

# Vegetable Fiber Reinforced Calcium Aluminum Cement based composites for construction materials VFRCCs

Doctoral thesis by:  
Nourjamal Gorgani

Directed by:  
Albert de la Fuente Antequera  
Josep Claramunt Blanes

Doctoral programme:  
Construction Engineering

Barcelona, June 2022



UNIVERSITAT POLITÈCNICA DE CATALUNYA  
BARCELONATECH

Department of Civil and Environmental  
Engineering

# DOCTORAL THESIS









Curs acadèmic: 2022-2023

## Acta de qualificació de tesi doctoral

Nom i cognoms

Nourjamal Gorgani

Programa de doctorat

Construction Engineering

Unitat estructural responsable del programa

Construction Engineering Department

## Resolució del Tribunal

Reunit el Tribunal designat a l'efecte, el doctorand / la doctoranda exposa el tema de la seva tesi doctoral titulada

\_\_\_\_\_.

Acabada la lectura i després de donar resposta a les qüestions formulades pels membres titulars del tribunal, aquest atorga la qualificació:

NO APTE

APROVAT

NOTABLE

EXCEL·LENT

(Nom, cognoms i signatura)	(Nom, cognoms i signatura)	
President/a	Secretari/ària	
(Nom, cognoms i signatura)	(Nom, cognoms i signatura)	(Nom, cognoms i signatura)
Vocal	Vocal	Vocal

\_\_\_\_\_, \_\_\_\_ d'/de \_\_\_\_\_ de \_\_\_\_\_

El resultat de l'escrutini dels vots emesos pels membres titulars del tribunal, efectuat per la Comissió Permanent de l'Escola de Doctorat, atorga la MENCIÓ CUM LAUDE:

SÍ

NO

(Nom, cognoms i signatura)	(Nom, cognoms i signatura)
President/a de la Comissió Permanent de l'Escola de Doctorat	Secretari/ària de la Comissió Permanent de l'Escola de Doctorat

Barcelona, \_\_\_\_ d'/de \_\_\_\_\_ de \_\_\_\_\_





*To all my family for their support  
A special thanks to my spouse Rajat Sewani  
To be by my side during 4 years of this doctoral programe  
A special thanks to my mother Maryam Seyedi and my sister Aijamal Gorgani  
And to my brothers even being far a way, they were my strength*



## **ACKNOWLEDGEMENTS**

I would like to thank to my tutors, Prof. Dr Albert de la Fuente (Department of Civil and Environmental Engineering, Polytechnic University of Catalunya– UPC) and Prof. Dr Josep Claramunt Blanes (Department of Agricultural Engineering ESAB, Polytechnic University of Catalunya– UPC) for their invaluable support and dedication during these 4 years. To Albert, for his trust and the opportunity he has given me to work with him during the development of this doctoral thesis. For his priceless guides when introducing the field of research to me. For encouraging me to experience the field as it should be experienced.

To Josep, for his endless support and patience to guide me during every step of the development of this doctoral thesis. For the opportunity he has given me to work with him and for introducing to me the amazing world of experimental field and his incredible dedication on every single part of this work. For encouraging me for 4 years and guiding and cheering me throughout its ups and downs. My gratitude for both of you, Albert and Josep goes well beyond to what these words can describe here.

My most sincere thanks to the coordinator, Prof. Dr Joan Ramon Casas Rius and all the members of the Department of Construction Engineering, Polytechnic University of Catalunya– UPC, I have had the opportunity of great educational experience to complete my doctoral degree in this Department.

In final, I would like to remember the moments I shared with my friends in the university are unforgettable. For this, a special thanks to Golshid Gilani to be a true friend by my side during these 4 years. To Payam Sadr, Ali Mahpoor and Vanessa to work and share time together in the lab. To Ali Farma, Parastoo and Nilufar for their true friendship in ups and downs. I had unforgettable moments with every single of you guys, thanks to be a part of the memories of these 4 years of this degree.

## ABSTRACT

Vegetable Fiber Reinforced Cement Composite Materials (VFRCC) have emerged as a potential construction material, providing adequate load-bearing capacity and ductility for non-structural applications. VFRCC have good mechanical properties (strength and ductility) which make them potentially suitable for non-structural construction applications.

The improved capacity of this material is due to the fact that, unlike ordinary mortar, a reinforcement is introduced that is distributed throughout the section of the piece, allowing the fibers to work throughout the entire tensile block. Commonly publications analyze the mechanical behavior of these materials in bending mode, their durability properties, chemical compositions and the micro-structure of matrix.

The objective of this doctoral thesis is to evaluate the mechanical behavior of VFRCC as a non-structural construction material. In this context, a cement-based matrix will be used which will be optimized by incorporating two different additives, a pozzolanic addition and two types of vegetable fibers (VF) as reinforcing elements, that will be introduced into the matrix in different proportions. The mechanical behavior will be carried out by means of three-point bending tests and four mechanical parameters will be analyzed, depending on the level of applied load: Limit of proportionality (LOP), maximum resistance to bending (MOR), Modulus of elasticity (MOE) and specific energy. The durability of the material will also be studied through an accelerated aging treatment consisting of 10 dry-wet cycles. The chemical composition of the matrix will also be analyzed by X-Ray diffractometry (XRD) and the micro-structure by scanning electron microscopy (SEM) and backscattered electron microscopy (BSEM) and atomic composition by energy dispersive X-Ray spectroscopy (EDX).

In terms of mechanical performance, it was found that the composites containing 10% cotton linter fiber with the polycarboxylate additive incorporated, exhibited higher flexural strength compared to the flax fiber composites, with good and sufficient deformability and ductility. At the same time, the influence of CAC on VFRCC demonstrated that this cement matrix could be a viable alternative to an OPC matrix in terms of VF durability for this type of material, compared to those conventional VF-OPC.

It was also observed that the accelerated aging cycles had a greater effect on the CAC matrix itself than on the VF, indicating that this matrix could be a viable alternative to produce a durable VFRCC. In terms of pozzolanic addition in CAC matrix, the results of BSEM/SEM and XRD analyzes revealed that, at higher concentrations of pozzolans, silica fume does not fully react with CAC, thus an excess of silica (SF) particles appeared in the micro-structure of the matrix. According to XRD results, new phases of strätlingite ( $C_2ASH_8$ ) were present in mixtures with low SF content. Simultaneously, the incorporation of silica fume in VFRCC appeared to further minimize fiber degradation. This doctoral thesis provides knowledge and data that can help to future researches and contribute to the future development of VFRCC design strategies.

Keywords: mechanical resistance; vegetable fiber reinforced cement composite; flexural post-cracking properties; durability properties; cotton linter fiber; flax fiber; additives

## RESUMEN

Los materiales Compuestos de Cemento Reforzado con Fibras Vegetales (CCRFV) han surgido como un potencial material de construcción, proporcionando una capacidad de carga y ductilidad adecuadas para aplicaciones no estructurales. Los CCRFV poseen unas buenas propiedades mecánicas (resistencia y ductilidad) que los hacen potencialmente adecuados para aplicaciones constructivas no estructurales.

La capacidad mejorada de este material se debe al hecho de que, a diferencia del mortero ordinario, se introduce un refuerzo que se distribuye en toda la sección de la pieza, permitiendo que las fibras funcionen en todo el bloque de tracción completo. Comúnmente, las publicaciones analizan el comportamiento mecánico de estos materiales a flexión, sus propiedades de durabilidad, composiciones químicas y microestructura de la matriz.

El objetivo de esta tesis doctoral es evaluar el comportamiento mecánico de los CCRFV como un material de construcción no estructural. En este contexto, se utilizará una matriz a base de cemento que se optimizará incorporando dos aditivos distintos, una adición puzolánica y dos tipos de fibras vegetales (FV) como elementos de refuerzo, que se introducirán en la matriz en diferentes proporciones. El comportamiento mecánico se llevará a cabo mediante ensayos de flexión de tres puntos y se analizarán, en función del nivel de carga aplicada, cuatro parámetros mecánicos: Límite de proporcionalidad (LOP), resistencia máxima a flexión (MOR), Módulo de elasticidad (MOE) y Energía específica. También se estudiará la durabilidad del material mediante un tratamiento de envejecimiento acelerado compuesto por 10 ciclos seco-húmedo. También se analizarán la composición química de la matriz mediante difracción de rayos x (DRX) y la microestructura mediante microscopía electrónica de barrido (SEM) y microscopía de electrones retrodispersados (BSEM) y composición atómica mediante espectroscopia de rayos X con dispersión de energía (EDX).

En términos de rendimiento mecánico, se encontró que los compuestos que contenían 10% de algodón con el aditivo de policarboxilato incorporado, exhibieron mayor resistencia a la flexión en comparación con los compuestos de fibra de lino, con una buena y suficiente capacidad de deformación y ductilidad. Al mismo tiempo, la influencia del CAC en los CCRFV demostró que esta matriz de cemento podría ser una alternativa viable a una matriz de OPC en términos de durabilidad de las FV para este tipo de material, en comparación con los FV-OPC convencionales.

También se observó que los ciclos de envejecimiento acelerado tenían un efecto mayor en la propia matriz de CAC que en las FV, lo que indica que esta matriz podría ser una alternativa viable para producir CCRFV durable. En términos de adición puzolánica en matriz CAC, los resultados de los análisis BSEM/SEM y XRD revelaron que, con concentraciones más altas de puzolana, el humo de sílice no reacciona por completo con el CAC, por lo que aparecía un excedente de partículas de SF en la microestructura de la matriz. Según los resultados de XRD, las nuevas fases de la strätlingita ( $C_2ASH_8$ ) estaban presentes en mezclas con bajo contenido de SF. Simultáneamente, la incorporación de humo de sílice en CCRFV pareció minimizar aún más la degradación de la fibra. Esta tesis doctoral proporciona conocimientos y datos que pueden ayudar a futuras investigaciones y contribuir al desarrollo futuro de estrategias de diseño de CCRFV.

Palabras clave: Propiedades mecánicas; compuesto de cemento reforzado con fibras vegetales; propiedades post-fisuración por flexión; durabilidad; fibra de algodón; fibra de lino; aditivos.

## Resum

Els materials compostos de Ciment Reforçat amb Fibres Vegetals (CCRFV) han sorgit com un possible material de construcció, proporcionant una capacitat de càrrega i ductilitat adequades per a aplicacions no estructurals. Els CCRFV tenen unes bones propietats mecàniques (resistència i ductilitat) que els fan potencialment adequats per a aplicacions constructives no estructurals.

La capacitat millorada d'aquest material es deu al fet que, a diferència del morter ordinari, se n'introdueix un que es distribueix en tota la secció de la peça, permetent que les fibres funcionin a tot el bloc de tracció complet. Comunament, les publicacions analitzen el comportament mecànic d'aquests materials a flexió, les seves propietats de durabilitat, composicions químiques i microestructura de la matriu.

L'objectiu d'aquesta tesi doctoral és avaluar el comportament mecànic dels CCRFV com un material de construcció no estructural. En aquest context, s'utilitzarà una matriu a base de ciment que s'optimitzarà incorporant dos additius diferents, una addició putzolànica i dos tipus de fibres vegetals (FV) com a elements de reforç, que s'introduiran a la matriu en diferents proporcions. El comportament mecànic es durà a terme mitjançant assaigs de flexió de tres punts i s'analitzaran, segons el nivell de càrrega aplicada, quatre paràmetres mecànics: Límit de proporcionalitat (LOP), resistència màxima a flexió (MOR), Mòdul d'elasticitat (MOE) i Energia específica. També s'estudiarà la durabilitat del material mitjançant un tractament d'envelliment accelerat compost per 10 cicles secs-humit. També s'analitzaran la composició química de la matriu mitjançant difractometria de raigs x (DRX) i la microestructura mitjançant microscòpia electrònica d'escombrada (SEM) i microscòpia d'electrons retrodispersats (BSEM) i composició atòmica mitjançant espectroscòpia de raigs X amb dispersió d'energia (EDX).

En termes de rendiment mecànic, es va trobar que els compostos que contenen 10% de cotó i amb Sika Viscocrete incorporat, van exhibir més resistència a flexió en comparació dels compostos de fibra de lli, amb una bona i suficient capacitat de deformació i ductilitat. Simultàniament, la influència del CAC als CCRFV va demostrar que aquesta matriu de ciment podria ser una alternativa viable a una matriu de ciment Portland comú en termes de durabilitat de les FV en aquests materials, en comparació dels FV-OPC convencionals.

També, es va observar que els cicles d'envelliment accelerat tenien un efecte més gran a la mateixa matriu de CAC que a les FV, cosa que indica que aquesta matriu podria ser una alternativa viable per produir CCRFV durables. En termes d'addició putzolànica en matriu CAC, els resultats de les anàlisis BSEM/SEM i XRD van revelar que, amb concentracions més altes de puzolana, el fum de sílice no reacciona del tot amb el CAC, per la qual cosa apareixia un excedent de partícules de SF a la microestructura de la matriu. Segons els resultats de XRD, les noves fases de la strätlingita ( $C_2ASH_8$ ) estaven presents en barreges amb baix contingut de SF. Simultàniament, la incorporació de fum de sílice a CCRFV va semblar minimitzar encara més la degradació de la fibra. Aquesta tesi doctoral proporciona coneixements i dades que poden ajudar a investigar futures i contribuir al desenvolupament futur d'estratègies de disseny de CCRFV.

Paraules clau: Propietats mecàniques; compost de ciment reforçat amb fibres vegetals; propietats post-fisuració per flexió; durabilitat; fibra de cotó; fibra de lli; additius.



## TABLE OF CONTENTS

<b>1. Introduction .....</b>	<b>27</b>
1.1. Introduction .....	27
1.2. Motivation.....	32
1.3. Research objective .....	32
1.4. Research method .....	33
1.4.1. Vegetable fiber reinforcement in CAC-based matrix.....	33
1.4.2. Influence of pozzolanic -Silica Fume- addition on CAC matrix .....	34
1.4.3. Influence of pozzolanic -Silica Fume- addition in VFRCC .....	35
<b>2. State of the art .....</b>	<b>36</b>
2.1. Introduction .....	36
2.2. Cementitious materials .....	37
2.2.1. Introduction to chemistry and mineralogy in CAC.....	37
2.2.2. CAC applications .....	38
2.2.3. Hydration mechanisms of CACs .....	39
2.3. Pozzolanic materials, silica fume .....	41
2.3.1. Influence of pozzolanic materials on CAC matrix .....	41
2.4. Vegetable fibers as reinforcement material in FRC .....	45
2.4.1. Classification of vegetable fibers .....	45
2.4.2. Characteristics of vegetable fibers .....	47
2.4.3. Morphological structure of vegetable fibers .....	49
2.5. Vegetable fibers reinforced cement composites VFRCC .....	51
2.5.1. Mechanical behavior of vegetable fibers in cement composites.....	51
2.5.2. Application area of VFRCC.....	52
2.5.3. Critical factors of vegetable fiber reinforced cement composites.....	53
2.6. Effect of fiber degradation/durability of VFRCC .....	55
2.6.1. Methodologies for durability improvement of VFRCC .....	57
<b>3. Experimental program .....</b>	<b>61</b>
3.1. Experimental program outline .....	61
3.2. Materials .....	63
3.2.1. Calcium cement aluminate.....	63
3.2.2. Fluidifying additives .....	63
3.2.3. Vegetable fibers .....	64
3.2.4. Silica fume .....	65
3.3. Specimen preparation.....	66
3.3.1. Specimen preparation procedure for 1 <sup>st</sup> -2 <sup>nd</sup> stages .....	66

---

3.3.2. Specimen preparation procedure for 3 <sup>rd</sup> -4 <sup>th</sup> stages .....	68
3.3.3. Accelerated aging cycles .....	70
3.4. Mechanical performance characterization .....	71
3.5. Microstructure and chemical composition analysis .....	72
3.5.1. X-Ray diffraction analysis .....	72
3.5.2. BSEM/SEM microstructure analysis .....	73
<b>4. Results and discussions .....</b>	<b>74</b>
4.1. Flexural strength performance .....	74
4.1.1. Modulus of elasticity (MOE) .....	74
4.1.2. Limits of proportionality (LOP) .....	78
4.1.3. Modulus of rupture (MOR) .....	79
4.1.4. Specific energy, Toughness (SE) .....	82
4.2. Durability analysis of composite materials .....	83
4.2.1. Modulus of elasticity (MOE) .....	83
4.2.2. Limits of proportionality (LOP) .....	87
4.2.3. Modulus of rupture (MOR) .....	88
4.2.4. Specific energy absorption (SE) .....	90
4.3. Mechanical, microstructure-chemical composition analysis of silica fume-calcium aluminate cement pastes .....	91
4.3.1. Flexural strength performance .....	91
4.3.2. Compression strength performance .....	93
4.3.3. X-Ray Diffraction, chemical composition analysis .....	96
4.3.4. BSEM, microstructure analysis .....	99
4.4. Mechanical resistance, durability and microstructure analysis of silica fume-calcium aluminate cement composites .....	106
4.4.1. Flexural strength performance .....	106
4.4.2. Durability of composites after aging cycles .....	108
4.4.3. BSEM, microstructural analysis of unaged-aged compounds .....	111
4.4.4. SEM, analysis of the fracture surface .....	117
<b>5. Conclusions .....</b>	<b>122</b>
VFRCC in CAC-based matrix as alternative reinforcement .....	123
Influence of pozzolanic addition, silica fume incorporation in CAC-based matrix; a low alkaline medium .....	124
VF reinforcement in SF-CAC-based matrix .....	125
Future perspectives .....	126
<b>6. References .....</b>	<b>128</b>

---



## LIST OF FIGURES

Figure 1.1 The brick making process by Egyptians .....	27
Figure 1.2 The scheme of Hatschek fiber cement production process .....	28
Figure 1.3 Hardie’s Fibrolite .....	29
Figure 1.4 The Interbau housing in Hansavuliding, by Walter Gropius, Berlin .....	29
Figure 1.5 The Ricola storage facility in Laufen, by Herzog & De Meuron .....	29
Figure 1.6 The loop chair designed by Willy Guhl.....	30
Figure 1.7 Relative comparison between vegetable fiber and glass fiber .....	31
Figure 1.8 1 <sup>st</sup> -2 <sup>nd</sup> experimental stages methodology, flexural strength of VFRCC .....	34
Figure 1.9 3 <sup>rd</sup> experimental stage methodology, mechanical resistance of SF-CAC ...	34
Figure 1.10 4 <sup>th</sup> experimental stage methodology, flexural strength of SF-VFRCC .....	35
Figure 2.1 The composition range of CAC compared to OPC .....	37
Figure 2.2 Typical application of CAC concrete .....	38
Figure 2.3 The schematic strength development of CAC at w/c ratio of 0.4 .....	41
Figure 2.4 The SEM micrograph of platy strätlingite crystallites .....	42
Figure 2.5 Photographic sources of some vegetable fiber types .....	45
Figure 2.6 Vegetable fiber types according to their physical and application form .....	46
Figure 2.7 Flax fiber plant’s stem cross-section compositions .....	48
Figure 2.8 The scheme of vegetable fiber structure from plant to cellulose chains .....	50
Figure 2.9 Fiber arrangement in 1-D, 2-D and 3-D dimension classifications.....	52
Figure 2.10 The application area of natural fibers.....	53
Figure 2.11 The fiber orientation effects on tensile strength of composites.....	55
Figure 2.12 A schematic representation, water absorption at fiber/matrix interface .....	56
Figure 2.13 Fiber/matrix interface in VFRC composites .....	57
Figure 2.14 Fiber decomposition process .....	59
Figure 3.1 The out-line of experimental program and test methods procedures .....	62
Figure 3.2 Raw calcium aluminate cement .....	63
Figure 3.3 Vegetable fibers subjected to wet/dry cycles and dried in stove .....	65
Figure 3.4 Raw silica fume grains before treatment .....	65
Figure 3.5 The silica fume milling treatment procedure .....	66
Figure 3.6 The schematic representation of 1 <sup>st</sup> -2 <sup>nd</sup> experimental stages .....	67
Figure 3.7 The schematic representation of 3 <sup>rd</sup> -4 <sup>th</sup> experimental stages .....	69
Figure 3.8 The wet/dry cycles, specimens subjected to aging cycles .....	70
Figure 3.9 Flexural strength and compression strength tests .....	71

Figure 3.10 Flexural stress-strain curves obtained for cellulosic cement composite	71
Figure 3.11 X-Ray Diffraction analysis, specimen preparation	72
Figure 3.12 BSEM-SEM analysis, specimen preparation procedure	73
Figure 4.1 The average values of modulus of elasticity MOE (GPa)	75
Figure 4.2 Flexural stress-displacement relationships for 0AD-Cotton linter	76
Figure 4.3 Flexural stress-displacement relationships for SP380-Cotton linter	76
Figure 4.4 Flexural stress-displacement relationships for SVC3425-Cotton linter	76
Figure 4.5 Flexural stress-displacement relationships for 0AD-Flax fiber	77
Figure 4.6 Flexural stress-displacement relationships for SP380-Flax fiber	77
Figure 4.7 Flexural stress-displacement relationships for SVC3425-Flax fiber	77
Figure 4.8 The average values of limits of proportionality LOP (MPa)	78
Figure 4.9 The average values of modulus of rupture MOR (MPa)	80
Figure 4.10 Effect of cotton linter/flax fibers on the post-cracking	82
Figure 4.11 The average values of specific energy SE (kJ/m <sup>2</sup> )	82
Figure 4.12 The average values of modulus of elasticity MOE (GPa)	84
Figure 4.13 Flexural stress-displacement relationships for 0AD-Cotton linter	85
Figure 4.14 Flexural stress-displacement relationships for SP380-Cotton linter	85
Figure 4.15 Flexural stress-displacement relationships for SVC3425-Cotton linter	85
Figure 4.16 Flexural stress-displacement relationships for 0AD-Flax fiber	86
Figure 4.17 Flexural stress-displacement relationships for SP380-Flax fiber	86
Figure 4.18 Flexural stress-displacement relationships for SVC3425-Flax fiber	86
Figure 4.19 The average values of limits of proportionality LOP (MPa)	87
Figure 4.20 The average values of modulus of rupture MOR (MPa)	88
Figure 4.21 Effect of aging cycles on the post-cracking load carrying capacity	89
Figure 4.22 The average values of specific energy SE (kJ/m <sup>2</sup> )	90
Figure 4.23 The average values of flexural modulus of elasticity MOE (GPa)	92
Figure 4.24 The average values of flexural modulus of rupture MOR (MPa)	93
Figure 4.25 The average values of compression modulus of elasticity MOE (GPa)	93
Figure 4.26 The average values of compression modulus of rupture MOR (MPa)	94
Figure 4.27 X-Ray diffraction results for 0%SF-CAC paste at 7, 28 and 56 days	97
Figure 4.28 X-Ray diffraction results for 5%SF-CAC paste at 7, 28 and 56 days	97
Figure 4.29 X-Ray diffraction results for 15%SF-CAC paste at 7, 28 and 56 days	98
Figure 4.30 BSEM micrograph results for 0%SF-CAC paste at 7 days, presents polyphasic particles, indicating EDS analysis areas	99
Figure 4.31 BSEM micrograph results for 0%SF-CAC paste at 7 days, presents polyphasic particles	100

Figure 4.32 BSEM micrograph results for 0%SF-CAC paste at 28, 56 days, presents polyphasic particles, indicating EDS analysis areas .....	100
Figure 4.33 BSEM micrograph results for 5%SF-CAC paste at 7, 28 days, presents polyphasic particles and hydrated zones, indicating EDS analysis areas .....	101
Figure 4.34 BSEM micrograph results for 5%SF-CAC paste at 7, 28, 56 days, presents polyphasic particles mapping .....	102
Figure 4.35 BSEM micrograph results for 15%SF-CAC paste at 7, 28 days, presents polyphasic particles and hydrated zones indicating EDS analysis areas .....	103
Figure 4.36 BSEM micrograph results for 15%SF-CAC paste at 7, 56 days, presents polyphasic particles mapping .....	104
Figure 4.37 BSEM micrograph results for 15%SF-CAC paste at 28 days, presents polyphasic particles and hydrated zones .....	105
Figure 4.38 BSEM micrograph results for 0%SF-CAC paste at 7, 28, 56 days cured binders differentiation.....	105
Figure 4.39 Flexural stress-displacement relationships for SF-CAC-SVC342510%CO composites at 28, 56 days .....	106
Figure 4.40 Flexural strength parameters for SF-CAC-SVC342510%CO composites at 28, 56 days.....	106
Figure 4.41 Flexural stress-displacement relationships for SF-CAC-SVC342510%CO composites at 28D and 28D+10% accelerated aging cycles .....	108
Figure 4.42 Flexural strength parameters for SF-CAC-SVC342510%CO composites at 28D and 28D+10% accelerated aging cycles .....	108
Figure 4.43 BSEM micrograph results for 0%SF-CAC-10%CO at 28 days, presents polyphasic particles and hydrated zones, indicating EDS analysis areas .....	111
Figure 4.44 BSEM micrograph results for 0%SF-CAC-10%CO at 28 days, presents polyphasic particles and hydrated zones mapping .....	112
Figure 4.45 BSEM micrograph results for 0%SF-CAC-10%CO at 28D+10 accelerated aging cycles, presents polyphasic particles and hydrated zones, indicating EDS analysis areas .....	113
Figure 4.46 BSEM micrograph results for 0%SF-CAC-10%CO at 28D+10 accelerated aging cycles, presents polyphasic particles and hydrated zones mapping .....	114
Figure 4.47 BSEM micrograph results for 5%SF-CAC-10%CO at 28D cured compound identification phase .....	114
Figure 4.48 BSEM micrograph results for 5%SF-CAC-10%CO at 28D cured compound, presents polyphasic particles and hydrated zones mapping.....	115
Figure 4.49 BSEM micrograph results for 5%SF-CAC-10%CO at 28D+10 accelerated aging cycles, presents polyphasic particles and hydrated zones.....	116
Figure 4.50 BSEM micrograph results for 5%SF-CAC-10%CO at 28D+10 accelerated aging cycles, presents polyphasic particles and hydrated zones mapping.....	117
Figure 4.51 SEM micrograph showing the cement hydration compounds in the lumen and surface of the vegetable fibers .....	118
Figure 4.52 SEM micrograph of cotton linter compounds at 28D and 28D+10 accelerated aging cycles in CAC and SF-CAC mixtures .....	118

Figure 4.53 SEM micrograph of cotton linter compounds at 28D in CAC matrix ..... 119

Figure 4.54 SEM micrograph of cotton linter compounds at 28D in CAC and SF-CAC mixtures ..... 120

Figure 4.55 SEM micrograph of cotton linter compounds at 28D+10 accelerated aging cycles in CAC and SF-CAC mixtures ..... 121

## LIST OF TABLES

Table 1.1 The specific objectives for each main subjects of the doctoral thesis .....	33
Table 2.1 The basic differences in OPC/CAC cements .....	37
Table 2.2 The chemical composition in different types of CAC cements .....	38
Table 2.3 The chemical composition of CAC hydrates .....	40
Table 2.4 The chemical composition of cellulosic fibers .....	48
Table 2.5 The mechanical properties of cellulosic fibers .....	48
Table 3.1 The chemical composition of calcium aluminate cement.....	63
Table 3.2 The properties of additives applied in mixtures .....	64
Table 3.3 The properties of vegetable fibers .....	64
Table 3.4 The chemical composition of silica fume .....	65
Table 3.5 The dosage of mixtures for 1 <sup>st</sup> -2 <sup>nd</sup> experimental stages .....	66
Table 3.6 The w/c ratio of mixtures for 1 <sup>st</sup> -2 <sup>nd</sup> experimental stages .....	68
Table 3.7 The dosages of mixtures for 3 <sup>rd</sup> experimental stage .....	68
Table 3.8 The dosages of mixtures for 4 <sup>th</sup> experimental stage .....	70
Table 3.9 The equations for calculations of MOR, MOE and Strain ( $\partial$ ) .....	72
Table 4.1 The average values of the modulus of elasticity MOE (GPa) .....	75
Table 4.2 The average values of the limits of proportionality LOP (MPa).....	78
Table 4.3 The average values of the modulus of rupture MOR (MPa) .....	80
Table 4.4 The average values of the specific energy absorption SE (KJ/m <sup>2</sup> ) .....	83
Table 4.5 The average values of the modulus of elasticity MOE (GPa) for unaged-aged compounds.....	84
Table 4.6 The average values of the limits of proportionality LOP (MPa) for unaged-aged compounds.....	88
Table 4.7 The average values of the modulus of rupture MOR (MPa) for unaged-aged compounds.....	89
Table 4.8 The average values of the specific energy absorption SE (KJ/m <sup>2</sup> ) for unaged-aged compounds .....	90
Table 4.9 The average values of flexural strength parameters MOR and MOE of Silica Fume-CAC mixtures .....	92
Table 4.10 The average values of compression strength parameters MOR and MOE of Silica Fume-CAC mixtures .....	94
Table 4.11 The detected phases in X-Ray Diffraction analysis.....	98
Table 4.12 The average values of flexural strength parameters of Silica Fume-CAC-10%Cotton linter fiber compounds .....	107
Table 4.13 The average values of flexural strength parameters of unaged-aged Silica Fume-CAC-10%Cotton linter fiber compounds .....	109



## Abbreviations and Symbols

$Al_2O_3$	Aluminum oxide
$CaO$	Calcium oxide
$Fe_2O_3$	Iron oxide III
$TiO_2$	Titanium oxide
$Na_2O$	Sodium oxide
$K_2O$	Potassium oxide
$CaAl_2O_3$	Monocalcium Aluminate
$SiO_2$	Silicon oxide
$FeO$	Iron oxide
$S_2$	Sulfide
$SO_3$	Sulfate
$MgO$	Magnesium oxide
$Ca$	Calcium
$H_2O$	Water
$OH$	Hydroxide
$CH$	Calcium Hydroxide/Portlandite
$Ca_3A_{12}(SiO_4)_{3-x}(OH)_{4x}$	Katoite
$AH_3$ or $Al(OH)_3$	Gibbsite
$Ca_2Al_2SiO_7 \cdot 8H_2O$ ( $C_2AS$ )	Gehlenite
$C_2ASH_8$	Strätlingite (Hexagonal platy hydrates)
$C_2AH_8$	Lamellar calcium aluminate hydrates (Meta-stable phases – Hexagonal hydrates)
$C_3AH_6$	hydrogarnet (Stable phases – Cubic hydrates)
$CA$	Monocalcium Aluminate
$CAH_{10}$	Monocalcium Aluminate (Meta-stable phases – Hexagonal hydrates)
$CA_2$	Grossite
$CA_6$	Hibonite
$C_{12}A_7$	Mayenite
$C_2S: 2CaO \cdot SiO_2$	Belite
$CAC$	Calcium Aluminate Cement
$OPC$	Ordinary Portland Cement
$VF$	Vegetable Fiber
$VFRC$	Vegetable Fiber Reinforced Cement Composite
$pH$	Potential Hydrogen
$SF$	Silica Fume
$MK$	Metakaolin
$SL$	Slag
$FA$	Fly Ash
$FL$	Flax Fiber
$CO$	Cotton Linter Fiber
$SP380$	Superplasticizer 380
$SVC3425$	Sika ViscoCrete 3425

---

<i>OAD</i>	<i>Without Additives</i>
<i>W/D</i>	<i>Wet/Dry</i>
<i>HR</i>	<i>Relative Humidity</i>
<i>W</i>	<i>Water</i>
<i>D</i>	<i>Day</i>
<i>M</i>	<i>Months</i>
<i>Y</i>	<i>Year</i>
<i>MPa</i>	<i>Megapascal</i>
<i>GPa</i>	<i>Gigapascal</i>
<i>kJ/</i>	<i>Kilojoule per square meter</i>
<i>N</i>	<i>Newton</i>
<i>kN</i>	<i>Kilo Newton</i>
<i>cm</i>	<i>Centimeter</i>
<i>g</i>	<i>Gram</i>
<i>μm</i>	<i>Micrometer</i>
<i>nm</i>	<i>Nanometer</i>
<i>XRD</i>	<i>X-Ray Diffraction</i>
<i>BSEM</i>	<i>Backscattered Scanning Electron Microscopy</i>
<i>EDS</i>	<i>X-Ray Energy Dispersive Spectroscopy</i>
<i>SEM</i>	<i>Scanning Electron Microscopy</i>
<i>∂</i>	<i>Strain</i>
<i>F</i>	<i>Load (force)(N)</i>
<i>l</i>	<i>Length of the support span (mm)</i>
<i>f</i>	<i>Maximum deflection (mm)</i>
<i>b</i>	<i>Thickness of specimen (mm)</i>
<i>h</i>	<i>Width of specimen (mm)</i>
<i>LOP</i>	<i>Limits OF Proportionality</i>
<i>MOR</i>	<i>Modulus OF Rupture</i>
<i>MOE</i>	<i>Modulus OF Elasticity</i>
<i>SE</i>	<i>Specific energy absorption</i>



# 1. INTRODUCTION

## 1.1. INTRODUCTION

Vegetable Fiber Reinforced Cement Composites (VFRCCs) have emerged as a potential construction material, providing proper tensile stress bearing capacity and ductility. The use of fibers to improve the mechanical properties of brittle materials was already implemented by ancient Egyptians by 1500 BCE (See [Figure 1.1](#)), such as (i.e., straws or horsehair) to reinforce mud bricks. (E. Baldwin- Smith, 1938).



BRICK MAKING, TOMB OF REKHMARA, THEBES

P. E. Newberry, *The Life of Rekhmara* (1900, Pl. XXI).

**Figure 1.1.** The brick making process by Egyptians. (E. Baldwin- Smith, 1938).

Ludwig Hatschek an Austrian textile engineer, invented *fiber (asbestos) cement* in the late 19th century,. In 1893, he established the first Austro-Hungarian asbestos factory and began researching on new products. He studied for 7 years developing the fire-resistant roof panels which were light, low cost, and durable. By 1900, he patented a machine which enabled the incorporation of thin asbestos sheets in Portland cement paste. [Figure 1.2](#) presents the scheme of Hatschek fiber cement production process.

The 9:1 (90 parts of cement-10 parts of asbestos) ratio utilized to produce these panels ensured that the desired both mechanical and physical properties as a building material were obtained. (Ludwig Hatschek, 1900, Patent GB190006455A). In 1942 the ETERNIT- Werke Ludwig Hatschek, the cellulose fiber containing fiber cement products, was patented. (Ludwig Hatschek, 1942, Patent CH234322A).

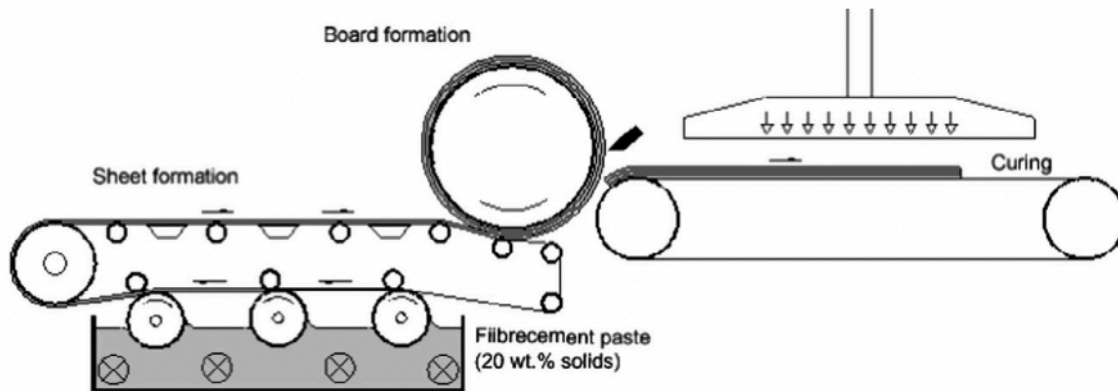


**Figure 1.2.** The scheme of Hatschek fiber cement production process. (M. Ardanuy, J. Claramunt, 2015).

James Hardie and Coy Pty, Fibrolite, an Australian factory produced the first fiber cement products, replacing some asbestos mixture and integrating cellulose fibers in its fiber cement products by 1938. Fibrolite, according to the historical commercial brochure (Figure 1.3), is a strong, durable and fire retardant material, manufactured from OPC and asbestos fiber into various classes of building and roofing materials, including flat sheets for walls, ceiling, partitions, etc. (James Hardie, Coy Pty, Fibrolite, 1938).

The decade of 1945–55 was an incipient period in the development of building materials and procedures that would revolutionize the construction industry. The use of manufacturers' fibro (asbestos cement), strawboard, and other products were promoted by Modernism. (S. Marsden, 2003).

In 1938, Solomit established a strawboard factory in Freeling (the first strawboard house at Freeling, in Australia was built by 1949). Solomit SA grew into a significant rural industry in the 1950s-1960s, fabricating thousands of strawboard sheets for acoustic ceilings. (S. Marsden, 2003).

Architects like Walter Gropius pioneered the use of coated fiber cement panels with the ventilated facade system as (rain-screen) technology in the 1950s (Figure 1.4). In his book, "The New Architecture and the Bauhaus, 1935" Gropius wrote: "The role of walls is restricted to mere screens stretched between the vertical columns of the frame to avoid rain, cold and noise. (Gropius, 1965).

Herzog & De Meuron used uncoated fiber cement panels to design the Ricola storage facility in Laufen in 1987 (See Figure 1.5). The cladding is made of Eternit panels that are larger at the top than at the bottom, emphasizing the difference between the lower part, where numerous individual foundations support the façade construction. (Herzog & de Meuron 1978-2007).

February 24, 1938. BUILDING 55

*Roofed to Endure!*



Approx. 112,500 sq. ft. of "FIBROLITE" Super-Six Corrugated Sheets were used for roofing, and 9,800 sq. ft. for walling, these large Works and Office buildings for Messrs. H. V. McKay Massey Harris Pty. Ltd., Concord, Sydney.

Architects: Messrs. Stephenson Meldrum & Turner.

Engineers: Mr. C. S. Steels.

Builders: Messrs. William Hughes & Co. Ltd.

Rust, corrosion or the elements cannot harm the roofs of these large Works for Messrs. H. V. McKay Massey Harris Pty. Ltd., Concord. They're covered with Hardie's "Fibrolite" Super-Six Corrugated Sheets. They will endure with the building . . . painting will never be required . . . maintenance costs throughout their long life will be negligible.

**Specify Hardie's Genuine "Fibrolite"**

ILLUSTRATED CATALOGUE MAILED ON REQUEST.

•

**JAMES HARDIE & COY. PTY. LTD.**  
"Asbestos House," Cr. York & Barrack Sts., Sydney  
And at Newcastle, Melbourne, Brisbane, Perth and Auckland, N.Z.

**HARDIE'S FIBROLITE**  
CORRUGATED ASBESTOS CEMENT ROOFING

TRIED, TESTED AND PROVED FOR OVER 20 YEARS

Advertisers will be pleased to send Catalogues and Price Lists on application.

Figure 1.3. Hardie's Fibrolite (James Hardie, Coy Pty, Fibrolite, 1938).



Figure 1.4. The Interbau housing in Hansaviendingen houses of Walter Gropius in Berlin, 1955-1957 (Gropius, 1965).

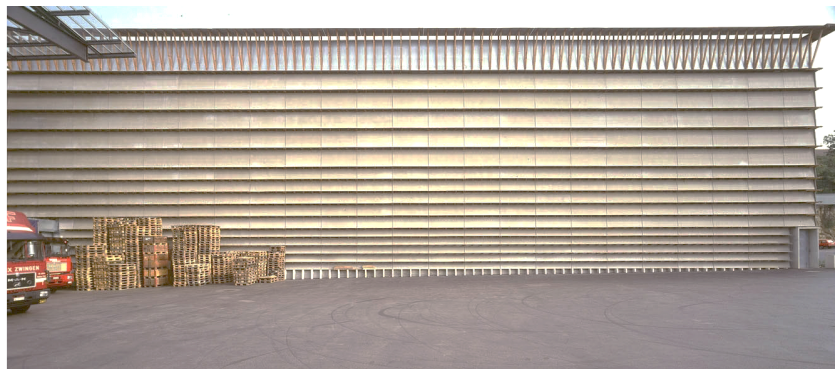
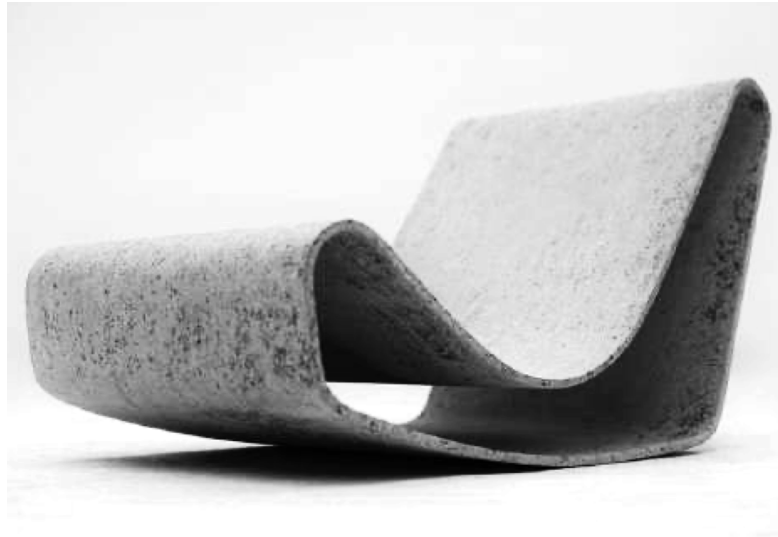


Figure 1.5. The Ricola storage facility in Laufen in 1987 designed by Herzog & De Meuron (Herzog & de Meuron 1978-2007).

The designer Willy Guhl created the famous "loop chair" in 1954 (See [Figure 1.6](#)), which was made up of a single piece made of this material, which the basic properties of the fiber cement are still evident in this design: thinness, lightness, durability, and elegance. The Guhl chair, made from recyclable fiber cement, adds a touch to any living landscape, where the grooves in the back provide additional stability. ([A. Esquinas Herrera, 2019](#)).



**Figure 1.6.** The loop chair designed by Willy Guhl, in 1954 ([A. Esquinas Herrera, 2019](#)).

In the early 1970s and 1980s, a worldwide campaign was launched to legislate the removal of asbestos reinforcing from a wide range of construction materials. ([Wilke. HJ, 1976](#)). A successful material throughout seven decades of their use, it began to be prohibited by law in industrialized countries due to the serious health hazard issues this material presents to human beings. Unfortunately, even though these prohibitions asbestos-cement products are still produced in the developing countries. ([T. Filho, K. Scrivener 2000](#)).

According to the legislated law of December 7 in 2001, products containing asbestos fibers intentionally added was prohibited in Spain. ([Decree 1406/1989, Spain 2001](#)). After banning asbestos fibers due to its hazardous effects on human health, finding alternatives fibers has drawn the researcher's attention. ([M. Khorami, E. Ganjian 2011](#)).

Owing to the major use of asbestos as cement reinforcement all around the world, new fiber alternatives for cement-based composite reinforcement were introduced as substitutes to asbestos fibers ([H. Savastano, P.G. Warden 2003](#)). Since then, experimenting the asbestos-free alternatives, with the wide variety of synthetic and natural fibers have been in progress in different laboratories throughout the world. ([R.S.P Coutts 2005](#)).

The engineering interest has been focused from monolithic materials to fiber-reinforced polymeric materials in recent decades. These polymeric materials are; (i.e., aramid, carbon, glass fiber, polypropylene, among others), are the most widely used to reinforce cement-based composites due to their low cost which present proper mechanical properties. ([P. Wambua 2003](#)). Currently, the synthetic fibers (i.e., polypropylene (PP), polyethylene (PE), and polyvinyl alcohol (PVA)) are being used in engineered cementitious composites (ECC). Among those, PVA fibers have a higher tensile strength than PP fibers, while ECC reinforced with PVA fiber present more toughness and flexural strength than ECC reinforced with PP fiber. ([E.H. Yang, V.C. Li 2010](#)).

Regardless of presenting good durability performance, synthetic fibers compared to natural fibers present some drawbacks; (i.e., higher density, higher cost, hardly recyclable, high energy consumption, among others). Instead natural fibers are renewable, recyclable, low cost and low energy consumption. Figure 1.7 presents the relative comparison between vegetable fiber and glass fiber. (M. Li, Y. Pu 2020).

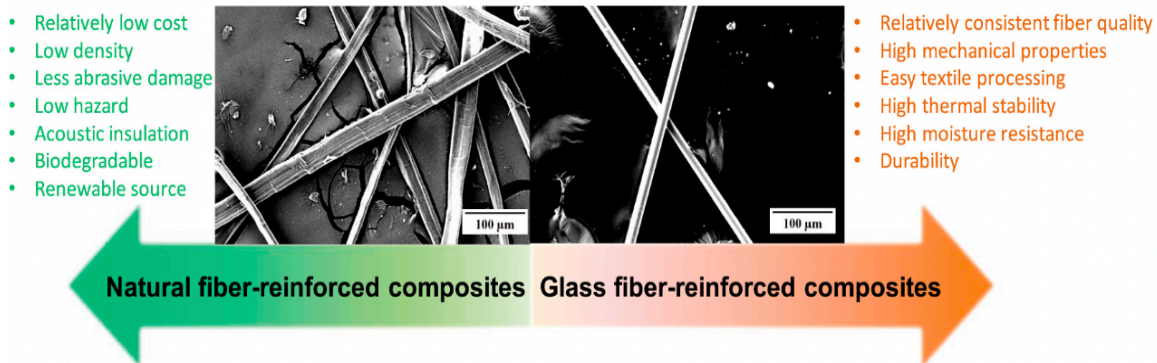


**Figure 1.7.** Relative comparison between vegetable fiber and glass fiber for composite manufacturing. The SEM photos of (left) alkaline mercerized ramie fiber, (right) E-glass fiber (M. Li, Y. Pu 2020).

VFs are available in most of the developing countries, and VFs could be suitable as reinforcement element for brittle matrices; however, VFs present deficiencies in terms of durability performance compared to synthetic fibers. (V. Agopyan, H. Savastano 2005). For this reason, most of the researches on VFRCCs were focused on the durability aspects (B.J. Mohr, J.J. Biernacki 2006). These studies have been boosted during the last 2 decades, due to the demand for sustainable, energy-efficient building materials (L.C. Roma 2008).

The development of *green products* based on natural resources for construction applications, include new pathways to produce; (i.e., better mechanical and physical properties, long term durability, thermal stability, low cost and others.). (K. G. Satyanarayana, G. G. C. Arizaga 2009).

Apart from the positive outcomes derived from the research on durability of VFRCCs, the use of these is increasing, due to the proven suitable mechanical properties; (i.e., enhanced toughness, ductility, flexural capacity and crack resistance, low thermal conductivity, their availability and low cost) for building components when compared to other non-fiber-reinforced cement materials. (J. Claramunt, M. Ardanuy 2010). The main advantage of VFRCCs is the control of the crack width once the element is cracked (V. Agopyan, H. Savastano 2005), since these fibers bridge the matrix crack and transfer the loads (M. Ardanuy, J. Claramunt 2015).

Despite all the advantages mentioned above, the industrial production of VFRCCs is currently constrained by the long-term durability problems. (T. Filho, K. Scrivener 2000). VFRCCs undergo into an ageing process when exposed to humidity, which causes severe strength reductions.

This durability issue is associated with an increase in fiber fracture and decrease in fiber pull-out strength. (T. Filho, K. Ghavami 2003), (T. Filho 1997), (Gram HE 1983), these being consequences of the combination of some factors: (1) fiber weakening caused by alkali attack; (2) fiber mineralization caused by hydration product migration to lumens, and (3) volume variation caused by their high water absorption (T. Filho, K. Scrivener 2000). The efficiency of fiber reinforcement is influenced by how fibers are conserved within the matrix over the time. If

this matter is not treated properly, this can lead to a decline in the flexural tensile strength performance (T. Filho, Kh. Ghavami 2003) and, thus, these are unsuitable for structural applications since -for this purpose- long-term mechanical performance must be maintained within the reliable levels. This is an aspect upon which further research is required to fully understand this phenomenon. Some studies have been carried out as a review on the long term durability of VFRCCs (M. Ardanuy, J. Claramunt 2015).

Other researchers (H. Savastano, V. Agopyan 1999), (H. Savastano, P.G. Warden 2000, 2003 and 2005), (V. Agopyan, H. Savastano 2005), (B.J Mohr, H. Nanko 2005), (B.J Mohr, J.J. Biernaki 2006), (J. Claramunt, M. Ardanuy 2010), (P. Soroushian, J. Pil Won 2012) studied durability properties and alternative VFs for cement-based composites and the microstructure of those materials.

## 1.2. MOTIVATION

Buildings have an important role in framing societies, and environments in which humans interact and develop vital activities. Furthermore, buildings have a major role in the use of energy in the transition to a low-carbon, resilient, and sustainable society, and are among the largest sources of greenhouse gas (GHG) emissions in most nations. (Housing 2030, Report of ONU-Habitat).

To shift that dependency to renewables, architects and engineers must use systems-level approach to building design, seeing structures as energy producers rather than exclusively or predominantly as energy sinks. With today's technology, it is possible to adapt buildings and construction materials to correspond with the greatest standards of health, comfort, low cost, aesthetic and sustainability, including enhancing energy productivity and reducing CO<sub>2</sub> emissions, at prices equivalent to or close to those of old systems. (ECE 2017).

In this context, the necessity to regulate the construction industry and environmental implications and the climate change crisis has prompted the architects and engineers toward designing high-performance and environmentally friendly buildings and durable materials. The façade of a building, being part of the enclosure unquestionably is no exception to this requirement. The façade design, however, is given the less attention it deserves, despite the huge potential for energy savings and reduced environmental impacts (S. Moghtadernejad, L.E. Couinard 2020).

## 1.3. RESEARCH OBJECTIVE

The *main objective* of this doctoral thesis is to perform an experimental program to characterize from the mechanical and durability-VFRCCs by considering the following aspects:

- The effect of using different VFs types and contents –considering different additives– as reinforcement for CAC-based composited on the flexural performance of non- and aged panels.
- The effect of pozzolanic addition in CAC matrix on the partial replacement of CAC with Silica Fume (SF) and on the hydration reactivity of the matrix;

- The effect of using VF reinforced SF-CAC composites on the flexural performance of thin panels subjected and non-subjected to aging cycles.

To attend the general objectives, several specific objectives were proposed. Table 1.1 highlights the specific objectives for each subject.

**Table 1.1.** The specific objectives for the main subjects investigated in the doctoral thesis.

Subject	Specific objectives
Vegetable-Fiber reinforcement in CAC-based matrix as alternative reinforcement	<ul style="list-style-type: none"> <li>• Evaluate the influence of different VFs types and contents on flexural strength of VFRCCs (the efficiency of the VFs).</li> <li>• Evaluate the influence of different additive types on flexural strength of VFRCCs (the efficiency of the additives).</li> <li>• Evaluate the influence of accelerated aging cycles on flexural strength of VFRCCs (durability- long-term efficiency of VFs).</li> <li>• Evaluate the influence of cement matrix type (CAC) on the VFs properties; (the efficiency of CAC).</li> <li>• Evaluate the influence of short term-long term curing times; (the mechanical performance efficiency of VFs).</li> </ul>
Influence of pozzolanic addition; Silica Fume incorporation in CAC-based matrix; A low alkaline medium	<ul style="list-style-type: none"> <li>• Evaluate the mechanical behaviour of SF-CAC with different SF/CAC ratios.</li> <li>• Evaluate the chemical composition analysis (to assess the influence of SF on the hydration phases of CAC).</li> <li>• Evaluate the micro-structure analysis (to assess the influence of SF on the micro-structure of CAC).</li> </ul>
Vegetable-Fiber reinforcement in SF-CAC based matrix;	<ul style="list-style-type: none"> <li>• Evaluate the influence of SF on flexural strength of VFRCCs</li> <li>• Evaluate the influence of accelerated aging cycles on flexural strength of SF-VFRCCs</li> <li>• Evaluate the micro-structure analysis, (to assess the influence of SF on the micro-structure and hydrations phases of SF-VFRCCs).</li> <li>• Evaluate the VF surface analysis, (to assess the influence of SF on the VFs durability and VFs mineralization ).</li> </ul>

## 1.4. RESEARCH METHOD

This research is focused on characterization of the mechanical properties of VFRCCs oriented to non-structural construction applications (i.e., façade panels). To this end, an extensive experimental program involving the production and testing cotton linter fiber and flax fiber in a CAC and SF-CAC cement-based matrices was carried out. As this experimental program was meant to cover different relevant features, this was designed dividing the experimental efforts by the phases described below.

### 1.4.1. Vegetable fiber reinforcement in CAC-based matrix

The experimental stage was focused on characterizing VFRCC produced with CAC matrices –as a potential alternative for conventional OPC-based VFRCCs– and their fiber mineralization drawbacks due to alkaline attack. With this purpose, this stage was based on testing flexural performance of thin VFRCCs before and after this having been subjected to accelerated aging cycles. The specimens were produced with two type of VFs (cotton linter and flax fibers) and different fiber contents. Two type of admixtures meant to improve workability of the composites were used. The outline of this stage is schematized in [Figure 1.8](#).

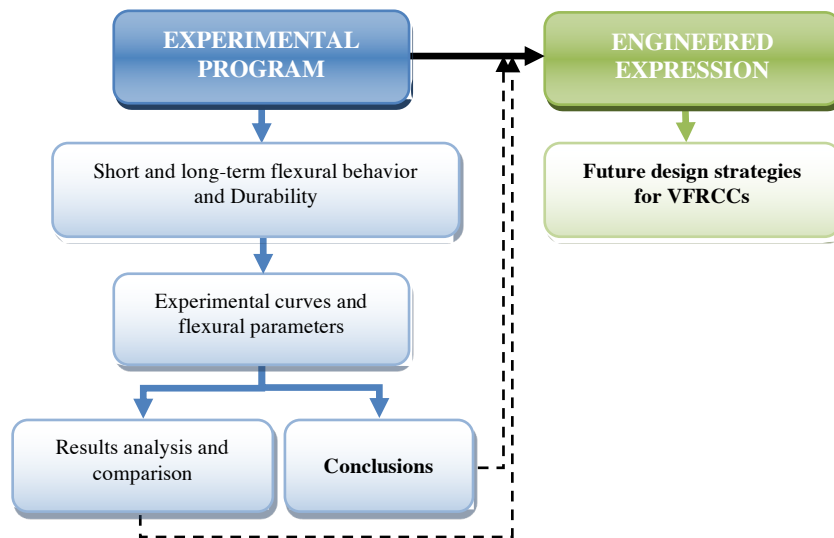


**Figure 1.8.** The 1<sup>st</sup> and 2<sup>nd</sup> experimental stages methodology, short and long term flexural performance of VFRCCs non and aged compounds (durability of VFRCCs).

#### 1.4.2. Influence of pozzolanic –Silica Fume– addition on the CAC matrix

The 3<sup>rd</sup> experimental stage was focused on characterizing the influence of pozzolanic (Silica Fume) addition in CAC based cement –as a low alkaline matrix for VFRCCs–. Moreover its chemical compositions and micro-structure of mixtures were assessed due to –the conversion phenomenon caused by environmental temperature and humidity changes over the time in CAC-based cements–. With this purpose, this stage was based on testing mechanical properties (flexural and compression performance) of SF-CAC with 5 different ratios. The chemical composition and micro-structure of mixtures were evaluated by XRD and BSEM analysis. The outline of 3<sup>rd</sup> experimental stage is schematized in Figure 1.9.

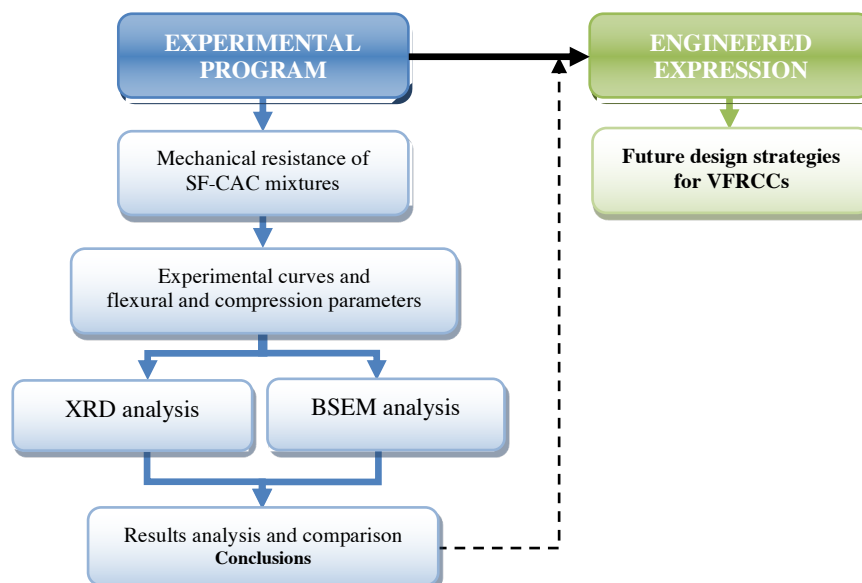


**Figure 1.9.** The 3<sup>rd</sup> experimental stage methodology, the influence of silica fume addition on the CAC matrix, the flexural and compression performance of SF-CAC mixtures.

#### 1.4.3. Influence of pozzolanic –Silica Fume– addition in VFRCC, the flexural strength of SF-VFRCCs

The 4<sup>th</sup> experimental stage was focused on characterizing the influence of pozzolanic (Silica Fume) addition in VFRCC. Moreover the micro-structure of compounds were assessed – the durability of VFs in CAC-based cements. With this purpose, this stage was based on testing flexural performance of non and aged SF-VFRCC compounds. The micro-structure of mixtures and the fiber surfaces were assessed by BSEM-SEM analysis on non and aged compounds. The outline of this stage is schematized in Figure 1.10.

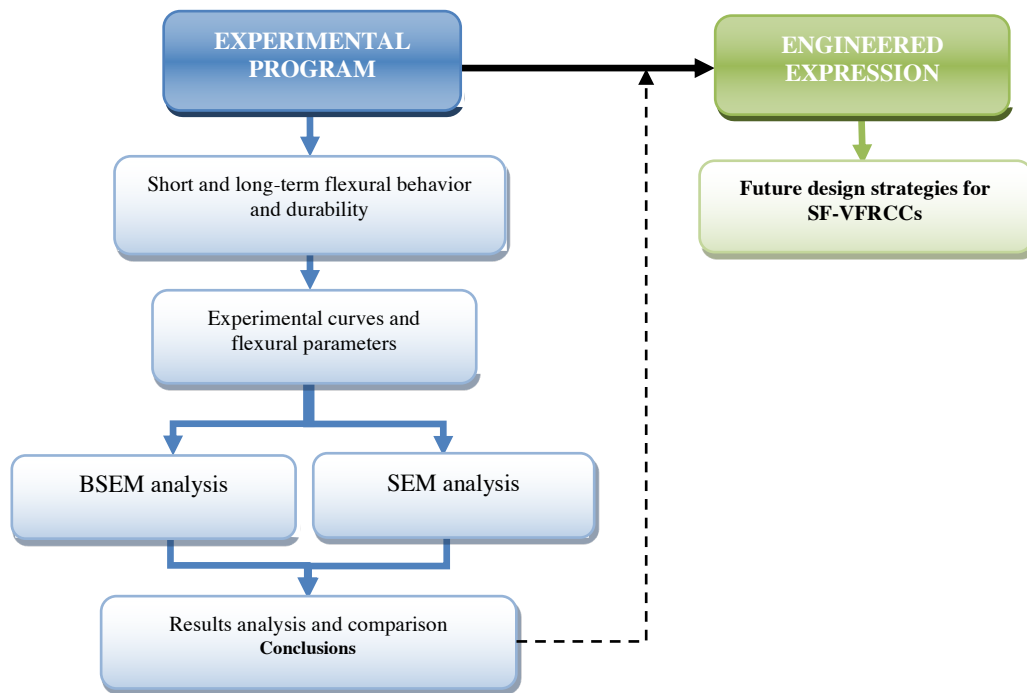


**Figure 1.10.** The 4<sup>th</sup> experimental stage methodology; The flexural resistance of SF-VFRCC mixtures. The influence of SF addition in the micro-structure of VFRCCs.

## 2. STATE OF THE ART

### 2.1. INTRODUCTION

Vegetable Fiber Reinforced Cement Composites (VFRCCs) have emerged as a potential construction material, providing proper tensile stress bearing capacity and ductility. (V. Agopyan, H. Savastano 2005). VFRCCs could be a qualified material for non-structural construction applications. (B.J. Mohr, H. Nanko 2005), (R.S. Teixeira, G.H.D. Tonoli 2012). The enhanced performance of this material is due to the fact that, unlike ordinary concrete the reinforcement in VFRCC is distributed across the entire cement panel section, allowing the fibers to function throughout the full tensile block. (J. Claramunt 2016). Commonly, publications describe the mechanical behavior of these materials in flexion mode, their durability properties, chemical compositions and micro-structure of the matrix.

This chapter reviews the fundamental properties of the VFRCCs that are still need to be improved and identified. Hence, this state of the art peruses to briefly review the literature on numerous themes that will be addressed in this dissertation. These approaches are described in the following sections. Firstly, an introduction to the cementitious materials, Calcium Aluminate Cement as a potential matrix for VFRCCs, its chemistry and morphological characteristics, the hydration phases and its components, and CAC applications have been reviewed.

Likewise, the incorporation of pozzolanic additions in CAC matrix has been reviewed through the literature. Given that, the proposed research focuses on the mechanical behavior of VFRCCs, hence, the vegetable fibers are overviewed through the literature; the fiber classifications, its morphological structure to have a deep understanding of its structure. In final, the VFRCC and its application area which is the principal core of this work, has been focused on the critical factors that influence the mechanical properties of VFRCCs. To that end, several methodologies that improves the durability drawbacks of these materials are explored. All these approaches are described in the following sections.

## 2.2. CEMENTITIOUS MATERIALS

### 2.2.1. Introduction to chemistry and mineralogy in CAC

Calcium aluminate cement (CAC) is suitable cementitious material for fast-setting concrete. In terms of its quick strength gain capabilities, CAC develops the majority of its strength within a very short period of time after setting time. However, due to its strength loss with time, the use of CAC in structural applications is limited. This reduction in strength is caused by a chemical reaction known as conversion (E. Garcia, P. Garces 2000), that will be described further in next sections.

Concretes based on CAC cements are suitable in specific conditions, including resistance to acid attack, corrosion, and abrasion in hydraulic structures. CAC's these properties has broaden this material's application ranges. CAC, like Portland cement contains calcium, silicon, aluminium, and iron oxides. However, their compositions are considerably distinct; Figure 2.1 depicts the approximate composition zone of calcium aluminate cements inside the CaO-SiO<sub>2</sub>-Al<sub>2</sub>O<sub>3</sub> system, and the composition zones of OPC and blast-furnace slag (K.L. Scrivener, J. Newman 2003).

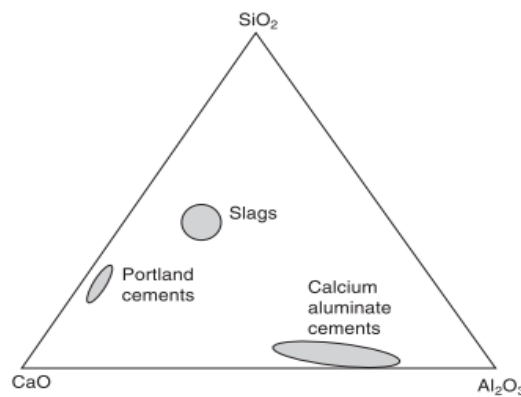


**Figure 2.1.** The composition range of Calcium Aluminate Cements compared to Portland Cements. (K.L. Scrivener, J. Newman, 2003).

The primary difference between Portland cement and Calcium aluminate cement is the nature of their active phases, which lead to setting and hardening. Table 2.1 illustrates the fundamental difference between OPC and CAC cements. (K.L. Scrivener, L. Cabiron, 1999). In general terms, CAC is classified into three types based on the percentage of Al<sub>2</sub>O<sub>3</sub> Content. Table 2.2 presents the classification of CAC cements and its chemical compositions. (V. Antonovič, J. Keriene, 2013).

**Table 2.1.** Basic difference in OPC/CAC. (N.B. Sing 2002), (K.L. Scrivener 1999).

CEMENT	ORIGEN	COMPONENT	HYDRATION
OPC	Limestone Silicate (Clay)	Tricalcium-Dicalcium Silicate C <sub>2</sub> S/C <sub>3</sub> S	C-S-H/CH
CAC	Limestone Bauxite	Mono Calcium Aluminate CaAl <sub>2</sub> O <sub>4</sub>	C-A-H/AH

**Table 2.2.** The chemical composition in different types of CAC (V. Antonovič, J. Keriene, 2013).

COMPONENTS	CAC		
	40% Al <sub>2</sub> O <sub>3</sub>	50% Al <sub>2</sub> O <sub>3</sub>	70% Al <sub>2</sub> O <sub>3</sub>
Al <sub>2</sub> O <sub>3</sub>	37.5-45.5	50.8-54.5	68.5-71.0
CaO	36.5-39.5	36.0-39.0	28.0-31.0
SiO <sub>2</sub>	1.6-5.0	2.0-5.5	0.2-0.6
FeO+Fe <sub>2</sub> O <sub>3</sub>	12.0-18.0	1.0-10.0	<0.5
TiO <sub>2</sub>	<4.0	<4.0	<0.5

The Mono-Calcium Aluminate (CA or CaAl<sub>2</sub>O<sub>4</sub>) is a common property in all CAC types, which is the principal reactive phase in cements that the content can reach up to 40% to 60% of the cement. This mineral reacts slowly in water at ambient temperature, although this process can be accelerated at higher temperatures. Mayenite is the other reactive phase (C<sub>12</sub>A<sub>7</sub>), which quickly interacts with water and plays a major role in the nucleation of calcium aluminate hydrates, is commonly found in cements containing a high concentration of Al<sub>2</sub>O<sub>3</sub> (V. Antonovič, J. Keriene 2013). Other phases include Belie (C<sub>2</sub>S), Gehlenite (C<sub>2</sub>AS), spinel phase and ferrite solid solution. (K.L. Scrivener, J. Newman, 2003).

### 2.2.2. CAC applications

The principal motivation for CACs development was to discover new cement chemistries that would be more resistant to sulphate attack than ordinary Portland cement (K.L. Scrivener, J. Newman 2003). However, it is beyond the scope of this section, two major fields of CAC applications are in refractory concrete for industrial use, involving high temperatures (i.e., steel making), and in so-called "building chemistry" where it is a component of complex mixtures of mineral and organic ingredients for applications such as; self-levelling screeds and tile cements. Furthermore, it is commonly used in conventional concrete to provide exceptional endurance in harsh environments. Figure 2.2 presents the typical applications of CAC concrete. (K. L. Scrivener, L. Cabiron 1999).



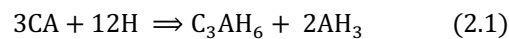
**Figure 2.2.** Typical applications of CAC concrete: 1. Bridge widening, rapid hardening. 2. Dam flushing gate, abrasion resistance. 3. Foundry floor, abrasion and thermal shock resistance. (K. Scrivener, J. Newman, 2003).

Today, CAC cements have a wide range of applications; which are widely employed as admixtures in conjunction with other mineral binders such as Portland cement, calcium sulphate, lime to generate a variety of very unique mortars for applications such as repair, floor levelling, tile adhesives, and grouts (K.L. Scrivener, J. Newman 2003). CAC with 40% Al<sub>2</sub>O<sub>3</sub> is used in concretes that can be applied at temperatures up to 1300 °C. CAC containing 70% Al<sub>2</sub>O<sub>3</sub> oxide can withstand high temperatures from 1500 °C to 1800 °C (V. Antonovič, J. Keriene 2013).

### 2.2.3. Hydration mechanisms of CACs

Hydration is the chemical reaction that occurs when cements react with water to form a rigid solid. The physical process is the same for both CACs and OPCs - however, the hydration products of CAC are chemically distinct from those of calcium silicate phases found in OPC (K.L. Scrivener, J. Newman 2003). When CAC is placed in water, calcium ions and aluminate ions dissolve in water to form a solution, however, the nature of the formed hydrates depends on the temperature of its hydration phases. With lower temperatures producing CAH<sub>10</sub>, moderate temperatures producing C<sub>2</sub>AH<sub>8</sub> and AH<sub>3</sub>, and thus higher temperatures producing C<sub>3</sub>AH<sub>6</sub> and AH<sub>3</sub>, plus a poorly crystallized gel-like phase (K.L. Scrivener, L. Cabiron 1999).

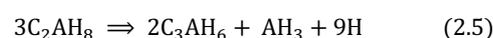
To have a general understanding of how these various hydrates of CAC develop, in the following description the hydration phases are detailed: When distinct phases are formed, same phases prefer to recombine to form a new mixture of phases with the lowest energy, this is the stable phase assemblage. However, due to the ion rearrangement that must occur, sometimes it is difficult for stable phases to form quickly. In such circumstances, it is common distinct phases to develop temporarily, that are meta-stable phases. The meta-stable phase has less energy than the initial nucleation phase, which acts as a driving factor in its creation, but still, it has more energy than the stable phase. Hence, a driving force persists for the meta-stable phases to give the stable phase assemblage. The stable hydrates of CA calcium aluminate are, C<sub>3</sub>AH<sub>6</sub> (a form of hydrogarnet) and AH<sub>3</sub> (gibbsite): (K.L. Scrivener, J. Newman, 2003).



C<sub>3</sub>AH<sub>6</sub> has a cubic crystal structure, it usually has a morphology of compact equiaxed faceted crystals, whereas AH<sub>3</sub> is often poorly crystalline and deposited in formless masses, because these hydrates are stable. The other phases that may occur initially will convert over time depending on the temperature and moisture of the surrounding environment. C<sub>3</sub>AH<sub>6</sub> nucleation is very slow at temperatures around 65 °C, and at temperatures up to 27-35 °C, the first hydrate to form is normally CAH<sub>10</sub>, while C<sub>2</sub>AH<sub>8</sub> and AH<sub>3</sub> dominate initially between 35 and 65 °C:



And the subsequent conversion reactions to the stable phases are as following:



These reactions occur in solution, where the reacting phases dissolve and the resultant phases precipitate. Although it is possible for  $\text{CAH}_{10}$  to convert directly to  $\text{C}_3\text{AH}_6$ ,  $\text{C}_2\text{AH}_8$  is commonly formed as an intermediary phase due to the ease of nucleation. Once stable phases have formed, they will continue to develop even if the temperature drops. From a practical standpoint, the formation of these distinct hydrates is significant because they have different densities and contain varying amounts of combined water; thus, when the conversion of meta-stable to stable hydrates occurs, the following CAC matrix properties change:

- I. *There is a decrease in solid volume, which leads to an increase in porosity, as a result, a decrease in strength at an equivalent degree of hydration.*
- II. *Water is liberated, that can be available to hydrate any remaining anhydrous phases.*

There are several methods to lower this conversion system, one of the methods for minimizing the conversion of metastable to stable hydrates is to cure CAC at high temperatures (H. M. Son, S. Park 2019). Despite the fact that the W/C ratio is the primary parameter determining the properties of all concretes, the impact on microstructure before and after conversion underscores its importance for CAC cements (K.L. Scrivener, J. Newman 2003). According to K.L. Scrivener et al (K.L. Scrivener, L. Cabiron 1999), good long-term durability of CAC requires a W/C ratio of 0.4 or less in the absence of superplasticizers. The Hexagonal-Cubic Phases of CAC hydrates are shown in Table 2.3. (H.M. Son, S. Park 2018-2019).

**Table 2.3.** The chemical composition of (Hexagonal-Cubic Phase) CAC hydrates.

HYDRATES	The chemical composition			Structure	Density (g/cm <sup>3</sup> )
	CaO	Al <sub>2</sub> O <sub>3</sub>	H <sub>2</sub> O		
CAH <sub>10</sub>	16.6	30.1	53.3	hexagonal	1.743
C <sub>2</sub> AH <sub>8</sub>	31.3	28.4	40.3	hexagonal	1.950
C <sub>3</sub> AH <sub>6</sub>	44.4	27.0	28.6	Cubic	2.527
AH <sub>3</sub>	-	65.4	34.8	hexagonal	2.420

At higher W/C ratios (0.7), the impact of conversion phases is major. If the temperature is kept low, there is enough water and space for almost all reactive anhydrous phases to give meta-stable hydrates ( $\text{CAH}_{10}$  -  $\text{C}_2\text{AH}_8$ ), and because these hydrates have a lower solid density, they fill most of the space originally occupied by water, resulting in lower porosity. And hence, when the conversion occurs, the generation of dense stable hydrates ( $\text{C}_3\text{AH}_6$  -  $\text{AH}_3$ ) results in a significant loss in solid volume, resulting in an increase in porosity, and as a result, a decrease in matrix strength (K.L. Scrivener, J. Newman 2003).

When the W/C ratio is lower than 0.4, there is insufficient water and space for the cement particles to generate meta-stable hydrates. In this case, the water released by the conversion phase will be available to react with the anhydrous cement particles to produce further hydrates. The net reduction in solid volume and increase in porosity will be lessened, and the matrix will be dense with the low porosity microstructures obtained after conversion, resulting in a higher matrix strength (K.L. Scrivener, J. Newman 2003). Figure 2.3 depicts the schematic growth of CAC strength at a W/C ratio of 0.4 (K.L. Scrivener, L. Cabiron 1999).

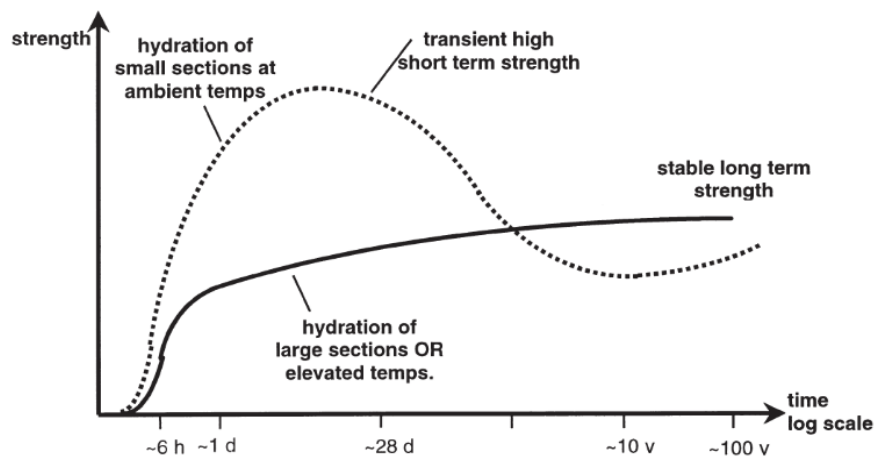


**Figure 2.3.** Presents the schematic strength development of CAC at a w/c ratio of 0.4 (K.L. Scrivener, L. Cabiron, 1999).

## 2.3. POZZOLANIC MATERIALS, SILICA FUME

### 2.3.1. The influence of pozzolanic materials on CAC matrix

Pozzolanic materials including silica fume have received attention significantly in the academic and industry areas recently. The effect of silica sources on the hydration characteristics and mechanical properties of OPC has been extensively investigated in previous studies (Bentur, A, Diamond, S 1987), (Schreiner, H, Holmen, L 2002), (R.D. Toledo Filho, Kh. Ghavami 2003), (B.J Mohr, J.J. Biernacki 2007) and many others.

Pozzolanic materials have been assessed as a partial weight replacement for cement in order to minimize the alkalinity of the cement matrix while simultaneously refining the pore structure of the matrix. Silica fume appears to dramatically reduce composite deterioration owing to wet/dry cycles when employed in reasonably high volumes (i.e., 30 percent or larger replacement of cement by weight). (Schreiner, H, Holmen, L 2002). However, the investigations on the incorporation of silica sources in CAC is limited compared to those of OPCs, hence the information for a better understanding of this phenomenon is missing currently, necessitating a further research on it (H.M. Son, S. Park, 2018).

According to the literature, in terms of CACs, integrating silicate sources such as slag, fly ash, metakaolin, and silica fume, may minimize the conversion phenomena (J. Ding, Y. Fu 1995), (A. Hidalgo, J.L. García 2009), (E. Sakai, T. Sugiyama 2010), (N.K. Lee, K.T. Koh 2017). The incorporated silicate source reacts with the hydrated calcium aluminate (CA), resulting in the generation of strätlingite ( $C_2ASH_8$ ). (B. Lothenbach, P. Durdzinski 2015). When silica fume is added into a CAC matrix, it can prevent the loss in compressive strength induced because of conversion by forming a stable phase of strätlingite  $C_2ASH_8$  (H.M. Son, S. Park 2019). Mostly, Pozzolanic materials not only act as a filler but also are useful to create a cementitious binder that contribute to improve the matrix strength within the cement composites (M. Khorami, E. Ganjian 2013).

Figure 2.4 shows the SEM micrograph of platy strätlingite crystallites (H. Pöllmann 2012).

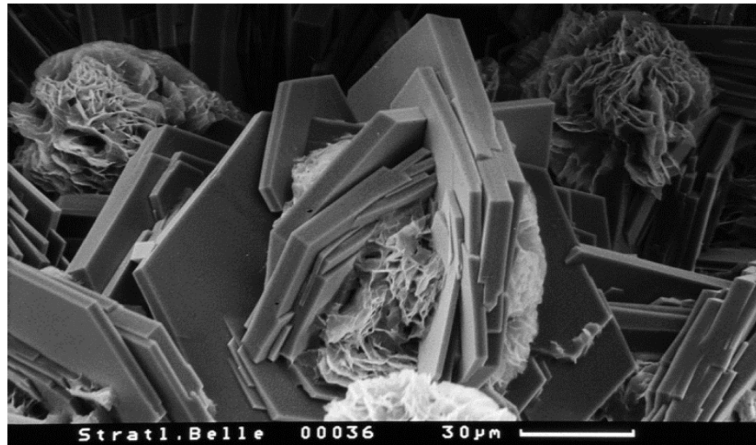


Figure 2.4. The SEM micrograph of platy strätlingite crystallites (H. Pöllmann 2012).

Strätlingite, a siliceous phase that is associated with blended cement hydration, frequently determined as a fixed composition of  $(2\text{CaO} \cdot \text{Al}_2\text{O}_3 \cdot \text{SiO}_2 \cdot 8\text{H}_2\text{O})$  which (develops as hexagonal platy crystals), although our knowledge of its stability and compatibility with other phases is limited. Strätlingite has a rather constant composition and is compatible with C–S–H and hydrogarnet solid solutions at acceptable temperatures, but it is incompatible with portlandite and decomposes in its presence. Strätlingite is stable in cement hydrate systems containing a high aluminosilicate concentration, such as CACs. However, its stability declines with increasing temperature, with an upper limit of stability about  $90 \pm 5 \text{ }^\circ\text{C}$  above which it decomposes progressively to various solids, primarily hydrogarnet solid solution (M. Okoronkwo, F. Glasser 2016). When reactive silica is added to CAC, strätlingite ( $\text{C}_2\text{ASH}_8$ ) is formed instead of  $\text{C}_2\text{AH}_8$ . This phase is stable at temperatures ranging from  $20 \text{ }^\circ\text{C}$  to  $70 \text{ }^\circ\text{C}$ . The inter-laminar water is lost at roughly  $175 \text{ }^\circ\text{C}$ , while the internal water is lost at around  $210 \text{ }^\circ\text{C}$ . (B. Lothenbach, P. Durdzinski 2015).

The addition of pozzolans to CAC results in the development of alumino-silicate phases such as hydrogarnet ( $\text{C}_3\text{AH}_6 \cdot \text{Ca}_3\text{Al}_2(\text{SiO}_4)_{3-x}(\text{OH})_{2x}$ ) a solid solution and strätlingite ( $\text{C}_2\text{ASH}_8 \cdot \text{Ca}_2\text{Al}_2\text{SiO}_7 \cdot 8\text{H}_2\text{O}$ ). This reaction could occur in the following phases: the mineral addition's silica content would react with calcium aluminates CA, avoiding the generation of the hexagonal form  $\text{C}_2\text{AH}_8$  and hence the conversion to the cubic form  $\text{C}_3\text{AH}_6$ , instead of this cubic phase, it is proposed a hexagonal aluminate hydrate containing silica, known as strätlingite, to be generated (A. Hidalgo, J. García 2008). The addition of pozzolans such as fly ash, metakaolin, and silica fume to CAC has been studied by some authors:

Midgley, stated that traces of strätlingite ( $\text{C}_2\text{ASH}_8$ ) were found in ancient hydrated high alumina cement. Midgley proposed that the strätlingite compound offers a better mechanical property than those cubic hydrates of CAC, hydrogarnet ( $\text{C}_3\text{AH}_6$ ) (H.G. Midgley 1967).

Bentsen et al. pointed out that micro silica promotes the development of strätlingite, gehlenite. He also noted that the strätlingite compound crystallizes as a stable phase at temperatures ranging from  $20$  to  $70 \text{ }^\circ\text{C}$  (S. Bentsen, A. Seltveit 1990).

Majumdar et al, considered that the amount of  $\text{C}_2\text{ASH}_8$  is determined by the ability of a mineral admixture to release silica. He reported that with cement based on equal contents of CAC-

BFS cured at either 20 or 38 °C, the compressive strength increased over 1 years, whereas samples made without BFS addition showed a significant decrease in their strength associated with the CAC conversion system only after 1 week. In another study, they concluded that, in mixes based on CAC with a silica fume content between 30% and 50% wt. the gehlenite is the main hydration product before a week ( $T_a < 40^\circ\text{C}$ ) (A. Majumdar, B. Singh 1989, 1990, 1992).

Xiandog et al. reported that the reaction that avoids the conversion process might be achieved as follows: the silica content of the mineral admixtures would react with the calcium aluminates initially, avoiding the generation of  $\text{C}_2\text{AH}_8$  and, subsequently the conversion to  $\text{C}_3\text{AH}_6$ . As a result, instead of this cubic phase, a hexagonal hydrate known as gehlenite ( $\text{Ca}_2\text{Al}_2\text{SiO}_7 \cdot 8\text{H}_2\text{O}$ ;  $\text{C}_2\text{ASH}_8$ ) is hypothesized to be formed (C. Xiandog, R. Kirkpatrick 1993).

Collepari et al. studied the 15%-30% SF wt. and 20%-40% FA wt. incorporation by weight in CAC matrix. They reported that using 15% SF wt. almost completely reduces the strength loss at 20-40°C due to the development of strätlingite  $\text{C}_2\text{ASH}_8$  and hence the transformation of hexagonal aluminate hydrates ( $\text{CAH}_{10}$ ,  $\text{C}_2\text{AH}_8$ ) into the cubic hydrates ( $\text{C}_3\text{AH}_6$ ) is hindered. In contrary, the usage of Fly Ash is not especially beneficial in minimizing the transformation of hexagonal hydrates into the cubic phase, due to a significant rise in FA content of (>40%) wt. of CAC and hence, a higher w/c ratio that is required in order to identify the effect of FA on this transition, in result a decrease in the compressive strength (M. Collepari, S. Monosi 1995).

Bensted et al. investigated the pozzolanic effect of SF on CAC, they discovered that when SF is incorporated into CAC, the absence of calcium hydroxide (CH) as a hydration product and the much lower alkali medium in CAC matrix compared to OPC, inhibits the pozzolanicity of SF (due to CH, portlandite) as generally it was observed with OPC (J. Bensted 1996).

J. Rivas Mercury et al. reported that in the CAC-SF system, silica reacts with the calcium aluminate phases in the cement and water to form different crystalline hydrates (with varying proportions of Ca, Al, Si) such as  $\text{Ca}_2\text{Al}_2\text{SiO}_7 \cdot 8\text{H}_2\text{O}$  ( $\text{C}_2\text{ASH}_8$ ; strätlingite or gehlenite),  $\text{Ca}_3\text{Al}_2(\text{SiO}_4)_{3-x}(\text{OH})_{4x}$  ( $0 < x < 3$ ) (katoite), and not very well defined and complex zeolite-type phases (J. Rivas Mercury, A. De Aza 2003).

A. Hidalgo et al, investigated the microstructure development in mixes of calcium aluminate cement with Silica Fume and Fly Ash. the samples of 20%-30%-50% SF wt. and 30%-50% FA wt. in CAC matrix have been tested in sealed conditions of (98% relative humidity and  $293 \pm 2$  K) hydrated at 2, 7, 30, 90 days. They reported a lower level of gibbsite and a larger content of hexagonal hydrates in samples with mineral additions in their formulations These findings are connected to the slowing of the so-called conversion reaction. CAC-SF mixes in higher silica content, contain more hexagonal hydrates than CAC-FA mixes for the same percentage of mineral addition (A. Hidalgo, J. García 2009).

Mostafa et al. has investigated the chemical activation of CAC with different mixes of 20% FA wt. CAC, 20% SF wt. CAC and 10% FA+10% SF wt. CAC cured at 38°C. It was reported that the addition of FA and SF to CAC inhibits the conversion reactions. The addition of sodium sulphate  $\text{Na}_2\text{SO}_4$  as an activator increases the inhibition efficiency of both FA and SF on the conversion reactions, however, the FA was more reactive to form the strätlingite  $\text{C}_2\text{ASH}_8$  than SF (N. Mostafa 2012).

Abd El-Hamid et al. studied the influence of nano-silica addition on CAC as biomaterial, the results demonstrated that the addition of nano-SiO<sub>2</sub> particles to CA cement plays an essential role in suppressing CA cement conversion reactions and, as a result, increasing the physic-mechanical properties of the cement paste. The data showed that mixing 10% wt. nano-silica with CAC produced the greatest physic-mechanical results, good suppression of the conversion reactions, and hence, a denser microstructure (H. El-Hamid, M. Radwan 2019).

M. Ramírez and J. Claramunt investigated the influence of Metakaolin on the CAC based matrix reinforced with non-woven flax fiber composites, according to the results of BSEM and XRD they confirmed, the reactions that is hypothesized to be formed as strätlingite is not observed but instead acted as a filler, aiding in the nuclear precipitation of the CAC phases and reducing matrix porosity. Due to this lack of hypothesized reaction, the addition of larger amounts of metakaolin in CAC mixtures resulted in a reduction of binding compounds, as a result, a reduction in the mechanical behavior of composites (M. Ramírez, J. Claramunt 2020).

M. Idrees et al. investigated the hydration behavior of CAC with mineral admixtures, 10%-30%-60% of each GGBFS and FA wt. and 5%-10%-15% SF wt. at different temperatures of 20 °C and 38 °C. it was reported that silica fume used mixtures had relatively lower strength compared to GGBFS and FA, but showed some strength improvement at higher temperatures at late ages –10% and 25% increase at 90 days for 5% and 15% SF wt. respectively– (M. Idrees, O. Ekincioglu 2021).

At 40, 65, and 95 °C, the primary phases hydrated as a consequence of the interaction of C<sub>12</sub>A<sub>7</sub>, CA, and CA<sub>2</sub> with silica and water are Katoite of the form Ca<sub>3</sub>A<sub>12</sub>(SiO<sub>4</sub>)<sub>3-x</sub>(OH)<sub>4x</sub> with x ranging from 0 ≤ 3-x ≤ 0.334, and gibbsite Al(OH)<sub>3</sub>. The crystal phase of gehlenite of the form Ca<sub>2</sub>Al<sub>2</sub>SiO<sub>7</sub>.8H<sub>2</sub>O is observed at temperatures below ≤90 °C and (W/C = 2) (J. Mercury, X. Turrillas 2006).

The mineral additions such as silica, resulting in the development of aluminum-silicate phases (J. Zapata, A. Henry 2020), however, the mechanisms behind their creation remain unknown still. After the conversion, strätlingite interacts with calcium oxide and prevents the formation of C<sub>2</sub>AH<sub>8</sub> and C<sub>3</sub>AH<sub>6</sub>. The hydration reaction for CAC with silica addition is followed by the strätlingite crystallizing in a stable phase in the temperature range T ~ 20 - 90 °C (J. Zapata, A. Henry 2020).

## 2.4. VEGETABLE FIBER REINFORCEMENT IN COMPOSITE MATERIALS

### 2.4.1. Classification of vegetable fibers

Vegetable Fibers (VFs) have been utilized to toughen bricks and pottery since very beginning of civilization, but the principles of vegetable fiber reinforcement of fragile matrices have only recently become scientifically understood. Initially, it was proposed that utilizing tightly spaced fibers might greatly increase the cracking strain of brittle matrices such as cement paste, mortar and concrete (T. Filho 1997). VFs have been traditionally used to manufacture high-quality textiles, due to their good mechanical qualities the use of these fibers in the composites sector is increasing substantially, and it is being researched continuously around the world. (V. Agopyan, H. Savastano 2005), (B.J Mohr, H. Nanko, K.E. Kurtis 2005), (P. Soroushian, M. Elzafraney 2006), (H. Savastano, A. Turner 2006), (G.H.D. Tonoli, H. Savastano 2009, 2010), (J. Claramunt, M. Ardanuy 2010, 2011, 2013, 2015), (H. Ventura 2017).

There are certain advantages worth mentioning: Widespread availability, a wide range of morphologies (short fibers, staples, pulp, strands, tufts, technical fibers), low cost, non-hazardous nature, safer working conditions, bio-degradability for a more sustainable world, CO<sub>2</sub> neutrality, well-balanced stiffness, toughness, and strength, good thermal and acoustic insulation, easily adjustable surface that can be modified to achieve more hydrophilicity or hydrophobicity (P.N. Balaguru, S.P. Shah 1992), (P. Wambua, J. Ivens 2003), (A. Bentur, S. Midness 2006), (M. Ardanuy, J. Claramunt 2015), (H. Ventura 2017), (M. Ramírez 2020).

Unfortunately, VFs present drawbacks such as: swelling due to moisture and water absorption, lower durability, poor fire resistance, limited processing temperature, distinct quality due to variability in their diameter and length, surface roughness, chemical compositions that depend on many other factors such as harvesting time and weather conditions among others (M. Ardanuy, J. Claramunt 2015), (H. Ventura 2017), (M. Ramírez 2020). Nonetheless, certain treatments can be treated to improve their qualities. Figure 2.5 presents photographic sources of some vegetable fibers.

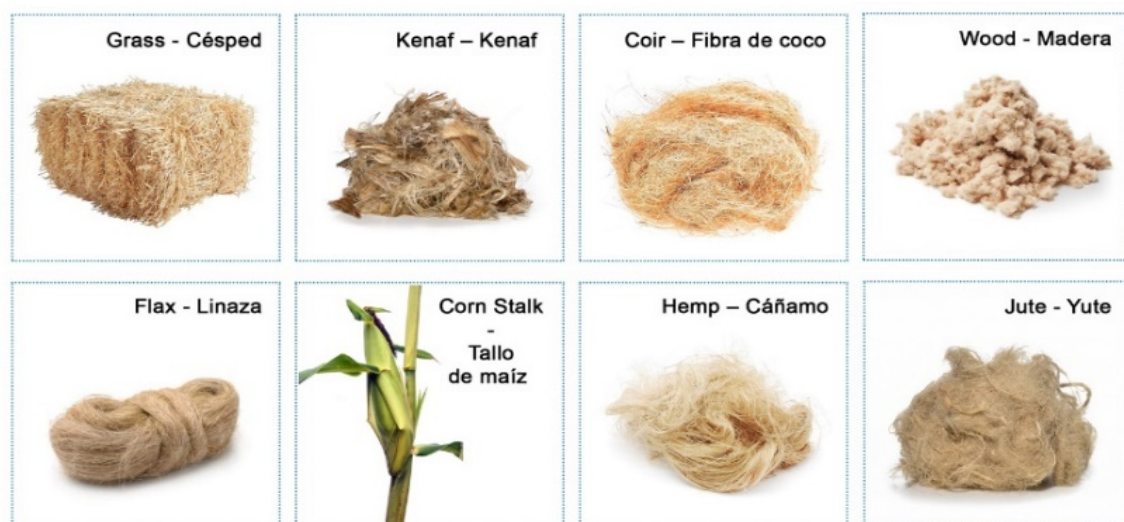


**Figure 2.5.** Depicts photographic sources of some vegetable fibers (M. Ardanuy, J. Claramunt 2015), (M. Ramírez 2020), (M. Sriram, K.R. Aswin Sidhaarth 2022).

VFs are divided into six different categories based on their origin (driven component from the plant). They are described as following (M. Ramírez 2020), (M. Sriram, K.R. Aswin Sidhaarth 2022): Figure 2.6 presents the types of fibers according to their physical form and the application method in composites materials (Biagiotti, J, Puglia, D 2008), (M. Jawaid, H.P.S. Abdul Khalil 2011), (M. Ardanuy, J. Claramunt 2015).

- I. **Bast fiber:** Bast fiber is extracted from the outer part of plant stems. Jute, flax, abaca, and kenaf are some examples of bast fibers. Retting is the extraction process of these bast fibers, which is performed through biological or chemical breakdown of cut plant stems. Their typical characteristic is their strong tensile strength.
- II. **Leaf fibers:** Leaf fibers are coarse and rough fibers extracted from leaf tissues by hand scraping after beating/retting or mechanically extracted. Leaf fibers include sisal, caroa, henequen, and pineapple.
- III. **Seed fiber:** Coir fiber is a type of seed fiber that is collected from the coconut husk. There are some other different type of seed fiber that is taken from the pod or boll of various plant seeds. Cotton, kapok, and milkweed floss are a few examples.
- IV. **Stalk fiber:** These fibers are derived from plant stalks and commonly are collected from sugarcane, corn, eggplant, sunflower, wood, and the straw of various grain crops such as barley, wheat, rice.
- V. **Grass and other fiber crop residue:** These fibers are abundant in tall grasses such as ryegrass, elephant grass, switchgrass and bamboo. Fibrous crop leftovers such as pulse seed coat, peanut shell, hazelnut husk, corn husk, millet stover, and others can be potentially used as fiber reinforcements in cement-based composites.
- VI. **Wood fibers:** These fibers are sourced from a wide range of trees. They are in abundant supply all around the world. Softwood and hardwood are the two main categories of wood fibers.

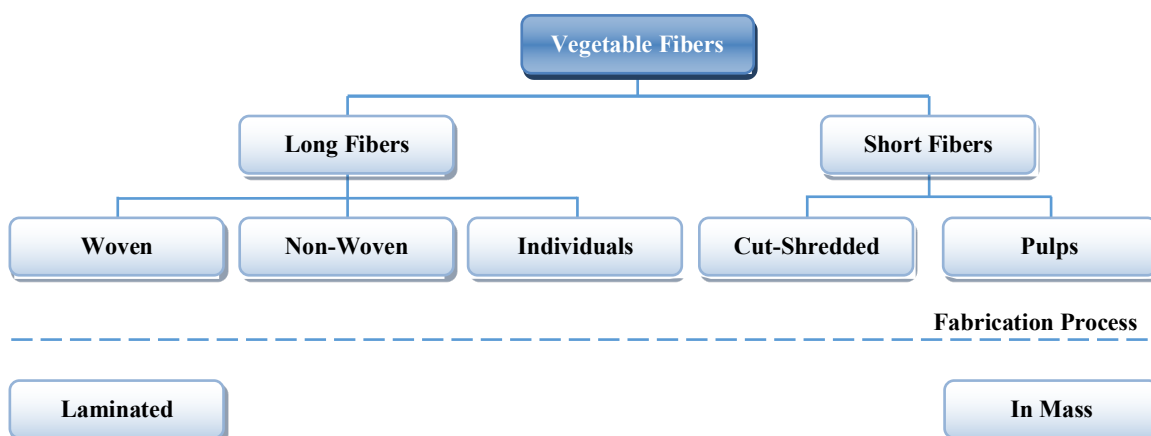


**Figure 2.6.** Depicts the types of fibers according to their physical form and the application method in composites materials. (M. Ramírez 2020).

#### 2.4.2. Characteristics of vegetable fibers

The insertion of VFs into cementitious matrix boosts the water uptake of composites due to the formation of hydrogen link between the water hydroxyl groups of cellulose, hemicellulose and lignin. The hydrophilic nature of vegetable fiber results in decreased compatibility with hydrophobic matrices, as well as poor dimensional stability, because water uptake induces swelling of these fibers (U. Huner 2015).

Therefore, it is necessary to determine the nature and compositions of vegetable fiber, in order to obtain a deep understanding of the decomposition processes associated with these materials (Z. Azwa, B. Yousif 2013). VFs are also known as ligno-cellulosic-fibers, composed of the following components: The principal components are cellulose, lignin and hemicellulose and with minor components including pectin, waxes and inorganic substances.

Table 2.4 presents the chemical compositions of cellulosic fibers and Table 2.5 presents the mechanical properties of cellulosic fibers (E.H. Gram 1983), (R.S.P. Coutts 1992), (V. Agopyan, H. Savastano 2005), (D. Dittenber 2012), (H. Ventura 2017).

The cell wall is organized with three layers: middle lamella, primary cell wall and secondary cell wall (S. Mathias, A. Dickson 2016). A single natural filament has a diameter of around 10  $\mu\text{m}$  and can be considered a sort of natural composite material itself. The cell walls are composed of lignin–hemicellulose matrix and microfibrils that are orientated in different directions in each cell wall. Each microfibril has a diameter of around 10 nm and it is composed of 30–100 cellulose molecules (Z. Azwa, B. Yousif 2013), (S. Mathias, A. Dickson 2016).

The micro-fibrillar angle, which is orientated off of filament's axis, that is responsible for the mechanical properties of fibers, as lower angles generally lead to higher strength and stiffness, whilst larger angles contribute to better ductility of fibers. The fiber filaments are joined into a bundle by lignin, and attached to the stem by pectins. The lignin and pectin are weaker polymers than cellulose, therefore it must be removed if the fibers are necessary to be effective as reinforcing element, and they are often removed as undesirable cell wall components during the retting process (D. Dittenber 2012).

Previously stated, cellulose is the primary component of VFs, it is a linear polymer formed of  $\beta$  (1 $\rightarrow$ 4) linked D-glucose repeating units, with cellobiose (two glucose) being the repeat unit. Each glucose molecule includes 3 free hydroxyl (-OH) moieties that can interact to form hydrogen bonds. These bonds are important in the aggregation of cellulose chains and in determining the cellulose crystal structure. (Z. Azwa, B. Yousif 2013), (S. Mathias, A. Dickson 2016).

Hemicellulose is an amorphous polymer that forms a cross-linking with cellulose molecules, resulting the cell's major structural component. Hemicelluloses have a smaller molecular weight, a poorer strength and thermal stability, it is hydrophilic and hence easily hydrolyzed, and its great sensitivity to moisture makes it the most hydrophilic component of fibers. As a result, it plays an important role in water absorption, biological attacks and thermal degradation of cellulosic fibers. Regarding to lignin, it is a complex hydrocarbon polymer that offers the plant firmness and aids in water conveyance. It is hydrophobic, which makes it resistant to UV destruction and microorganism attacks (H. Ventura 2017), (Z. Azwa 2013). Lignin and hemicellulose do not contribute to the tensile strength of fiber, however, due to their cross-linked structure, they act as a “Matrix,” providing structural solidity to the walls while providing flexibility (H. Ventura, J. Claramunt 2016).

**Table 2.4.** The chemical composition of common cellulosic fibers (K. Pickering 2016).

Fiber	Cellulose (wt.%)	Hemicellulose (wt.%)	Lignin (wt.%)	Pectin (wt.%)
Flax	60-81	14-18.6	2-3	1.8-2.3
Jute	51-72	12-20.4	5-13	0.2
Sisal	43-88	10-13	4-12	0.8-2
Kenaf	36	21	18	2
Hemp	70-78	17.9-22	3.7-5	0.9
Ramie	68.6-76	13.1-15	0.6-1	1.9-2
Cotton	82.7-92	2-5.7	0.5-1	5.7
Coir	43	0.3	45	4
Banana	60-65	6-19	5-10	3-4
Wood	45-50	23	27	-

**Table 2.5.** The mechanical properties of common cellulosic fibers (K. Pickering 2016).

Fiber	Density (g/cm <sup>3</sup> )	Diameter (μm)	Elongation at break (%)	Tensile Strength (MPa)	Young Modulus (Gpa)
Flax	1.4-1.5	40-620	2.7-3.2	343-1035	27-80
Jute	1.3-1.5	30-140	1.4-3.1	187-773	3-55
Sisal	1.3-1.5	100-300	2-2.9	507-855	9-28
Kenaf	1.22-1.4	40-90	3.7-6.9	2.95-930	22-53
Hemp	1.4-1.5	16-50	1.3-4.7	580-1110	3-90
Ramie	1.5	40-60	3.6-3.8	400-938	44-128
Cotton	1.5-1.6	16-21	2-10	287-597	5.5-12.6
Coir	1.25-1.5	11-450	15-47	106-270	3-6
Banana	1.3-1.35	50-280	3-10	529-914	7.7-32

### I. Bast fiber

Among all vegetable fibers listed above, bast fibers such as jute, flax, ramie and sisal are the most commonly used as reinforcement elements for composites. Bast fibers, they consist mainly Cellulose (60-75%), Hemicellulose (between 2-6%), and Lignin (between 1-6%), (J.A Garcia Hortal 1988). The cellulose and hemicellulose degrade between 250 °C and 400 °C (with a weight loss of over 75%), whereas the lignin decomposes between 200 °C and 500 °C. (L. Gonzalez-Lopez, J. Claramunt 2021). Which can be found in fiber bundles in the interior section of plant stems. Figure 2.7 presents a cross section of a flax fiber stem with bundles of bast fibers. On a macroscopic scale, the stem is composed of: (G. Beckerman, K. Pickering 2008).

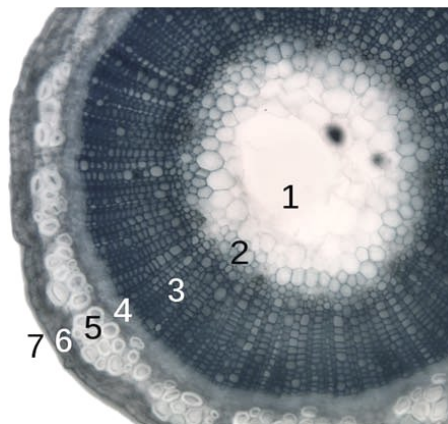


**Figure 2.7.** Demonstrate a Flax plant's stem cross-section composed of following sections: (1) pith (2) protoxylem (3) xylem (4) phloem (5) bast tissue (6) cortex (7) epidermis (H. Ventura 2017).

The flax fiber's properties are including biodegradability, low cost, low density of 1.4 to 1.54 g/cm<sup>3</sup>, moisture absorption of 7% (P. Wambua, J. Ivens 2003), strong thermal and acoustical insulation. They are excellent materials for composite reinforcement element due to their mechanical qualities, high stiffness of 27-80 GPa, good strength of 345-1830 MPa. Taking into account other special qualities of these fibers, for instance, its low elongation 1.2-3.2% (K. Pickering 2016), which is a crucial issue for obtaining stiff composites with high stress transmission. However, the mechanical characteristics of flax fibers are influenced by numerous factors (D. Dittenber 2012), (L. Yan 2014); The plant species, the cultivation procedure, the position of the fibers in the plant, and the meteorological conditions, in order of their direct influence on the plant's growth. The harvesting phases determine the cell wall thickness, coarseness, microfibril angle, porosity, size and shape of the lumen. The extraction processes, retting types, and fiber bundle separation conditions. The transportation and storage circumstances, as well as the age of the fibers.

## II. Seed fiber

Cotton linters are defined as the short fluffy fibers that remain on the cotton seed after the ginning process. Cotton linters are made up of staple lint fibers, short immature lint fibers, and fuzz fibers. Linters are a low-cost raw material used in the pulp and paper industries. As a papermaking fiber, linters pulp has excellent durability, bulk, brightness and forming. However, linters are thick-walled, have a relatively short fiber length, and a low bonded area when compared to staple lint fibers, resulting in low conformability (flexibility), weak tensile, rupture strength, and, ultimately, poor bending stiffness due to inadequate interfacial bonding (L. Titcombe 1992).

The waxy materials and pectins are responsible for the hydrophobic properties of the raw cotton (R. Freytag, J. Dinze 1983). The primary and two secondary hydroxyl groups, as well as the glycosidic link, are the key properties of the cellulose molecule in terms of chemical reactivity. Other than hydrolysis, alcoholises, or the action of some concentrated or anhydrous acids, the glycosidic bond is not easily broken. However, when the primary and secondary hydroxyl groups are subjected to conventional alcohol interactions, they can be easily oxidized (T. Nevell 1985).

### 2.4.3. Morphological structure of vegetable fibers

Fiber is a term used by authors using natural fibers in composites investigations. However, fiber has a strict botanical meaning, which describes a single elongated, thick-walled, plant cell. (S. Mathias, A. Dickson 2016). In terms of the morphological structure, these fibers have a complex structural system that often includes: long elementary fibers with a polygonal hollow section, a smooth surface and nodes, thick walls and a central well-defined hollow (Lumen). Previously stated, the mechanical properties of fiber are determined by the thick central layer of the secondary cell wall. It is made up of helically cellular microfibrils formed of long chain cellulose molecules. Each cell wall is composed of three major components: cellulose, hemicelluloses, and lignin. Lignin-hemicelluloses act as the matrix and the microfibrils (formed of cellulose molecules) act as the fibers. (H. Ventura 2017).

The central cell walls or layers surrounding a hole are referred to (Lumen), and each layer formed of microfibrils has a different chemical composition and structure. The outer thin layer, primary cell wall, acts as a coat roughly 0.2 µm thick in flax fibers, and the micro-fibrillar angle with regard to the fiber axis is around 35°. The inner layer, the secondary cell wall, has a thickness of 5-15 µm and contains the majority of the fibers. The secondary cell wall is also composed of three layers (S. Mathias, A. Dickson 2016), (Mi Li, P.Y. Thomas 2020).

The  $S_1$  layer regulates the stability of fiber in compression by inhibiting lateral cell expansion. The  $S_2$  layer is very important because of its relative size to the  $S_1$  and  $S_3$  layers and it plays an important role in the characteristics of fiber as a result. It contains amorphous hemicelluloses and cellulose that is orientated at about  $10^\circ$  (S. Mathias, A. Dickson 2016). (H. Ventura 2017).

Regarding to cotton linter, the outer wall of cotton linter contains waxes, lipids, and pectin. Similarly, the primary wall contains waxes and pectin, although it is mostly composed of cellulose in the form of microfibrils. The secondary wall is composed of a thin outer layer  $S_1$  and an inner layer  $S_2$  that is 95% of the dry weight of the fiber and can be up to  $5 \mu\text{m}$  thick. In contrast to the microfibrils of the primary wall, which are randomly arranged, the microfibrils of the  $S_2$  layer are oriented at  $20^\circ$ -  $30^\circ$  with regard to the fiber axis. Similarly, to flax fibers the lumen forms a hollow in the center of cell walls. Microfibrils are composed of parallel cellulose chains that are joined together by hydrogen bonding. Elementary fibrils are smaller groups of highly crystalline clump and aggregated molecules (3-6 nm wide). Cellulose, which accounts for 95% of the cell's composition, is the most abundant renewable natural resource found in fibers. It is a polymeric carbohydrate composed of D-anhydro glucopyranose units (cellulose chains) linked together by bonds (L. Titcombe 1992). Figure 2.8 depicts the schematic structure of vegetable fiber from the plant to the cellulose crystals.

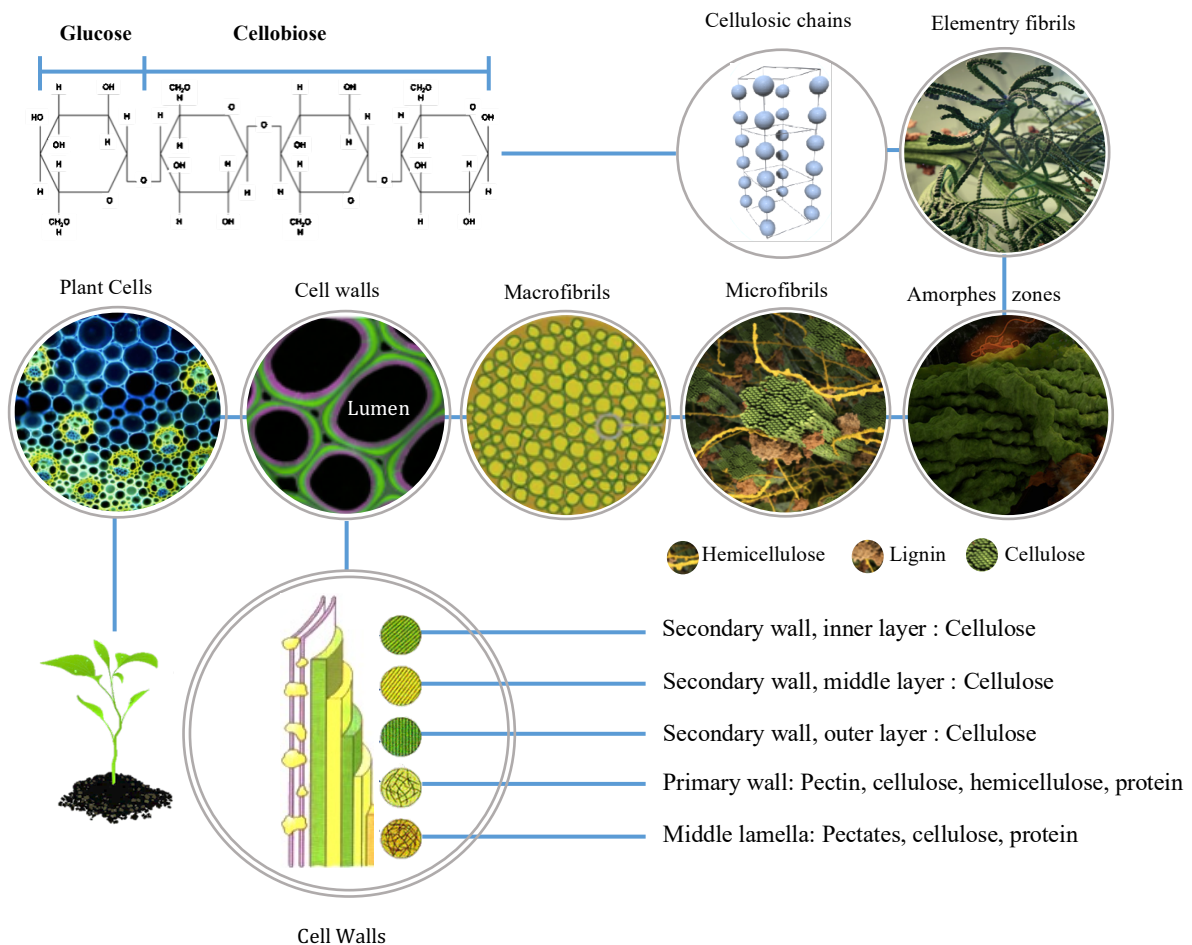


**Figure 2.8.** The scheme of vegetable fiber structure from the plant to the cellulose crystals.

## 2.5. VEGETABLE FIBER REINFORCED CEMENT COMPOSITES (VFRCC)

The number of applications in which vegetable fiber reinforced composite (VFRCC) is used is continuously growing due to its improved properties, such as toughness, ductility and brittle performance. VFRCC has been studied as a suitable material for a variety of non-structural applications including: Roofing tiles (Z. Berhane 1994), (V. Agopyan, H. Savastano 2005), (R.S. Teixeira, G.H.D. Tonoli 2013), Exterior applications (B.J. Mohr, H. Nanko 2005), Wall panels (V. Agopyan, H. Savastano 2005), Facade panels (H. Ventura, M. Ardanuy 2014), (J. Claramunt, 2016), (J. Claramunt, M. Ardanuy 2017), (J. Claramunt, H. Ventura 2018), (J. L. Gonzalez-Lopez, J. Claramunt 2021), (P. Astrolabe, J. Claramunt 2022), Pavement panels (M. Ramírez 2020), (A. Gere mew, P. D. Winne 2021).

These construction applications can withstand cyclic loads and stresses in its joints, climatic critical periods which are projected to last for millions of cycles. This cyclic load may cause mechanical properties failure and affect the characteristics of these materials significantly (i.e., strength, stiffness, toughness, durability). These enhanced properties are achieved by added VFs into the cementitious matrix, which are able to act as stress transfer elements to control cracking, and giving a greater ductility, increasing post-cracking tensile strength, toughness, impact resistance and other engineering properties of this material. (A. Bentur, S. Mindess 2006).

The use of VFRCCs provides advantages not only in terms of non-structural applications response, but also in terms of production. Resulting in more light-weight reinforced construction materials, improved production efficiency and economic competitiveness compared to the traditional methods. The non-structural use and manufacturing advantages of VFRCCs indicate that it is a cost-effective and competitive alternative to traditional reinforcement methods, however, the growing demand for the use of VFs in these applications must be accompanied by the development of simplified methods for the design of optimized VFRCCs sections. (J. Claramunt 2016).

The identification of the most accurate and appropriate process for designing VFRCC is a critical factor in assisting with the expansion of this material's application area. This procedure should contain an appropriate constitutive model, test methodologies to assess the material's performance that are indicative of the real application, and numerous factors that influence their mechanical properties which will be discussed in upcoming sections.

### 2.5.1. *The mechanical behaviour of vegetable fibers in cement composites*

When compared to unreinforced composites, the ability to limit and control the crack propagation, increased ductility of these materials during post cracking time is an effect of added VFs as reinforcement in such composites (N. Flores 2014).

According to Shanks's report, fiber/matrix are two major constituents of these composites, where the reinforcement elements play a key role as structural element of material, giving the composite remarkable strength and the matrix that surrounds VFs with elastic interaction that holds them in place and transfers the force between fibers, resisting against the applied load (R. Shanks 2014).

Generally, the mechanical behavior of material is determined by composite's structure. Thus, the internal structure must be specified in order to analyse and anticipate their performance under various conditions. Three major constituents of these materials that should be considered are as following (A. Bentur, S. Mindess 2006):

- I. The bulk cementitious matrix's structure.
- II. Fiber shape and dispersion.
- III. The fiber/matrix interface structure.

In general terms, the pastes/mortars are used as based matrix for thin sheet components, where the fibers act as reinforcement element with a range of 5–15% by weight of cement. A denser microstructure and enhanced rheology in these composites allow for the integration of 2–6% by volume of short fibers, which can provide efficient reinforcing. In final, The fiber/matrix interface characteristics perform multiple effects that should be taken into account when considering the fiber/matrix and bonding/de-bonding process through the interface. The particulate nature of the matrix has a strong influence on the microstructure of transition zone in composites. The mechanical property that is mainly influenced by fibers is the residual post-cracking tensile strength, and that represents an important design parameter for VFRCC (A. Bentur, S. Mindess 2006). The following items are the various forms of fiber-reinforcing arrangements presented in Figure 2.9. (H. Ventura 2017):

- I. Continuous reinforcement, which consists of long fibers inserted into a matrix using processes such as filament winding (twisting)/layering of fiber matting.
- II. Discrete short fibers, often less than 50 mm in length, that are introduced into the matrix using procedures such as spraying and mixing.

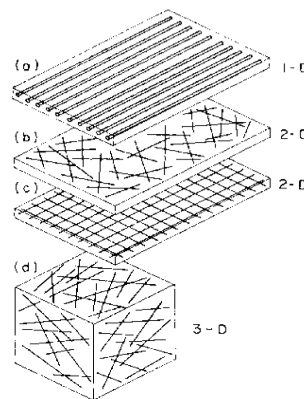


**Figure 2.9.** Fiber arrangements in 1-D, 2-D, and 3-D dimensions are classified as continuous (a, c) or discrete, short fibers (b, d) (A. Bentur, S. Mindess 2006).

### 2.5.2. Application area of VFRCC

Previously stated, VFs are increasingly being used as reinforcement elements in composite materials and its mechanical properties are being investigated in order to maximize its full potential as a substitute for synthetic fibers. VFRCCs application area is now limited to interior and non-structural applications due to their lower mechanical properties and poor durability and poor moisture resistance of VFs (Z. Azwa 2013). Non-structural construction applications are addressed to thin wall panels or façade panels (the outer skin of buildings), thin-sheet products such as partitions, building envelopes, or ceiling flat sheets, thin pavement panels, or roofing tiles. (J. Claramunt 2016). The natural fiber composites materials are mainly used in construction, and some other industry such as textile, sports, transport industries. (Y. Shireesha, G. Nandipati 2019). Figure 2.10 presents the application area of natural fibers.

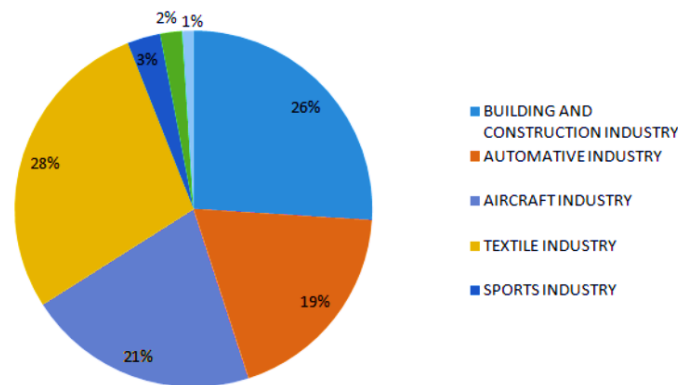


**Figure 2.10.** The application area of natural fibers (Y. Shireesha, G. Nandipati 2019).

The ventilated façades are multi-layered building envelopes that consist of an exterior layer mechanically connected to an inner layer and a ventilated air gap that usually comprises thermal insulation in contact with the inner layer. This outer membrane, in addition to its aesthetic function, should protect against heat radiation, rain and wind by producing an air chamber. Ceramics, natural stones, wood-resin and aluminium-resin composites, and increasingly fiber cements are being used for these envelopes due to the benefits that stated previously, improved flexural strength, toughness, and crack resistance of cement-based matrices by adding stiffness, strength, and bonding capacity. (J. Claramunt 2016). Today many attempts are being accomplished to broaden the application area of these composites.

### 2.5.3. Critical factors of vegetable fibers reinforced cement composites

The improved performance of this material is due to the fact that, unlike ordinary concrete, the reinforcement in VFRCC is distributed across the entire cement panel section, allowing the fibers to function throughout the full tensile block (J. Claramunt 2016). Due to this feature, the added VFs in construction applications are subjected to, dynamic stresses applied in various directions that can be very effective. The crack bridging mechanism of VF is especially useful in applications involving local mechanisms, where concentrated loads caused by surrounding circumstance, stresses in the joints that can produce cracking. In this instance, the crack reduction and long term endurance become critical to assure quality, sealing, and avoiding excessive repair costs associated with the formation of these cracks.

Therefore, manufacturing VFRCCs involve certain crucial factors that must be taken into account. It is reported by (K. Pickering 2016) that the mechanical properties of these materials are significantly influenced by fiber/matrix selection, interfacial strength, fiber dispersion/orientation, porosity and production procedures. These key factors are summarized below as follows:

#### I. Fiber/Matrix selection

Several factors should be addressed before selecting a fiber as reinforcement element. The most important factors are (i.e., availability, cost, mechanical properties, length, quality, chemical composition, harvesting time, extraction methods, treatment, storage conditions. In this context, the changes in fiber strength have been documented in the literature to be roughly 15 to 20% as a result of harvesting time or extraction procedures. To achieve an optimal mechanical performance, fibers with high cellulose concentrations and microfibrils, such as bast fibers that

are preferable (H. Ventura 2017). Furthermore, low moisture absorption and high lignin content of fibers are favored due to their long-term resistance and improved thermal stability. However, geographical location has a significant impact in fiber selection, as availability is dependent on climate conditions (M. George 2016).

In order to achieve a composite with good mechanical performance, an optimal matrix which is less aggressive to VFs, with lower pH and alkalinity. Regarding to the outcome of mentioned aspects above, the flexibility of the fiber/matrix is also a significant challenge as the stress transfer will be performed depending on both factors (H. Ventura 2017).

## II. Fiber/Matrix interaction

The stress-transfer will be immediately affected, If the interface between fibers/matrix is inadequate, resulting in a poor reinforcing effect. A good fiber/matrix interaction is frequently demonstrated by an increase in strength and toughness; the stiffness is usually increased regardless of the moisture absorption capabilities of fiber. Although the fracture can occur even if there is a strong fiber/matrix interaction, but there are numerous effective feasible options for strengthening this compatibility between fiber/matrix that will be discussed in following sections (K. Pickering 2016).

## III. Fiber content/porosity

The increase in fiber content is referred to, an increase in the composite's mechanical characteristics. A higher fiber content will imply a higher stiffness and in result, a higher composite strength. However, this can lead to a number of constraints, particularly in VFRCC, the fiber content can be increased to a certain extent, that the water uptake of applied fiber is not a side effect for the material (M. George 2016).

Regarding to this limitation, which it is directly associated with obtaining a balance between fiber content and moisture absorption, and hence a successful stress transfer in composites. Due to this, there is a critical volume fraction (expectedly <10%) which reduced VF content has a negative influence on composite strength, resulting in the formation of pores/holes in the matrix (K. Pickering 2016), which the porosity has a significant impact on the ultimate properties of these composites.

## IV. Fiber orientation/dispersion

This factor is important in determining the orientation of fibers with regard to the direction of the applied load, as shown in (Figure 2.11) fibers aligned in the direction of the applied load have strong mechanical characteristics (H. Ventura 2017). Despite this, VFs are more difficult to align due to their restricted length in comparison to synthetic man-made fibers, which are manufactured in continuous length and dimensions. However, there are several approaches based on multiple systems that can be used to get the appropriate aligned VF. (K. Pickering 2016).

On the one hand, depending on the final use of the composite, the fiber orientation can be a favorable or a negative factor. In terms of fiber dispersion, it is a relevant factor particularly in composites with short fiber reinforcement, since a random and good distribution of fibers is required to produce an isotropic material. Therefore the fibers must be fully surrounded by the matrix, and not clustered in order to achieve a good stress-transfer (K. Pickering 2016).

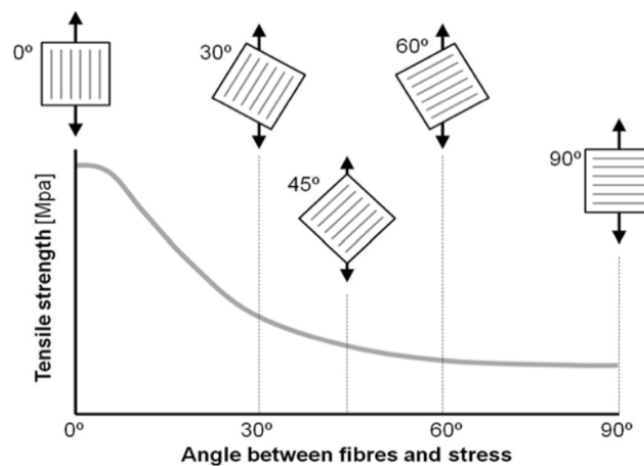


**Figure 2.11.** The fiber orientation effect on tensile strength of composite (H. Ventura 2017).

## V. Manufacturing process

The manufacturing procedure utilized to produce a composite is determined by the properties of the target application, such as size, form, length, reinforcing type, manufacturing costs, etc. (M. George 2016). The reinforcing morphology might also be a critical issue in composite manufacture. In this context, processing techniques can determine the good distribution of fibers in composites, such as the use of textile structures or the maximum content of fiber that can be applied or the maximum fiber length that can be processed; depending on all of these factors, the manufacturing procedure and its conditions play a key role in determining the final properties of produced composites (H. Ventura 2017). Apart from all these factors mentioned above, long-term durability of VFRCC is a critical issue in the design of these materials, as it has a substantial impact on mechanical resistance. The main challenge with cellulosic vegetable fibers in cementitious applications is their durability, which will be discussed in coming section in details and the methods to improve the durability of these materials.

## 2.6. EFFECT OF FIBER DEGRADATION/DURABILITY OF VFRCC

Long-term durability is the main challenge in the design procedure of VFRCCs as it has a substantial impact on mechanical performance of this material (J. Claramunt 2011). The dissolving of lignin and hemicellulose joining individual fiber cells by alkaline pore solution is the primary cause of VF degradation. This degradation is accelerated by alkaline hydrolysis induced depolymerization of fibers, which causes linked glucose molecules to become disordered and the length of molecular chain to be shortened. The rate of deterioration, however, is determined by crystallinity and fibrillar morphology of cellulose contained in VF structure. As a result, the degradation rate decreases as cellulose crystallinity increases (O. Onuaguluchi 2016). According to the literature, the majority of VFRCCs are based on OPC, which hardens by the hydration of anhydrous compounds, giving a rise to calcium silicate hydrate (C-S-H Gel), Ettringite and Calcium Hydroxide (CH-Portlandite). Several authors (HE Gram 1983), (A. Bentur, S.A.S. Akers 1989), (R.D.T Filho 1997), (H. Savastano, V. Agopyan 1999), (R.D.T Filho, K. Scrivener 2000) reported that the presence of calcium hydroxide (CH) causes fiber breakdown and mechanical strength loss. Especially when these composites are subjected to wet/dry (accelerated ageing cycles) either in a laboratory environment or in a natural atmosphere with high humidity.

The structure of VFs and their hydrophilic nature are responsible for their sensitivity to moisture when exposed to humidity or immersed in water; when the water is absorbed and diffused into cracks and pores of matrix, thus along the reinforced fibers. However, once the water enters in fibers, produces swelling and reaches to the gaps in surrounding fiber/matrix, in final results in de-bonding of fibers and a weakening of the fiber/matrix adhesion (J. Claramunt, M. Ardanuy 2010), (M. Ardanuy, J. Claramunt 2011). In this context, the use of a considerable volume of VFs may have a detrimental impact on long-term qualities of composites due to greater fiber degradation by moisture absorption (K. Pickering 2016).

Furthermore, the moisture absorption raises the possibility of microbiological attacks, which are related with the final biodegradation of these composites as well (J. Claramunt, M. Ardanuy 2010). According to a process suggested by Mohr et al, the VFs degradation during wet/dry cycling is accomplished gradually: (1) initial fiber-cement debonding, (2) reprecipitation of secondary ettringite within the hollow space at the former fiber-cement interface (kraft fibers only), (3) fiber embrittlement due to reprecipitation of CH within the fiber lumen or cell wall. This process, with some modifications, is also applicable to other fiber-cement composites (B.J. Mohr et al. 2005a-2005b). Figure 2.12 depicts a schematic representation of water absorption at fiber/matrix interface. This process is also postulated for fiber degradation in Figure 2.13 which shows the VF surfaces deposited by a barrage of CH calcium hydroxide (H. Ventura 2017):

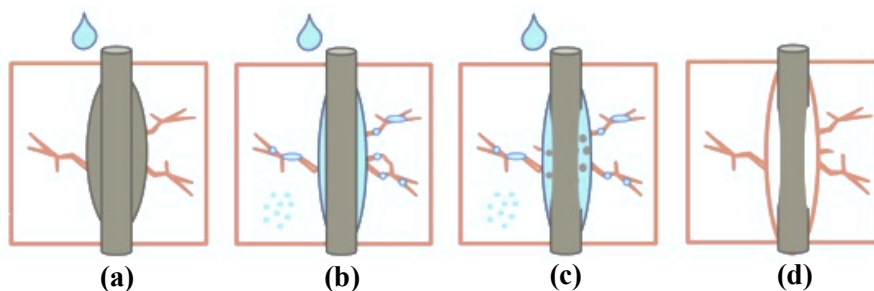


**Figure 2.12.** A schematic representation of water absorption at fiber/matrix interface (H. Ventura 2017).

- I. The first humid cycle: The fibers swell by absorbing water, and this is where some micro-cracks occur around the enlarged fibers size. Figure 2.12. (a).
- II. The first dry cycle: as a result of water loss, the cross section of fiber decreases, resulting in lack of adhesion between the fiber/matrix, where, a gap (the fiber/matrix de-bonding) begins to emerge. Figures. 2.12. (d) and 2.13. (a, b).
- III. The second humid cycle: (the capillary mechanism, where water molecules travel along the fiber/matrix interface), resulting in water diffusion through the matrix. Figure 2.12 (b, c).
- IV. The second humid cycle: (the capillary mechanism, where water molecules travel along the fiber/matrix interface), resulting in water diffusion through the matrix. Figure 2.12 (b, c).
- V. The second dry cycle: This cycle occurs when the water in the matrix and fiber evaporates, causing the dissolution to proceed into the fibers and deposit "calcium hydroxide" on the surface and lumen of the fibers (Figure 2.12 (c) and Figure 2.13. (e)).

- VI. Incoming cycles: This process is continued indefinitely, resulting in a flood of calcium hydroxide CH on cellulose plant fibers. This attack induces densification of the fibers' surface and lumen with highly alkaline chemicals, resulting in a reduction in mechanical strength.

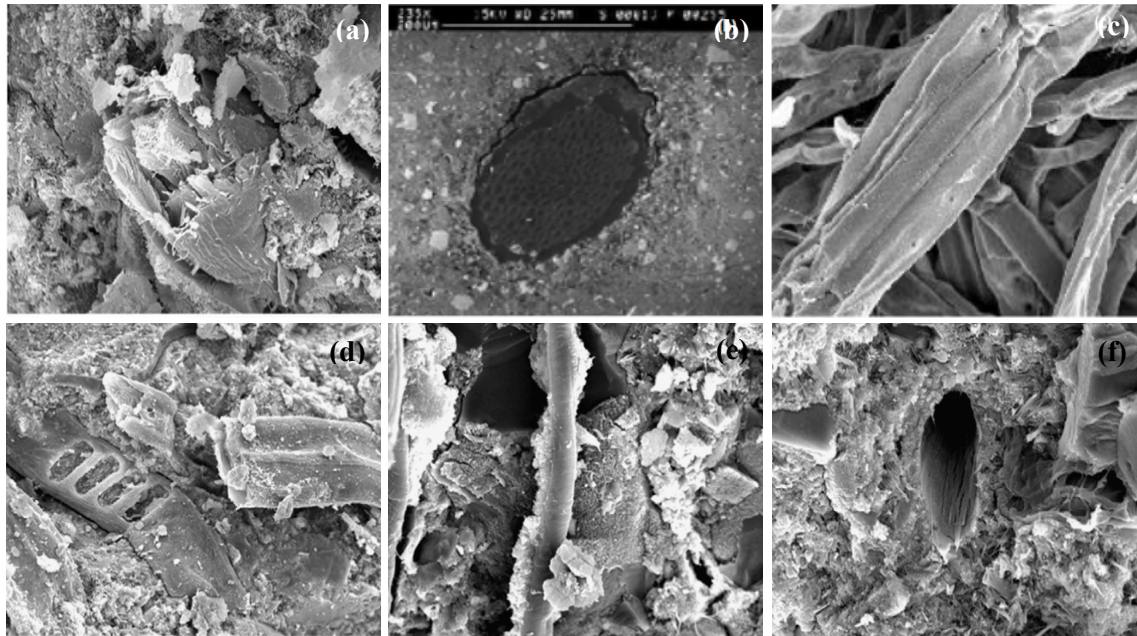


**Figure 2.13.** (a), (f) Fiber decomposition (b) The gap between fiber/matrix, (c) Untread fibers, (d), (e) CH deposited on fibers (V. Agopyan, H. Savastano 2005), (J. Claramunt, M. Ardanuy 2011).

### 2.6.1. Methodologies for durability improvement of VFRCC

Because of all factors discussed above, there are numerous fiber treatments that can assist to lower the hydroxyl groups and as a result, the hydrophilicity of cellulosic fibers. The fiber debonding results in inadequate stress-transfer, and therefore the inferior mechanical characteristics. According to the literature review, there are two strategies for enhancing the durability of cellulose fiber reinforced cement composites. The first strategy is, to modify the matrix to reduce or eliminate the alkaline chemicals found in cementitious matrices. The second method is, to modify the fiber's surface (through chemical or physical treatments) in order to increase their stability in the cementitious matrix, as follows (M. Ardanuy, J. Claramunt 2015), (H. Ventura 2017):

#### I. Modifying Matrix

There are two procedures available to remove or lower the portlandite (CH) content of cementitious matrix in general: (i.e., adding pozzolanic materials or the carbonation process). (M. Ardanuy, J. Claramunt 2015), (O. Onuaguluchi 2016). However, discussing about these strategies is beyond the scope of this section, thus in short it will be discussed about the addition of pozzolanic materials in the cement matrix as the experimental approach of this study is centered on this method. Previously stated, the pozzolanic reaction occurs during the hydration process of calcium hydroxide and amorphous silica, which results in hydrated calcium silicate a very stable salt (M. Ardanuy, J. Claramunt 2015).

A partial substitution of cement with this pozzolanic addition reduces the alkalinity of cement-based mixes, by reducing the soluble alkali content of matrix and the reduction of portlandite via pozzolanic reactions (M. Ramírez 2020). Pozzolanic additives are such as micro-silica or silica fume, metakaolin, blast furnace slag or fly ashes. Many researchers have been examined methods to reduce the alkalinity of cement matrix reinforced with VF, according to the literature the reported results of some authors are as following:

E.H. Gram reported the silica fume replacements of 17% and 33% of cement by weight reduced the pore water pH from 13.2 to 12.9 and 12.0, respectively. (E.H. Gram 1983). He has also reported that the replacement of cement with 70% slag by weight reduced the pore solution pH from only 13.2 to 13.0 and did not improve the durability of sisal fiber–mortar composites after 120 wet/dry cycles. Similar results were obtained using fly ash as a partial weight replacement of Portland cement.

Toledo Filho et al revealed the reduced alkalinity through partial replacement of cement by undensified silica fume was very effective method in preventing the deterioration of vegetable-based fibers in cement composites, but the replacement of 40% by weight of OPC matrix with slag did not reduce the embrittlement of the composite. (T. Filho, K. Ghavami 2003). In another study Filho reported, the partial replacement of Portland cement with 40% slag by weight did not significantly improve the durability of sisal fiber–mortar composites after 46 wet/dry cycles. (T. Filho, G.L. England 2003).

Despite considerable lignin degradation observed in coir fibers, extracted from 12 years old low alkaline ground granulated blast furnace slag cement composite, these extracted fibers appeared to be intact, according to John et al reports. Thus, the cited research demonstrated that the addition of pozzolanic materials could improve the durability of vegetable-based fiber reinforced cement composites (V. John, M. Cincotto 2005).

According to Mohr et al study, the binary and ternary mixes of slag, metakaolin and silica fume were beneficial in preventing the degradation of kraft pulp fiber reinforced cement composites exposed to wet/dry cycles. Composites containing 30% SF, 50% SF, 90% SL wt. and 30% MK wt. apparently eliminated degradation due to wet/dry cycling, as measured by changes in strength and toughness with progressive cycling. (B.J. Mohr, K. Biernacki 2007).

In another study, Toledo Filho et al stated that the use of a free calcium hydroxide cement matrix (*by adding metakaolin and calcined waste crushed clay brick to consume the calcium hydroxide*), might minimize the loss of toughness and long-term embrittlement of sisal fiber cement based laminates (F. Silva, T. Filho 2010).

J. Claramunt et al reported, the pozzolanic additions (i.e., Silica fume and Metakaolin) into OPC based matrix reinforced with flax nonwoven fibers led to a reduction in the  $\text{Ca}(\text{OH})_2$  content of the matrix, mainly with higher pozzolan contents. (J. Claramunt 2016). The study done by (M. Ramírez, J. Claramunt 2020) reported that CAC matrices with up to 10% MK wt. incorporation in composite reinforced with flax nonwoven fabrics can be obtained a good mechanical performance and high durability of the material.

## II. Modifying Fibers

Dimensional instability of vegetable-based fibers and their tendency to water absorption in different humidity conditions has a significant influence on fiber/matrix bonding behavior; thus, various procedure to decrease such properties in natural fibers are available to improve this issue: (i.e., silane treatment, acetylation, acrylation, alkali treatment, pulping, hornification, bleaching) (O. Onuaguluchi 2016).

Since, discussing about all these strategies is beyond the scope of this section, here it has been focused more on the hornification of VFs, as the experimental approach of this doctoral thesis is centered on this method. Hornification, is a process in which fibers are alternatively dried and re-wetted to irreversibly reduce their water retention value, which it does not modify the fiber's strength and length, but leads to a reduction in cell wall thickness. It has been found to improve fiber-cement bonding and fiber durability in cement matrix. (J. Claramunt, M. Ardanuy, J. A. García-Hortal 2009, 2010, 2011).

The fiber wall collapse begins after the first drying cycle and has the significant impact on fiber walls, and it continues to work after each drying and rewetting cycle, and after two or three cycles, it stabilizes. The process is depicted in Figure 2.14. The wet fiber before drying is shown by stage (a). With around 30% humidity content, water drainage begins to cause morphological changes in the fiber cell wall shown in stage (b), and capillary forces cause the fiber wall lamellae to approach each other. In result, the fiber cavity (lumen) may collapse during this stage. With more drying, the spaces between lamellae continue to shrink, reaching stage (c), which the open voids in the cell wall's lamellar structure become closed. Water removal occurs in the fine structure of the fiber wall near the conclusion of drying in stage (d). During the final stages of drying, when solid levels exceed 70-80 percent, the fiber shrinks dramatically and uniformly. The shrinking occurred in stage (d) is considered to be permanent. (S.F. Santos, G.H.D. Tonoli 2015).

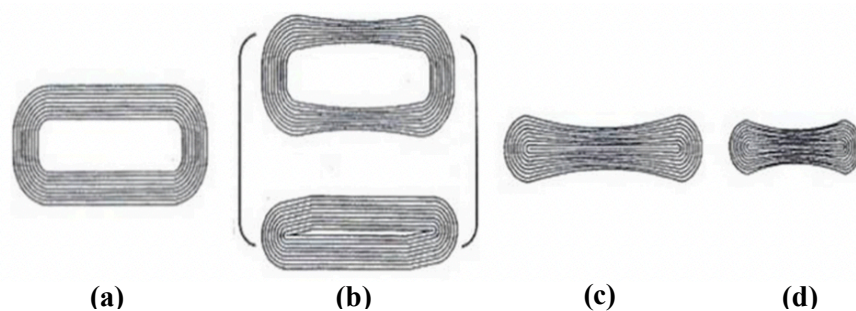


**Figure 2.14.** (a) Fiber decomposition, (b) The gap between fiber/matrix, (c) Untread fibers, (d) deposited on fibers (S.F. Santos, G.H.D. Tonoli 2015).

Modifying fiber characteristics including physical/chemical alteration of fiber's surface in order to improve fiber/matrix adhesion and to make them less susceptible to alkaline medium of cement matrix and environmental humidity. Around 13% (Pinus pulp) and 21% (cotton linter) higher values of flexural strength and around 20% (Pinus pulp) and 10% (cotton linter) higher values of compressive strength relative to the untreated fibers were obtained for the aged composites. (J. Claramunt, M. Ardanuy 2011), (M. Ardanuy, J. Claramunt 2015).

The formation of hydrogen bonds in cellulose causes natural fibers to shrink during drying and rewetting cycles, as it is well known. This irreversible effect (U. Weise, H. Paulapuro 1999), happens in the cell wall matrix of the VFs, and it is measured as a percentage reduction in water retention values (WRV), resulting in intensely bonded structures. The reduced WRV of hornificated fibers has beneficial effects on VFRCC. Moreover, the hornificated VFs have higher dimensional stability (Garcia-Hortal, 2007), and hence leads in higher fiber–matrix adherence.

With the lower WRV of hornificated VFs, consequently a reduction in the formation of CH coating on the surface and lumen of fibers will be and hence a reduction in the degradation of cellulose in VF reinforced cement matrix is expected. Taking this into account, to understand the effects of wet/dry cycles on the structure and characteristics of VFs to analyse the potential use of hornificated VFs in improving fiber/matrix adhesion and durability of VFRCC. (J. Claramunt, M. Ardanuy 2010, 2015).

According to a study by Ferreira et al, the adhesion stress and frictional stress of hornified fibers of the same length in a cement mortar matrix increased by 40%-50%, as compared to 25 mm long untreated fibers, respectively (S. Ferreira, P. Lima 2014).

Many other researchers have been examined different methods to reduce the dimensional instability of vegetable-based fibers. (O. Onuaguluchi 2016), (T. Filho, K. Ghavami 2003), (G. Tonoli, M. Belgacem 2012), (S. Ferreira, P. Lima 2014). These treatments, however, must be compatible with the matrix, because different matrices necessitate different fiber surface qualities and treatments that must be considered (H. Ventura 2017).

Pre-treatment of fibers with alkalis can eliminate natural and artificial contaminants and break down the fiber bundle into smaller fibers, increasing the effective surface area of fibers. It can provide a rough surface on the outer skin of fibers, increasing fiber resistance to pull-out from the matrix (O. Onuaguluchi 2016). Findings by Toledo Filho et al indicated that the immersion of sisal and coconut fibers in a silica fume slurry before their addition to cement mortar was very effective in reducing the embrittlement of the composite (T. Filho, K. Ghavami 2003).

Bleaching eliminates residual lignin and extractives from the cell wall of fibers, enhancing their whiteness/brightness for instance in pulp fibers. However, the depolymerization reaction during the bleaching process weakens fibers, diminishing their tensile strength, the bleaching process also has an impact on the permeability and bond behavior of fibers in cement composites (G. Tonoli, M. Belgacem 2012).

## 3. EXPERIMENTAL PROGRAM

### 3.1. EXPERIMENTAL PROGRAM OUTLINE

The specimens were designed using materials and methods adhered to the relevant standards. Calcium aluminate cement (CAC) as a based matrix with a low pH and low alkaline medium compared to OPC were investigated. Two types of fluidifying additives for the workability improvement of pastes with the recommended dosages were applied. Flax and cotton linter fibers as reinforcement elements with different contents of 2%, 6% and 10% wt. based on the literature review were incorporated to the matrix. Silica fume as pozzolanic binder in different contents ranging from 0% SF to 20% SF wt. to improve CAC matrix chemical properties was selected.

The experimental program was divided into 4 stages:

- **Stage 1.** The primary dosages and fiber/cement relation on the matrix of CAC-vegetable fibers were investigated. Flexural strength of specimens with VF contents ranging from 2%, 6% and 10% wt. with the dimensions of 10x40x160 mm were tested after 28 days, 6 months, and 1 year of curing in the humid chamber at ( $20\pm 1^{\circ}\text{C} > 90 \text{ HR}$ ). The three-point bending test was performed by a multi-test hydraulic press, according to the norm UNE-EN 196-1:2005.
- **Stage 2.** Following the stage 1, the flexural strength of specimens was examined, after completing 28 days curing and hereafter subjected to 10 accelerated aging cycles at ( $20\pm 1^{\circ}\text{C} > 90 \text{ HR}$ ). The three-point bending test was performed following the procedure established in stage 1.
- **Stage 3.** This stage was dedicated to the investigation of enhancing the durability and chemical properties of CAC matrix by evaluating the pozzolanic additions in CAC matrix such as Silica Fume (SF). The w/c relation was analyzed, SF contents ranging from 0%

to 20% wt. were considered in order to obtain derive conclusion. The flexural and compression strength of the specimens with the dimensions of 40x40x160 mm were tested after 7, 28 and 56 days of curing in the humid chamber of ( $20\pm 1^\circ\text{C} > 90 \text{ HR}$ ).

- Stage 4.** Following the previous stages, the suitable ratio between CAC-VF and CAC/SF was selected; hereafter, phase 4 was focused on the durability of SF-VFRCCs based on the outcomes of compatible VFRCCs (Stage 1-2) and SF-CAC matrix (Stage 3). In this case, the specimens with the dimensions of 10x40x160 mm were exposed to 28 days of curing period in the humid chamber before being subjected to 10 wet/dry cycles ( $20\pm 1^\circ\text{C} > 90 \text{ HR}$ ).

The out-line of test methods and the calculation procedures are detailed below in Figure 3.1.

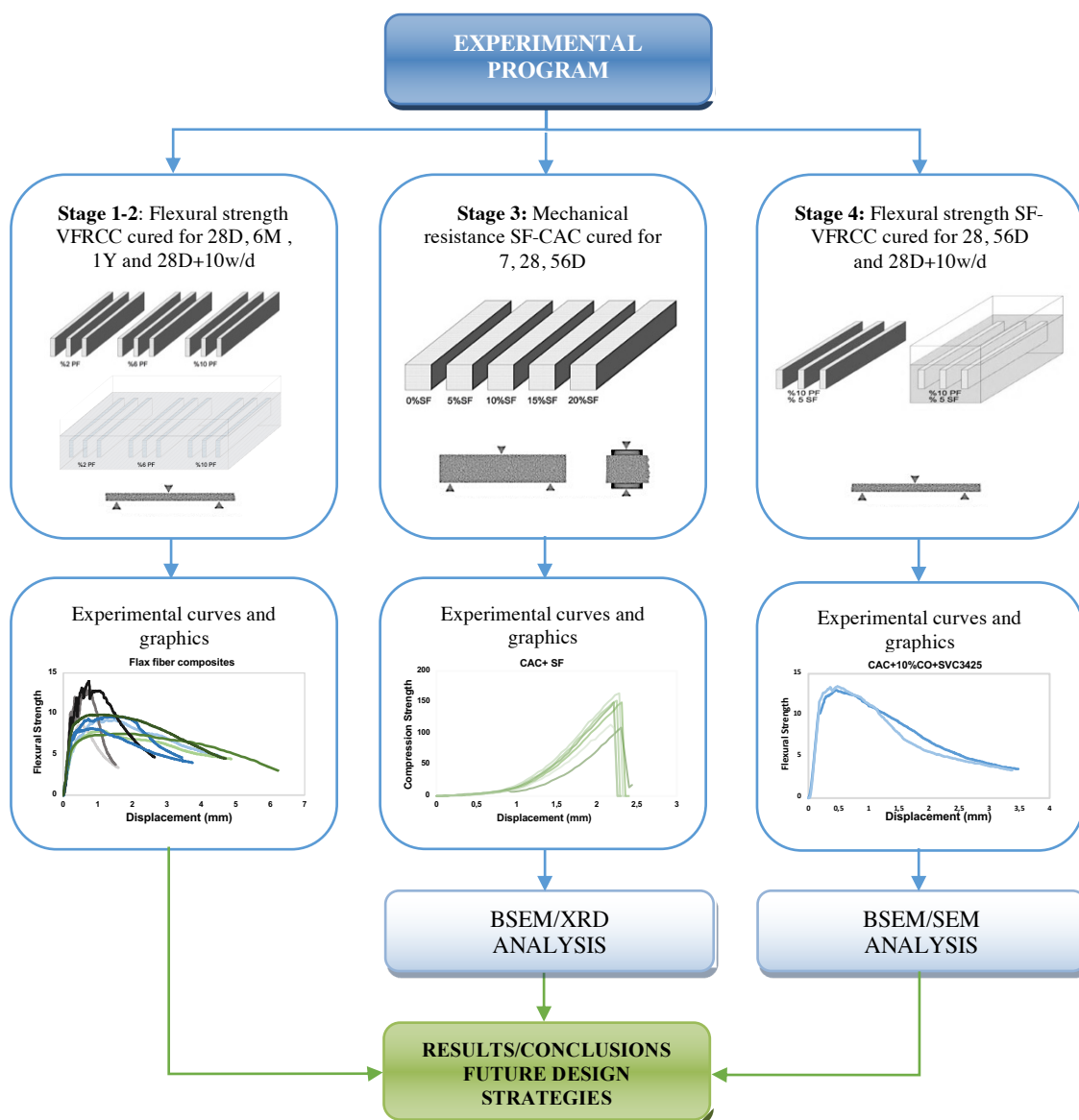


**Figure 3.1.** The out-line of experimental program and test methods procedures.

## 3.2. MATERIALS

### 3.2.1. Calcium cement aluminate

Calcium Aluminate Cement (CAC) with an alumina concentration of 41.5% provided by the company Cements Molins Ltd. was utilized as the basis cementitious matrix. Figure 3.2 presents the raw Calcium Aluminate Cement and Table 3.1 indicates the chemical compositions of CAC.

**Table 3.1.** The chemical composition of calcium cement aluminate (data provided by the manufacturer).

Chemical	Oxide equivalent (wt. %)
SiO <sub>2</sub>	3.7
Al <sub>2</sub> O <sub>3</sub>	41.5
CaO	38.1
MgO	0.43
SO <sub>3</sub>	0.01
Na <sub>2</sub> O	0.14
K <sub>2</sub> O	0.02
TiO <sub>2</sub>	1.72
MnO	0.01
Fe <sub>2</sub> O <sub>3</sub>	13.20
Loss on ignition	1.41



**Figure 3.2.** Raw Calcium Aluminate Cement.

### 3.2.2. Fluidifying additives

Sika ViscoCrete 3425 and Sika Plast 380 were used in this experimental program. On the one hand, Sika ViscoCrete 3425 is a superplasticizer oriented to high-performance concrete. It is a high-activity superplasticizer that combines different mechanisms of action. Due to surface adsorption and steric effect that separate the particles, the following properties can be achieved by using this additive in the cement mixtures.

On the other hand, Sika Plast 380 is high performance superplasticizer for the manufacture of all types of concrete made in ready-mix concrete plants; especially those with fluid consistency improving pumpability. It does not exert any corrosive action on the reinforcements due to the fact that it is a product free of chlorides, Table 3.2 presents the properties of these additive types.

**Table 3.2.** The properties of Additives applied in the mixtures (data provided by the manufacturer).

Additives	Chemical Base	Dosage (wt. %)	Physical Properties	Characteristics
Sika ViscoCrete 3424	Water-based modified polycarboxylate	0.2 - 0.8	Yellowish White Liquid	High density, resistance and impermeability
Sika Plast 380	Modified polymers in aqueous solution	0.5 - 1.8	Green Liquid	Mechanical strength, impermeability and durability improvement

### 3.2.3. Vegetable fibers

Flax fiber distributed by Fibers Recherche Development in Technophile de lube in Champagne and cotton linter fiber that is distributed by Celsur (Cotton South, S.L., Spain) were used. The main physical and chemical properties of both fibers are described in Table 3.3. Approximately 1.5 kg of each fiber type were treated, using the hornification of vegetable fiber method (J. Claramunt, M. Ardanuy 2011).

According to this method following the cutting and resizing, the fibers are gradually immersed in distilled water to be posteriorly cleaned and purified. The fibers must be saturated of the water, which is achieved when their color turn into a darker tone (immersed in water 4 days for an optimal result). Afterwards, the excess water is removed manually to facilitate and speed up the drying process. The fibers are placed in a container (steel tray, thoroughly scattered), and placed in a stove at temperature of 60°C for 3 days, until completely dry. This method is done for 5 cycles (See Figure 3.3), (1 cycle is a period of 1 week).

**Table 3.3.** The properties of vegetable fibers utilized in the program (data provided by the manufacturer).

Properties	Flax Fiber	Cotton Linter	
Length	≤ 6 cm	0.79 mm	 <p style="text-align: center;"><b>Flax fiber</b></p>
Diameter	98 ± 26 μm	16 - 21 μm	
Density	1.46 g/cm <sup>3</sup>	1.5 - 1.6 g/cm <sup>3</sup>	
Stiffness	30.4 GPa	5.5 - 12.6 GPa	
Strength	730 MPa	287 - 597 MPa	
<b>Chemical Composition</b>			 <p style="text-align: center;"><b>Cotton linter fiber</b></p>
Cellulose Content	77.1 ± 0.0%	82.7 - 92 wt.%	
Hemicellulose content	6.7 ± 0.2%	2 - 5.7 wt.%	
Lignin content	2.6 ± 0.2%	0.5 - 1 wt.%	
Content of gums, Fatty Acids, waxes and others	13.1 ± 0.3%	5.7 wt.%	
Minerals content	0.5 ± 0.0%	-	
Residual shive content	15.8 ± 2.3%	-	

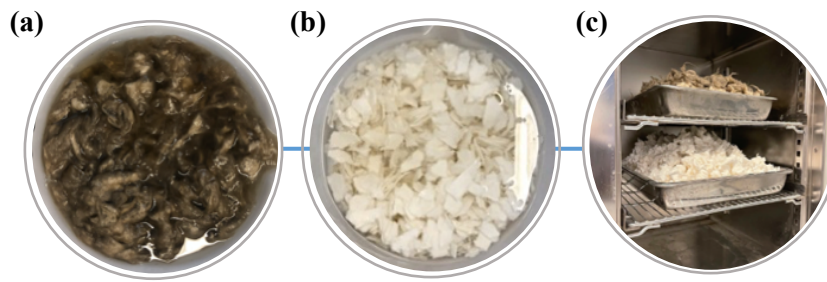


**Figure 3.3.** The vegetable fiber subjected to 5 wet/dry cycles. VFs soaked in distilled water (a) flax fiber, (b) cotton linter fiber, (c) drying cycle of VFs in stove.

### 3.2.4. Silica Fume

The silica fume (SF), is supplied by Arciresa, Gijon, Asturias, Spain. The mineralogical composition of the SF is presented in [Table 3.4](#) , [Figure 3.4](#). In a research done by Byung-Wan et al, it is reported that the adding process of finely grounded solid components to cement is a well-established procedure ([Byung-Wan, Chang-Hyun 2007](#)).

By following similar method a procedure presented in [Figure 3.5](#) a 1:1 ratio of silica fume and distilled water was mixed precisely and posteriorly grained in a milling machine shown in the figure below was milled for 15 minuts in order to get the fine-grounded silica fume grains.

**Table 3.4.** The chemical composition of silica fume (data provided by the

Chemical	Oxide equivalent (wt.%)
SiO <sub>2</sub>	93.5
Al <sub>2</sub> O <sub>3</sub>	0.32
CaO	0.39
MgO	0.2
SO <sub>3</sub>	0.03
Na <sub>2</sub> O	0.23
K <sub>2</sub> O	0.28
TiO <sub>2</sub>	-
MnO	-
Fe <sub>2</sub> O <sub>3</sub>	0.11
Loss on ignition	3.44



**Figure 3.4.** Raw silica fume grains before treatment

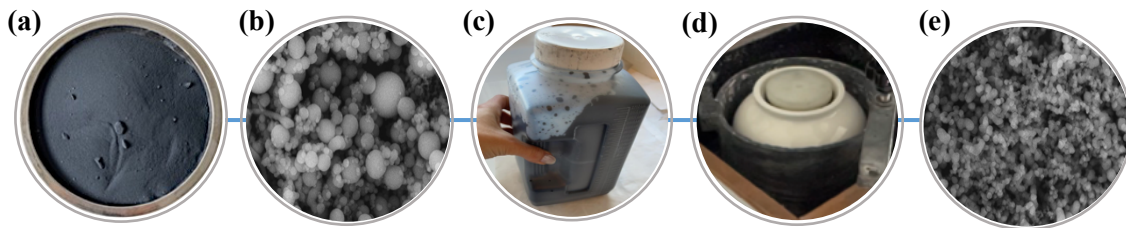


**Figure 3.5.** The silica fume milling treatment procedure: (a) raw silica fume, (b) microscopic image of silica fume particles before milling, (c) prepared 1:1 ratio of SF/W before milling, (d) milling machine, (e) microscopic image of silica fume particles after milling process.

### 3.3. SPECIMEN PREPARATION

#### 3.3.1. Specimen preparation procedure for the 1<sup>st</sup>- 2<sup>nd</sup> experimental stages

Calcium aluminate cement, distilled water, treated flax and cotton linter fiber in varied proportions of 2%, 6% and 10% of cement weight, de-molding oil to facilitate specimen removal and Sika ViscoCeret 3425 and Sika Plast 380 were used. [Table 3.5](#) presents the dosages of mixtures for the 1<sup>st</sup> and 2<sup>nd</sup> experimental stages:

**Table 3.5.** The dosage of mixtures for the 1<sup>st</sup>-2<sup>nd</sup> experimental stages.

Mixtures	CAC g	Fiber Content wt. %	Flax Fiber g	Cotton Linter g	SP380 wt. %	SVC3425 wt. %	Distilled water g	W/C
CAC	500	2%	10	10	-	-	200	0,40
	500	6%	30	30	-	-	375	0,75
	500	10%	50	50	-	-	500	1
CAC-Flax Fiber	500	2%	10	-	0,5 %	0,2 %	200	0,40
	500	6%	30	-	0,5 %	0,2 %	375	0,75
	500	10%	50	-	0,5 %	0,2 %	500	1
CAC- Cotton Linter	500	2%	-	10	0,5 %	0,2 %	200	0,40
	500	6%	-	30	0,5 %	0,2 %	375	0,75
	500	10%	-	50	0,5 %	0,2 %	500	1

The specimens were casted within a steel mold of internal dimensions of 40x40x160 mm according to UNE-EN 196-1:2005. The w/c was established by varying this parameter in different mixtures (See [Table 3.5](#)). The fibers were manually stirred until these were evenly scattered in the paste. In the case of cotton linter fibers, it was firstly blended with water, posteriorly it was added into the cement, manually stirred until a smooth paste was obtained.

The paste was weighed evenly for each cell and poured into the mold. To remove the excess of water, 100 kN load was applied during the period of 24 h. To obtain the desired w/c ratio, the mold was placed in a tray and the eliminated water was measured. The specimens were de-molded the day after, and the excess water was quantified. Finally, the specimens were placed in the humid chamber ( $20\pm 1^\circ\text{C}$ ;  $\text{HR} > 90\%$ ) during 28D, 6M, and 1Y.

Figure 3.6 presents schematic representation of the specimen preparation of 1<sup>st</sup>-2<sup>nd</sup> experimental stages. The process involves from the specimen manufacturing, cutting, cleaning-purifying fibers, wet/dry cycles applied to the VFs, the composites with aging cycles. According to the literature, (Scrivener, Cabiron 1999) the minimum amount of water necessary for the hydration of CAC is 0.25 o.w.c in order to obtain a durable CAC concrete. In this regard, the amount of water that fibers absorb has to be considered as the fibers used were dry, and a considerable amount of water was required to maintain the mixture's homogeneity. A total of 108 specimens with dimensions of 10x40x160 mm were produced according to UNE-196-1:2005. When fabricating the specimens, the amount of paste required for each cell was weighed and placed into the mold. The excess of paste was measured and after compressing, the excess of water was measured and removed, the final w/c ratio was determined (See Table 3.6).

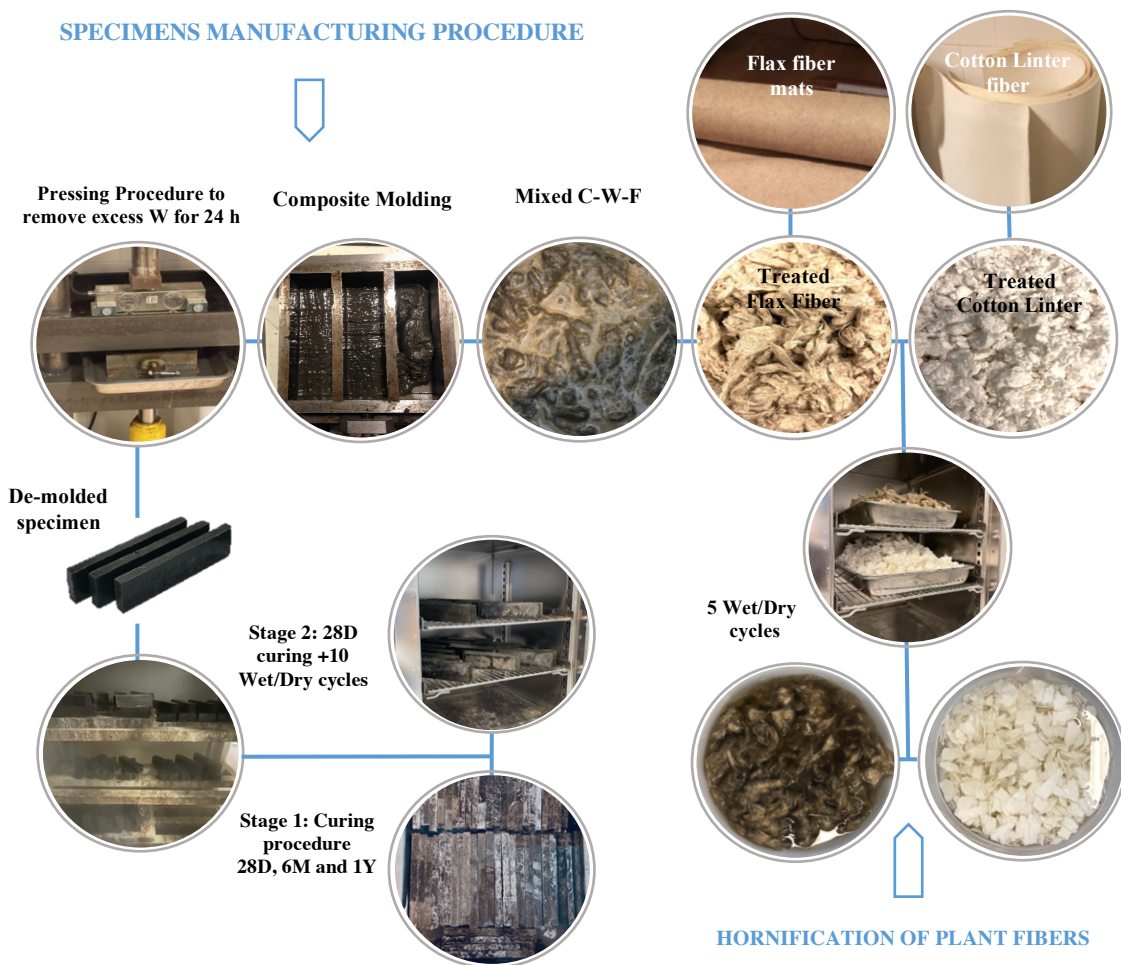


Figure 3.6. The schematic representation of 1<sup>st</sup> - 2<sup>nd</sup> experimental stages.

**Table 3.6.** The final W/C ratio for the 1<sup>st</sup> - 2<sup>nd</sup> experimental stages.

Specimen	Initial CAC g	Initial W g	Initial F g	Initial W/C	Initial P g	Excess P g	Used P g	Used W in P g	Excess W g	Used CAC g	Final W g	Final W/C
Flax	500	200	10	0.40	710	10	700	197.19	74	492.96	123.19	0.24
	500	375	30	0.75	905	205	700	266.73	96.5	355.64	170.73	0.48
	500	500	50	1	1050	350	700	253.53	135.5	253.53	118.03	0.46
Flax SP380	500	200	10	0.40	710	10	700	197.19	55.5	492.96	141.96	0.28
	500	375	30	0.75	905	205	700	266.73	108.9	355.64	157.83	0.44
	500	500	50	1	1050	350	700	253.53	110.5	253.53	143.03	0.56
Flax SVC 3425	500	200	10	0.40	710	10	700	197.19	86.5	492.96	110.69	0.22
	500	375	30	0.75	905	205	700	266.73	141.5	355.64	125.23	0.35
	500	500	50	1	1050	350	700	253.53	132	253.53	121.53	0.47
Cotton Linter	500	200	10	0.40	710	10	700	197.19	53.5	492.96	143.69	0.29
	500	375	30	0.75	905	205	700	266.73	88.9	355.64	177.83	0.50
	500	500	50	1	1050	350	700	253.53	130.5	253.53	123.03	0.48
Cotton Linter SP380	500	200	10	0.40	710	10	700	197.19	61.5	492.96	135.69	0.27
	500	375	30	0.75	905	205	700	266.73	141	355.64	125.73	0.35
	500	500	50	1	1050	350	700	253.53	135.5	253.53	118.03	0.46
Cotton Linter SVC 3425	500	200	10	0.40	710	10	700	197.19	66.5	492.96	130.69	0.26
	500	375	30	0.75	905	205	700	266.73	107.5	355.64	159.23	0.44
	500	500	50	1	1050	350	700	253.53	133	253.53	120.53	0.47

### 3.3.2. Specimen preparation procedure for the 3<sup>rd</sup>- 4<sup>th</sup> experimental stage

Calcium aluminate cement, distilled water, silica fume in varied proportions were used, the combinations were identified with a percentage of 95/5 where 95 corresponds to percentage of CAC content and 5 corresponds to percentage of SF content, 90/10, 85/15 and 80/20, demolding oil to facilitate specimen removal. Table 3.7 presents the dosages of mixtures for 3<sup>rd</sup> experimental stages:

**Table 3.7.** The dosage of mixtures for the 3<sup>rd</sup> experimental stage.

CAC wt. %	SF wt. %	W/C	W/C+SF	CAC-SF g	CAC g	SF g	Total W g	W+SF g	Final W g
1	0	0.35	0.35	1400	1400	0	490	0	490
0.95	0.05	0.35	0.35	1400	1330	70	490	140	420
0.90	0.10	0.35	0.35	1400	1260	140	490	280	350
0.85	0.15	0.35	0.35	1400	1190	210	490	420	280
0.80	0.20	0.35	0.35	1400	1120	280	490	560	210

The specimens were casted within a steel mold as previous section, according to UNE-EN 196-1:2005. A total of 30 specimens with dimensions of 40x40x160 mm were produced. The W/C and SF/C ratio were established by varying these parameters in different mixtures (See Table 3.7). The SF was firstly milled with water with the ratio of 1:1, posteriorly the mixture was added into the measured cement, and manually stirred until a smooth paste is obtained. The paste was weighed evenly for each cell and poured into the mold. The excess of the paste was removed, and then to remove the air bubbles the mold was placed on vibration machine and 120 vibration were applied. The specimens were de-molded the day after, and finally the specimens were placed in the humid chamber (20±1°C; HR > 90%) during 7, 28, 56 days.

Figure 3.7 presents schematic representation of the specimen preparation for 3<sup>rd</sup> and 4<sup>th</sup> experimental stages. The process involves from the specimen manufacturing, milling SF and in final the composites with the accelerated aging cycles for stage 4.



Figure 3.7. The schematic representation of the specimen production and equipment for the 3<sup>rd</sup>-4<sup>th</sup> experimental stages.

According to results of stage 1<sup>st</sup>-2<sup>nd</sup> and 3<sup>rd</sup>, the stage 4 was programmed to conclude this investigation. Therefore, the optimal VF type and content of stage 1-2 was incorporated into the optimal SF-CAC matrix of stages 3. Hereafter, the flexural strength of matrix was investigated after 28-56 days. Finally, the durability performance of specimens subjected to 10 wet/dry cycles were assessed. A total of 12 specimens with dimensions of 10x40x160 mm were produced according to UNE-196-1:2005 (See Figure 3.7). Table 3.8 indicates the dosages of each CAC-SF-CO mixture of 4<sup>th</sup> stage:

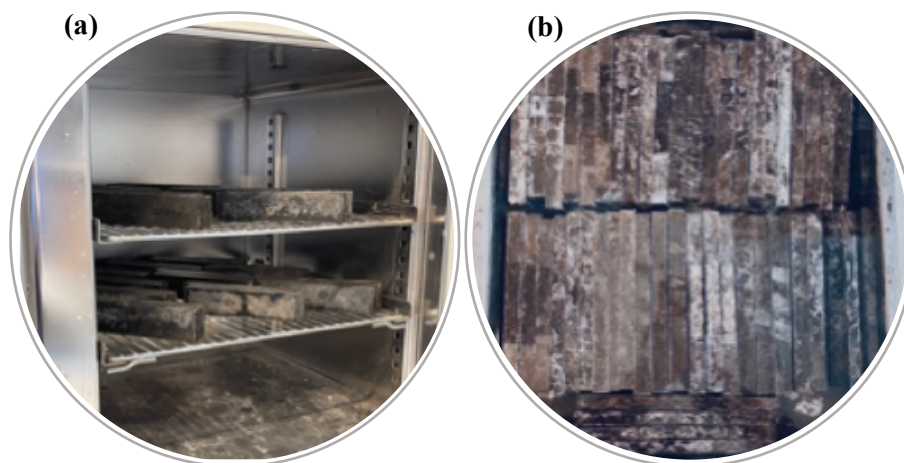
**Table 3.8.** The dosage of mixtures for the 4<sup>th</sup> experimental stage.

CAC Wt.%	SF Wt.%	W/C	W/C+SF	CAC-SF g	CAC g	SF g	Fiber g	Total water g	W+SF g	Final W g
1	0	1	0	500	500	0	50	500	0	500
0.95	0.05	1	1	500	475	25	50	500	50	475

### 3.3.3. Accelerated aging cycles

The specimens were subjected to wet/dry cycles once the curing time was achieved. On the one hand, the dry cycle consisted of placing the specimens into a stove, uncovered, as shown in Figure 3.8, the temperature was kept constant at 60°C for three days. On the other hand, the wet cycle consisted of immersing the specimens in distilled water during 4 days at laboratory's ambient temperature.

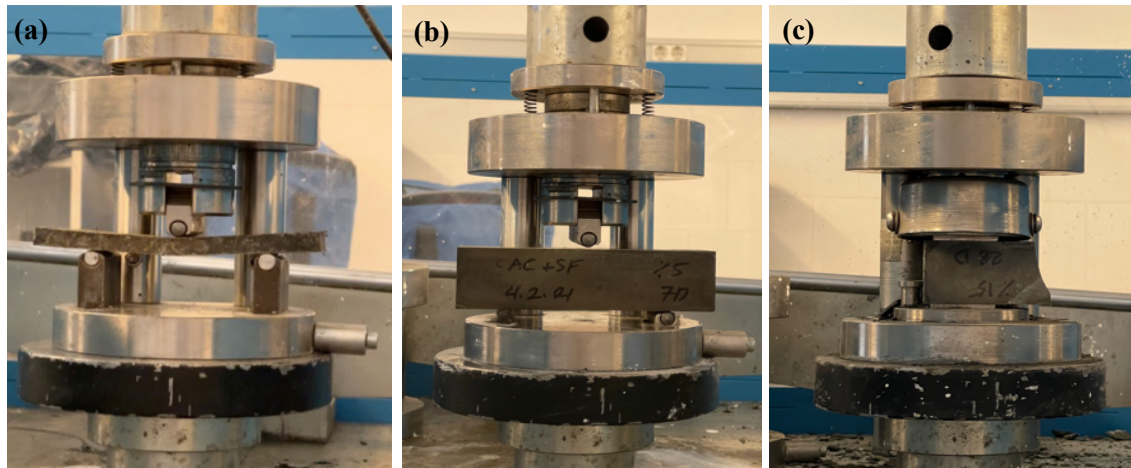
A complete cycle lasted of 1 week, and 10 cycles were performed continuously for each tested specimen. Posteriorly, the specimens were subjected to load in order to characterize the aged mechanical properties.



**Figure 3.8.** The wet/dry cycles procedure; (a) dry cycle of the specimens in the stove, (b) wet cycle of the specimens immersed in distilled water.

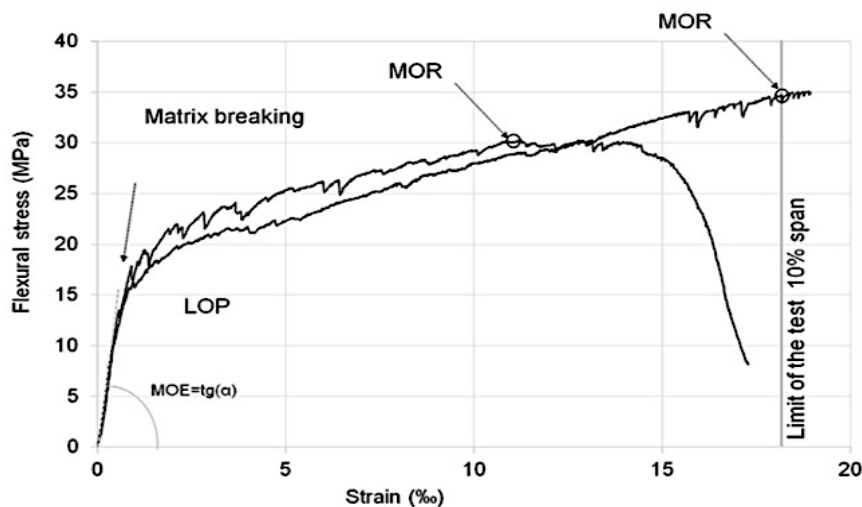
### 3.4. MECHANICAL PERFORMANCE CHARACTERIZATION

The compressive and flexural (at pre- and post-cracking stages) performance was characterized for the VFRCC, SF-CAC, and SF-VFRCC after specimens were produced and cured according to subsections 3.3.1 and 3.3.2. The weight and thickness of the specimens were measured using a digital balance and a Vernier caliper, respectively. The mechanical tests were performed with a Incotecnic multi-test press equipped with a load cell (See Figure 3.9).



**Figure 3.9.** (a), (b) flexural tests on different size prismatic specimens and (c) compression test.

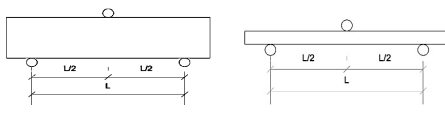
The three-point bending tests configuration was selected for characterizing the flexural strength following the UNE-EN 196-1:2005. Three (3) specimens for each mixture were tested for flexural strength, two pieces of each tested specimen were kept for performing the compression test (a total of specimens for each mixture). Both tests were carried out under a displacement-control (1 mm/min) configuration so that the post-cracking and post-failure phenomena could be properly captured. Flexural strength – strain (or deflection) relationships as the one depicted (quantitative) in Figure 3.10 were to be obtained and to be the basis of the analysis.



**Figure 3.10.** Flexural stress-strain curves obtained for cellulosic cement composites (M. Ardanuy, J. Claramunt 2015).

The limit of proportionality stress (LOP), the modulus of elasticity (MOE), the energy absorption (or toughness), and the strain are the parameters and constitutive parameters measured during the flexural tests. The equations (M. Ardanuy, J. Claramunt 2015) that were used to compute these parameters are presented in Table 3.9. In hardening-deflection materials, RILEM (RILEM TFR4-test 1984) recommends that MOR is established as that flexural strength corresponding to 10% of the span.

**Table 3.9.** Equations for calculations of MOR, MOE and Strain ( $\theta$ ) for three-point bending configuration.

		
MOR	$\frac{3 \cdot F \cdot l}{2 \cdot b \cdot h^2}$	F = the load (force) (N). l = length of the support span (mm). f = maximum deflection (mm). b = width of the specimen (mm). h = thickness of the specimen (mm).
MOE	$\frac{F \cdot l^3}{4 \cdot f \cdot b \cdot h^3}$	
$\theta$	$\frac{6 \cdot f \cdot h}{l^2}$	

### 3.5. MICROSTRUCTURE AND CHEMICAL COMPOSITION ANALYSIS

#### 3.5.1. X-Ray diffraction analysis

X-Ray Diffraction analysis (XRD) was used to identify the mineralogical composition of specimens for each experimental stage (Stage 3, SF-CAC) and (Stage 4, SF-VFRCC). The chemical composition was determined by X-ray diffraction (XRD) analysis with a diffractometer model X'Pert PRO MPD DY-3197 (PANalytical, Netherlands). Data were collected on the  $2\theta$  range from  $5^\circ$  to  $40^\circ$  at a resolution of  $0.02^\circ$  and a speed of  $1\text{s}/0.02^\circ$ . This procedure provides a limited information on the hydrated elements of specimens. The specimens (See Figure 3.11) were prepared grinding the small pieces of specimens immersed in isopropyl alcohol using an agata mortar, followed by immersion in acetone for 20s to freeze the hydration reactions. Afterwards the samples were washed with isopropyl alcohol and stored in a desiccator under vacuum until performing the analysis, a total produced powder was about 10 gr.

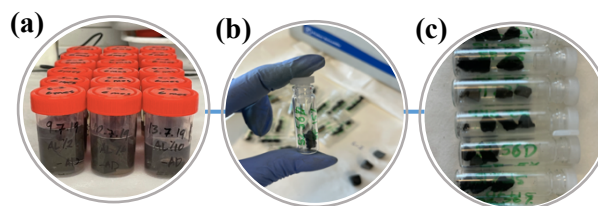


**Figure 3.11.** X-Ray Diffraction, specimen preparation for chemical composition analysis. (a) frozen hydration of specimen in isopropanol, (b), (c) prepared specimens for XRD analysis.

### 3.5.2. BSEM/SEM microstructure analysis

The microstructure was analyzed by means of BSEM-SEM imaging, performed in an SEM model JSM-6300 (JEOL, Japan) equipped with an energy dispersive X-Ray spectrometer (EDS) model Link ISIS-200 (Oxford Instruments, United Kingdom) for EDS analysis. The following description is the procedure of the method:

To prepare the specimens, small pieces from the flexural mode tested samples were immersed in isopropyl alcohol followed by encapsulation in epoxy resin and polishing to have parallel faces. For the study of the phases and their compositions in each mixture, the different phases observed were characterized by X-Ray analysis and associated with a grey tone range in the 8-bit SEM image. The distribution of the phases was determined by image treatment, consisting of brightness filtering for selection of the grey tone range and, in some cases, with further colour inversion. [Figure 3.12](#) presents the specimen preparation procedure for BSEM-SEM analysis.

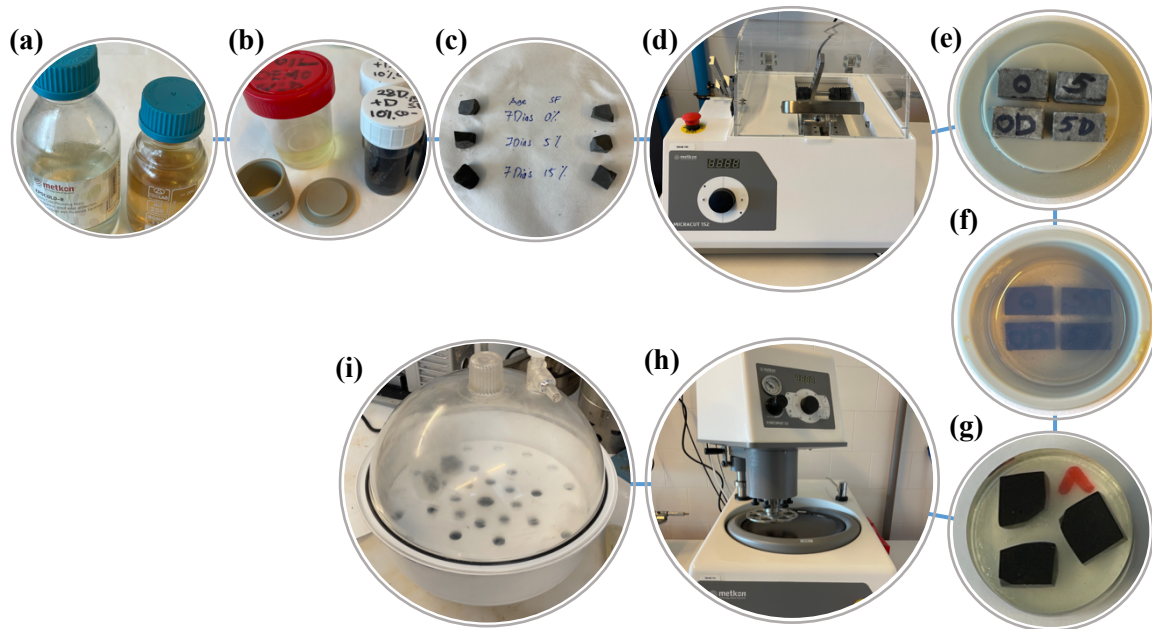


**Figure 3.12.** Experimental procedure; (a) epoxy resin (b) mold and specimens soaked in isopropanol (c) specimens before cutting, (d) cutting machine, (e) polished specimen, (f) specimens encapsulated by epoxy resin in mold, (g) demolded specimen next 24h, (h) polishing machine, (i) specimens kept in desiccator before BSEM/SEM analysis.

## 4. RESULTS AND DISCUSSION

### 4.1. FLEXURAL STRENGTH PERFORMANCE

In this section, the results obtained from the experimental characterization of the flexural strength by means of the 3-point bending tests are presented. The flexural stress-displacement curves derived for the tested composites, and the values of Modulus of Elasticity (MOE), Limits of Proportionality (LOP), Modulus of Rupture (MOR), and Specific Energy (SE) are computed and compared. The specimen groups are revealed the sets from 2%, 6% and 10% of VFs wt.% with two different additives incorporated and a reference specimen with no additive incorporation (0AD) cured for 28 days (28D), 6 months (6M) and 1 year (1Y). The graphs reveal the dependency of flexural strength and toughness on the curing times, distinct VF type and content ((FL) Flax fiber – (CO) Cotton Linter fiber) and the different additives considered.

Figures 4.2, 4.3 and 4.4 present the flexural strength – displacement relationships obtained for the cotton linter fiber-0AD (0AD-CO), cotton linter fiber-SP380 (SP380-CO) and cotton linter fiber-SVC3425 (SVC3425-CO), respectively. Figures 4.5, 4.6 and 4.7 present the flexural strength – displacement relationships obtained for the flax fiber-0AD (0AD-FL), flax fiber-SP380 (SP380-FL) and flax fiber-SVC3425 (SVC3425-FL), respectively, for the different curing periods (28D, 6M and 1Y). The stress-deflection has a linear relationship, which can be used to calculate the elastic modulus accurately (MOE).

#### 4.1.1. Modulus of elasticity (MOE)

Figure 4.1 and Table 4.1 present the flexural modulus of elasticity obtained from bending mode curves for both cotton linter and flax fiber compounds. The flexural strength-displacement relationships are shown in Figures 4.2, 4.3 and 4.4 for cotton linter compounds, and Figures 4.5, 4.6 and 4.7 for the flax fiber compounds. The initial stress-deflection response is linear elastic for both fiber type as the specimens exhibit sufficient stiffness, with sufficiently high first crack strain capacity for some applications, (*At this linear range the response is dominated by the matrix/VFs*).

This linear relationship before first crack was steeper at 28D for both fiber type compounds, but the slope was decreased after 6M-1Y hydration stages (as it is expected for CAC matrix due to the conversion system that occurs in such matrices). However, in some cases the cotton linter fiber compounds behavior was opposite trend when superplasticizers were added. The stiffness of the both cotton linter and flax fiber reinforced compounds are sufficiently high to keep the newly formed cracks from widening, however, in some specimens the crack widening appeared. (See Figures 4.3 and 4.4 in specimen with 6%VF hydrated for 28D and Figure 4.4 the specimen with 6%VF hydrated for 1Y). As it can be seen in Figure 4.1 the two composite systems present a distinct behavior at this elastic linear zone, in cotton linter compounds when the VF content was increased the MOE averages was increased while in flax fiber compounds the opposite trend is observed. Nevertheless, in both compound system there is a reduction rate in MOE means with time. MOE averages at 28D hydrated cotton linter compounds ranged from 8,30 to 9,80 GPa for 0AD-CO compounds, from 7,25 to 8,97 GPa for SP380-CO and for SVC3425-CO ranged from 7,37 to 10,52 GPa. This compound exhibited a reduction of 45% after 1Y hydration with 5,73 GPa. At 1Y the SP30-Co has shown the lowest averages ranged from 3,74 to 4,99 GPa.

Flax fiber compounds exhibited MOE averages ranged from 6,20 to 10,27 GPa at 28D and 5,14 to 9,69 GPa at 6M and 3,10 to 5,23 GPa at 1Y, with the lowest MOE mean of 3,10 GPa for SVC3425-10%FL compound.

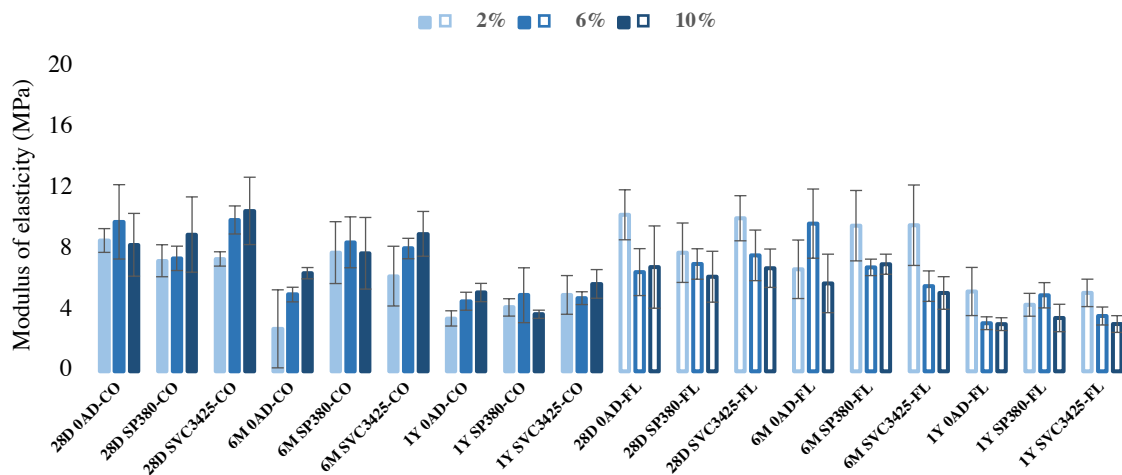
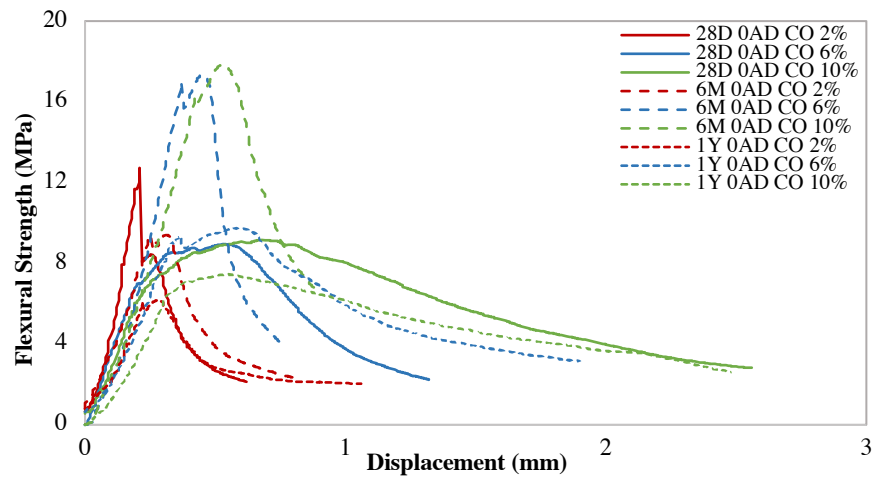


Figure 4.1. The average values of modulus of elasticity MOE (GPa) at different curing ages.

Table 4.1. The average values of the modulus of elasticity MOE (GPa)

Curing Days	28 Days			6 months			1 year			
	Fiber Content wt.%	2%	6%	10%	2%	6%	10%	2%	6%	10%
Co-0AD		8,58 (0,78)*	9,80 (2,44)	8,30 (2,06)	2,78 (2,56)	5,03 (0,48)	6,43 (0,37)	3,47 (0,50)	4,59 (0,59)	5,17 (0,60)
Co-SP380		7,25 (1,05)	7,41 (0,80)	8,97 (2,47)	7,78 (2,03)	8,46 (1,67)	7,74 (2,35)	4,19 (0,57)	4,99 (1,80)	3,74 (0,27)
Co-SVC3425		7,37 (0,47)	9,93 (0,92)	10,52 (2,21)	6,24 (1,96)	8,05 (0,67)	9,02 (1,47)	5,01 (1,27)	4,80 (0,42)	5,73 (0,94)
FL-0AD		10,27 (1,64)	6,50 (1,54)	6,83 (2,70)	6,69 (1,92)	9,69 (2,27)	5,76 (1,92)	5,23 (1,58)	3,15 (0,42)	3,09 (0,42)
FL-SP380		7,78 (1,95)	7,04 (1)	6,20 (1,67)	9,55 (2,31)	6,82 (0,54)	7,02 (0,66)	4,36 (0,75)	4,98 (0,83)	3,49 (0,90)
FL-SVC3425		10,04 (1,48)	7,60 (1,66)	6,76 (1,26)	9,58 (2,64)	5,58 (1)	5,14 (1,07)	5,14 (0,90)	3,62 (0,59)	3,10 (0,55)

\* Values in parentheses are standard deviation



**Figure 4.2.** Flexural stress – displacement relationships for the cotton linter fiber-OAD composites at different curing ages.

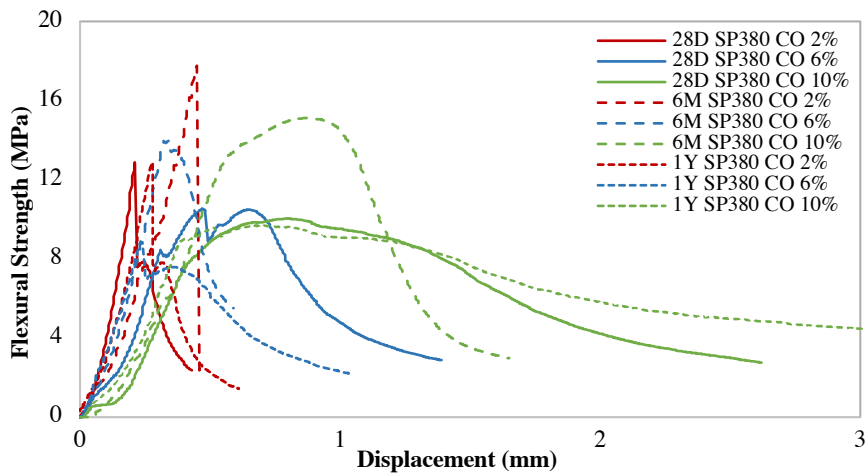


**Figure 4.3.** Flexural stress – displacement relationships for the cotton linter fiber-SP380 composites at different curing ages.

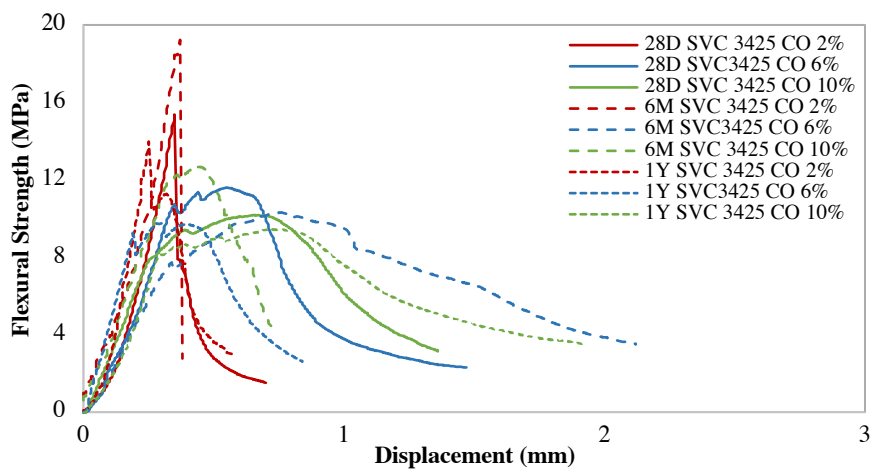


**Figure 4.4.** Flexural stress – displacement relationships for the cotton linter fiber-SVC3425 composites at different curing ages.

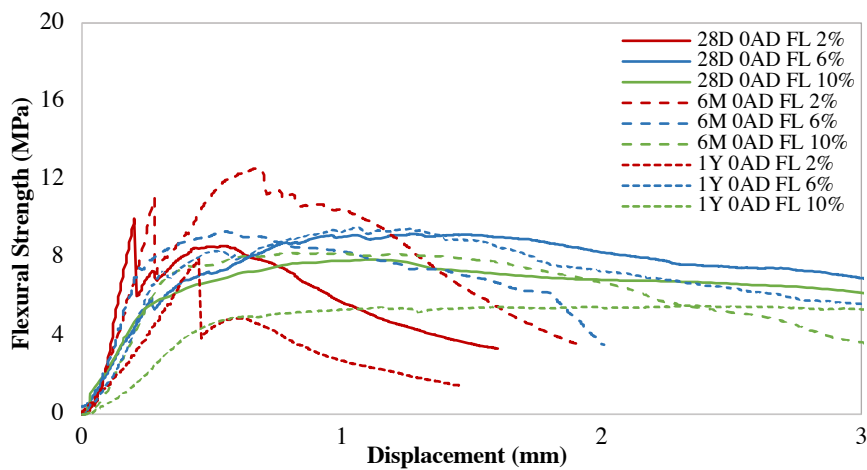


**Figure 4.5.** Flexural stress – displacement relationships for the flax fiber-0AD composites at different curing ages.

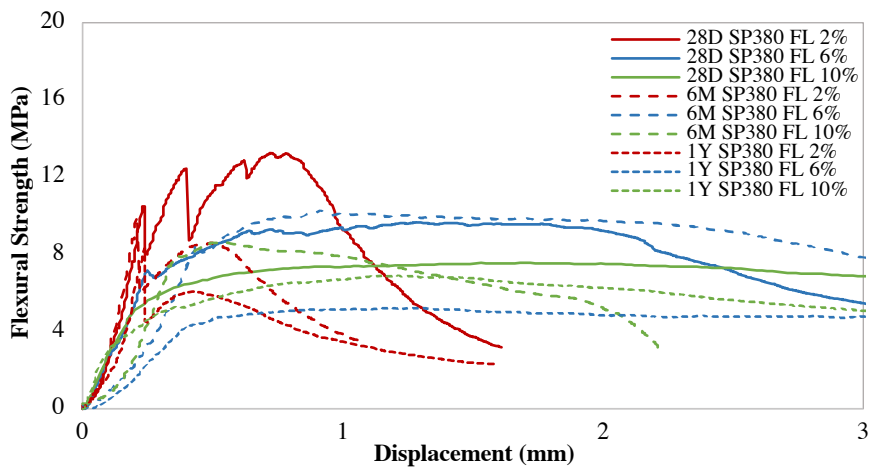


**Figure 4.6.** Flexural stress – displacement relationships for the flax fiber-SP380 composites at different curing ages.

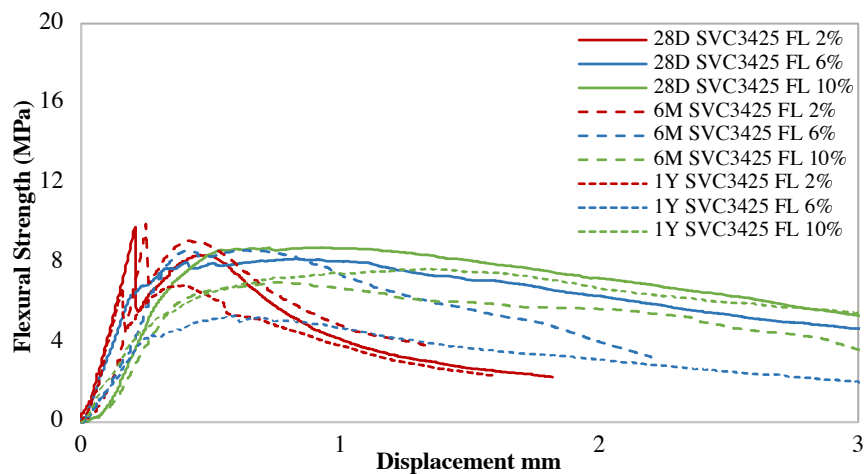


**Figure 4.7.** Flexural stress – displacement relationships for the flax fiber-SVC3425 composites at different curing ages.

#### 4.1.2. Limit of proportionality (LOP)

Three-point bending load–deflection typical curves obtained for cotton linter specimens are shown in Figures 4.2, 4.3 and 4.4. An elastic-linear range where the matrix and the fiber behave Linearly is observed up to a point where the matrix cracks. The end of the linear elastic range is delimited by lower and upper bound of the limit of proportionality (LOP). It was found that in specimens reinforced with 2%VF the means are almost twice higher than those of 6%-10%VF, (the means are significantly decreased for both compounds with 6%-10%VF). The 0AD-CO exhibited a decrease of 44% from (12,38 MPa for 2%VF to 6,93 MPa for 10%VF, See Table 4.2) in their means when the VF content was increased at 28D. This trend was also observed in other categories at 28D, SP380/SVC3425-CO exhibited decrease of 39% and 48% respectively. At 6M, remarkable increased mean was observed in compounds with both additives type, with SP380 performing better. Both compounds of SP380/SVC3425 with 10%VF exhibited increased LOP means of 28% and 22% respectively compared to their counterpart specimens at 28D. The 0AD-CO exhibited a decline of 50% in compound with 2%VF, but retained its means for 6%-10%VF compounds. In contrast at 1Y hydration, there is a significant change (decline of 67% from 12,48 to 4,15 MPa) in means of SP380-CO compounds compared to 6M hydration when VF was increased. The SVC3425-CO exhibited sustained means among others with average LOP ranged from 7,66 to 14,55 MPa at 1Y. (This compound is highlighted as an optimum mixture of this stage, the standard deviations varied from 0.48 to 2.83 MPa, See Table 4.2). Figure 4.8 and Table 4.2 present the flexural limits of proportionality obtained from bending mode curves for both cotton linter and flax fiber compounds.

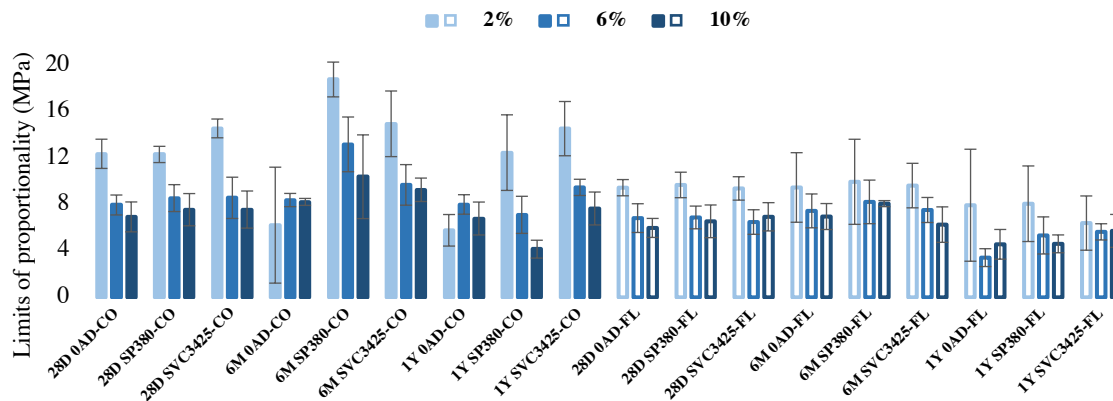


Figure 4.8. The average values of limits of proportionality LOP (MPa) at different curing ages.

Table 4.2. The average values of the limits of proportionality LOP (MPa)

Curing Days	28 Days			6 months			1 year		
	Fiber Content wt.%	2%	6%	10%	2%	6%	10%	2%	6%
Co-0AD	12,38 (1,26)*	7,96 (0,86)	6,93 (1,29)	8,22 (5)	8,39 (0,57)	8,23 (0,3)	5,78 (1,36)	8,01 (0,84)	6,8 (1,42)
Co-SP380	12,32 (0,7)	8,56 (1,16)	7,56 (1,39)	18,79 (1,5)	13,19 (2,36)	10,40 (3,61)	12,48 (0,9)	7,11 (0,83)	4,15 (2,04)
Co-SVC3425	14,57 (0,81)	8,58 (1,78)	7,57 (1,6)	14,96 (2,83)	9,70 (1,75)	9,27 (1,01)	14,55 (5,2)	9,48 (1,43)	7,66 (0,48)
FL-0AD	9,45 (0,7)	6,83 (1,24)	5,98 (0,82)	9,47 (3)	7,45 (1,46)	6,97 (1,12)	7,94 (4,83)	3,42 (0,77)	4,58 (1,28)
FL-SP380	9,69 (1,1)	6,89 (0,98)	6,55 (1,41)	9,96 (3,67)	8,23 (1,88)	8,08 (0,26)	8,07 (3,26)	5,34 (1,6)	4,62 (0,77)
FL-SVC3425	9,39 (1,01)	6,49 (1,06)	6,94 (1,22)	9,64 (1,92)	7,53 (1,08)	6,27 (1,53)	6,40 (2,34)	5,64 (0,7)	5,73 (1,42)

\* Values in parentheses are standard deviation.

Three-point bending load–deflection typical curves obtained for flax fiber specimens are shown in [Figures 4.5, 4.6 and 4.7](#). As can be seen a notable difference in the curves form of flax compounds are observed. It was found that, a decreased trend was observed with time in all categories. 0AD-FL compounds exhibited a decrease of (16%, 50% and 24% for 2%, 6% and 10%VF respectively) at 28D to 1Y with lowest LOP means ranging from 4,58 to 7,94 MPa among others. This trend was also observed in other categories SP380/SVC3425-FL. At 1Y, remarkable decreased means was observed in both compound types compared to 28D specimen counterparts, with SVC3425-FL performing better behavior after 1Y. SP380-FL exhibited a reduction of (17%, 23% and 30% for 2%, 6% and 10%VF respectively at 28D to 1Y with means ranging from 4,62 to 9,96 MPa, See [Table 4.2](#)). Whereas SVC3425-FL exhibited a reduction of (32%, 13% and 42% for 2%, 6% and 10%VF respectively at 28D to 1Y with means ranging from 5,64 to 9,39 MPa, the standard deviations varied from 0.7 to 2.34 MPa, See [Table 4.2](#)).

The post LOP range was characterized by a multiple cracking formation in compounds reinforced with 6%-10%VF at 1Y hydration. The failure of the cotton linter composites occurred after a mid-span deflection around 0,37-0,33 mm for 6%-10%VF respectively for (0AD-CO), 0,23-0,41 mm for 6%-10%VF respectively for (SP380-CO) and 0,20-0,27 mm for 6%-10%VF respectively for (SVC3425-CO). The failure of the flax fiber composites occurred after a mid-span deflection around 0,34-0,51 mm for 6%-10%VF respectively for (0AD-FL), 0,43-0,17 mm for 6%-10%VF respectively for (SP380-FL) and 0,23-0,30 mm for 6%-10%VF respectively for (SVC3425-FL). Failure of the both compounds were followed by a flexural-softening response in compounds with 6%VF due to the localization and widening of the existing cracks while in compounds with 10%VF the failure were followed by a flexural-hardening response.

Modulus of rupture (MOR) means were in the same range for both compound types. At 1Y hydration cotton linter compounds exhibited (9,48 and 8,22 MPa for SVC3425 (6%-10%CO respectively) whereas flax compounds exhibited (6,73 and 6,69 MPa for SVC3425 (6%-10%FL respectively), with cotton linter performing better results, but the energy absorption capacity (toughness) was approximately 50% higher for flax fiber composites.

#### 4.1.3. Modulus of rupture (MOR)

[Figure 4.9](#) and [Table 4.3](#) present the flexural modulus of rupture obtained from bending mode curves for both cotton linter and flax fiber compounds. It was found that the cotton linter specimens hydrated for 6M exhibited higher MOR means comparing to 28D and 1Y counterpart compounds, (the means are significantly increased for both compound types with additive incorporation). The 0AD-CO exhibited a decrease of 25% from (12,38 MPa for 2%VF to 9,28 MPa for 10%VF, See [Table 4.3](#)) in their means when the VF content was increased at 28D. This trend was also observed for SP380/SVC3425-CO, which exhibited decrease of 23% and 30% respectively. At 6M hydration, both compounds of SP380/SVC3425 with 10%VF exhibited a slight increase in MOR means of 32% and 8% respectively compared to their counterpart specimens at 28D. The 0AD-CO exhibited a retained means for 6%-10%VF compounds. At 1Y hydration, there were no significant changes (a decline of 19% from 9,23 to 7,47 MPa) in MOR of 0AD-10%CO compared to 6M hydration. The compounds with SP380/SVC3425-10%VF exhibited a reduction of 36% and 25% respectively, (from 13,79 to 8,86 MPa for SP380-CO and from 10,95 to 8,22 MPa for SVC3425-CO) with SVC3425 performing better among others with sufficient and sustained means. The compound exhibited the average MOR ranged from 8,22 to 14,55 MPa at 1Y. (the standard deviations varied from 0.15 to 4.25 MPa, See [Table 4.3](#)).

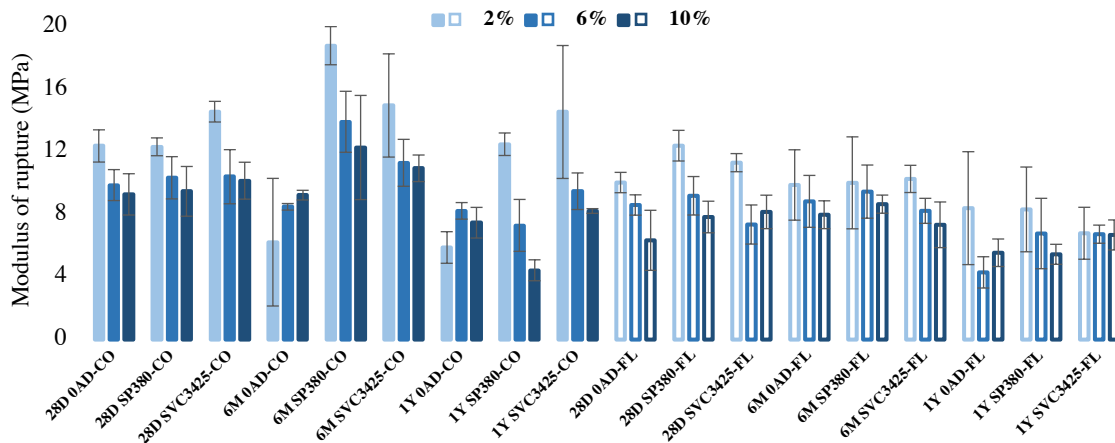


Figure 4.9. The average values of modulus of rupture MOR (MPa) at different curing ages.

Table 4.3. The average values of the modulus of rupture MOR (MPa)

Curing Days	28 Days			6 months			1 year		
Fiber Content wt. %	2%	6%	10%	2%	6%	10%	2%	6%	10%
Co-0AD	12,38 (ab) (1,03)*	9,87 (bcdef) (0,99)	9,28 (bcdef) (1,32)	8,35 (abcd) (4,08)	8,48 (ab) (0,21)	<b>9,23 (a)</b> <b>(0,31)</b>	5,78 (b) (1,01)	8,23 (ab) (0,53)	7,47 (b) (0,98)
Co-SP380	12,32 (abc) (0,57)	10,34 (bcde) (1,35)	9,47 (bcdefg) (1,59)	<b>18,79 (a)</b> <b>(1,22)</b>	13,92 (abc) (1,95)	13,79 (a) (3,33)	12,48 (ab) (0,72)	8,26 (ab) (1,66)	8,86 (ab) (0,67)
Co-SVC3425	<b>14,57 (a)</b> (0,66)	<b>10,41 (bcde)</b> (1,73)	<b>10,15 (bcde)</b> (1,18)	<b>17,22 (a)</b> (3,3)	<b>11,30 (bcd)</b> (1,5)	<b>10,95 (bcd)</b> (0,85)	<b>14,55 (a)</b> (4,25)	<b>9,48 (ab)</b> (1,17)	<b>8,22 (ab)</b> (0,15)
FL-0AD	10,04 (bcdefg) (0,65)	8,60 (defgh) (1,43)	6,34 (efghi) (1,92)	11,10 (bcd) (2,25)	8,83 (d) (1,66)	7,98 (d) (0,89)	8,40 (b) (3,61)	8,59 (ab) (1)	5,55 (b) (0,88)
FL-SP380	12,39 (abc) (0,98)	9,19 (cdefg) (1,23)	7,83 (efghi) (1,01)	10,02 (cd) (2,94)	9,46 (bcd) (1,7)	8,65 (d) (0,58)	8,32 (b) (2,71)	6,78 (b) (2,25)	5,45 (b) (0,64)
FL-SVC3425	11,31 (abcd) (0,58)	7,35 (efghi) (1,25)	8,16 (defghi) (1,07)	10,27 (bcd) (0,87)	8,23 (d) (0,8)	7,33 (d) (1,46)	6,79 (b) (1,66)	6,73 (b) (0,58)	6,69 (b) (0,96)

For the same system containing the same kind of coupling agent, means with the same letter for each property are not significantly different at the 5% significance level. \* Values in parentheses are standard deviations and Analysis of variance (Anova results)

On the other hand, It was found that the flax fiber compounds exhibited higher MOR means at 6M (in compounds with higher fiber content) comparing to 28D and 1Y counterpart compounds, (however, there is a minor influence on MOR with the additive incorporation), the MOR average values ranged from 7,33 to 11,10 MPa. The both 0AD/SP380-FL compounds exhibited a reduction of 37% in MOR means at 28D when VF content was increased, (10,04 MPa for 2%VF to 6,34 MPa for 10%VF) and (12,39 MPa for 2%VF to 7,83 MPa for 10%VF) respectively, See Table 4.3. This reduction rate was lower for SVC3425-CO mixture at 28D, which exhibited a reduction of 28%, performing better among others. At 1Y hydration, the both 0AD/SP380-10%FL content exhibited higher reduction rate in their MOR values (30% reduction from 7,98 to 5,55 MPa) and (37% reduction from 8,65 to 5,45 MPa) respectively, compared to 6M hydrated counterpart specimens. While SVC3425-10%VF exhibited a minor reduction of 9% (from 7,33 to 6,69 MPa) performing better behavior among others with time, with sufficient and sustained MOR means for some application. (the standard deviations varied from 0.58 to 1.66 MPa, See Table 4.3). From these results, it can be deduced that the addition of superplasticizer in both cotton linter and flax fiber compounds led to a more balanced performance in compounds with time, as the lowest LOP and MOR averages were obtained by 0AD (reference compounds). In final due the high dispersion of MOR averages these results were assessed for analysis of variance (ANOVA test), which compared the means in (VF type-content and curing times categories at 28D, 6M and 1Y). The Tukey test exhibited significant difference in VF type and curing time categories, but no remarkable differences were observed for applied VF ranges of 2%, 6% and 10% in both fiber type (See Table 4.3).

Figure 4.10 depicts effect of cotton linter and flax fibers with two types of additives (SP380/SVC3425) on the post-cracking load carrying capacity in the CAC-based (low alkaline matrix) VFRCCs. Stated previously, the first crack of both matrix presented reduction and increase for both short fiber (cotton linter fiber) and long fiber (flax fiber) in different hydration stages. In relation with the post-crack strength, it can be seen that the addition of long fibers, *flax fibers* increased the post-cracking load-carrying capacity of the composites. An interesting behavior can be observed in the load-deflection curves of this compounds (See Figure 4.5, 4.6 and 4.7).

A FCS deflection of about 0,30-0,50 mm the load-carrying capacity of the composites reached up to a deflection around 6.00 mm at 28D, 6M and 1Y. A ductile (Strain-softening-behavior in compounds with 6% VF content), and (an elastic-behavior in compounds with 10% VF content) which was mildly decreased with time. This can be attributed to the presence of flax fibers (6%-10%VF contents) the load is supported by the sufficient modulus of elasticity of flax fibers which can keep up to 90% or more of the composite *Post Crack Strength* at deflections as high as 4,0 to 6,0 mm.

On the other hand, 2%FL compound even as lowest fiber content exhibited interesting post-cracking behavior (Strain-softening behavior with multiple wide cracks at 28D and 6M (See Figure 4.6, 4.7). The interesting behavior of these mixtures shows the benefits of the *flax fibers* on the retained strength and toughness of the composites in all hydration categories.

Thus it can be deduced that the addition of long flax fibers in such composites led to an increase in the post-crack deflection (toughness) with the sufficient First/Post-crack strength reaching values of the same magnitude of the first crack strength in compounds with 10% VF even after 1Y hydration stage.

On the other hand, in relation with the post-crack strength of cotton linter compounds, it can be seen that the addition of short fibers, increased the post-cracking load-carrying capacity of the composites only with higher fiber contents of 6%-10% VF wt. Interesting behavior can also be observed in the load-deflection curves of these compounds (See Figure 4.2, 4.3 and 4.4). A FCS deflection of about 0,25-0,60 mm the load-carrying sufficient capacity of the composites reached up to a deflection around 1.50, 2,50 and 3,50 mm at 28D, 6M and 1Y. Likewise, a ductile (Strain-softening-behavior in both compounds with 10% VF content), and (Strain-softening behavior with multiple wide cracks in compounds with 6% VF content) which was mildly decreased with time after 1Y hydration stage.

This can be attributed to the presence of cotton linter fibers in compounds which the load is supported by the sufficient modulus of elasticity which can keep up to 30% to 40% of the composite First Crack Strength at deflections around 1,0 to 1,5 mm. These results show the benefits of the 6%-10%VF of cotton linter fiber led to a fairly good Strain-softening behavior at 28D, although with a gentle reduction with time in strength but with retained toughness (*even after 6M-1Y hydration stages, this can be observed clearly in Figures 4.2, 4.3 and 4.4*).

Therefore, it can be deduced that the addition of short cotton linter fiber in such composites led to a sufficient post-crack deflection and strength after 1Y hydration for some construction applications. In general, it was observed a superior number of post-cracks with lower crack width for the flax fiber composites in comparison to the cotton linter composites (*when the VF content was increased up to 10% wt.*). This behavior of flax fiber may indicate the higher bond strength for this composite therefore, resulting in a stiffer Post-Crack regions.

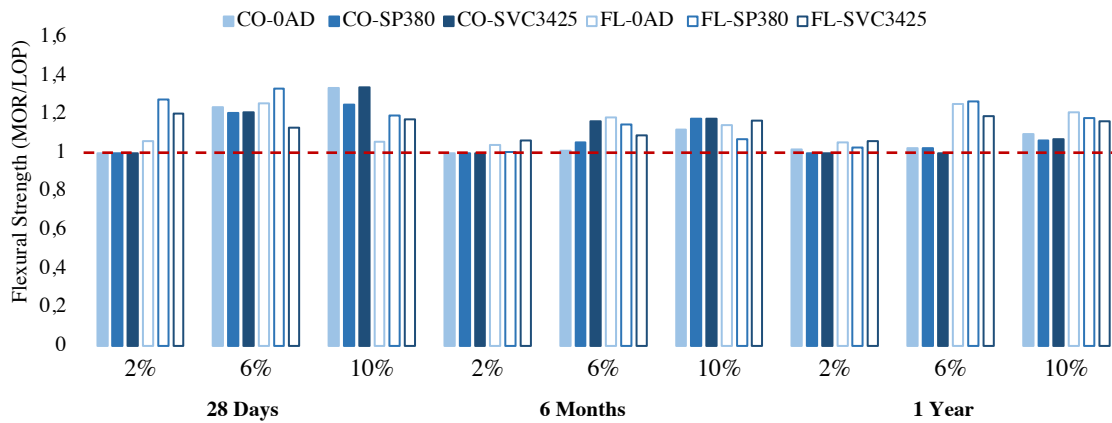


Figure 4.10. Effect of cotton linter/flax fibers on the post-cracking load carrying capacity of the VFRCs.

4.1.4. Specific Energy (SE)

The toughness was calculated as the area under the load vs. displacement curves presented for both composite systems depicted in Figures 4.2 to 4.7. The flexural specific energy absorption (SE, Toughness) obtained from bending mode curves for both cotton linter and flax fiber compounds are presented in Figure 4.11 and Table 4.4. As can be seen, there is a remarkable difference in toughness of both compound systems, flax fiber composites presented toughness triple as high as those of cotton linter composites. However, both compounds exhibited reduction in their toughness with time. Previously stated, the toughness of the long flax fiber composites can be considerably increased leading to a load capacity of 40 to 90% of composite’s first crack strength reaching to 6.0 mm deflections while the cotton linter fiber composite has already failed at lower deflections. Cotton linter compounds with 10%VF content, exhibited toughness means ranging from 4,98 to 22,37 kJ/m<sup>2</sup>, whereas flax fiber compounds with 10%VF content, exhibited means ranging from 17,19 to 38,90 kJ/m<sup>2</sup> at 28D to 1Y hydration, See Table 4.4). The ultimate highest toughness (kJ/m<sup>2</sup>) obtained at 1Y hydration for flax/cotton linter fiber composites with 10%VF content, were 28.75 and 9.92 kJ/m<sup>2</sup> respectively. With SVC3425 performing better in both compound system among others. These results indicates that by incorporating (long or short) cotton linter and flax fibers into a CAC matrix a high strength and tough material can be obtained becoming a promising material for the industrial production of vegetable fiber cement products.

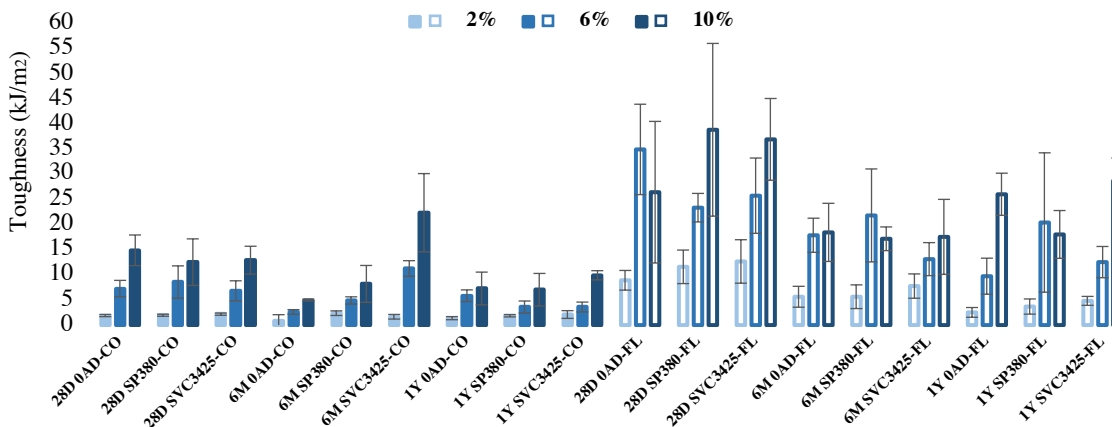


Figure 4.11. The average values of specific energy SE (kJ/m<sup>2</sup>) at different curing ages.

**Table 4.4.** The average values of the toughness, specific energy SE (kJ/m<sup>2</sup>)

Curing Days	28 Days			6 months			1 year		
	Fiber Content wt. %	2%	6%	10%	2%	6%	10%	2%	6%
Co-0AD	1.90 (0.22)*	7.27 (1.64)	14.90 (3.05)	0.81 (1.26)	2.62 (0.46)	4.98 (0.19)	1.38 (0.31)	5.85 (1.16)	7.29 (3.26)
Co-SP380	1.96 (0.2)	8.58 (3.22)	12.53 (4.64)	2.37 (0.46)	4.91 (0.72)	8.21 (3.67)	1.86 (0.23)	3.60 (1.2)	7.05 (3.24)
Co-SVC3425	2.18 (0.22)	6.82 (2)	12.93 (2.77)	1.66 (0.46)	11.27 (1.56)	22.37 (7.8)	2.10 (0.77)	3.60 (0.98)	9.92 (0.92)
FL-0AD	8.92 (1.96)	34.99 (9)	26.47 (14.1)	5.64 (2.08)	17.89 (3.4)	18.46 (5.79)	2.53 (0.97)	9.73 (3.59)	26.05 (4.2)
FL-SP380	11.60 (3.34)	23.39 (2.84)	38.90 (17.2)	5.65 (2.36)	21.84 (9.26)	17.19 (2.36)	3.69 (1.51)	20.4 (13.88)	18.06 (4.76)
FL-SVC3425	12.67 (4.33)	25.77 (7.5)	36.99 (8.14)	7.77 (2.42)	13.13 (3.29)	17.57 (7.47)	4.82 (0.89)	12.55 (3.11)	28.74 (4.55)

\* Values in parentheses are standard deviation

## 4.2. DURABILITY OF COMPOSITE MATERIALS

In this section, the results obtained from the experimental characterization of the flexural strength by means of three-point bending tests are presented. The flexural stress-displacement curves derived for the tested composites, and the values of Modulus of Elasticity (MOE), Limits of Proportionality (LOP), Modulus of Rupture (MOR), and Specific Energy (SE) are computed and compared. The specimen groups are revealed the sets from 2%, 6% and 10% of VFs wt. with two different additives incorporated and a reference specimen with no additive incorporation (0AD) cured for 28 days (Unaged), 28D+Subjected to 10 accelerated aging cycle (Aged). The graphs exhibit the dependency of flexural strength and toughness for unaged-aged compounds, reinforced with distinct VF type and content ((FL) Flax fiber - (CO) Cotton linter fiber) and different additives (SP380-SVC3425) are considered.

Figures 4.13, 4.14 and 4.15 present the flexural stress-displacement relationships obtained for cotton linter fiber-0AD (0AD-CO), cotton linter fiber-SP380 (SP380-CO) and cotton linter fiber-SVC3425 (SVC3425-CO), respectively. Figures 4.16, 4.17 and 4.18 present the flexural stress-displacement relationships obtained for flax fiber-0AD (0AD-FL), flax fiber-SP380 (SP380-FL) and flax fiber-SVC3425 (SVC3425-FL), respectively, for unaged and aged compounds.

### 4.2.1. Modulus of elasticity (MOE)

Figure 4.12 and Table 4.5 present the flexural modulus of elasticity obtained from bending mode curves for both cotton linter and flax fiber compounds. The flexural stress-displacement relationships are shown in Figures 4.13, 4.14 and 4.15 for unaged and aged cotton linter fiber compounds, and Figures 4.16, 4.17 and 4.18 for unaged and aged flax fiber compounds. (Stated previously, the initial stress-deflection response is linear elastic zone which in this linear range the response is dominated by the matrix/VFs).

In this context, the both compound system (Unaged cotton linter and flax fiber compounds) exhibited sufficient stiffness (MOE), and fairly good first crack strain capacity (LOP) before aging cycles, with cotton linter compounds performing better compared to flax fiber compounds (See Figure 4.12 and Table 4.5). However, in both compound type there is a reduction trend in stiffness means after being subjected to 10 accelerated aging cycles.

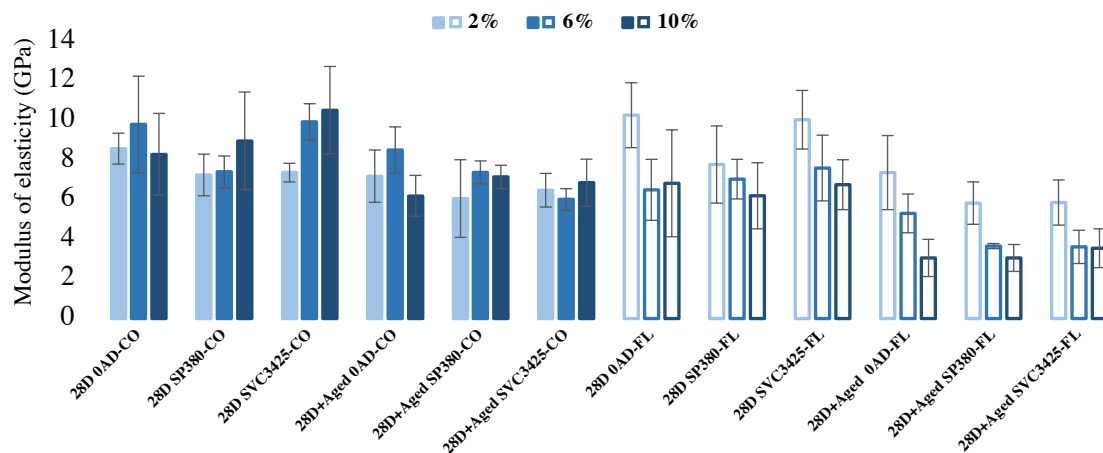


**Figure 4.12.** The average values of Modulus of elasticity MOE (GPa) for unaged and Aged composites.

**Table 4.5.** The average values of modulus of elasticity MOE (GPa)

Curing Days	Unaged			Aged			
	Fiber Content wt.%	2%	6%	10%	2%	6%	10%
Co-0AD		8,58 (0,78)	9,80 (2,44)	8,30 (2,06)	7,19 (1,32)*	8,51 (1,17)	6,20 (1,03)
Co-SP380		7,25 (1,05)	7,41 (0,80)	8,97 (2,47)	6,06 (1,96)	7,38 (0,58)	7,15 (0,59)
Co-SVC3425		7,37 (0,47)	9,93 (0,92)	10,52 (2,21)	6,48 (0,85)	6,01 (0,55)	6,86 (1,19)
FL-0AD		10,27 (1,64)	6,50 (1,54)	6,83 (2,70)	7,37 (1,87)	5,31 (0,98)	3,06 (0,94)
FL-SP380		7,78 (1,95)	7,04 (1,00)	6,20 (1,67)	5,83 (1,07)	3,67 (0,13)	3,06 (0,68)
FL-SVC3425		10,04 (1,48)	7,60 (1,66)	6,76 (1,26)	5,86 (1,14)	3,62 (0,84)	3,55 (0,98)

\* Values in parentheses are standard deviation

Shown in Figures 4.13 to 4.10, the linear relationship before LOP is steeper at 28D, but the incline is dropped after aging cycles. Stiffness of the both cotton linter/flax fiber reinforced compounds are sufficiently high to keep the newly formed cracks from widening, however, in some specimens the crack widening is appeared. (See Figures 4.15, 4.16 in cotton linter-6%VF cured for 28D, and Figures 4.17, 4.18 in flax fiber compounds 2%-6%VF wt. cured for 28D). Figure 4.12 and Table 4.5 shows the MOE means are increased when VF content was increased in both unaged-aged categories of cotton linter compounds. While flax fiber compounds exhibited an opposite trend. Means of aged cotton linter compounds exhibit a reduction of 13% to 25% ranged from 6,20 to 8,51 GPa for reference, with 20% reduction ranged from 6,06 to 7,38 GPa for SP380-CO (*this compound retained its mean with 6%VF wt.*). SVC3425-CO means were ranged from 6,01 to 6,86 GPa after wet/dry cycles, with a reduction of 35% from (10,52 to 6,86 GPa) for 10%FV content. On the other hand, both aged SP30/SVC3425-10%CO exhibited 14% - 10% improved means of 7,15 to 6,86 GPa respectively, compared to reference (See Table 4.5). This indicating the effectiveness (*however, insignificant*) of the incorporation of superplasticizers in CAC matrix. Aged flax fiber compounds exhibited an opposite trend, where the means were reduced with increased VF content. Aged 0AD-FL ranged from 3,06 to 7,37 GPa and revealed about 19% to 55% reduction after wet/dry cycles. Likewise, both SP30/SVC3425-FL compounds experienced around 50% reduction after cycles, with means ranged from 3,06 to 5,83 GPa and 3,55 to 5,86 GPa respectively (See Table 4.5).

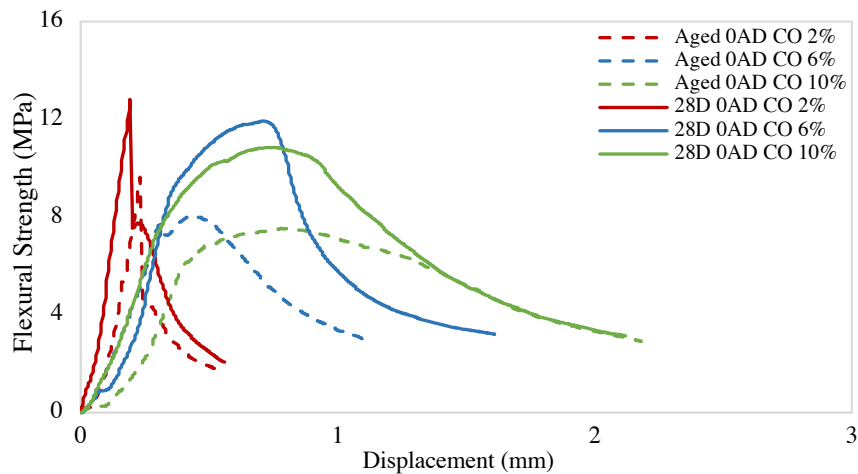


**Figure 4.13.** Flexural stress – displacement relationships for the cotton linter fiber-0AD composites at 28D and aged specimens.

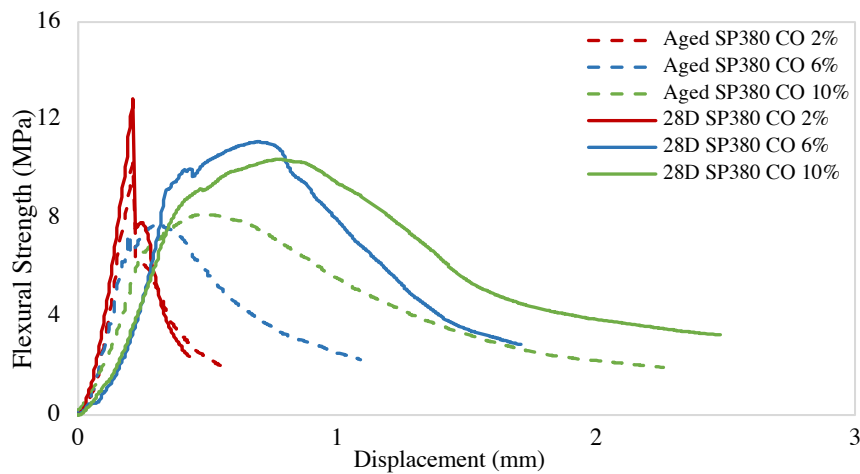


**Figure 4.14.** Flexural stress – displacement relationships for the cotton linter fiber-SP380 composites at 28D and aged specimens.

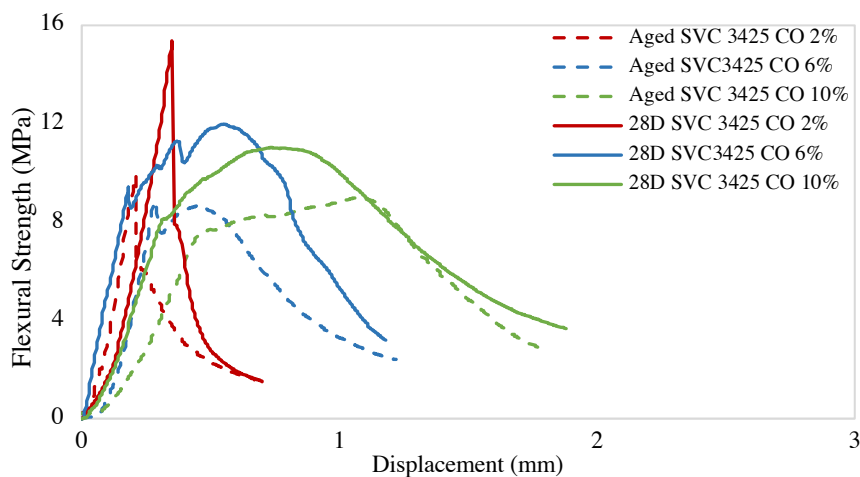


**Figure 4.15.** Flexural stress – displacement relationships for the cotton linter fiber-SVC3425 composites at 28D and aged specimens.

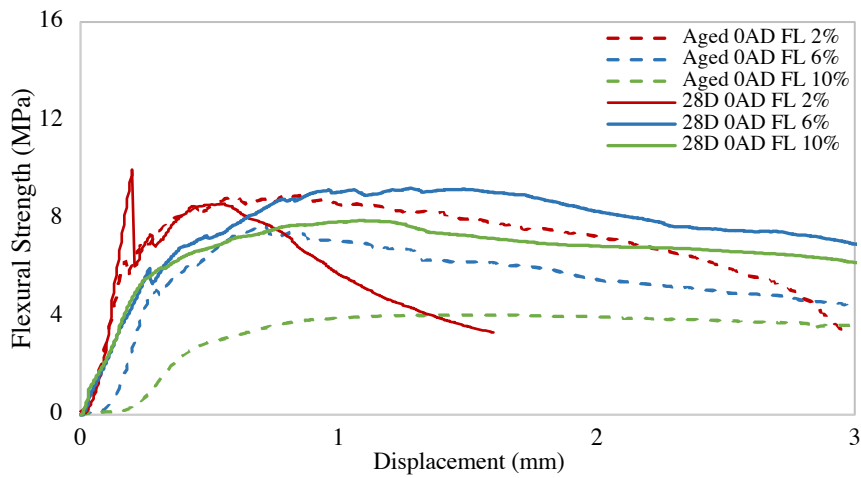


**Figure 4.16.** Flexural stress – displacement relationships for the flax fiber-OAD composites at 28D and aged specimens.

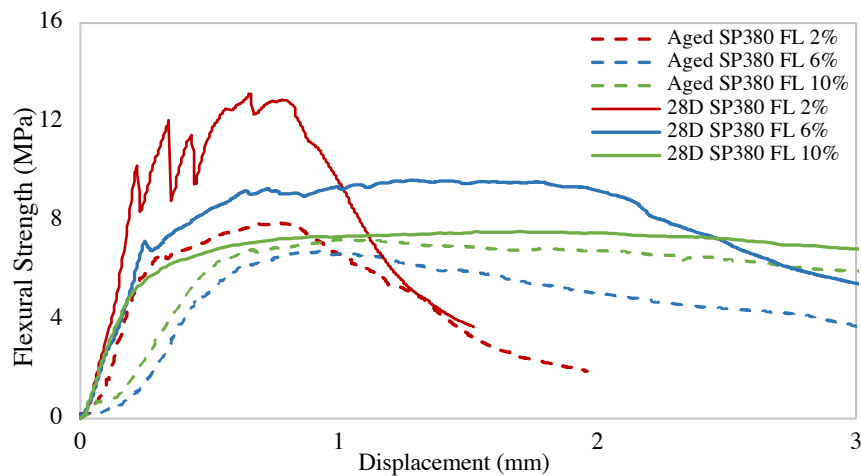


**Figure 4.17.** Flexural stress-displacement relationships for the flax fiber-SP380 composites at 28D and aged specimens.

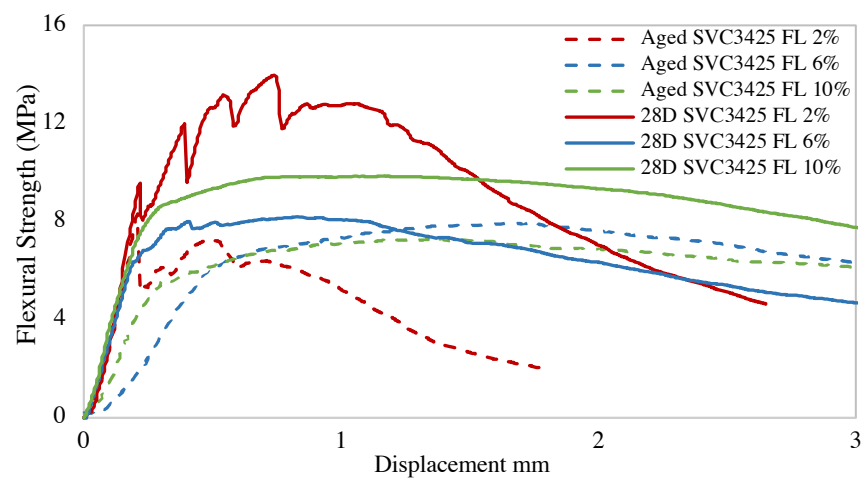


**Figure 4.18.** Flexural stress-displacement relationships for the flax fiber-SVC3425 composites at 28D and aged specimens.

#### 4.2.2. Limit of proportionality (LOP)

Three-point bending load–deflection typical curves obtained for unaged-aged cotton linter specimens are shown in Figures 4.13, 4.14 and 4.15. In general, it can be observed that the first crack strength (FCS) of the specimens was decreased up to 30% in compounds with 2%VF contents after being subjected to wet/dry cycles, while the compounds with higher fiber contents of 6%-10% VF wt. almost retained their FCS.

The specimens with 6%-10% VF wt. presented fairly good ductile behavior which was drastically decreased by the aging process (See Figure 4.19). It is important to observe that the deterioration in the all composites toughness was lower in compounds with higher FV contents, even after 10 cycles of wetting and drying.

In this context, aged cotton linter reference mixture exhibited around 7% of reduction from (6,93 to 6,51 MPa for 10% VF content, See Table 4.6) in their FCS means. The same trend was also observed in both aged SP380/SVC3425-10%CO compounds, exhibiting decrease of 9% and 5% respectively, with SVC3425 performing better FCS among others. Both compounds with 10%VF (*cotton linter fiber*) and incorporated SP380/SVC3425 in their matrix exhibited slightly higher LOP means of 5% and 10% respectively, compared to reference specimens after aging cycles. with SVC3425-10%CO performing slightly higher FCS (7,17 MPa) in this category after wet/dry cycles. (This category is highlighted as an optimum mixture of the durability stage, the standard deviations are varied from 0.80 to 1.16 MPa, See Table 4.6).

On the other hand, flax fiber compounds exhibited slightly lower FCS compared to cotton linter compounds (See Figure 4.19). Similarly here, a higher reduction in compounds with 2%VF was observed, however, LOP means for 6%-10%VF wt. compounds also was decreased. There is a significant reduction of (about 20% from 5,98 to 4,86 MPa) in FCS of reference compound with 10%VF after aging cycles. Whereas, the both aged SP380/SVC3425-10%FL wt. exhibited lower reduction rate, both about 13% in their FCS average with 5,71 to 6,00 MPa respectively, with SVC3425-10%FL wt. performing slightly higher FCS in this category as well.

Figure 4.19 and Table 4.6 present the flexural limits of proportionality obtained from bending mode curves for both cotton linter and flax fiber compounds.

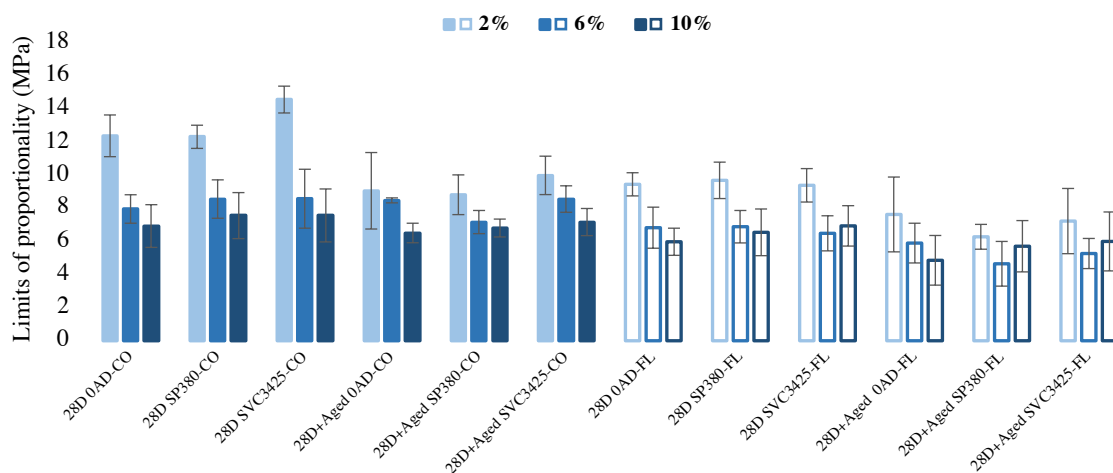


Figure 4.19. The average values of limits of proportionality LOP (MPa) for unaged-aged composites.

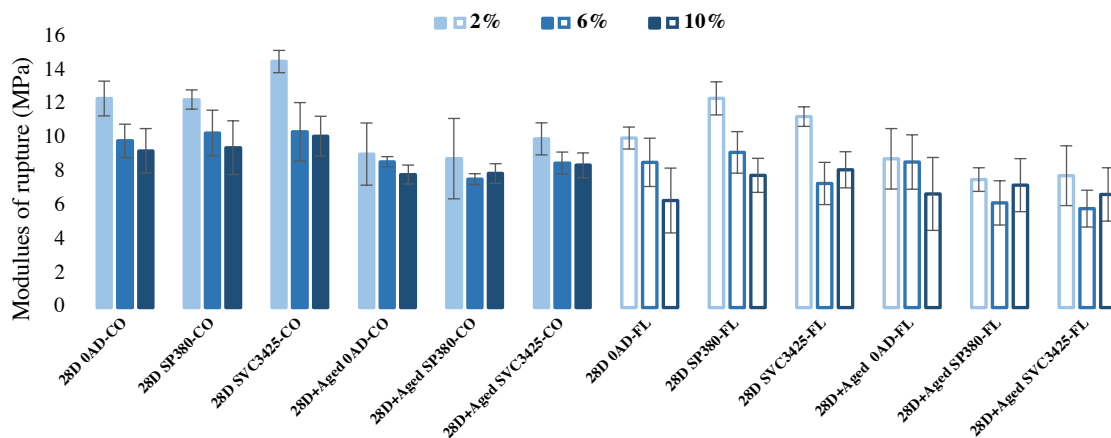
**Table 4.6.** The average values of limits of proportionality LOP (MPa)

Curing Days	Unaged			Aged			
	Fiber Content wt.%	2%	6%	10%	2%	6%	10%
Co-0AD		12,38 (1,26)*	7,96 (0,86)	6,93 (1,29)	9,06 (2,31)	8,48 (0,15)	6,51 (0,59)
Co-SP380		12,32 (0,7)	8,56 (1,16)	7,56 (1,39)	8,82 (1,2)	7,17 (0,7)	6,81 (0,54)
Co-SVC3425		<b>14,57 (0,81)</b>	<b>8,58 (1,78)</b>	<b>7,57 (1,6)</b>	<b>9,99 (1,16)</b>	<b>8,56 (0,8)</b>	<b>7,17 (0,82)</b>
FL-0AD		9,45 (0,7)	6,83 (1,24)	5,98 (0,82)	7,63 (2,26)	5,90 (1,2)	4,86 (1,5)
FL-SP380		9,69 (1,1)	6,89 (0,98)	6,55 (1,41)	6,28 (0,75)	4,65 (1,35)	5,71 (1,55)
FL-SVC3425		9,39 (1,01)	6,49 (1,06)	6,94 (1,22)	7,23 (1,97)	5,27 (0,91)	6,00 (1,78)

\* Values in parentheses are standard deviation

#### 4.2.3. Modulus of rupture (MOR)

Figures 4.20 and Table 4.7 present the flexural modulus of rupture (MOR) obtained from bending mode curves for both cotton linter and flax fiber compounds. Three-point bending load–deflection typical curves obtained for unaged-aged cotton linter specimens are shown in Figures 4.13, 4.14 and 4.15. It can be observed that non-aged cotton linter specimens with 6%-10%VF presented a ductile (Strain-Softening) behavior which was mildly decreased by the aging process (See Figures 4.13, 4.14 and 4.15). The post-crack strength (PCS) of reference specimens was decreased up to 13% to 15% in compounds with 6%-10%VF wt.% after aging cycles (See Table 4.7). For example, values of PCS in non-aged reference was ranging from 12.38 to 9.28 MPa, which PCS decreased from 9.06 to 7.88 MPa for 6%-10%VF wt.% respectively. And a reduction of 27% and 18% occur in compounds of SP380/SVC3425-6%VF respectively. This reduction, however, was lower in SP380/SVC3425-10%CO compounds with around 17% for both mixtures, with SVC3425 performing better among others. On the other hand, it was observed that the non-aged specimens presented a multiple-cracking behavior under bending loads, while the specimens submitted to cycles of wetting and drying presented a single crack formation (this was evident in compounds with 6% VF content, See Figure 4.14 and 4.15). It is important to observe that the deterioration in the composite's toughness is insignificantly affected by cycles of wetting-drying, this will be discussed further in coming section.

**Figure 4.20.** The average values of modulus of rupture MOR (MPa) for unaged-aged composites.

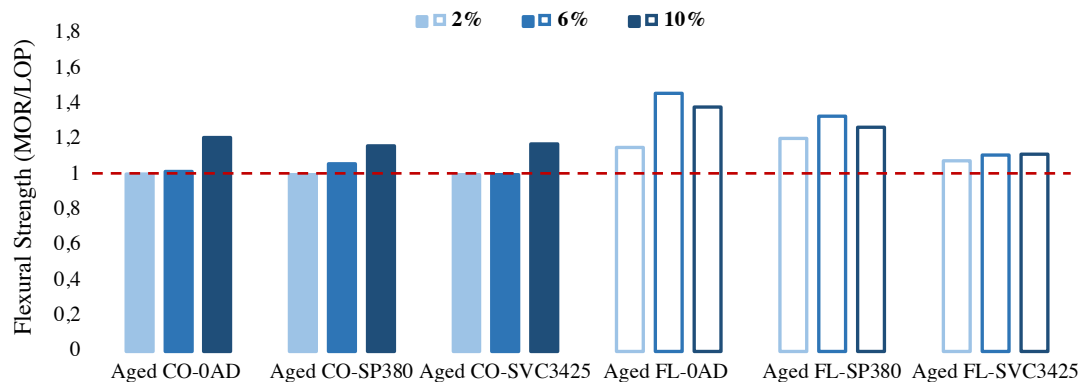
**Table 4.7.** The average values of modulus of rupture MOR (MPa)

Curing Days	Unaged			Aged			
	Fiber content wt. %	2%	6%	10%	2%	6%	10%
Co-0AD		12,38 (ab) (1,03)*	9,87 (bcdef) (0,99)	9,28 (bcdef) (1,32)	9,06 (bcde) (1,84)*	8,64 (defgh) (0,30)	7,88 (defghi) (0,54)
Co-SP380		12,32 (abc) (0,57)	10,34 (bcde) (1,35)	9,47 (bcdefg) (1,59)	8,82 (bcde) (2,38)	7,61 (efghi) (0,32)	7,94 (efghi) (0,42)
Co-SVC3425		14,57 (a) (0,66)	10,41 (bcde) (1,73)	10,15 (bcde) (1,18)	9,99 (bcdef) (0,95)	8,56 (defghi) (0,65)	8,42 (defghi) (0,71)
FL-0AD		10,04 (bcdefg) (0,65)	8,60 (defgh) (1,43)	6,34 (efghi) (1,92)	8,81 (defghi) (1,79)	8,62 (efghi) (0,82)	6,73 (fghi) (1,62)
FL-SP380		12,39 (abc) (0,98)	9,19 (cdefg) (1,23)	7,83 (efghi) (1,01)	7,58 (efghi) (0,76)	6,20 (hi) (0,91)	7,25 (efghi) (1,07)
FL-SVC3425		11,31 (abcd) (0,58)	7,35 (efghi) (1,25)	8,16 (defghi) (1,07)	7,81 (defghi) (1,77)	5,86 (ghi) (1,09)	6,70 (fghi) (1,47)

For the same system containing the same kind of coupling agent, means with the same letter for each property are not significantly different at the 5% significance level. \* Values in parentheses are standard deviation

Three-point bending load–deflection typical curves obtained for unaged-aged flax fiber specimens are shown in Figures 4.16, 4.17 and 4.18. It can be observed that non-aged flax fiber specimens with 6%-10%VF presented a ductile behavior; (Strain-Softening behavior and multiple cracking for 6%VF compound), and (almost elastic behavior with single crack for 10%VF compounds with SP380/SVC3425) which was gently decreased by the aging process (See Figures 4.16, 4.17 and 4.18), (Figure 4.21). It is important to observe that in contrast with the cotton linter compounds, the non-aged SP380/SVC3425-2%FL compounds exhibited a ductile (Strain-softening behavior with multiple wide cracking) which PCS values were affected drastically by wetting-drying cycles. (Figures 4.17 and 4.18), (Figure 4.21). On the other hand, the post-crack strength (PCS) of reference specimens retained their PCS values in compounds with 6%-10%VF after aging cycles (See Table 4.7). While a reduction of 33% and 8% occur in compounds of SP380 with 6%-10%VF respectively. This reduction in SVC3425/6%-10%FL compounds was around 20% for both mixtures, with SP380-10%FL performing better among others with 7,25 MPa for MOR (See Table 4.7). It is important to note that the deterioration in the composite's toughness was not significantly affected by cycles of wetting-drying.

In final due the high dispersion of MOR averages the results were assessed for analysis of variance (ANOVA), which compared the means in (VF type-content in unaged and aged compounds). Tukey test exhibited differences in VF *type* and in both *aged- unaged* categories, but no remarkable differences were observed for VF *content* ranges of 2%, 6% and 10% wt.% in both categories. (See Table 4.7 the values in parentheses).

**Figure 4.21.** Effect of aging cycles on the post-cracking load carrying capacity of the VFRCCs.

#### 4.2.4. Specific energy absorption (SE)

Stated previously, the toughness was calculated and computed as the area under the load vs. displacement curves presented for both composite systems depicted in Figures 4.13 to 4.18. The flexural specific energy absorption (SE, *Toughness*) obtained from bending mode curves for both unaged-aged cotton linter-flax fiber compounds are presented in Figure 4.22 and Table 4.8. There is a significant difference in toughness of both systems, flax fiber composites presented toughness of triple as high as those of cotton linter composites. Although a reduction in their toughness was observed after aging cycles. The toughness of the long flax fiber composites can be considerably increased leading to a load capacity of 40% to 90% of composite's FCS reaching to 6.0 to 8.00 mm deflections with sufficient PCS. In this context, the cotton linter fiber composite has already failed at very lower deflections, however, with higher FCS and MOR values. These compounds with 10%VF exhibited toughness ranging from 2,18 to 12,93 kJ/m<sup>2</sup> before aging cycles, whereas flax compounds with 10%VF exhibited toughness ranging from 12,67 to 36,99 kJ/m<sup>2</sup> before W/D cycles, See Table 4.8). The highest toughness obtained by aged flax-cotton linter fiber composites with 10%VF, were 27.92 kJ/m<sup>2</sup> (reference matrix) and 9.91 kJ/m<sup>2</sup> in SVC3425 matrix respectively. These results indicates that by incorporating (long or short) cotton linter and flax fibers into a CAC matrix a fairly good strength and tough material can be obtained becoming a promising material for the industrial production of vegetable fiber cement products.

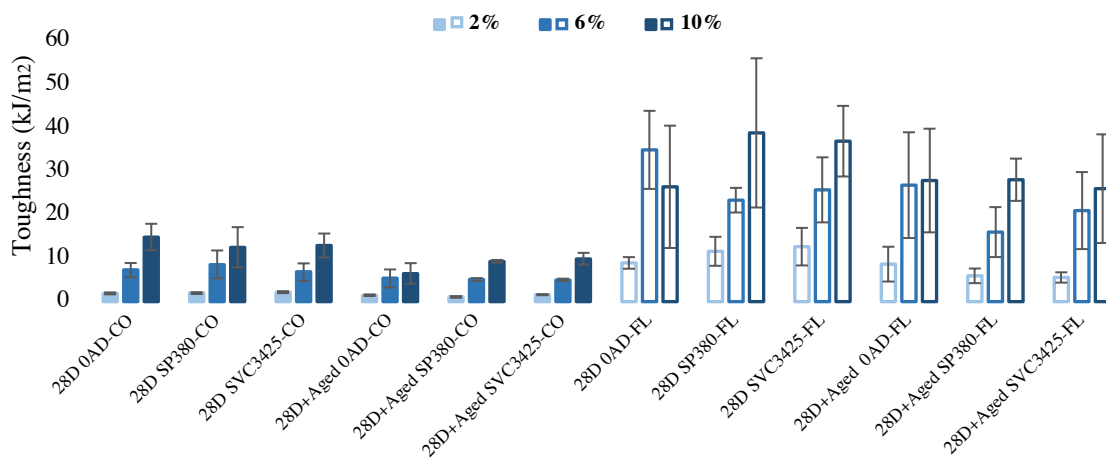


Figure 4.22. The average values of toughness, specific energy SE (kJ/m<sup>2</sup>) for unaged-aged compounds.

Table 4.8. The average values of toughness, specific energy absorption (KJ/m<sup>2</sup>)

Curing Days	Unaged			Aged			
	Fiber content wt.%	2%	6%	10%	2%	6%	10%
Co-0AD		1,90 (0,22)*	7,27 (1,64)	14,90 (3,05)	1,48 (0,18)*	5,34 (2,08)	6,51 (2,36)
Co-SP380		1,96 (0,2)	8,58 (3,22)	12,53 (4,64)	1,08 (0,19)	5,09 (0,33)	9,31 (0,3)
Co-SVC3425		<b>2,18 (0,22)</b>	<b>6,82 (2)</b>	<b>12,93 (2,77)</b>	<b>1,60(0,12)</b>	<b>5,03 (0,26)</b>	<b>9,91 (1,34)</b>
FL-0AD		8,92 (1,96)	34,99 (9)	26,47 (14,1)	8,64 (4,01)	26,85 (12,19)	27,92 (11,95)
FL-SP380		11,60 (3,34)	23,39 (2,84)	38,90 (17,2)	5,95 (1,69)	16,03 (5,76)	28,10 (4,87)
FL-SVC3425		12,67 (4,33)	25,77 (7,5)	36,99 (8,14)	5,57 (1,19)	20,99 (8,88)	26,04 (12,53)

\* Values in parentheses are standard deviation

The obtained results in both 1<sup>st</sup>-2<sup>nd</sup> stages, indicate that the decrease percentage in FCS was higher for specimens containing lower 2%VF content wt. (while compounds with 6%-10%VF contents for instance in the case of cotton linter fiber, compounds retained its FCS) when being subjected to aging cycles. This behavior could be related to a twofold action that combines (1) the lower degradation of the vegetable fibers in (*CAC with lower alkaline medium*) with the aging process and (2) the well-known conversion system reactions that occurs in CAC pastes with time depending on the temperature and humidity of the ambient (K.L. Scrivener, J. Newman, 2003), (K.L. Scrivener, L. Cabiron 1999).

It is also well known that VFs mineralization leads to a complete reduction in its strength and strain capacity (HE Gram 1983), (A. Bentur, S.A.S. Akers 1989), (R.D.T Filho 1997), (H. Savastano, V. Agopyan 1999), (R.D.T Filho, K. Scrivener 2000) and, therefore, it can be considered that this slight reduction in VFRCCs (*to some extent but not completely is due to fiber degradation*) in CAC-based matrix occurs after submitting the specimens to the wetting and drying cycles. On the other hand, it could be related to major extent of the conversion reactions which also can contribute to the decrease of the FCS values, as the hydration reactions of CAC still could be in progress at late stages of hydration, and in results of the porous produced by these reactions could be considered that the main reason of these degradations in composites are due to this issue.

On the one hand, the conversion phases, could also be involved to some extent by VF incorporation in matrix (*due to VF water absorption and an incomplete hydration phases because of low available water*). This claim possibly could be observed by SEM/BSEM results. The preserved mechanical performance of mixtures over the time despite of increased VF% (comparing 28D to 1Y hydration stages), indicates that CAC matrix is less aggressive toward the VFs. However, the understanding of this behavior demands the further and deeper investigations, as the FCS-PCS of the reference specimens have decreased up to 20% with the accelerated aging regime.

#### 4.3. MECHANICAL, CHEMICAL AND MICROSTRUCTURE ANALYSIS OF SILICA FUME-CALCIUM ALUMINATE CEMENT PASTES

##### 4.3.1. Flexural strength performance

In this section, the results obtained from the experimental characterization of the flexural strength by means of three-point bending tests are presented. The flexural stress-displacement graphs derived for the tested composites, and the average values of Modulus of Elasticity (MOE), Modulus of Rupture (MOR) are computed and compared. The specimen groups are revealed the sets from 0%, 5%, 10%, 15% and 20% of Silica Fume (SF) wt. cured for 7 days (7D), 28 days (28D), 56 days (56D).

Figures 4.23 and Table 4.9 present the flexural modulus of elasticity obtained from three point bending mode for CAC-SF mixtures up to 20%SF wt. hydrated for 7, 28 and 56 days. The mixtures exhibited low MOE values at 7D. However, at 28D hydration the means were gently higher than those 7D means. In general, 5%SF matrix achieved a greater means among others at 28D and 56D, although there were insignificant differences with the means of 5%, 15% and 20%SF wt. The 10%SF and the reference matrix (0%SF) exhibited lowest means at 28D.

At 56D, a gentle increase in MOE means of 5%SF and 10%SF wt. matrix were observed, while the reference matrix, 15%SF and 20%SF wt. exhibited a reduction at 56D. In this context, the mixtures at early 7D hydration stage exhibited values ranging from 0,16 to 0,63 GPa, with CAC-15%SF performing higher value among others. The standard deviations varied from 0,009 to 0,06 GPa. Likewise, at 28D the specimens revealed means ranged from 0,75 to 1,13 GPa, the standard deviations varied from 0,03 to 0,12 GPa. At 56D the means ranged from 0,76 to 1,18 GPa, with CAC-5%SF performing higher value among others. The standard deviations varied from 0,01 to 0,23 GPa.

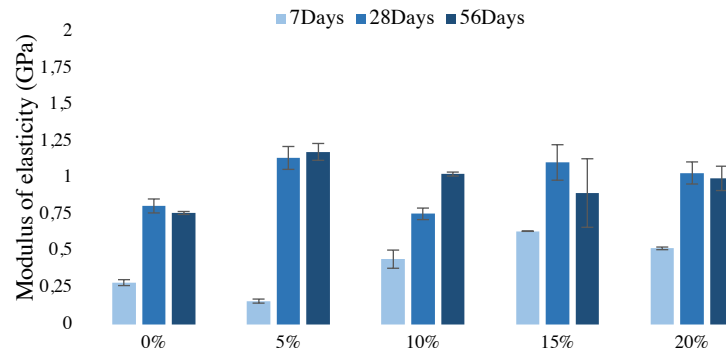


Figure 4.23. The average modulus of elasticity MOE (GPa) at different curing times.

Specimens	Flexural Strength	MOR (MPa)			MOE (GPa)		
	Curing Days	7 days	28 days	56 days	7 days	28 days	56 days
	CAC-0% SF	0,88 (b) (0,05)*	6,10 (ab) (0,58)	8,23 (a) (0,94)	0,28 (0,02)	0,81 (0,04)	0,76 (0,01)
CAC-5% SF	<b>0,88 (b)</b> <b>(0,25)</b>	<b>10,50 (a)</b> <b>(0,95)</b>	<b>14,62 (a)</b> <b>(0,83)</b>	<b>0,16 (0,01)</b>	<b>1,13 (0,07)</b>	<b>1,18 (0,05)</b>	
CAC-10% SF	2,63 (ab) (0,14)	4,27 (b) (0,10)	8,36 (a) (0,35)	0,44 (0,06)	0,75 (0,03)	1,02 (0,01)	
CAC-15% SF	6,69 (a) (0,55)	8,95 (ab) (1,59)	10,07 (a) (0,1)	0,63 (0,001)	1,10 (0,12)	0,89 (0,23)	
CAC-20% SF	3,68 (ab) (0,32)	9,38 (ab) (1,16)	5,76 (a) (0,27)	0,52 (0,009)	1,03 (0,07)	0,99 (0,08)	

For the same system containing the same kind of coupling agent, means with the same letter for each property are not significantly different at the 5% significance level. \* Values in parentheses are standard deviation.

Figure 4.24 and Table 4.9 present the flexural modulus of rupture obtained from three point bending mode for CAC-SF mixtures up to 20%SF, and hydrated for 7, 28 and 56 days. The mixtures revealed significant changes in different curing times, where with higher SF contents a reduction in MOR means were observed for 10%, 15% and 20%SF wt. 0%SF (reference matrix), 5%SF and 15%SF binders were evaluated by XRD and BSEM analysis, the micro-structural and chemical compositions of mixtures were assessed. With respect to MOR, 7D hydrated specimens exhibited very poor flexural strength in all mixtures which highest mean was achieved by 15%SF binder.

On the other hand, at 28D the MOR means increased significantly, whereas the highest means were obtained by 5% and 20%SF. Likewise, at 56D also significant changes were observed with an increased trend of 35%, 40%, 95%, 13% for binders of (0%, 5%, 10%, 15%SF wt. respectively) compared to 28D counterpart specimens. Except 20%SF binder which experienced a remarkable decline of 39% from 9,38 MPa at 28D to 5,76 MPa at 56D hydration.

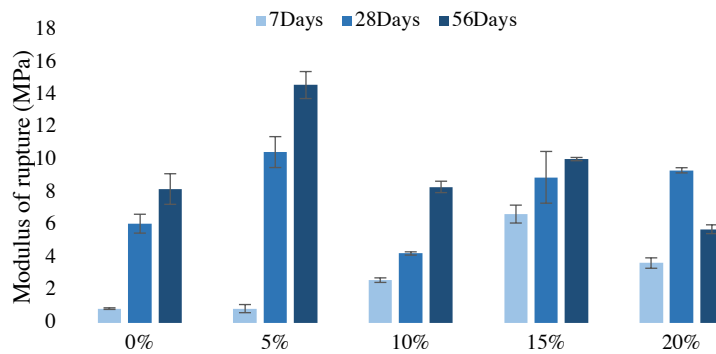


**Figure 4.24.** The average modulus of rupture MOR (MPa) at different curing times.

On the one hand, the 5%SF matrix exhibited about 40% increased mean, the highest mean among others at 56D with (14,62 MPa) compared to its mean at 28D. Despit of exhibiting very poor performance at 7D (0,88 MPa), a significant improvement at 28D was also observed with 10,50 MPa. The 15%SF mixture at 7D with 6,69 MPa, presented an increased mean about 33% at 28D with 8,95 MPa, this binder improved up to 37% with 10,07 MPa at 56D compared to 7D hydration. (See [Table 4.9](#)).

#### 4.3.2. Compression strength performance

In this section, the results obtained from the experimental characterization of the compression strength of the specimens tested under compression mode are presented. The compression tension-displacement graphs derived for the tested composites, and the average values of Modulus of Elasticity (MOE), Modulus of Rupture (MOR) are computed and compared. The specimen groups are revealed the sets from 0%, 5%, 10%, 15% and 20% of Silica Fume (SF) wt. cured for 7 days (7D), 28 days (28D), 56 days (56D).

[Figures 4.25](#) and [Table 4.10](#) present the compression modulus of elasticity obtained from compression tension-displacement graphs derived for the tested specimens for CAC-SF mixtures up to 20%SF, hydrated for 7, 28 and 56 days. As can be seen, a reduction in MOE means are observed with time in all groups of specimens, except for 5%SF binder that exhibited an opposite behaviour, with a mild increased mean with times. However, it can be observed that the higher SF content incorporation in matrix, exhibited a minor influence on the behaviour of mixtures, in which approximately similar means were achieved almost for all mixtures.

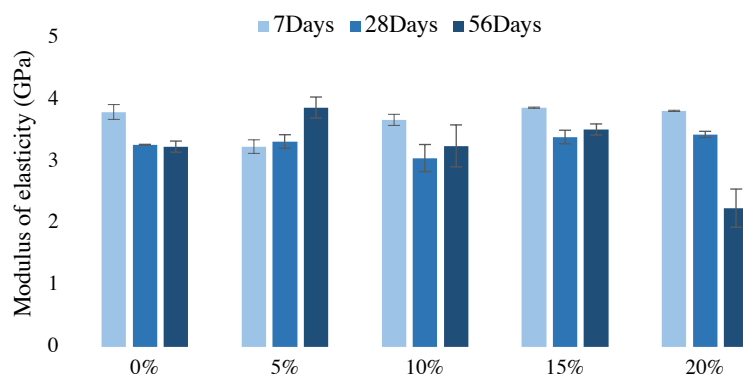


**Figure 4.25.** The average modulus of elasticity MOE (GPa) at different curing times.

TABLE 4.10. The average values of compression strength							
SAMPLES	Compression Strength	MOR (MPa)			MOE (GPa)		
		Curing	7 days	28 days	56 days	7 days	28 days
	CAC-0% SF		138,59 (a) (6,61)*	146,52 (a) (2,27)	147,96 (b) (0,88)	3,80 (0,12)	3,27 (0,005)
CAC-5% SF		113,25 (e) (3,49)	139,84 (a) (3,35)	178,02 (a) (10,77)	3,24 (0,11)	3,32 (0,11)	3,88 (0,17)
CAC-10% SF		133,85 (a) (4,27)	141,68 (a) (7,26)	146,07 (b) (10,16)	3,68 (0,09)	3,06 (0,22)	3,25 (0,34)
CAC-15% SF		136,03 (ab) (2,07)	148,32 (a) (2,78)	166,81 (ab) (6,42)	3,87 (0,01)	3,40 (0,11)	3,52 (0,09)
CAC-20% SF		126,64 (bc) (0,71)	151,63 (a) (3,68)	151,18 (ab) (7,09)	3,82 (0,01)	3,44 (0,05)	2,24 (0,01)

For the same system containing the same kind of coupling agent, means with the same letter for each property are not significantly different at the 5% significance level. \* Values in parentheses are standard deviation.

In this context, the mixtures at early 7D hydration stage exhibited MOE values ranging from 3,24 to 3,87 GPa, with CAC-15%SF performing higher value among others. The standard deviations varied from 0,01 to 0,12 GPa. Likewise, at 28D the specimens means ranged from 3,06 to 3,44 GPa, the standard deviations varied from 0,005 to 0,22 GPa. At 56D hydration the means ranged from 2,24 to 3,88 GPa, with CAC-5%SF performing higher value among others (3,88 GPa). The standard deviations varied from 0,01 to 0,34 GPa.

Figures 4.26 and Table 4.10 present the compression modulus of rupture obtained from compression tension-displacement graphs derived for the tested specimens for CAC-SF mixtures up to 20%SF, hydrated for 7, 28 and 56 days. As can be seen, it was observed insignificant differences in MOR values of binders in different curing times. Similarly, here, the 5%SF mixture which exhibited interesting behaviour among others. Simultaneously, incorporating higher SF% contents revealed a minor effect on the behaviour of mixtures, in which approximately resembling MOR values were achieved almost for all specimens. At 7D hydration the specimens exhibited slightly lower values compared to 28D and 56D hydration results. Among all specimens, the 5%SF binder exhibited a remarkable improved strength at 56D, the highest mean with 178 MPa, an increment of 57% compared to its value at 7D. Nevertheless this binder achieved the lowest MOR values of 113,25 and 139,84 MPa at 7D and 28D respectively (*with about 24% improved mean*).

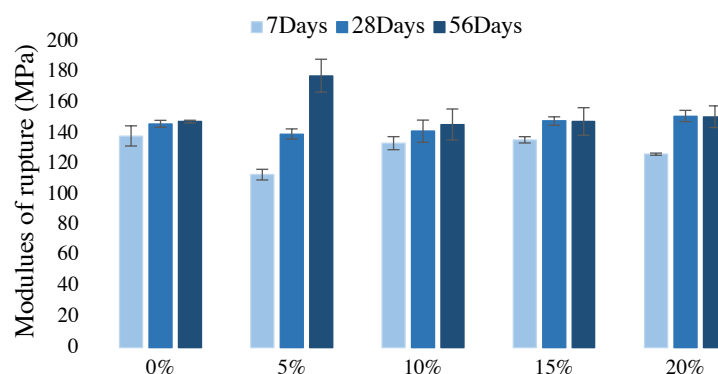


Figure 4.26. The average modulus of rupture MOR (MPa) at different curing times.

On the other hand, at 7D hydration stage the highest MOR was obtained by the reference matrix (0%SF) with 138,59 MPa, where the 10%SF-15%SF obtained gently lower than 0%SF with 133,85 and 136 MPa respectively. The 20%SF exhibited a value of 126,64 MPa at 7D.

Regarding to the 10%SF-15%SF-20%SF wt. at 28D, an increase of 6%, 9% and 19% were observed in MOR results with 141,68 – 148,32 and 151,63 MPa respectively compared to 7D counterpart specimens. The reference mixture exhibited 6% increase at 28D with 146,52 MPa. (See Table 4.10). At 56D in the MOR means of 0%, 10%,15% and 20%SF mixtures, it was observed an insignificant difference, the means ranged from 146,07 to 178,02 MPa, with 5%SF binder performing better among others. Hence, it can be considered that the pozzolanic additions (i.e., Silica Fume) into the CAC pastes, can lead to a high compression strength, as the specimens exhibited significantly high MOR means at 7D, 28D and 56D hydration stages. These results were also consistent with ANOVA test results, whereas the Tukey test revealed no significant changes in binders, when SF content was increased up to 20%SF.

From all these results, the observed behaviour of mixtures with respect to the influence of SF% content and curing time on the CAC matrix, it can also be attributed the following concluded phenomenon:

1. In general terms, the stress–strain curve of normal concrete shows that, an increase in the compressive strength reduces the ultimate strain, and, consequently, the concrete quick failure is due to brittle behavior of the matrix. Normally, the brittle behavior occurs in high-strength grades (M. R. Hamidian, P. Shafigh 2021). According to the results discussed, this type of failure can also be observed in CAC-SF mixtures. This behavior of binders at early hydration stage of 7D could be because of this brittle nature of these groups of concrete.
2. A reduction in the strength of binders in higher SF contents, could also be related to the unreacted SF particles in CAC paste as it would be an excess of SF particles in mixture, (*this claim will be discussed and demonstrated by BSEM analysis*). In such context, the higher SF content could be acting only as a filler particles rather than giving a complete pozzolanic reaction (*this could be observed in BSEM results of mixtures with 15%-20% of SF content*), Although to claim this a further and deep study is demanded.
3. Stated previously, conversion of hydrated phases of CAC could be hindered with pozzolanic addition in the matrix. *Silica fume* incorporation into the CAC matrix results in the development of alumino-silicate phases such as Hydrogarnet ( $C_3AH_6$ ) -a solid solution- and strätlingite ( $C_2ASH_8$  a hexagonal platy phase). This reaction can occur in following phases: the mineral silica content reacts with calcium aluminates CA, avoiding the generation of hexagonal forms of  $C_2AH_8$  and hence the conversion to cubic forms of  $C_3AH_6$ . Instead of this cubic phase, a hexagonal aluminate hydrate containing silica, known as strätlingite, is generated (A. Hidalgo and J. García 2009). When silica fume is added into a CAC matrix, it can prevent the loss in compressive strength induced because of conversion by forming a stable phase of strätlingite  $C_2ASH_8$  (H.M. Son and S. Park 2019).
4. The potential nucleation capacity of SF particles due to their specific spherical surface area, a further study demands to confirm this claim. SF particles could act as nucleating agents that accelerate the hydration process of CAC in the initial stages to generate a jelly, smooth and gummy kind of paste.

Accordingly, in binders of 5%SF the formation of *strätlingite*  $C_2ASH_8$  could be possible in early stages, (*this will be discussed and demonstrated by XRD/BSEM analysis in following*

sections). Therefore the conversion phases in CAC could be hindered due to the generation of *strätlingite* phase at 28D-56D hydration stages. Resulting in decreased porous and a compact matrix with higher mechanical resistance was obtained for 5%SF binders (prevailing (3)).

These can also be justified with (prevailing (1)) The poor flexural strength of binders at 7D compared to those of 28D-56D hydrated binders (prevailing (3)). On the other hand, the possible nucleation effect of SF particles in matrix (prevailing (4)) explaining the similarities in mechanical performance of mixtures despite of increased SF content (i.e., 10%, 15% and 20%SF wt.) due to the unreacted excess SF particles in mixtures, (prevailing (2)) which could also be caused by the low w/c ratio 0.35 that was not enough to hydrate all the cement and SF (K. Scrivener and L. Cabiron 1999).

Therefore, leading to an overall reduction in flexural strength of binders at 7D, while with very high compressive strength achieved at 7D. An apparently contradictory phenomenon, because of high variations in flexural and compressive strength of binders (prevailing (1)). In compression mode, the strength was maintained or gently increased. This also could be related to the incorporated silicate source to the matrix, resulting in the generation of stable phases of *strätlingite*, and hence, preventing the compressive strength loss induced because of conversion phases as well (prevailing (3)), (H.M. Son and S. Park 2019).

The relationship between conversion, porosity and compressive strength have been extensively studied for both CAC cements (T. Matusinović and J. Šipušić 2003) and Portland cements (I. Odler and M. Rößler 1985). The compression mechanisms are controlled mainly by the physical contact between the particles, this being much stronger for more compacted materials. Therefore, the conversion phases could have a greater influence than the hydration procedure on the evolution of bending performance of these tested compounds. Nevertheless, per our knowledge, this phenomenon hasn't been studied for the flexural strength of such matrices, as the particle adhesion mechanisms are responsible for tensile strength and therefore flexural performance could be involved (prevailing (1)). On the other hand, the precipitation of new hydrated compounds in the porous areas, triggered by an initial conversion of phases, which could be developing an adhesion mechanism but not strong enough to achieve a good tensile response that is capable of improving the flexural strength of binders at early stages.

#### 4.3.3. X-Ray Diffraction, chemical composition analysis

The results obtained from XRD analysis, are carried out on the reference (0%SF), 5%SF and 15%SF binders. Figures 4.27, 4.28 and 4.29 present XRD results obtained for each mixture (i.e., 0%SF, 5%SF and 15%SF wt.) respectively, at 7D, 28D and 56D with their observed hydration phases. These graphs exhibits a progressive transition in peaks corresponding to CAC-SF hydration phases, which decrease-increase respectively according to their SF content in mixtures.

Shown in Figure 4.27, for 0%SF binder it can be observed that at 7D hydration a certain amount of meta-stable phase of  $C_2AH_8$  is present (a), and at 56D hydration stable phases of  $C_3AH_6$  and  $AH_3$  are observed (c). Moreover, at 28D (b) the peak corresponding to anhydrous CA phase points to the existence of particles that remained for hydration, while at 56D (c) the CA phase is greatly reduced. Hence, a hydration of CA phase was experienced, this is also consistent with the results of mechanical resistance in previous section. Mainly, XRD spectra 0%SF revealed: 1. The presence of meta-stable phase of  $C_2AH_8$  at 7D hydration (a); 2. Complete

conversion of  $CAH_{10}$  phases into  $C_3AH_6$  and  $AH_3$  after 56D hydration (c); 3. Reduction of anhydrous phases of CAC (CA, CT and  $C_2A$ ) in specimens hydrated for 28D (b).

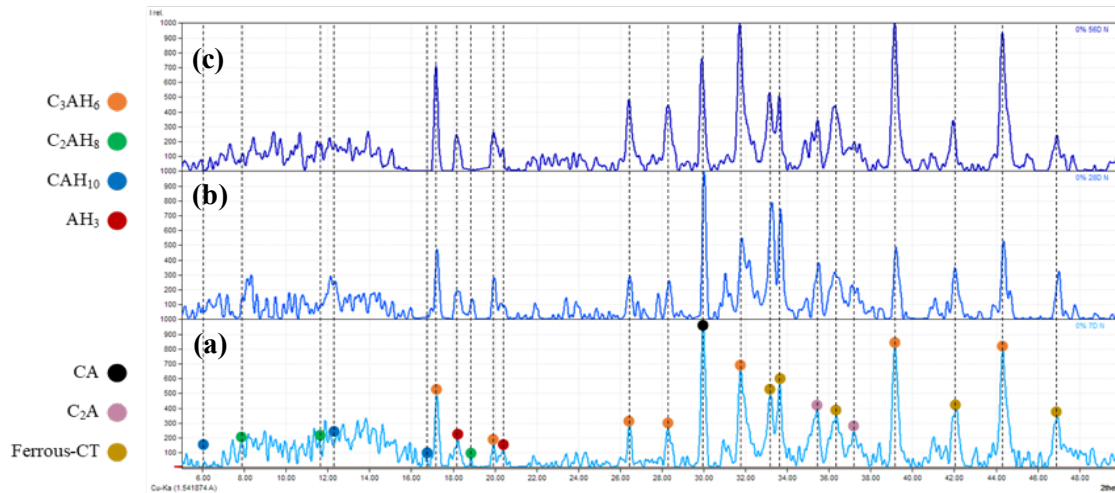


Figure 4.27. X-Ray Diffraction results for 0% SF-CAC paste cured for 7 (a), 28 (b) and 56D (c) present anhydrous polyphasic particles and hydrated zones of  $C_3AH_6+AH_3$

The XRD spectra for 5%SF matrix in Figure 4.28 revealed: 1. The presence of strätlingite phase  $C_2ASH_8$  in mixtures at early hydration stage of 7D (a); 2. The hindered conversion hydrates with  $C_2ASH_8$  formation and leading to an increased meta-stable  $CAH_{10}$  and  $C_2AH_8$  phases at 28D hydration, where these phases are present still after 56D hydration (c), resulting in a decrease in the presence of stable phases of  $C_3AH_6+AH_3$  at 56D (c); 3. Anhydrous phases of CA, Ferrous-CT and  $C_2A$  are present at 7D hydration (a), CA, Ferrous-CT were increased for those pastes cured for 28D and 56D (b, c) while  $C_2A$  amount was decreased. Therefore, it could be considered that the conversion phases of CAC paste could be possible with SF addition into CAC matrix, hence, the formation of new compounds of  $C_2ASH_8$  is confirmed.

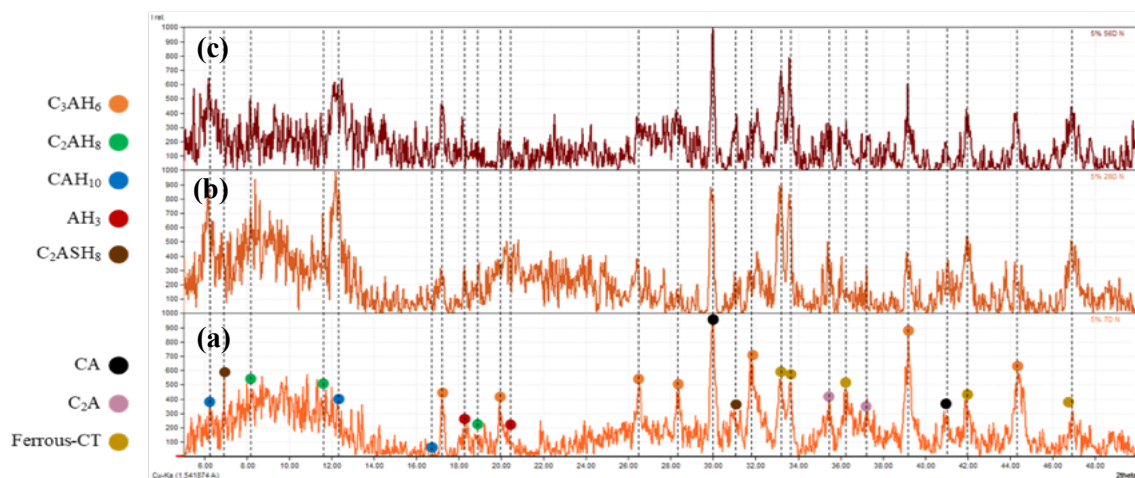
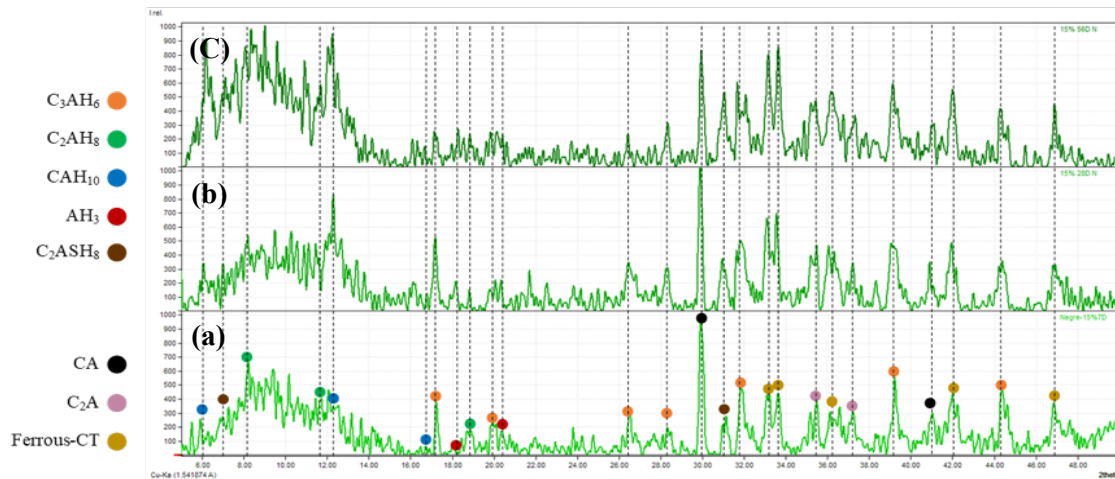


Figure 4.28. X-Ray Diffraction results for 5% SF-CAC paste cured for 7D (a), 28D (b) and 56D (c) present anhydrous polyphasic particles and hydrated zones of  $C_3AH_6+AH_3$

The XRD spectra of 15%SF binder is presented in Figure 4.29, this spectra reveals: 1. The presence of hexagonal platy phases of strätlingite  $C_2ASH_8$  in mixtures at 7D, 28D and 56D hydration stages, whereas these phases are increased significantly at 56D hydration (a, b, c); 2. The presence of meta stable  $CAH_{10}$  and  $C_2AH_8$  phases in mixtures at 7D and 28D hydration (b) that it was increased considerably at 56D hydration. These results confirming, the hindered conversion phases of  $C_3AH_6$  and  $AH_3$  which at 56D, these phases are considerably decreased; 3. The remarkable increased anhydrous phases of (CA, CT and  $C_2A$ ) of mixtures at 28D and 56D hydration (b, c).



**Figure 4.29.** X-Ray Diffraction results for 15% SF-CAC paste cured for 7(a), 28 (b) and 56D (c) present anhydrous polyphasic particles and hydrated zones of  $C_3AH_6+AH_3$

The detected phases in X-Ray Diffraction analysis are presented in Table 4.11 as following:

**Table 4.11.** The detected phases in X-Ray Diffraction analysis

Match! Entry	COD Entry	Identified as	Crystal system	Name
99-100-0020	0009431	Ferrous-CT	O	Brownmillerite
99-100-0164	0018046	Ferrous-CT	C	Wustite
99-200-0003	1007235	$C_3AH_6$	C	Dicalcium tricalcium oxide hexahydrate hydrogarnet
99-200-0018	1200016	$AH_3$	M	Aluminium hydroxide Gibbsite
99-200-0035	2002888	$C_2A$	M	Calcium dialuminium oxide
99-200-0036	2103045	$CAH_{10}$	H	Calcium aluminate decahydrate
99-200-0183	9005059	$C_2ASH_8$	H	Strätlingite
99-200-0040	4308075	CA	M	Calcium monoaluminate
Bibliographic	-	$C_2AH_8$	-	-

#### 4.3.4. BSEM, Microstructure analysis

The results obtained from BSEM analysis confirms the XRD results above revealed strong peaks that indicated the formation of new stable phases so called strätlingite  $C_2ASH_8$  in early hydration stage of mixtures at 7D. BSEM analysis were carried out on 0%SF, 5%SF and 15%SF wt. matrices cured for 7D, 28D and 56D as presented in following Figures 30, 31, 32. The analysis are carried out to determine the micro-structure of various zones in each mixture.

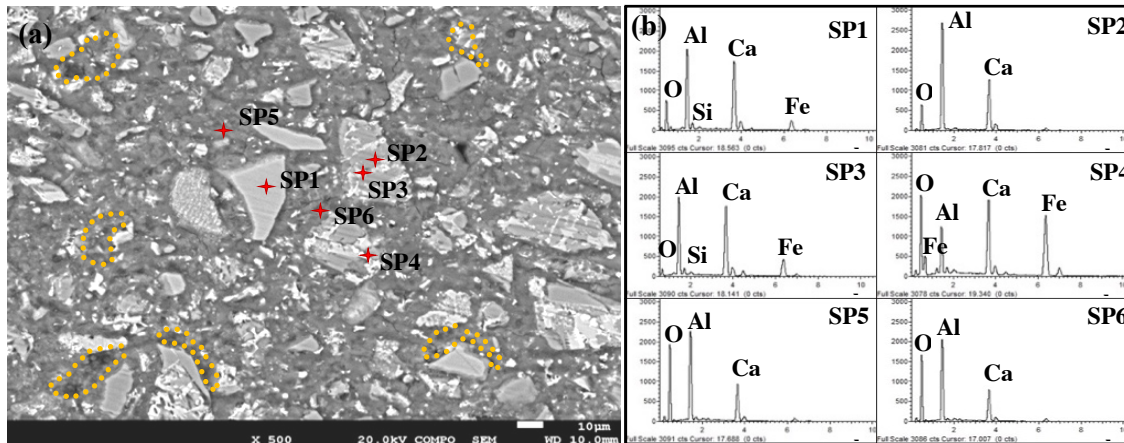


**Figure 4.30.** (a) BSEM image of 0%SF-CAC binder at 7D, (b) Anhydrous and hydrated phases, and their corresponding EDS spectra, SP1-SP2= anhydrous polyphasic phases; SP3-SP4 = anhydrous phases with high iron content of Ferro-CT; SP5-SP6 = hydrated phase, zones of  $C_3AH_6 + AH_3$ .

As it was expected analogous to XRD results above, Figure 4.30 indicates the presence of anhydrous polyphasic particles and hydrated zones in a pure CAC paste cured for 7D, likewise the common phases found in CAC matrix were detected. In this analysis three types of particles were identified: A uniform gray color phase, analyzed by SP1 spectrum, it could be mono calcium aluminate based on constituents detected here (CA phase). However, the components found in SP2 spectrum, the polyphasic particles are observed with two shades of gray, one neutral and a lighter gray, which also could be mono calcium aluminate (CA phase). The lighter sections are studied in SP3-SP4 that contains iron in addition to aluminum and calcium, these phases could be corresponded to Ferro-CT with a significant iron content (those white color particles). These phases could be corresponded to anhydrous constituents of lime aluminate cement, as the low oxygen content of SP3-SP4 spectrum seems to indicate it. However, in SP4 more of this chemical appears that could indicate a hydrated phase deposited on an anhydrous particle with a high iron content of AFm hydrated phase type. SP5-SP6 are corresponded to a darker gray zone of hydrated phases of CAC and chemically similar in compositions.

However, these dark gray zones have no perceptible morphology, given the high aluminum content relative to calcium, which could be amorphous  $AH_3$  mixed with  $C_3AH_6$ . On the other hand, there has been no indication of  $C_2AH_8$  existence in electron microscopy, which are generally immediately identifiable. Form all these it could be deduced that the meta-stable phases of  $CAH_{10}$  and  $C_2AH_8$  were converted to the stable phases of  $C_3AH_6$  and  $AH_3$ .

Moreover, porous areas indicated by dotted red circles in Figure 4.30 could be caused by conversion phases mentioned above. However, it is not highly widespread porosity, as didn't result a notable loss of resistance in mixtures. This could be due to the low w/c ratio of 0.35 that was used, under these conditions enough water or space was not available for CAC to form the

meta-stable hydrates. Hence, the water is released during conversion phases will be available to react with anhydrous phases to form more hydrates. Therefore, the net decrease in solid volume and the rise in porosity will be reduced, hence after conversion, a matrix will be compacted resulting in an increased strength. (K. Scrivener and J. Newman 2003), (K. Scrivener and L. Cabiron 1999). As result, hydrated phases from  $CAH_{10}$  to  $C_3AH_6$  of crystalline precipitation in cubic (the blue arrows in Figure 4.31(c)) was appeared with amorphous phases of  $AH_3$  (the red arrows). Due to decreased volume occupied by  $C_3AH_6$  compared to  $CAH_{10}$ , there are areas where the porosity is higher.

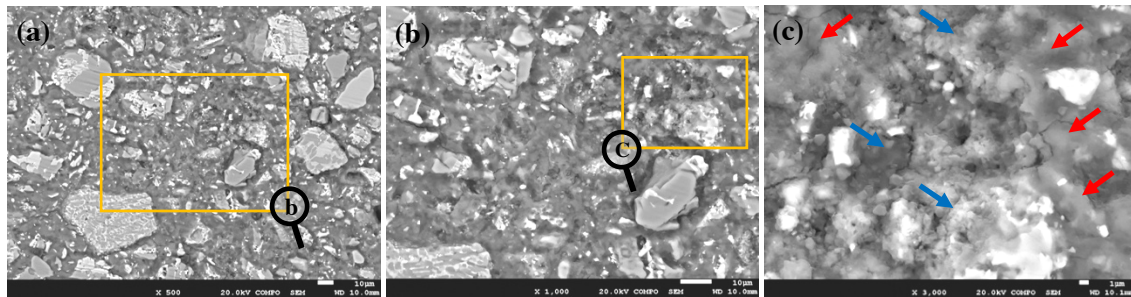


**Figure 4.31.** (a) BSEM image of 0%SF-CAC at 7D. (b) BSEM image showing the porous areas. (c) BSEM image showing hydrated phases of  $C_3AH_6$  and its crystalline precipitation in cubic and  $AH_3$  hydrated phase.

Figure 4.32 presents CAC paste at 28D along with some detailed images of previous binder at 7D, to note dissimilarity of mixtures over time. The changes in meta-stable phases ( $CAH_{10}$ -  $C_2AH_8$ ), some particles are included in details Da and Db obtained from Figure 4.30.

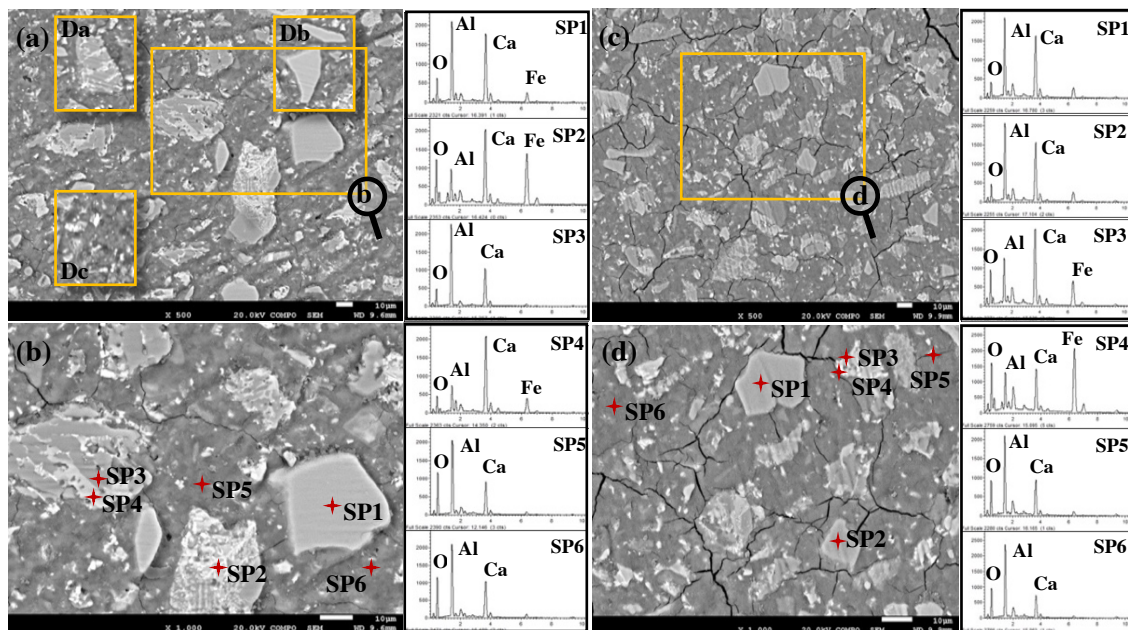


**Figure 4.32.** (a) BSEM image of 0%SF-CAC at 28D, at different magnification. (b) with EDS spectra corresponding to the points marked in image. SP1-SP4 = anhydrous phase; SP2= anhydrous phases with high iron content Ferro-CT; SP3-SP5-SP6 = hydrated phases of  $C_3AH_6+AH_3$ . (c) BSEM image of 0%SF-CAC at 56D, at different magnification (d) with EDS spectra corresponding to the points marked in image. SP1-SP2 = anhydrous phases; SP3-SP4 = anhydrous phases with high iron content Ferro-CT; SP5-SP6 = hydrated zones of  $C_3AH_6+AH_3$

The elements are identical as detected hydrates at 7D (Monophasic monocalcium aluminate particles, polyphasic calcium aluminates particles, Ferritic phases, etc.). Nevertheless, from a micro-structural point of view, there are some minor changes in the shape of particles, for instance the edges of indicated particles is becoming somewhat more rounded. This could be indicative of a more advanced phase of hydration, as a result a greater dissolution of particles in the medium. As can be seen, the pores in hydrated zone of binder are disappeared, it could be due to the formation of new hydrated compounds. (K. Scrivener and L. Cabiron 1999). As can be seen in detail Dc taken from previous Figure 4.31, to note the similarity of the geometry of hydrated zones in both mixtures. In Figure 4.32, the image (c) presents the paste at 56D, similarly SP1-SP2 are for anhydrous particles corresponded to those monocalcium aluminate, and SP3-SP4 along with some iron content, possibly belonging to small ferritic phase particle located on the right. The hydrated phases are analyzed in SP5-SP6 the zones of  $C_3AH_6+AH_3$ .

Indicated in Figure 4.33 the image (a) presents the microstructure of 5%SF-CAC mixture at 7D. In SP1-SP2-SP3 spectra of anhydrous particles giving results corresponded to those monocalcium aluminate SP1-SP3 along with some silica and iron, possibly belonging to small particles of ferritic phase located on the right. The SP2 spectra belong to a polyphasic particle where in addition to monocalcium aluminate, some Ferro-CT phases are appeared. The hydrated phases analyzed in SP4-SP5, in addition to aluminum and calcium, incorporated some silica contents. However, the detected silica is in low quantities, this could be due to the reaction of SF and calcium aluminates to form strätlingite  $C_2ASH_8$  phase. Finally as in image (b) new type of particle is appeared, SP6 indicates a remarkable SF particle that begun to react with calcium aluminate phases, resulting in the formation of  $C_2ASH_8$ . Nevertheless, the low calcium content may indicate that the formation of this compound is still in its early stages of reaction. Moreover, the fact of crushing SF by milling machine has made its particles to be no longer a spherical form, but to a polygonal structure, which is observable in image (b).

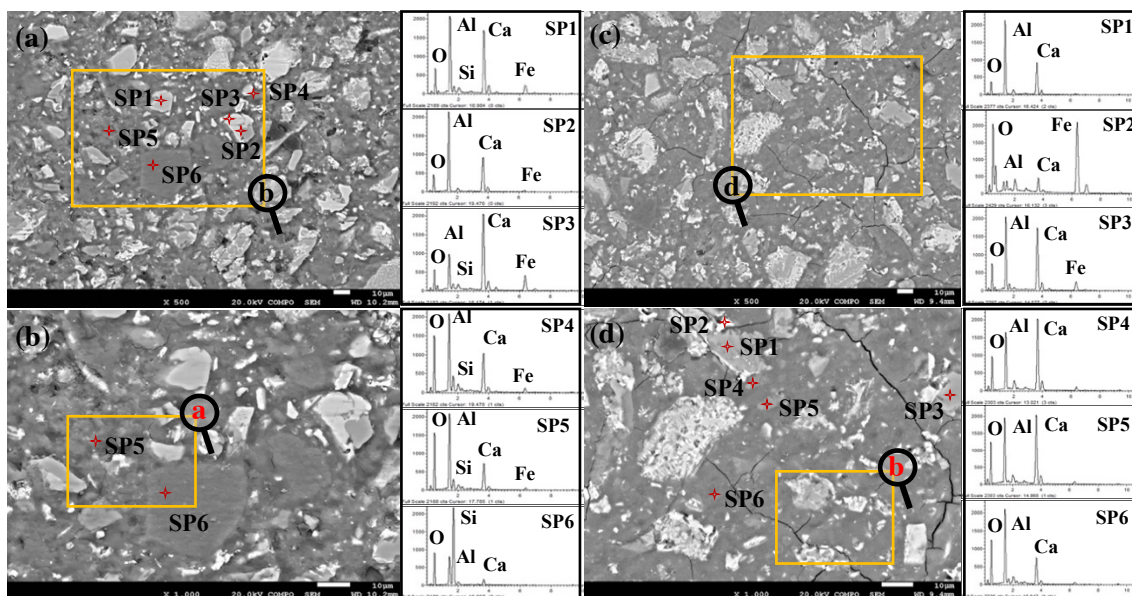


**Figure 4.33.** (a) BSEM image of 5%SF-CAC at 7D, at different magnification. (b) with EDS spectra corresponding to the points marked in image. SP1= anhydrous phase; SP2-SP3= anhydrous phases with high iron content Ferro-CT; SP4-SP5= hydrated phases with some silica contents, SP6= strätlingite  $C_2ASH_8$ . (c) BSEM image of 5%SF-CAC at 28D, at different magnification (d) with EDS spectra corresponding to the points marked in image. SP1= anhydrous phase; SP2-SP3 = anhydrous phases with high iron content Ferro-CT; and SP4-SP5-SP6= various types of hydrated calcium and aluminum.

Image (c) presents 5%SF-CAC at 28D, to observe the similarity of the geometry of hydrated zones in matrix at 7D-28D. Distinct from 0%SF, in this mixture the monophasic calcium aluminate particles are evident. Anhydrous phases of aluminates appear in SP1, SP2 and SP3 in image (c) belong to polyphasic particles with rich Ferro-CT phases that appeared. The dissolution and combination of calcium aluminate appeared in SP2-SP3 seem to be caused by SF incorporation in matrix. Furthermore, the particles of SF didn't appear here, which it was clearly detected in binders at 7D. SP4-SP5-SP6 in image (d) reveal various types of hydrated calcium and aluminum compounds; however, no significant silicon content is detected in any of these spectra. In the abscissa 1.73 and 2.31, only minor presences are identified. (Note: the abscissa 2.05 and 2.13 peaks in SP6 indicated with blue arrow correlate to the platinum in specimens' coating).

Figure 4.34 presents the mapping image of anhydrous particles 5%SF-CAC mixture. (a) 5%SF-CAC at 7D, (b) 5%SF-CAC at 28D and (c) 5%SF-CAC at 56D, where the anhydrous particles (lighter color parts), hydrated zones (plain medium gray color) along with the polygonal amorphous silica particles are observed.

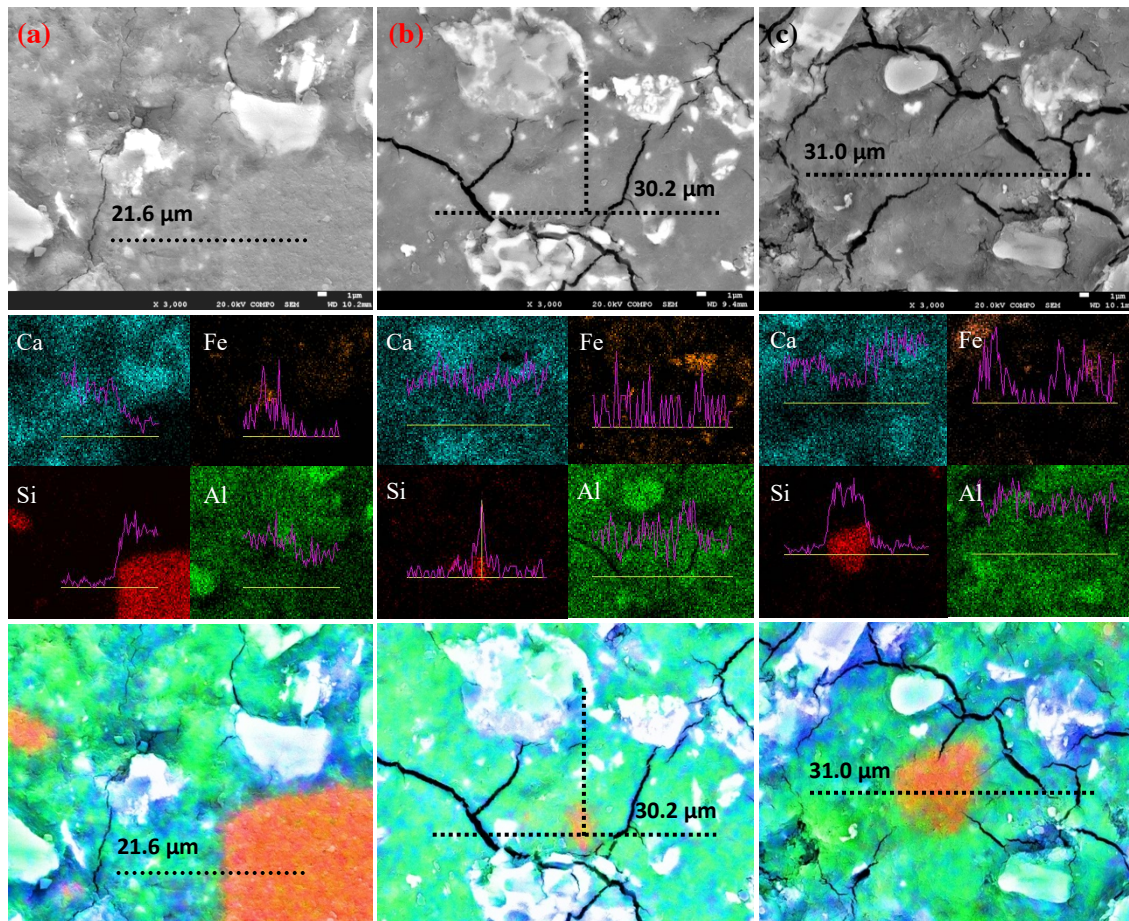


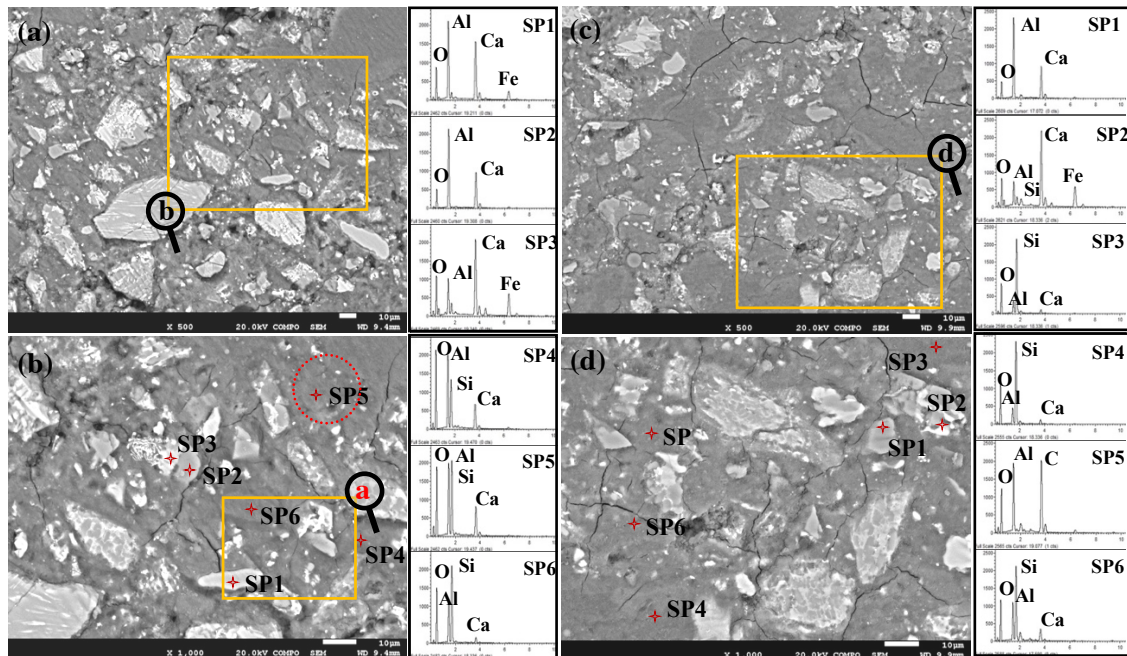
**Figure 4.34.** (a) BSEM image of 5%SF-CAC at 7D. (b) BSEM image of 5%SF-CAC at 28D. (c) BSEM image of 5%SF-CAC at 56D. Present the mapping of anhydrous polyphasic particles and hydrated zones and the new generated strätlingite  $C_2ASH_8$  compounds.

At the bottom of each column (a, b, c) the mappings corresponding to Ca, Si, Fe and Al elements are included. It indicates the concentrations of each element in corresponded figures that

in transparency zones with highest ion concentration are placed on the original image. The line scans are performed from central lower hydrated zone of SF particles in all sections. The Si mapping of 5%SF-CAC at 7D (a), silica contents of hydrated zone are very low in contents. Thus it can be deduced that SF reactions with calcium aluminate could be incomplete or unreacted. Moreover, in SF particle zone the spectrum indicates the certain amounts of Ca and Al, that could be a reaction between these particles with the possible formation of strätlingite.

In the combination of mappings in color in all images above, it is possible to perceive exactly the distribution of hydrated zones and the limits of SF particle, that a certain amount of  $C_2ASH_8$  could be forming. In Si mapping of 5%SF-CAC at 28D (b), a concentration of Si is detected exactly along with the presence of Ca and Al. This could be consistent with dissolving practically all calcium mono-aluminate particles, although Si concentration didn't appear as a clear particle. This could be due to: (1) the mineral phase wasn't notable as a specific particle or crystal, (2) it could be slightly covered by other hydrated phases. However, probably it is due to the possibility (1) since it appears that SF particles are dissolved in the medium. Furthermore, in section (c) 5%SF-CAC at 56D, likewise Si concentration is detected, which could be related to  $C_2ASH_8$  formation.

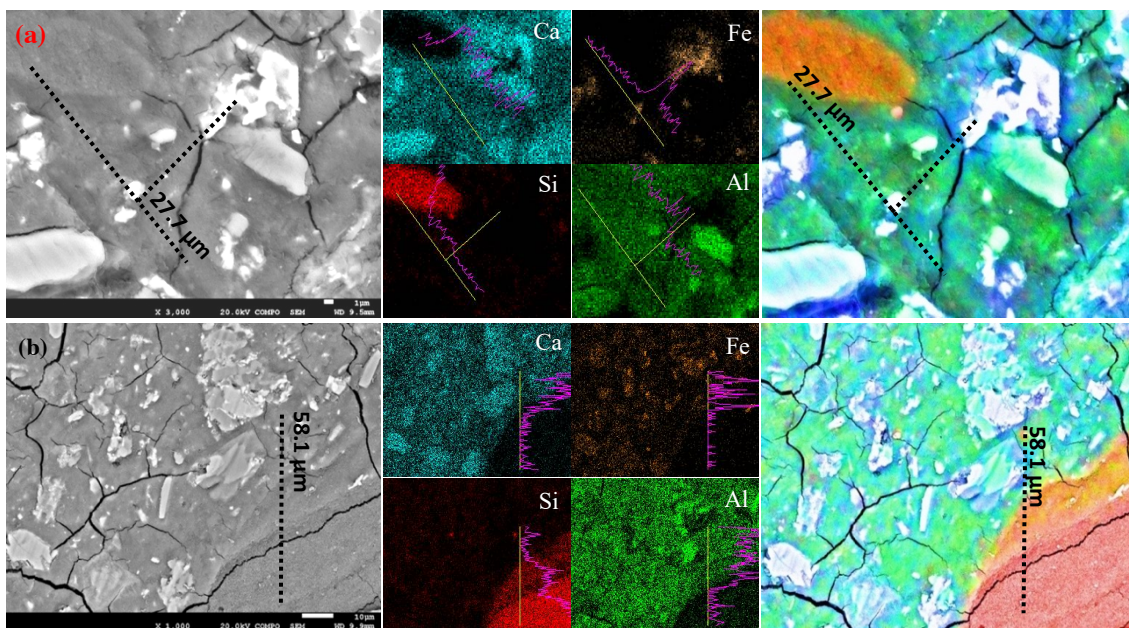
BSEM images of 15%SF-CAC at 7D-28D are shown in Figure 4.35, analogously to previous sections it is corresponded to anhydrous particles of mono-calcium aluminate along with some silica and iron, probably belonging to a small ferritic phase located at the bottom. SP2-SP3 belong to a polyphasic particles where monocalcium aluminate in SP2 and some rich Ferro-CT phases are appeared in SP3. The hydrated phases analyzed in SP4-SP5, in addition to aluminum and calcium, a considerable silica quantity is detected, hence, a possible strätlingite phase formation.



**Figure 4.35.** (a) BSEM image of 15%SF-CAC at 7D, at different magnification (b) with EDS spectra corresponding to the points marked in image. SP1= anhydrous phase; SP2-SP3 = anhydrous phases with high iron content Ferro-CT. SP4-SP5-SP6= hydrated zones and new strätlingite compounds (c) BSEM image of 15%SF-CAC at 28D, at different magnification (d) with EDS spectra corresponding to the points marked in image. SP1= anhydrous phase; SP2= anhydrous phases with high iron content Ferro-CT. SP3-SP4-SP5-SP6= hydrated zones of strätlingite.

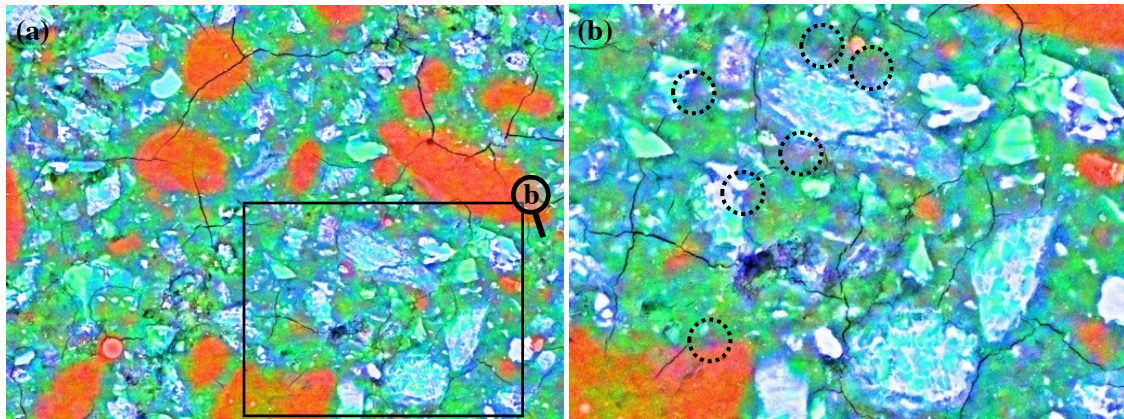
In SP5-SP6, Si content is very high among others, focusing closely on SP5 (red circle (b)) the SF particle can be detected with faded limits. Therefore, a part of this detected Si that could be SF particle, however, in hydrated zone of SP5 (d), no particular particle is detected, that would be consistent with the amounts of each element that are seen in this spectrum. Finally, the type of particle analyzed above appears as SF, where SP6 indicates identical as previous 5%SF-CAC mixture, a SF particle begun to react with calcium aluminate, hence, a possible formation of the  $C_2ASH_8$  could be deduced. Likewise in images (c, d), in SP1 the monocalcium aluminate particle is detected, in SP2 the polyphasic particle with high iron content (easily detectable due to its very light color), both anhydrous and hydrated darker gray area are composed of different combinations of aluminum and calcium in SP5. Nevertheless, the differences from 5%SF-CAC at 28D, SF particles are detected through SP3-SP4 which are easily detectable, while in images (c, d) the particle edges are faded, which are not as clear as those particles detected at 7D. Similarly, here the monocalcium aluminate particles almost disappeared, probably due to the presence of SF turning into new compounds of strätlingite detected in SP5-SP6.

Figure 4.36, image (a) presents the Si mapping for 15%SF-CAC at 7D and image (b) at 56D. It seems, there is a minor difference relative to those of 5%SF-CAC, as SF particle seemed to have a greater influence and reactivity in matrix. As shown, in silicon line scan (the perpendicular line to x axis in image (a)); before the line there are higher silicon values, also considerable in aluminum amount, although calcium value remains stable. This may indicate the formation of some  $C_2ASH_8$  content. In image (b) 15%SF-CAC matrix at 56D, the most relevant thing that is observed; the matrix seems to be very dense whereas some SF particles (Red zone) remains without reacting. In upper part of this large SF particle a phase with a lot of aluminum and silicon are formed, this could be related to  $C_2ASH_8$  formation, but with very little quantity of calcium. According to a study done by Collepari et al on 15%-30% SF-CAC, reported that using 15%SF almost completely reduces the strength loss of such matrix at 20-40°C due to the development of  $C_2ASH_8$ , then transformation of hexagonal aluminate hydrates into cubic hydrates are hindered (M. Collepari and S. Monosi 1995).



**Figure 4.36.** (a) BSEM image of 15%SF-CAC at 7D, (b) BSEM image of 15%SF-CAC at 56D, presents the mapping of anhydrous polyphasic particles and hydrated zones, the new strätlingite compounds.

Figure 4.37 presents the false color image with intensities of differentiated elements of Si (Red), Al (Green), Ca (Cyan) and Fe (White), where the dissolution of anhydrous phases to form hydrated phases is appeared clearly and the diffuse boundaries of particles are observed clearly. Although with 15%SF content in binder, it seems, many particles are unreacted or the reactions are incomplete, as if SF content were excessive in the matrix. Nevertheless, the formation of  $C_2ASH_8$  is present, the lilac areas indicated by black dotted circles in image (b). In final regardless of all analysis and discussions mentioned above, these mineral additions such as silica fume could result in the development of such compounds and aluminum-silicate phases but the mechanisms behind their creation still remain unknown.



**Figure 4.37.** BSEM image of 15%SF-CAC at 28D, at different magnification zones with false color image that presents the intensities of different elements with colors, Si (Red), Al (Green), Ca (Cyan) and Fe (White).

Figure 4.38, presents the particle analysis done by digital image analysis. The gray tone areas for anhydrous particles with regard to hydrated phases was determined in this particle analysis. Following that, the area in pixels of anhydrous phases was counted, the percentage of non-hydrated particles in image (a) accounts for 36.97% of the image. This proportion is 31.54% in the middle image of 28D cured specimens (b), and it drops to 22.14% at 56D cured specimens in image (c).

In terms of mean particle sizes, the 7D cured specimen is 774.04 pixels, the 28D cured one is 739.62 pixels, and the 56D cured one is 510.02 pixels. In short, it can be stated that over the time, the particles are dissolved and reduced their size. Note: The specimens with 15%SF haven't been analyzed because their color does not allow to be discriminated with respect to hydrated parts.

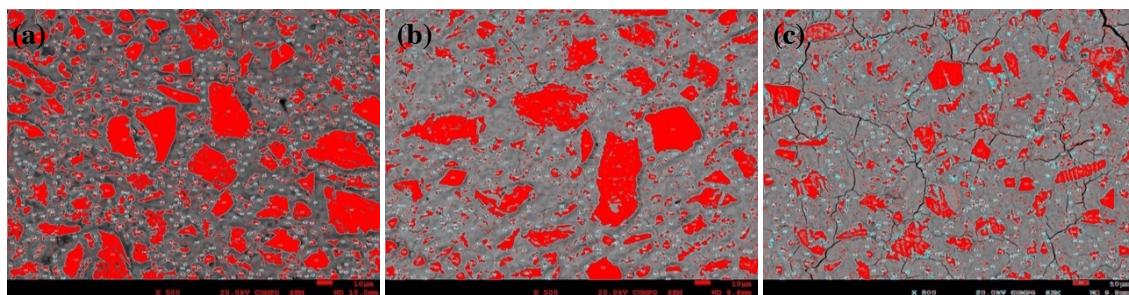


**Figure 4.38.** BSEM image of 0%SF-CAC paste (a) at 7D, (b) at 28D and (c) at 56D cured binders differentiation.

#### 4.4. DURABILITY AND MICROSTRUCTURE OF SILICA FUME-CALCIUM ALUMINATE CEMENT COMPOSITES

##### 4.4.1. Flexural strength performance

In this section, the results obtained from the experimental characterization of the flexural strength by means of three-point bending tests are presented. The flexural stress-displacement curves derived for the tested composites, and the values of Modulus of Elasticity (MOE), Limits of Proportionality (LOP), Modulus of Rupture (MOR), and Specific Energy (SE) are computed and compared. The specimen groups are revealed the sets from 0%SF (reference compound) and 5%SF reinforced with 10% cotton linter fiber in CAC based matrix cured for 28D and 56D.

Figures 4.39, 4.40 present the plot of flexural stress-displacement relationships obtained for SF-CAC-SVC342510%CO mixtures with varied SF content of (i.e., 0%SF, 5%SF). Table 4.11 present the average values of flexural strength parameters. The obtained results exhibited that the linear relationship before FCS was steeper at 28D, although it dropped gently at 56D. The failure of compounds occurred approximately in the range of 0.30-0.55 mm at 28D-56D, where the PCS deflection reached up to 2.80-5.00 mm at 28D for both compounds. 5%SF specimen's bearing capacity approached to its limit (FCS) accompanied by the specimen failure, while PCS of this mixture generated a curve resembled to the flexural load-deflection for a ductile material with (Strain-softening behaviour), with a sufficient FCS-PCS for some applications.

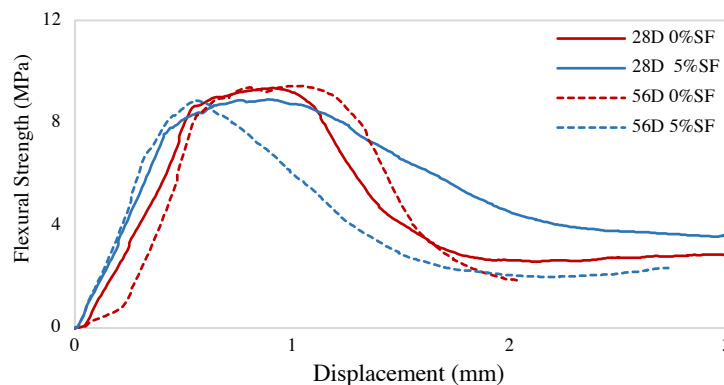


**Figure 4.39.** Flexural stress-displacement relationships for the SF-CAC-SVC342510%CO composites at 28D and 56D.

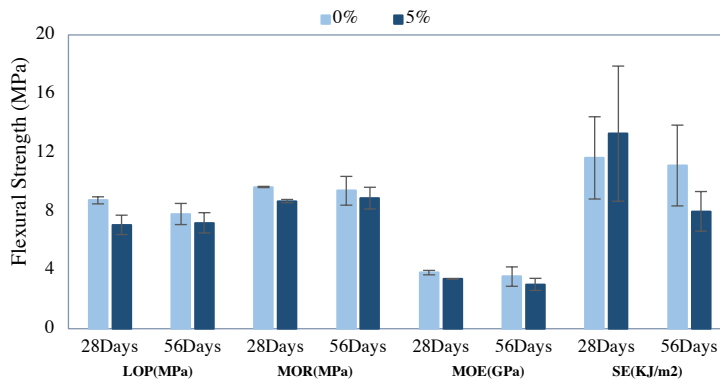


**Figure 4.40.** Flexural strength parameters for SF-CAC-SVC342510%CO composites at 28D and 56D.

On the other hand, it was observed that a superior number of post-cracks with lower crack width for the composites with 5%SF in comparison to the reference composites. This behavior of compound indicates the higher bond strength for this mixture therefore, resulting in a stiffer Post-Crack regions. According to MOE average values, it was observed that when 5%SF was added to the matrix a decline about 11% exhibited in means ranged from 3,82 to 3,39 GPa at 28D. This specimen exhibited about 14% reduction from 3,50 to 3,02 GPa at 56D hydration. Considering each mixture individually, a decreased trend was observed in means over the time. 0%SF binder experienced about 9% from 3,82 to 3,50 GPa, and 5%SF binder achieved about 11% lower mean from 3,39 GPa at 28D to 3,02 GPa at 56D. (See Table 4.11).

Regarding to the limits of proportionality (LOP), reference composite exhibited slightly higher FCS than 5%SF compounds (See Figure 4.40). with respect to the curing time classification, 0%SF matrix decreased about 10% its mean at 56D hydration, in contrast 5%SF binder retained its FCS. Although there is insignificant difference between the means of both mixture. This behaviour of compounds could be related to the strätlingite  $C_2ASH_8$  formation stated in previous sections by (*i.e.*, XRD, BSEM analysis). Overall, in both 28D-56D hydration stages when the SF was incorporated, this matrix is experienced a decrease about 19% from 8,74 to 7,07 MPa at 28D and around 8% reduction in the FCS of specimens at 56D from 7,81 to 7,21 MPa was observed (See Table 4.11).

The reference matrix exhibited, a better performance than 5%SF matrix in modulus of rupture average values. The same behaviour as LOP was observed for MOR, with 0%SF performing better at both 28D and 56D hydration. The matrix exhibited a reduction in its strength about 10% when 5%SF was added, from 9,65 to 8,69 MPa at 28D hydration. Same trend appeared at 56D, although with lower reduction rate around 5%. The reference compound exhibited around 6% greater mean with 9,39 MPa than 5%SF with (8,89 MPa) at 56D. It is important to observe that, these changes are not remarkable, but still it can be seen that, 5%SF could retain its MOR value at 56D (this binder improved gently its mean around 3%), in contrast 0%SF binder decreased its value around 3% after 56D hydration. (See Table 4.11).

The toughness of the specimens are calculated as the area under the load-deflection shown in Figure 4.39. As can be seen in Figure 4.40, the 5%SF compounds exhibited around 15% higher toughness value than reference mixture from (11,60 kJ/m<sup>2</sup> for 0%SF) to (13,28 kJ/m<sup>2</sup> for 5%SF) at 28D hydration. Specimens exhibited an opposite trend at 56D hydration which the toughness value reduced by 28% from (11,11 kJ/m<sup>2</sup> for 0%SF) to (7,99 kJ/m<sup>2</sup> for 5%SF) when silica fume was added to the matrix. Considering each compound individually, 5%SF compound has shown a greater reduction about 40% lower value (7,99 kJ/m<sup>2</sup> at 56D) comparing to its value at 28D. This trend was lower in the reference mixture, with only 5% reduction in mean over the time. (See Table 4.11).

Table 4.11. The average values and standard deviations of Flexural Strength

Specimen	Flexural Strength	LOP (MPa)		MOR (MPa)		MOE (GPa)		SE (kJ/m <sup>2</sup> )	
		28 days	56 days	28 days	56 days	28 days	56 days	28 days	56 days
	Curing Days								
CAC-0%SF-10%CO		8,74 (0,24)	7,81 (0,72)	9,65 (a) (0,04)*	9,39 (a) (0,98)	3,82 (0,15)	3,55 (0,66)	11,6 (2,8)	11,11 (2,7)
CAC-5%SF-10%CO		7,07 (0,66)	7,21 (0,69)	8,69 (a) (0,11)	8,89 (a) (0,74)	3,39 (0,02)	3,02 (0,41)	13,28 (4,6)	7,99 (1,35)

\*Values in parentheses are standard deviation

#### 4.4.2. Durability of composites after aging cycles

In this section, the results obtained from the experimental characterization of the flexural strength by means of three-point bending tests are presented. The flexural stress-displacement curves derived for the unaged-aged tested composites, and the values of Modulus of Elasticity (MOE), Limits of Proportionality (LOP), Modulus of Rupture (MOR), and Specific Energy (SE) are computed and compared. The specimen groups are revealed the sets from 0%SF (reference compound) and 5%SF reinforced with 10% cotton linter fiber in CAC based matrix cured for 28D and 28D+10 accelerated aging cycles. Figures 4.41, 4.42 present a plot of flexural stress-displacement for varied SF content of (i.e., 0%SF, 5%SF) in CAC-SVC3425-10%CO composite, and Table 4.12 presents its flexural strength parameter's average values. The obtained results exhibited the linear relationship before FCS was steeper in both compound types after being subjected to aging cycles, in unaged specimens the incline was dropped considerably at 28D. The failure of unaged compounds occurred approximately in deflection range of 0.40-0.55 mm, while the failure of aged compounds was in range of 0.20 mm. Where, PCS deflections reached up to 3.50 to 4.00 mm in both unaged-aged compounds. Both aged 0%-5%SF specimen's bearing capacity approached to its limit (FCS) accompanied by the specimen failure, while PCS of mixtures generated a curve resembled to flexural load-deflection for a ductile material with (Strain-softening behaviour), with a sufficient FCS-PCS and toughness for some applications.

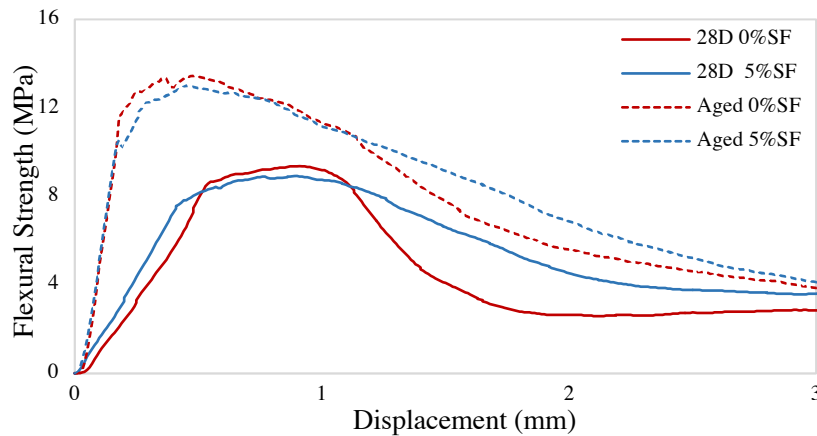


**Figure 4.41.** Flexural stress-displacement relationships for the SF-CAC-SVC342510%CO composites at 28D and 28D+10 accelerated aging cycles.

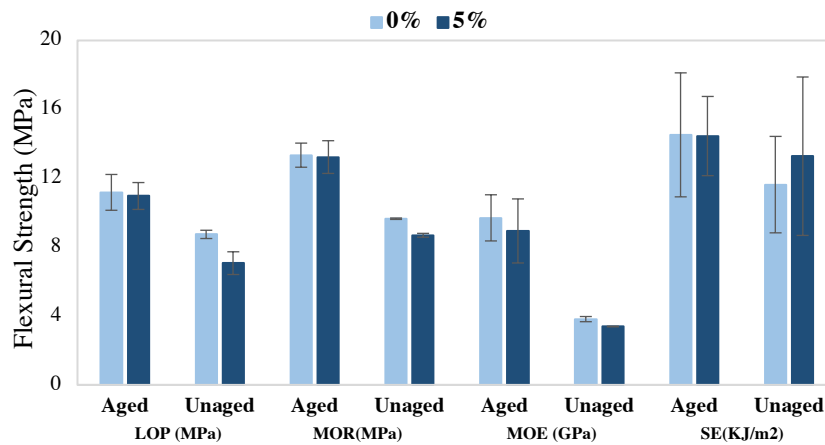


**Figure 4.42.** Flexural strength parameters for SF-CAC-SVC342510%CO composites at 28D and 28D+10 accelerated aging cycles.

The compounds exhibited about 10% decrease in their modulus of elasticity average value with the addition of 5%SF in matrix from 3,82 to 3,39 GPa in unaged compounds cured for 28D. While the aged counterpart specimens exhibited same trend but gently lower rate about 8% from 9,70 to 8,94 GPa after 10 accelerated aging cycles. Considering the mixtures individually, significant improvement in means was observed after wet/dry cycles. 0%SF binder exhibited about 154% improvement from 3,82 to 9,70 GPa and the 5%SF exhibited about 164% higher mean after aging cycles, from 3,39 to 8,94 GPa. (See Table 4.12).

The results obtained for limits of proportionality indicate that the reference compound achieved slightly higher average value than 5%SF binders in both unaged-aged compounds. Unaged compounds exhibited around 20% reduction in their means from (8,74 to 7,07 MPa) with 5%SF addition to the matrix, while aged compounds almost retained its values (11,18 to 10,97 MPa), (See Table 4.12). Both 0%SF and 5%SF binders increased their mean after aging cycles, about 28% from (8,74 to 11,18 MPa) and 55% from (7,07 to 10,97 MPa) respectively.

With respect to MOR, the results are consistent with what was observed for LOP, the unaged compound experienced a strength loss about 10% with 5% silica fume addition to the matrix, whereas the aged compounds retained their means. Reference composite obtained MOR average value of 13,34 MPa, and 5%SF binder achieved up to 13,23 MPa after 10 accelerated aging cycles. Likewise, aged reference mixture exhibited an increase of 38% in its mean from (9,65 to 13,34 MPa). Same increase trend was observed in 5%SF compound about 34% increase in its value from (8,69 to 13,23 MPa). (See Table 4.12).

Toughness means in both aged mixtures was increased after cycles, a fairly good strain-softening behaviour with sufficient deformation capacity (FCS and PCS) were achieved in both binders, due to the formation of multiple cracks. As stated in previous studies with similar reinforcement systems (J. Claramunt 2016), (J. Claramunt and H. Ventura 2017).

The unaged specimens exhibited an increase of 15% with 5%SF addition in matrix, from 11,63 kJ/m<sup>2</sup> to 13,28 kJ/m<sup>2</sup>, and aged compounds retained their values, from 14,52 kJ/m<sup>2</sup> to 14,45 kJ/m<sup>2</sup>. Each compound revealed a greater mean of (25% higher), from 11,63 kJ/m<sup>2</sup> for unaged 0%SF compound comparing to its aged compound with 14,52 kJ/m<sup>2</sup>. Same trend is observed in compound with 5%SF, about 9% increased value (13,28 to 14,45 kJ/m<sup>2</sup>) after 10 accelerated aging cycles.

**Table 4.12.** The average values and standard deviations of flexural strength

Specimen	Flexural Strength	LOP(MPa)		MOR (MPa)		MOE (GPa)		SE (KJ/m <sup>2</sup> )	
	Curing Days	Aged	Unaged	Aged	Unaged	Aged	Unaged	Aged	Unaged
		CAC-0%SF-10%CO	11,18 (1,04)	8,74 (0,24)	13,34 (a) (0,7)*	9,65 (a) (0,04)	9,7 (1,34)	3,82 (0,66)	14,52 (3,6)
CAC-5%SF-10%CO	10,97 (0,78)	7,07 (0,66)	13,23 (a) (0,95)	8,69 (a) (0,11)	8,94 (1,86)	3,39 (0,41)	14,45 (2,3)	13,28 (4,6)	

\*Values in parentheses are standard deviation

The obtained results in 4<sup>th</sup>, indicate that the both reference (0%SF) and 5%SF compound exhibited similar behaviour and values in terms of FCS-PCS and toughness containing 10%VF content. Both compounds increased its FCS after being subjected to aging cycles. This behavior could be related to a twofold action that combines (1) the lower degradation of the vegetable

fibers in CAC with the aging process and (2) due to the formation of well-known phase of strätlingite ( $C_2ASH_8$ ) in CAC pastes with pozzolanic additions (J. Ding, Y. Fu 1995), (A. Hidalgo, J.L. García 2009), (E. Sakai, T. Sugiyama 2010), (N.K. Lee, K.T. Koh 2017), (H.M. Son, S. Park 2019).

It was also stated in the results of previous 1<sup>st</sup> - 2<sup>nd</sup> stages that, it can be considered that the slight reduction in VFRCCs that occurred could be (*to some extent but not completely is due to fiber degradation*) after submitting them to the wetting and drying cycles. While it could be related to a major extent of conversion reactions which could contribute to the decrease of the FCS values. On the other hand, regarding the results obtained in 3<sup>rd</sup> stage, the conversion system was hindered in mixture of 5%SF matrix, and the new phases of strätlingite ( $C_2ASH_8$ ) was present and sufficient FCS was obtained by these mixtures.

According to stated and confirmed results in previous sections, the mechanical behavior of specimens expected to be influenced with incorporated SF in VFRCC matrix. While here, the reference compound revealed almost identical performance as 5%SF specimens. Moreover, both compounds increased their FCS-PCS even after accelerated aging cycles, it can be considered that the fiber strength does not appear to be affected by aging cycles, regarding to higher values of flexural strength obtained by both unaged-aged compounds. Therefore, it could be considered that:

1. The durability of such materials developed in a CAC-based matrix, demonstrated a significant improvement over previously reported cementitious composites reinforced with vegetable fibers. As CAC is a lower pH matrix, as result an appropriate matrix for such materials (J. Claramunt and H. Ventura 2016).

2. Due to SF incorporation in matrix, there is a lower content of cement to degrade the VF, in other words, the alkaline medium of CAC is controlled by silica fume additions, at the same time the hindered conversion phenomenon in CAC matrix (M. Collepardi and S. Monosi 1995).

These claims will be evaluated by BSEM/SEM analysis in coming sections. The improved and preserved mechanical performance of both mixtures (0%SF-10%CO, 5%SF-10%CO) after being subjected to wetting and drying cycles, despite of increased content of 10%VF indicates that CAC, SF-CAC matrices are less aggressive toward the VFs. However, the understanding of this behavior demands the further and deeper investigations.

#### 4.4.3. BSEM, Microstructure analysis of unaged-aged compounds

Figure 4.43 indicates BSEM microphotograph of 0%SF-CAC-10%CO compound cured for 28D (as reference matrix) along with the anhydrous polyphasic particles and hydrated zones of  $C_3AH_6+AH_3$ . The chemical particles are identical as those detected hydrates in previous experimental section, such as (Monophasic mono-calcium aluminate particles, Polyphasic calcium aluminates particles and Ferritic phases, etc.). Stated clearly in detail previously, a more advanced phase of hydration are detected at 28D hydrated matrix, that indicates the change of meta-stable phases of  $CAH_{10}-C_2AH_8$  to stable phases of  $C_3AH_6+AH_3$ .

BSEM microphotograph results reveal strong peaks, indicating the formation of the stable phases during the hydration stages of 0%SF-CAC-10%CO compound. As anticipated, the presence of anhydrous polyphasic particles and hydrated zones in 0%SF-CAC-10%CO compound at 28D is indicated. The chemical analysis identified the following types of particles in matrix: SP1 revealed a uniform gray color phase, which could be mono-calcium aluminate based on constituents detected here (CA phase). The polyphasic particles found in SP2-SP3 are observed with two shades of gray, one neutral and a lighter gray, which also could be mono-calcium aluminate with some silicon content in SP2 (CA phase).

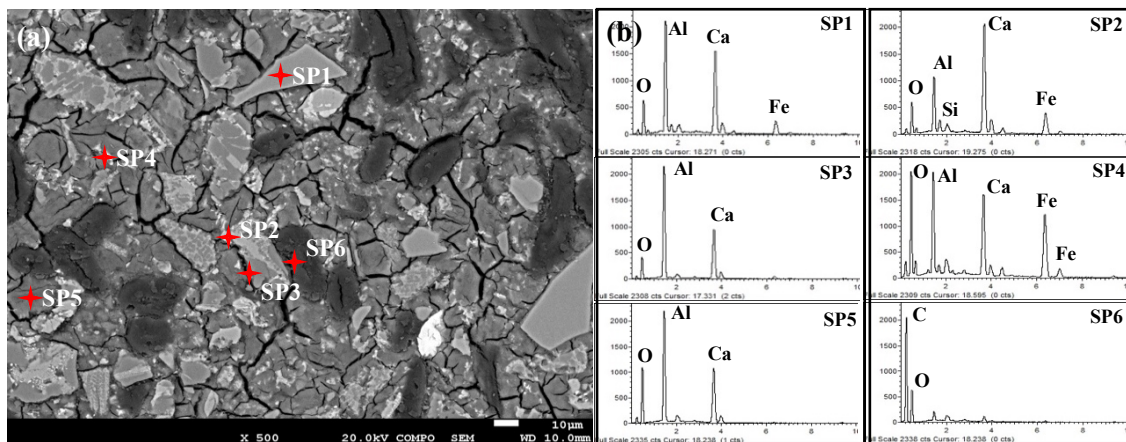


**Figure 4.43.** (a) BSEM image of 0%SF-CAC-10%CO at 28D, (b) with EDS spectra corresponding to the points marked in image. SP1-SP2= anhydrous phase with some silica and ferretic phases; SP3-SP5= hydrated phases SP4= anhydrous phases with high iron content Ferro-CT; SP6= Cotton linter fiber.

The lighter sections that studied in SP4, contains iron in addition to aluminum and calcium, that could be corresponded to Ferro-CT phases, with a high iron content. All these phases are related with anhydrous constituents of aluminate cement, as the low oxygen content of spectrum must indicate that. However, there is more of this chemical (oxygen) in SP4, that indicate a hydrated phase deposited on an anhydrous particle with a high iron content of hydrated phase type.

Spectra SP5 is corresponded to the dark gray area of cement's hydrated phases, that are chemically similar in composition. Given the high aluminum content relative to calcium, these dark gray areas could be amorphous  $AH_3$  mixed with  $C_3AH_6$ . There has been no evidence of  $C_2AH_8$  existence in electron microscopy, generally there are easily identified. This could imply that the meta-stable phases  $CAH_{10}$  and  $C_2AH_8$  have been converted to stable phases  $C_3AH_6+AH_3$ . SP6 correspond to the dark gray color of cotton linter fiber.

Figure 4.44 presents the mapping details of the previous figure; image (a) 0%SF-CAC-10%CO compound at 28D, image (b) the anhydrous particles (lighter parts), hydrated zones (plain medium gray), and some bean shaped particles dark grey corresponding to cotton linter fiber. Image (c) BSEM mappings for the elements Ca, O, Fe, and Al are included at the bottom in color, where indicates the concentrations of aforesaid elements. In transparency zones with the highest ion concentration placed on the original image. As can be seen, in mapping image the Ca and Al contents of hydrated zone are very high, which indicates the mono calcium aluminate (CA phase).

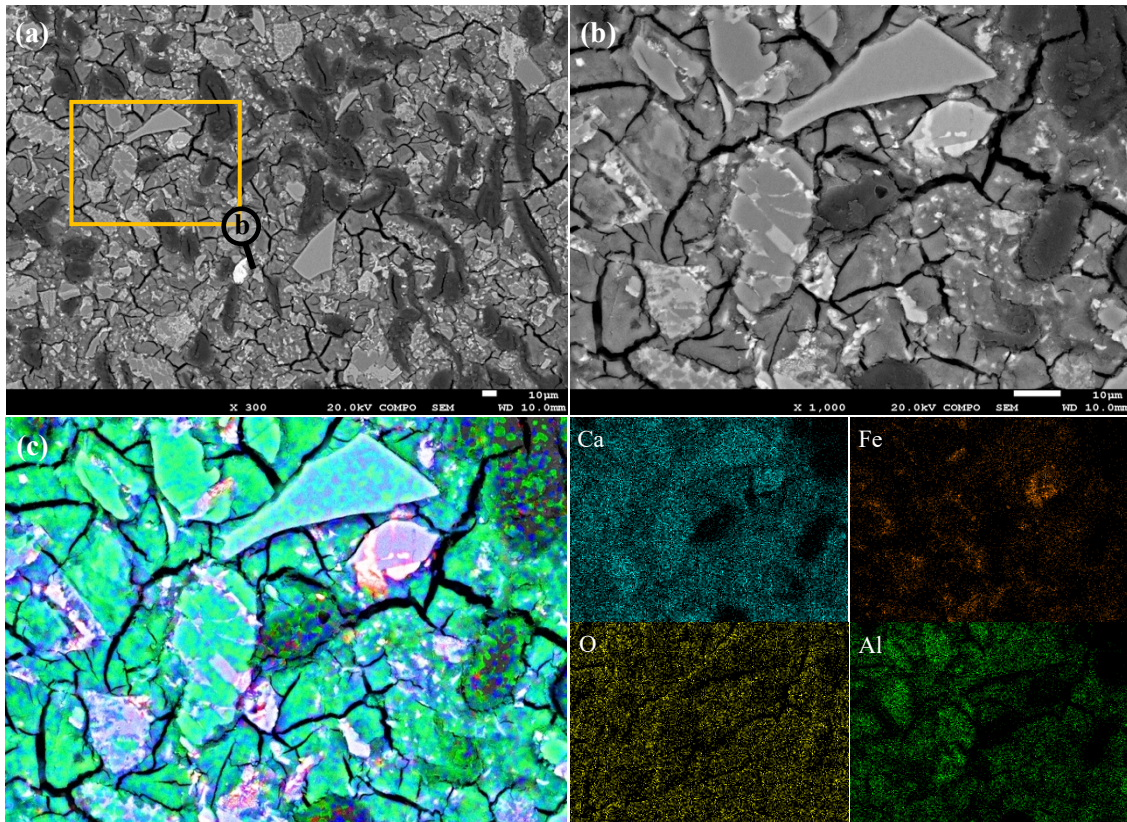


**Figure 4.44.** (a) BSEM image of 0%SF-CAC-10%CO at 28D (b, c) at different magnification zones that presents the mapping of anhydrous polyphasic particles and hydrated zones of  $C_3AH_6+AH_3$ .

Figure 4.45 presents BSEM microphotograph of 0%SF-CAC-10%CO compound at 28D and subjected to 10 accelerated aging cycles. The results show strong peaks indicating the formation of stable phases during the compound's hydration stages. The anhydrous polyphasic particles and hydrated zones are present and identified as following particle types:

As it is well observed in SP1, a uniform gray color of anhydrous monocalcium aluminate, that slightly has faded away in outer parts of the particle. The hydrated phase which can be observed clearly in spectra SP2, where the Ca content increases significantly with some iron contents. The lighter gray elements studied in SP3-SP4-SP5, contain iron in addition to aluminum and calcium with higher contents, this could be corresponded to the iron-rich Ferro-CT phases. As can be seen, in SP5 there are more of this chemical elements with a high iron content of the hydrated phase type. The SP6 spectra correspond to a darker gray area of cement's hydrated phases, they are chemically similar in composition. These dark gray areas could be amorphous  $AH_3$  combined with  $C_3AH_6$ . Hence, due to the high aluminum content relative to calcium, this

could indicate that the metastable phases  $CAH_{10}$  and  $C_2AH_8$  have been converted to the stable phases of  $C_3AH_6$  and  $AH_3$ . The SP7 spectra correspond to hydrated phase where the Ca content increases significantly with some iron contents, and SP8 correspond to the dark gray color of cotton linter fiber.

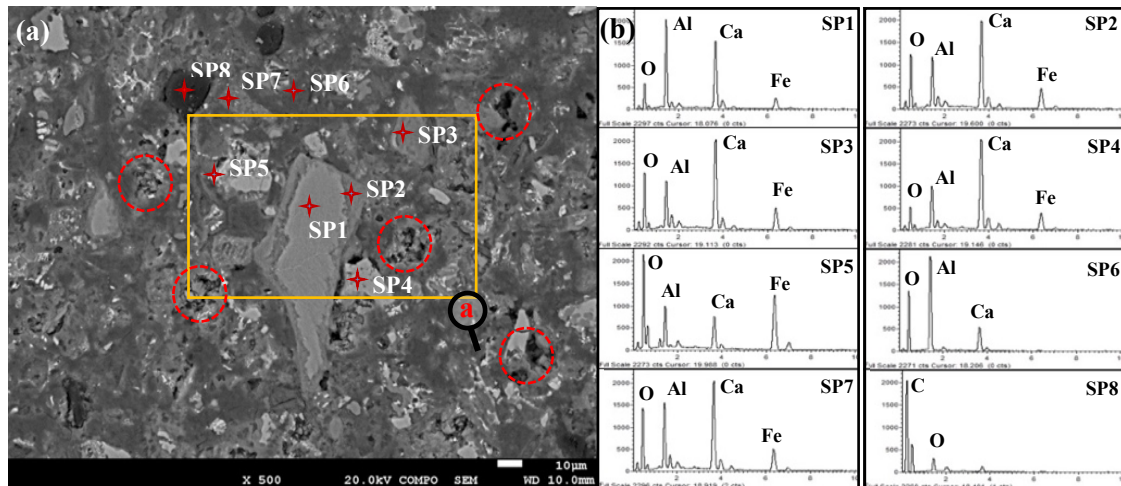


**Figure 4.45.** (a) BSEM image of 0%SF-CAC-10%CO at 28D, (b) with EDS spectra corresponding to the points marked in image. Spectra SP1-SP2= anhydrous phase; SP3-SP4-SP5= anhydrous phases with high iron content Ferro-CT; SP6 = hydrated phases of  $C_3AH_6 + AH_3$ , SP7= hydrated Ferro-CT phase, SP8= Cotton linter fiber.

However, aging cycles caused dissolution of some phases together with the migration and reprecipitation of calcium ion in certain areas. BSEM mapping phase in [Figure 4.46](#) image (c), (image (Ca) taken from [Figure 4.44](#) indicated by yellow line), to differentiate the similarities and dissimilarities that can be observed in both compounds before and after accelerated aging cycles. It appears to be, aluminum and calcium phases are combined (the color is a uniform bluish-green).

Moreover, in aged compound they are not uniformed (See image (c)), there are very bluish areas with higher Ca content and greenish areas with Al content, which coincide with the darker gray areas (lower atomic number) of the electron microphotograph and other parts with higher Al content (lighter gray areas and higher atomic number). This could indicate that, the dissolved phases are dissociated and precipitated, by modifying the relative contents of Ca and Al in matrix. This was observed clearly also in [Figure 4.45](#).

The SP1 spectra corresponds to anhydrous monocalcium aluminate and SP2 corresponds to hydrated phase, with an increased Ca content, in contrast with SP6 where Ca content is very low. Previously said, in unaged compound no porosity is observed, although there are many cracks. Regardless of considering these cracks, it seems that the matrix is very compacted and there are no visible porous areas compared to compounds exposed to aging cycles (indicated with yellow circles in [Figure 4.45](#)).

This indicates a conversion from  $CAH_{10}$  to  $C_3AH_6$  with the volume reduction implicit in the change. On the other hand, it seems that a part of porosity is filled with deposits of new phases of calcium aluminates rich in Al. This difference can be observed from the SP6 ([Figure 4.45](#)) and SP7 spectra ([Figure 4.46](#) (b)). In SP7 it is observed how the relative content between Al and Ca is much more balanced than in SP6 where a higher Al content is observed in darker hydrated zones which didn't appear in unaged 28D compound.

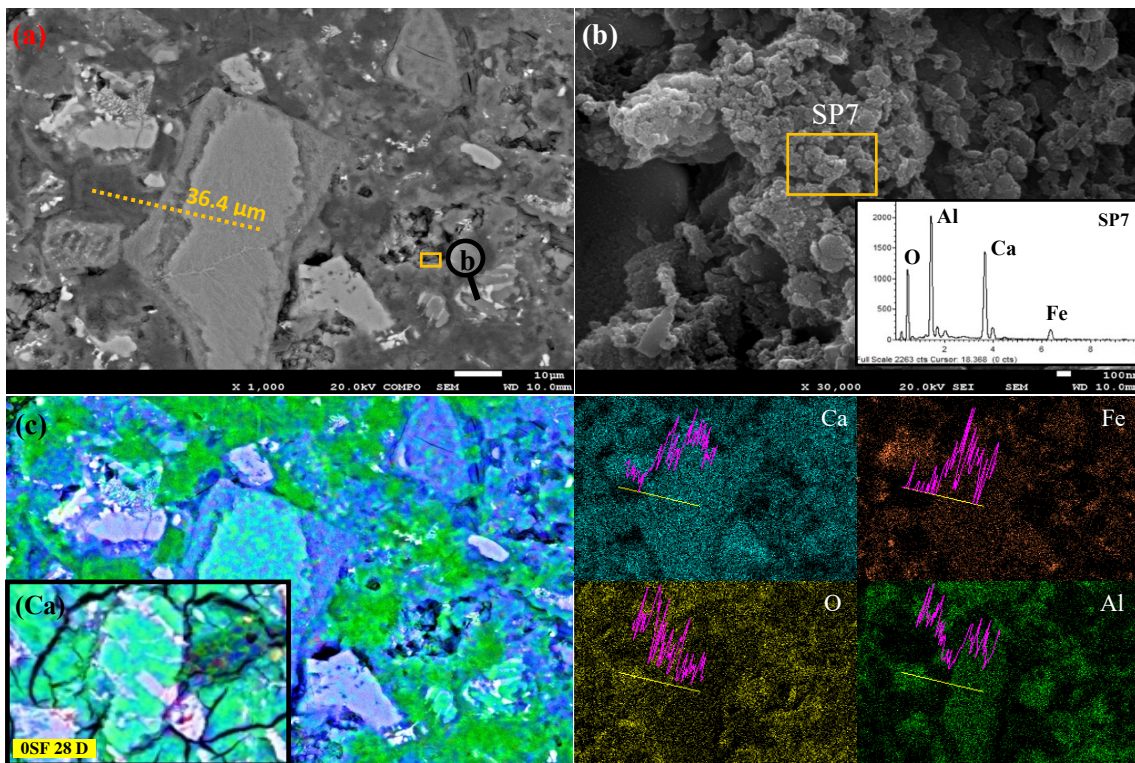


**Figure 4.46.** (a) BSEM image of 0%SF-CAC-10%CO at 28D+Subjected to 10 accelerated aging cycles, (b) with EDS spectra corresponding to the points marked in image, (c) the mapping of anhydrous polyphasic particles and hydrated zones of  $C_3AH_6+AH_3$ .

Figure 4.47 presents BSEM microphotograph of 5%SF-CAC-10%CO compound cured for 28D as the identification for the hydration phases, the monophasic calcium aluminate particles are visible in this specimen, as opposed to the specimen without SF in images (a, b). In SP1 spectra, the anhydrous particles rich in aluminates (lighter gray parts), hydrated zones (plain medium gray) and a part of amorphous silica particle are observed. In this case monophasic calcium aluminate particles are not evident, probably due to the presence of significant silicon content (in SP1 spectra), reacting and turning into strätlingite ( $C_2ASH_8$ ) that is detected in SP1. The cotton linter particles can be detected in SP2 with a high carbon content and lower oxygen content (easily detectable due to its dark gray color and oval bean shaped particles).

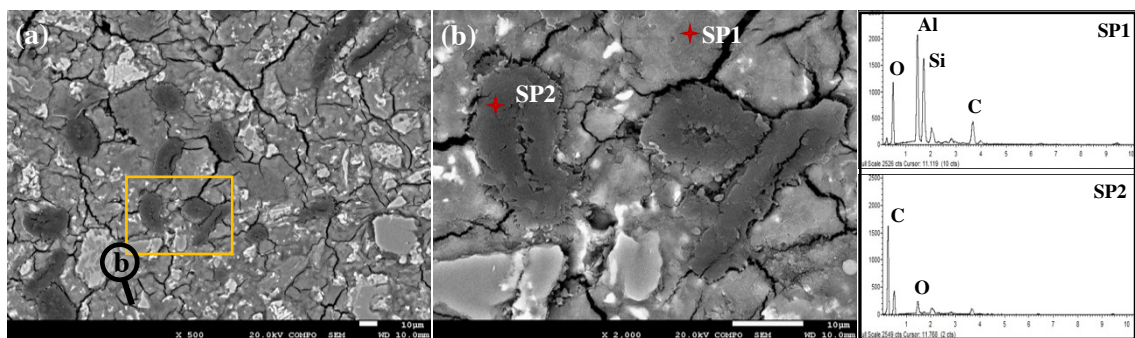


**Figure 4.47.** (a) BSEM image of 5%SF-CAC-10%CO 28D cured compound identification phase, (b) with EDS spectra corresponding to the points marked in image, SP1= possible formation of strätlingite phase ( $C_2ASH_8$ ), SP2= Cotton linter fiber.

The Si mapping in colors of 5%SF-CAC-10%CO at 28D, is presented at the bottom of each BSEM microphotograph in Figure 4.48, corresponding to Ca, Si, Fe and Al elements. Which indicates the concentrations of each element, the transparency zones with highest ion concentration are placed on the original image. As shown in Si mapping image (b), the silica content of hydrated zone is considerably high. This could indicate that the reaction with calcium aluminate compound has occurred, hence the possible formation of  $C_2ASH_8$  can be detected. On the other hand, SF particles are surrounded with a certain amount of Ca and Al, indicating that there has been a reaction between compounds. In combination of maps in color, it is possible to observe clearly the distribution of hydrated phases and in the limits of SF particles.

However, regardless of considering the cracks appeared in unaged compound which could be related to hydration drying procedure of matrix. The unaged matrix seems to be very well compacted and without porous, This is also indicated in Figure 4.50 at the bottom in the yellow rectangle which differentiate the dissimilarities.

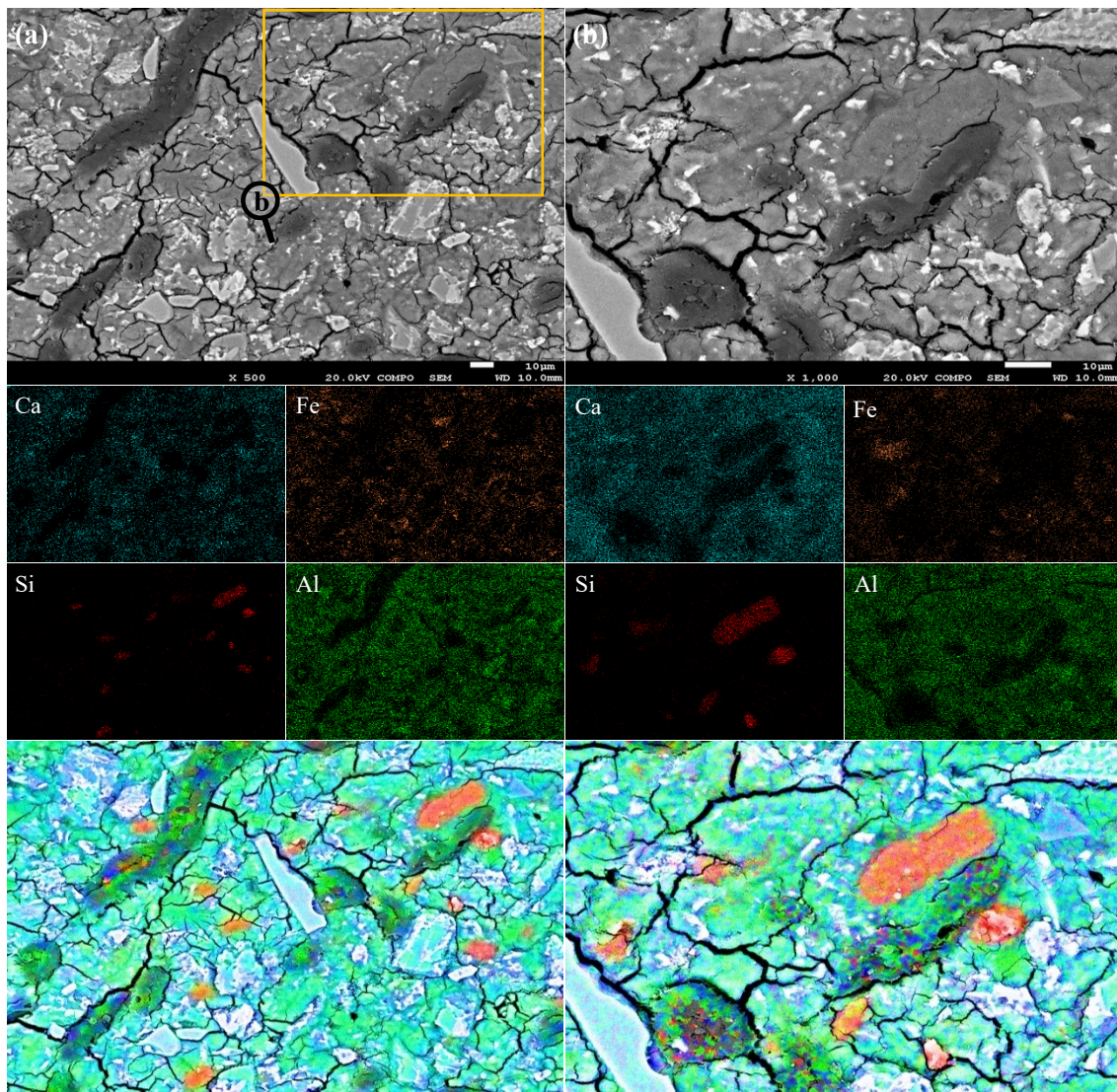


**Figure 4.48.** (a, b) BSEM image of 5%SF-CAC-10%CO compound 28D, at different magnification zones that presents the mapping of anhydrous polyphasic particles and hydrated zones.

Figure 4.49 indicates BSEM microphotograph of 5%SF-CAC-10%CO compound at 28D and subjected to 10 accelerated aging cycles. The results presents strong peaks of Ca and Al indicating the formation of stable phases during the compound's hydration stages in SP1-SP2-SP3. The anhydrous polyphasic particles and hydrated particles are identified as following particle types: It is observed in SP1 spectra, a uniform gray color of the anhydrous monocalcium aluminate, which slightly has faded away as hydrated phase that can be observed clearly in spectra SP3, with a high Ca content.

The SP4 spectra corresponds to a darker gray area of cement's hydrated phases, these dark gray areas could be amorphous  $AH_3$  combined with  $C_3AH_6$ . Due to the high aluminum content compared to calcium, this could be because of the converted metastable phases  $CAH_{10}$  and  $C_2AH_8$  to the stable phases of  $C_3AH_6$  and  $AH_3$ . For instance, it can be seen in the green circled zone it seems there is a precipitated compound about to close a pore.

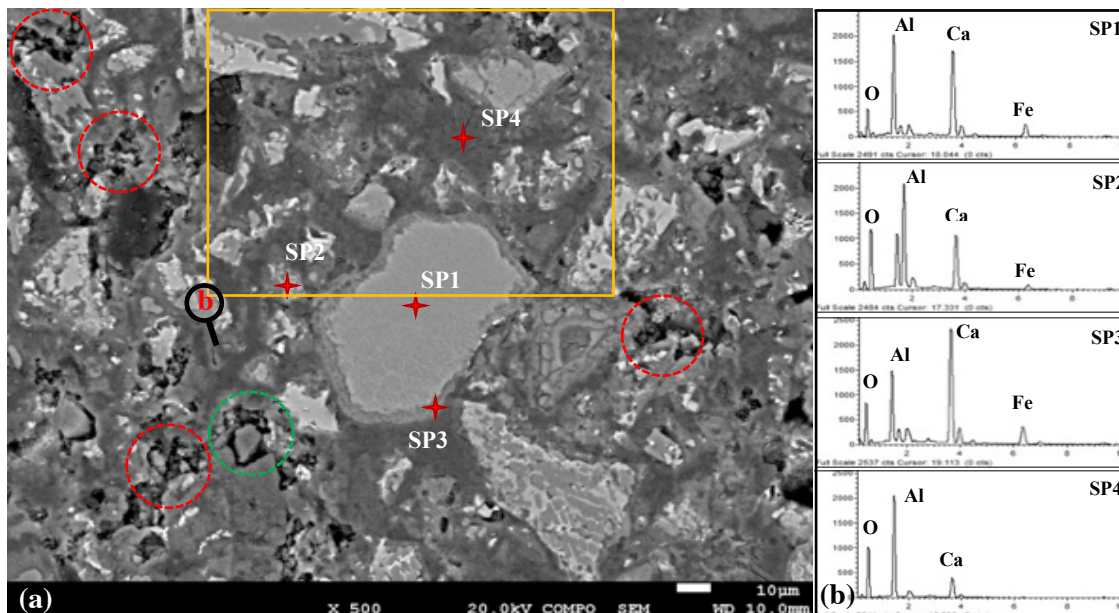


**Figure 4.49.** BSEM image of 5%SF-CAC-10%CO compound at 28D, subjected to 10 accelerated aging cycles, presents the anhydrous polyphasic particles and hydrated zones. Indicating the spectra corresponding to SP1-SP2-SP3= anhydrous polyphasic phases with high iron content Ferro-CT; SP4 = hydrated phases.

Figure 4.50 presents the Si mapping of 5%SF-CAC-10%CO compound subjected to 10 accelerated aging cycles. As can be observed in images (a, b and c) there are reprecipitation of Ca (blue zones), it appears that cotton linter fiber didn't interact in this process. In image (a) there are green zones close to fibers and blue areas which there is no fiber close by this zone. In image (c) seems that blue zones are more closer to fibers and green zones are a part from fibers. Therefore, there is no a clear tendency towards one of mentioned zones or the other. In line scan of image (c) can be seen that the content of Ca and Al in fibers zone is low.

Regarding to Si content in unaged compound, the particles are observable with their well-defined shapes. In Si mapping the particles are seen and no dispersion of Si ions are observed in the rest of specimen. On the other hand, in mapping of aged compound, the particles are blurred at their edges and Si ion appears scattered throughout the compound.

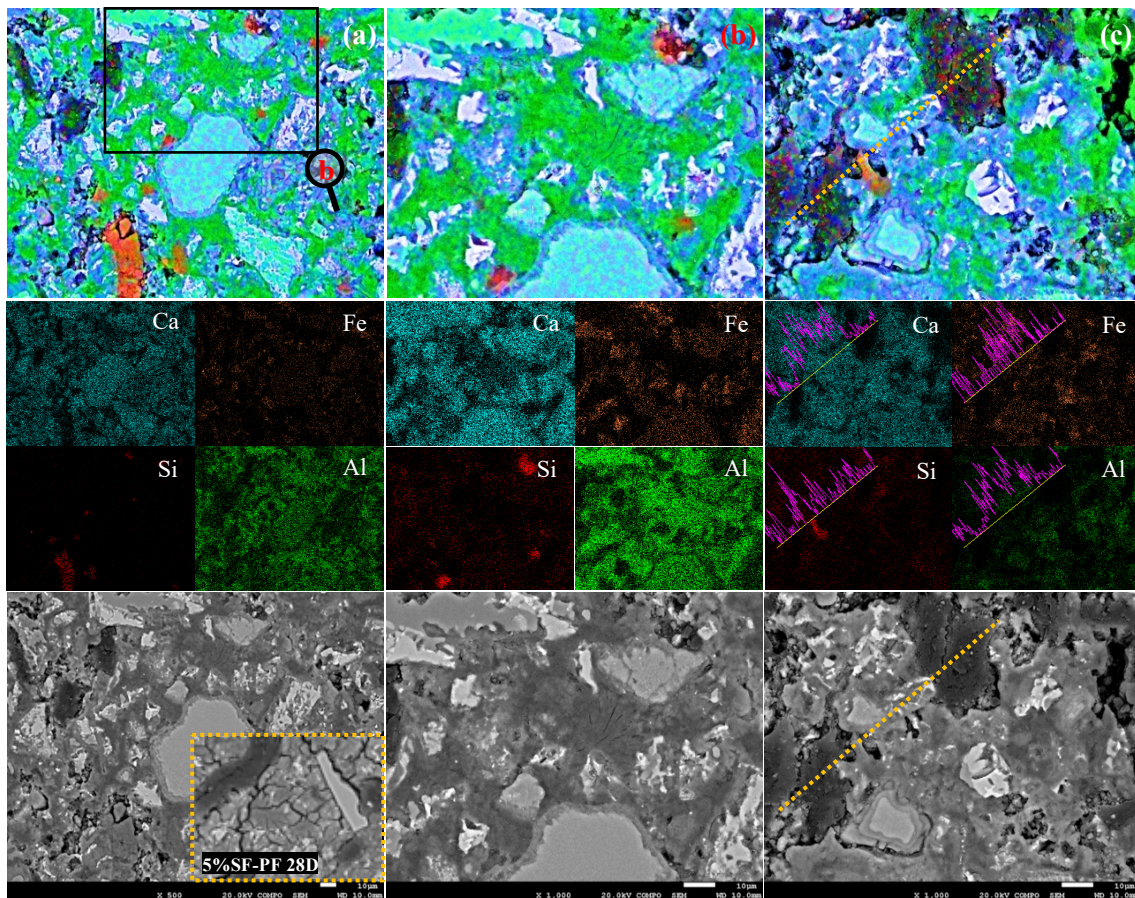
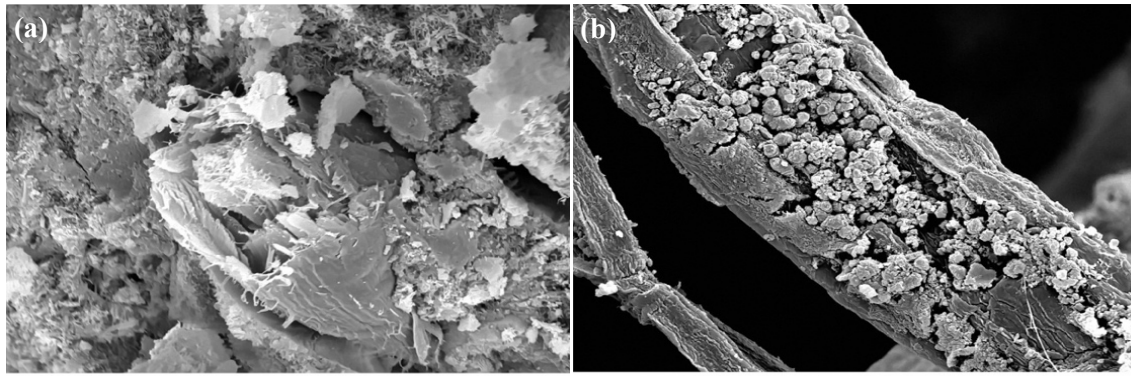


**Figure 4.50.** (a, b, c) BSEM image of 5%SF-CAC-10%CO compound at 28D, and subjected to 10 accelerated aging cycles, at different magnification zones that presents the mapping of anhydrous polyphasic particles and hydrated zones.

#### 4.4.4. SEM, Analysis of the fracture surface

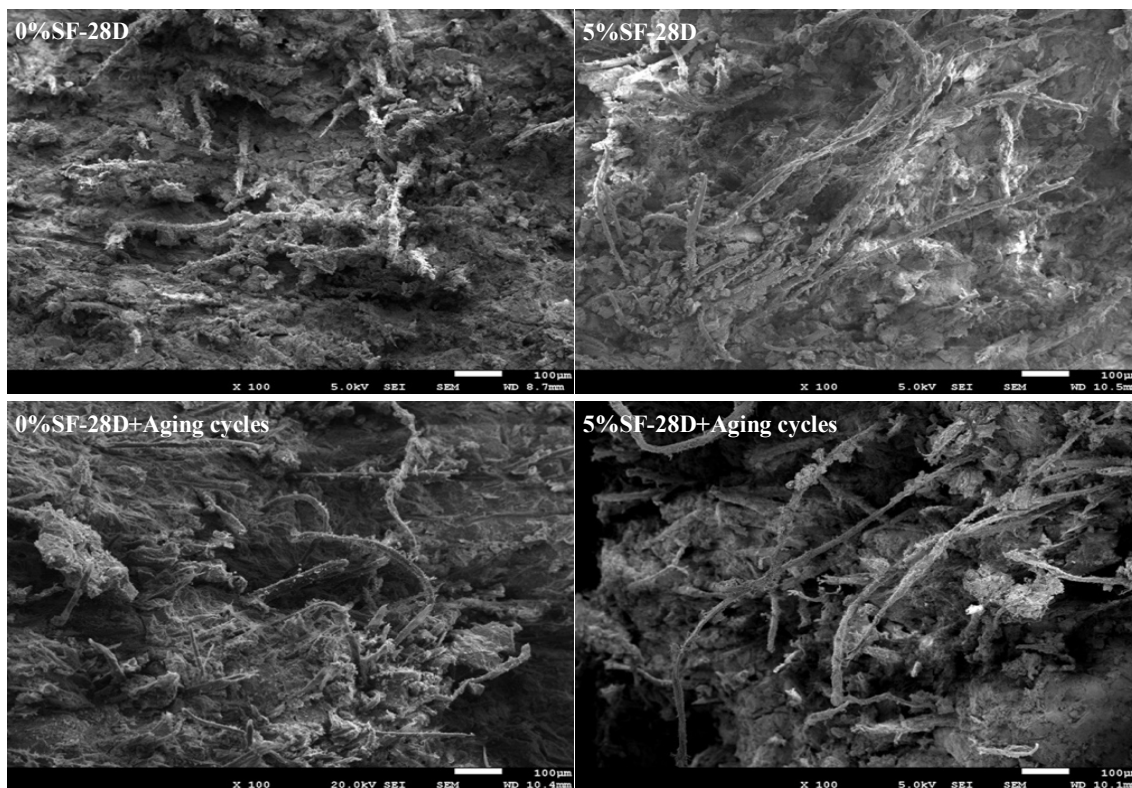
To evaluate the changes in the cotton linter fiber of both unaged-aged compounds were analyzed by SEM microphotograph images. Generally speaking, the clean fibers present a smooth surface (as indicated in Figure 4.51 for comparison purposes, the fibers are subjected to wet/dry cycles in Portland cement matrix). As can be seen, it is clearly possible to observe the damages on the surface of fibers corresponded to the effect of alkaline compounds of Portland cement paste. Image (a) correspond to fibers of portland mortars reinforced with Kraft pine fibers subjected to 4 dry-wet cycles of 1 week each. It can be observed that the fiber breaks at the level of the fracture surface.

Image (b) indicates the surface of a fiber which in its surface appears numerous transverse cracks as the result of fiber degradation suffered after the accelerated aging process. This degradation is the consequence of the dissolution of the amorphous zones of the cellulose which chains are truncated by the combination with the calcium ions coming from the portlandite of the matrix. (M. Ardanuy and J. Claramunt 2015).



**Figure 4.51.** SEM images showing cement hydration compounds in the lumen and surface of the vegetable fibers. (M. Ardanuy and J. Claramunt 2015).

Therefore, in SEM results of compounds shown in [Figure 4.52](#), it seems that there are not significant differences between the break sections of specimens. In all specimens, a multitude of cotton linter fibers can be seen protruding from the surface of the matrix. This can indicate that the vegetable fibers are not degraded in the CAC matrix. Regarding to the shape of the rupture sections, perhaps, that of aged 5%SF compound seems to be more disaggregated, and hence, it could be deduced that aged 5%SF compound could have higher deformability (this claim can also be verified with the results of bending mode curves and data). Although all specimens have maintained a high degree of ductility (Strain-softening behaviour was observed). (See [Figure 4.53](#))



**Figure 4.52.** SEM images of cotton linter compound at 28D in CAC and SF-CAC mixtures. SEM images of the cotton linter compound at 28D+Subjected to aging cycles in CAC and SF-CAC mixtures.

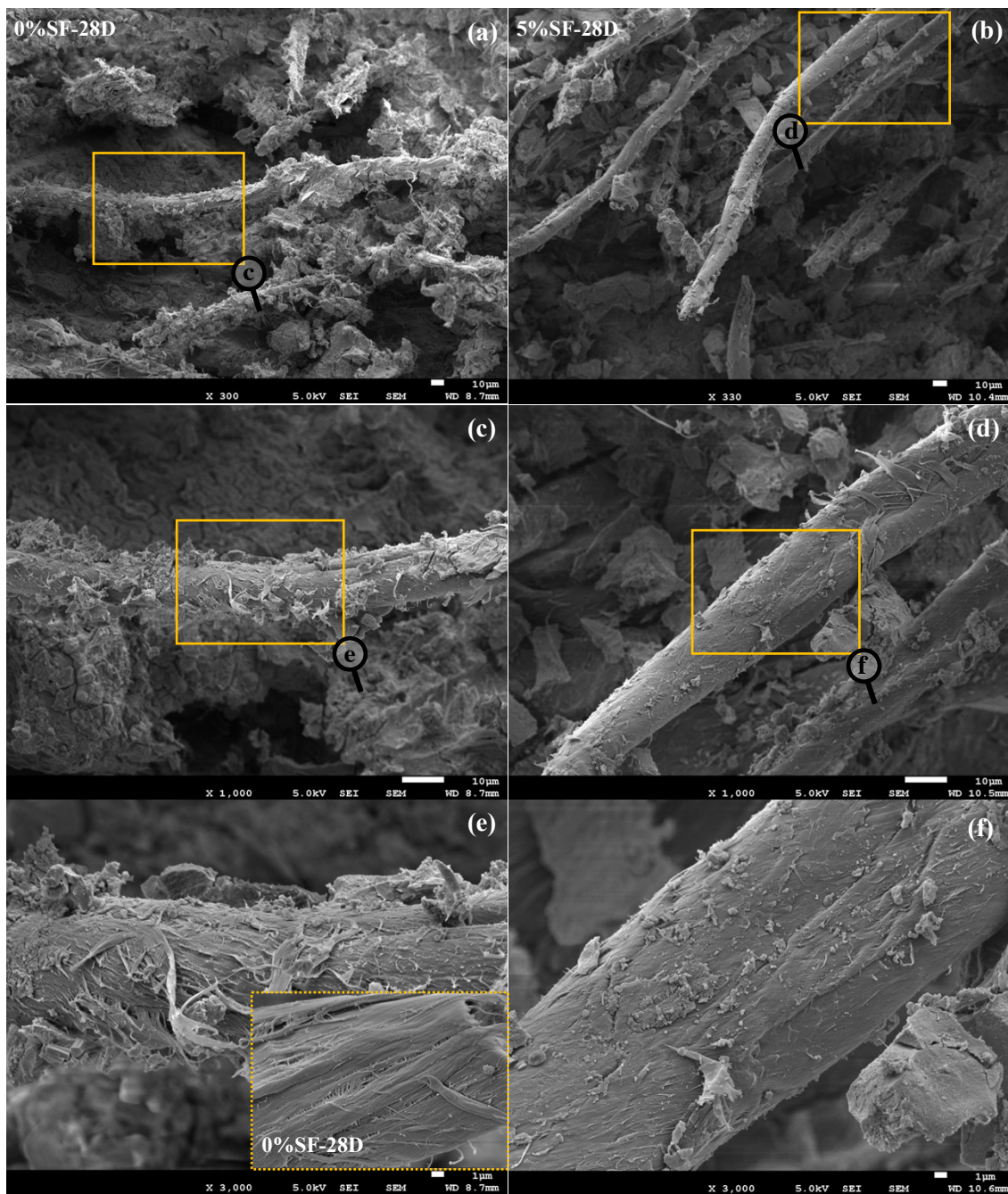


**Figure 4.53.** SEM images of cotton linter compound at 28D in pure CAC matrix and 5%SF-CAC binder.

In researches done on the VFRC composites with CAC-based matrix, VFs maintain their elasticity and have sufficient tensile strength to overcome the adherence to the matrix walls. In compounds without SF, a detachment of outer macro-fibril layers is observed (See [Figure 4.55](#)), while in specimen with 5%SF, this degradation didn't appear and the fiber's surface still remains relatively smooth. (See [Figure 4.54, 4.53](#)). Regarding to the differences between aged and unaged compounds, only slight longitudinal cracks can be observed in the direction of macro-fibrils in matrix. It is possible that aging cycles degrade the peptide polymer chains that act as the binder between macro-fibrils.

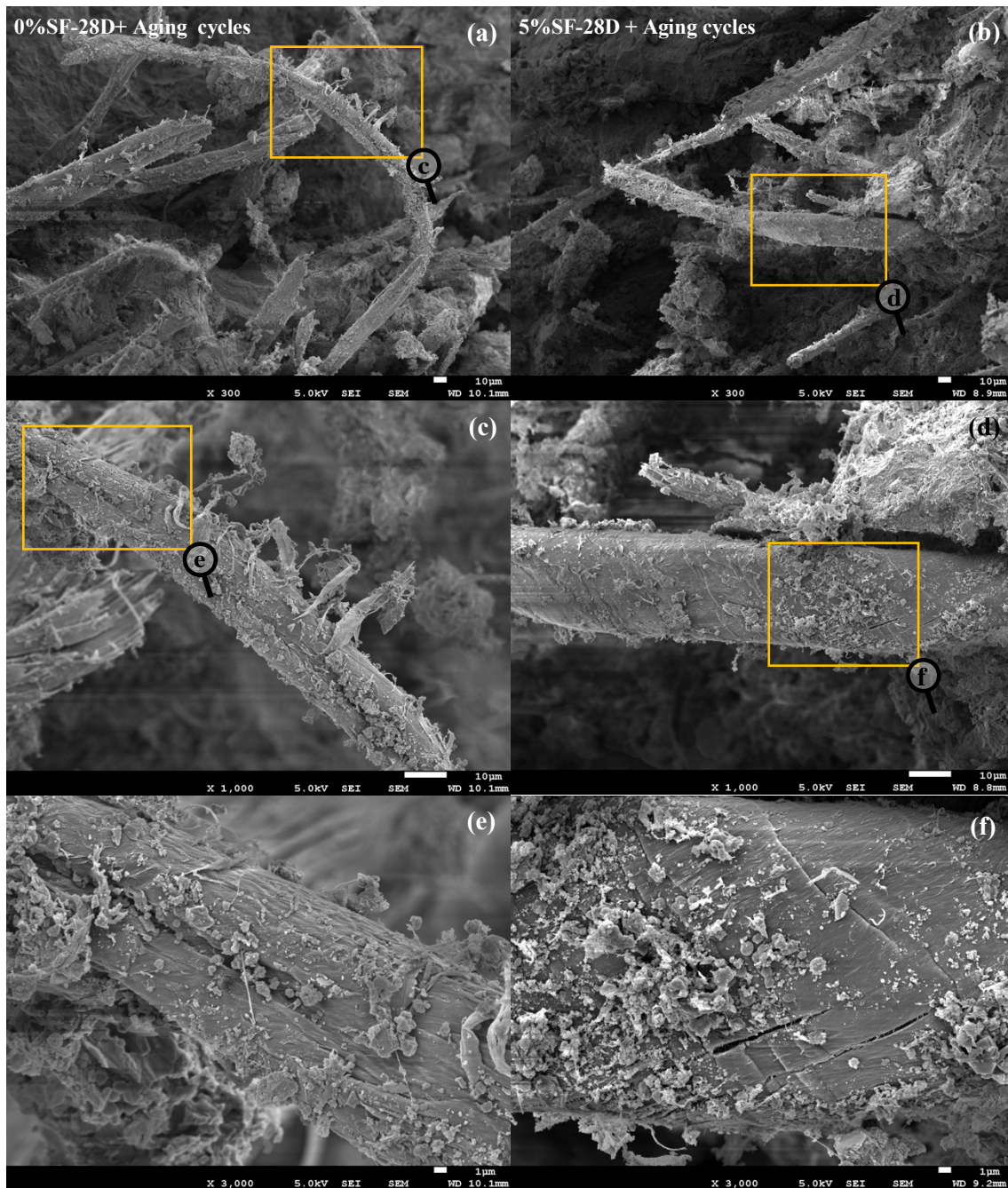


**Figure 4.54.** SEM images of cotton linter compound at 28D+ Subjected to aging cycles in pure CAC and 5%SF-CAC mixtures.

As can be seen, these cracks seem not to affect excessively the tensile strength of cotton linter fibers, since they are only separated from each other, while maintaining the integrity of cellulosic polymer chains. This can be seen in the following microphotographs of aged 0%SF, the surface layer of fiber has lost and it can be seen that how the macro-fibrils still retain their integrity. These results indicate that the CAC matrix is less aggressive toward vegetable fibers compared to Portland cement based composites. (See [Figure 4.55](#)).

A part from that, the addition of SF to CAC matrix could help to a further reduce of fiber damage in this matrix. This could be related to the absence of portlandite formation in CAC pastes, and also due to the reduction of cement content (however, in a very low content even with 5%SF addition) when the silica fume is incorporated to the matrix.

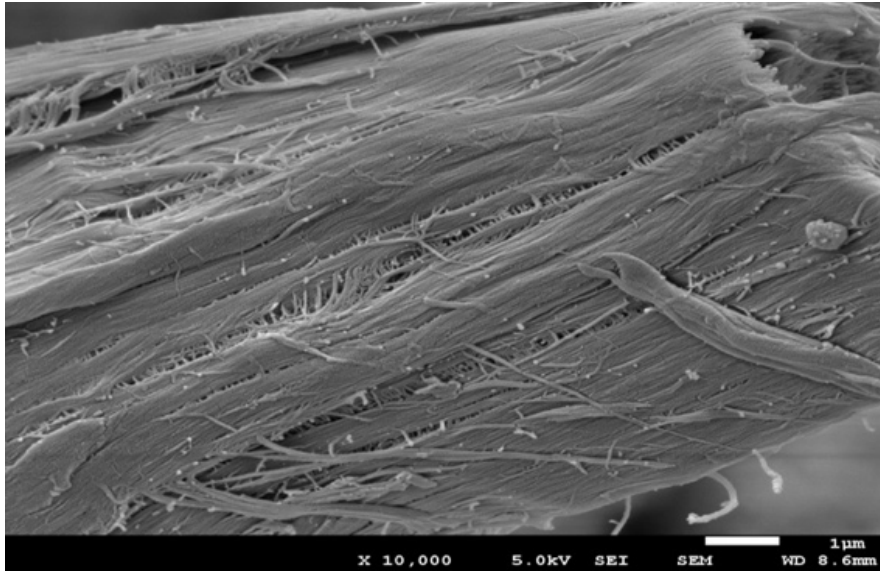


**Figure 4.55.** SEM image of cotton linter compound at 28D in CAC paste.

## 5. CONCLUSIONS

Vegetable Fiber Reinforced Cement Composite (VFRCC) has been proven to be a suitable material for non-structural construction applications, although because of the durability drawbacks of these materials, the studies on the flexural tensile behavior of these compounds after aging cycles in long term period of time is still required. For this reason, the presented investigation intended to respond to some extent the missing aspects by conducting an extensive experimental program together with some theoretical studies on the flexural tensile behavior of calcium aluminate cement reinforced with different types of vegetable fibers and contents.

In particular, (1) The long-term flexural strength and the influence of aging cycles on the strength of these compounds, (2) The influence of pozzolanic addition (silica fume) on CAC hydration phases and (3) In final the Vegetal Fiber Reinforced in SF-CAC matrices (VFRSFCC) were investigated. Based on the analysis of the results obtained, a conceptual analysis were proposed. In response to the general and specific objectives proposed in chapter 1, the general conclusions addressed in the thesis are presented next:

- CAC cement-based composites reinforced with vegetable fibers (i.e., cotton linter and flax fibers) can yield substantial improvements in the flexural properties of these materials. By incorporating (long or short) cotton linter and flax fibers into a CAC matrix a fairly good strength and tough material can be obtained becoming a promising material for the industrial production of vegetable fiber cement products.
- The incorporation of *Silica Fume* in CAC pure pastes can hinder the well-known conversion phenomenon for the specimens containing lower pozzolan contents.
- The incorporation of *Silica Fume* in VFRC in CAC-based matrix can improve the flexural behaviour of the composites in unaged-aged compounds.

*Vegetable-Fiber reinforcement in CAC-based matrix as alternative reinforcement*

- The incorporation of VFs was efficient in both fiber type (cotton linter and flax fiber). In terms of flexural performance, it was found that cotton linter compounds containing 6%-10% of VF exhibited flexural Strain-Softening behavior, with a sufficient deformation capacity (about 40% of FCS deflection) and a multiple post-cracking (wide cracks in compounds with 6%CO). These compounds obtained higher LOP and MOR values about 20% compared to those of flax fiber compounds. In compounds with lower contents (i.e., 2%VF), LOP and MOR were higher about (30%) in comparison to those with higher percentage of VF, although with a remarkable lower (80%) in their toughness. In general, cotton linter (*short fibers with the length of 0.79 mm*) composites exhibited a better performance in terms of flexural strength with sufficient toughness for some applications.
- While flax fiber compounds exhibited remarkably higher about (65%) toughness than those cotton linter fiber composites, as it was expected for (*long fibers with the length of  $\leq 2$  cm according to flax fibers used in this research*). The toughness of the long flax fiber composites were considerably increased leading to a load capacity (deformation) of 40% to 90% of composite's FCS reaching to 6.0 to 8.00 mm deflections with sufficient PCS. The highest toughness was obtained by flax fiber compounds.
- The results and analyses related with the influence of different additive types on the flexural strength of VFRCCs revealed that the both incorporated superplasticizer improved (about 10%) the general mechanical behaviour of the cotton linter fiber in compounds with higher VF contents compared to the reference matrix (without additive) at 1 year hydration. With SVC3425 performing a better behaviour. On the other hand, there was a minor influence of the both superplasticizer on the flexural strength of flax fiber compounds. However, considering individually the Sika ViscoCrete 3425 (SVC3425) proved a better performance than SikaPlast 380 (SP380) after long term period of 1 year hydration.
- Accelerated aging cycles results exhibited that the flexural strength of cotton linter and flax fiber composites was slightly affected –specially in compounds with higher VF contents–. The compounds containing 6%-10% VF wt. were subjected to (20%) degradation of the flexural deformation capacity, however, good deformation capacity was still maintained after aging cycles. In this context, the cotton linter led to (25%) higher flexural performance in comparison with the flax fiber after aging cycles in compounds with 10% VF wt. with SVC3425 being more effective than SP380. Furthermore, accelerated aging cycles had a significant effect on the matrix (while not on the VFs), confirming that the use of a CAC-based matrix is recommendable to produce durable VFRCCs.
- The findings of the influence of cement matrix (CAC) on the VFs properties and on the mechanical flexural strength confirmed that, due to the absence of portlandite formation in such mixtures, CAC pastes are less aggressive toward the VFs. It was found that CAC cements could be a viable alternative to Portland cements in terms of VF reinforcement durability.

*Influence of pozzolanic addition; Silica Fume incorporation in CAC-based matrix; A low alkaline medium*

- The incorporation of silica fume in CAC matrix was efficient. In terms of flexural performance, it was found that at early hydration stage of 7D the matrices exhibited very poor flexural behavior (*about 90% lower for MOR in paste with 5% of SF content*) compared to those of 28D hydrated matrices. With higher SF contents (i.e., 15%, 20% SF), MOR were higher (30% to 35%) in comparison with the reference matrix (without SF incorporation) at 28D. In general terms, the both binders (with 5% and 15% of SF) exhibited increased (40% and 14% respectively) flexural performance over the time (at 56D compared to 28D hydration) among others. However considering each mixture individually, the matrix with 5% of SF content led to a notably higher (45%) strength than the binder with 15% of SF.
- In terms of compression strength, the results do not reveal significant changes in all hydration categories (i.e., 7D, 28D and 56D) except the binders with 5% and 15% of SF contents with an increased MOR (*about 58% and 23% for respectively*) at 56D compared to those of 7D hydrated matrices. Incorporated silicate source to the matrix, resulting in the generation of stable phases of strätlingite, preventing the compressive strength loss induced because of conversion phases in a pure CAC paste. These binders exhibited higher MOR (*20% and 13% for binders with 5% and 15% of SF contents respectively*) in comparison with the reference matrix at 56D. In general terms, considering each binder individually, the matrix with 5% of SF content led to slightly higher (7%) compression strength than the mixture with 15% of SF at 56D.
- The findings of the chemical composition (XRD) analysis of SF-CAC mixtures (i.e., 0%, 5% and 15% of SF contents) exhibited the presence of strätlingite phase  $C_2ASH_8$  at early hydration stage of 7D in the both binders of 5% and 15% of SF contents. With the hindered conversion hydrates because of  $C_2ASH_8$  formation and increased meta-stable phases of  $CAH_{10}-C_2AH_8$  at 28D and 56D hydration stages, leading to a decreased stable phases of  $C_3AH_6+AH_3$  compared to the reference matrix.
- The micro-structure (BSEM) analysis of SF-CAC mixtures (i.e., 0%-5%-15% of SF contents) confirmed that the pozzolanic reaction (*strätlingite  $C_2ASH_8$  phase*) was achieved in mixtures. The matrix with 15% of SF content at 56D exhibited a very dense matrix, but some SF particles remained without reacting as if the SF content was excess in the mixture. Simultaneously, the silica fume addition aid in the nucleation of CAC phase precipitation while lowering the matrix porosity. Regarding to the reference matrix, the common phases found in pure CAC were detected, the presence of anhydrous polyphasic particles and hydrated zones at 7D were evident. The meta-stable phases of  $CAH_{10}-C_2AH_8$  were converted to the stable phases of  $C_3AH_6-AH_3$  at 7D and some minor changes in the shapes of meta-stable phases, the edges were somewhat more rounded at 28D, which could be indicative of more advanced phases of hydration in such matrix.

### *Vegetable-Fiber reinforcement in SF-CAC based matrix*

- The incorporation of 5% SF wt. in cotton linter reinforced CAC-based matrix compound exhibited insignificant changes on the flexural performance of compounds at the both 28D and 56D hydration stages. It was found that the cotton linter compound containing 10% of VF exhibited slightly lower FCS and PCS (about 11% for MOR) and (about 24% for LOP) compared to the reference compound at 28D. Nevertheless, this decrease rate was lower (about only 5%) at 56D, indicating that the conversion phases of the matrix with 5% SF wt. content was hindered. In terms of LOP the reduction rate was lower (8%) at 56D in comparison to the results at 28D, confirming the results concluded in previous sections, the presence of strätlingite phase  $C_2ASH_8$  in this matrix and hence a hindered conversion phase. This compound exhibited slightly higher (15%) toughness than the reference mixture at 28D.
- Accelerated aging cycles (10 cycles) results revealed that the flexural strength of the both cotton linter and the reference composites was highly affected –an improved flexural strength after aging cycles–. The compound containing 5% SF wt. reinforced with 10% of cotton linter fiber increased (34% for MOR) with the flexural Strain-Softening behaviour, and a sufficient deformation capacity was still maintained even after aging cycles. The reference compound led to (27%) higher flexural performance after aging cycles, with 5% SF being more effective than 0% SF contents when compared individually each compound. Despite of that, the results revealed insignificant change (*the influence of 5% SF wt.*) on the mechanical performance of the compound comparing to the reference compound, the durability of VF and hence the compounds developed in such matrix, demonstrated significant improvement over previously reported cementitious composites reinforced with VF.
- VFs maintained their elasticity and had sufficient tensile strength to overcome the adherence to the matrix walls. In compounds without SF, a detachment of outer macro-fibril layers was observed in aged reference compounds, which VF were affected by only slight longitudinal cracks in the direction of macro-fibrils in matrix. It is possible that aging cycles degrade the peptide polymer chains that act as the binder between macro-fibrils. this degradation didn't appear in specimen with 5%SF and the fiber's surface still remains relatively smooth.
- The results of the micro-structure (BSEM) analysis of unaged compounds (i.e., 0% and 5% SF wt. with 10% of cotton linter wt.) confirmed that the pozzolanic reaction (*strätlingite  $C_2ASH_8$  phase*) was achieved in mixture with 5% SF wt. The amorphous silica particle was present and the monophasic calcium aluminate particles were not evident, due to reacting and turning into strätlingite ( $C_2ASH_8$ ). This matrix exhibited a very dense matrix and without porous at 28D. Regarding to the reference compound, a more advanced phase of hydration at 28D was evident, indicating the change of meta-stable phases of  $CAH_{10}$ - $C_2AH_8$  to stable phases of  $C_3AH_6$ + $AH_3$ , and no visible porous areas in the matrix was present and the matrix was well compacted.
- The BSEM analysis of aged compounds (i.e., 0% and 5% SF wt. with 10% of cotton linter fiber wt.) confirmed that the metastable phases  $CAH_{10}$ - $C_2AH_8$  have been converted to the stable phases of  $C_3AH_6$ - $AH_3$  with the volum reduction in the reference mixture. Aging cycles led to dissolution of some phases together with the reprecipitation of calcium ion in certain areas of this matrix. It was confirmed that a part of porosity was filled with

deposits of new phases of calcium aluminate rich in Al. Regarding to the aged compound with 5% SF wt. the reprecipitation of Ca was evident where cotton linter fiber didn't interact with this process.

- The SEM analysis on the surface and the durability of cotton linter fiber after 10 accelerated aging cycles in the both (i.e., 0% and 5% SF wt. with 10% cotton linter fiber wt.), in the break sections a multitude of cotton linter fibers was evident protruding from the surface of the matrix, indicating that the fibers were not degraded. In compound with 5% SF wt. the break section was more disaggregated, this claim was also confirmed by results of flexural strength that the compound maintained a high ductility after aging cycles. Regarding to the reference matrix the fiber maintained a sufficient tensile strength to overcome the adherence to the matrix walls, but a detachment of outer macro-fibril layers was evident, although the macro-fibrils still retained their integrity. Whereas in the compound with 5% SF wt. this degradation didn't appear and the fiber's surface still remained relatively smooth.

### *Future perspectives*

The investigation performed in this doctoral thesis stated significant aspects and allowed to develop a material to predict the flexural behavior of vegetable fiber reinforced in CAC-based cement composite. The investigated compounds respond to applications with relevant non-structural responsibility. Which only small thin panels reinforced with VF in CAC and SF-CAC based mixtures were investigated. In this regard, the real scale specimens and the combination of different vegetable fiber types, the effect of accelerated aging cycles (with higher number of cycles), and the effect of different silica fume contents (with higher SF contents) on the CAC hydration phases. Moreover, taking into account that CAC is a type of refractory cement, a resistant material against chemical agents such as (i.e., sulfates), in other words, the other types of properties of this cement such as (i.e., its behavior at high temperature, or its behavior in harsh environments as it provides exceptional endurance, or incorporating other types and contents of vegetable fibers) could be the points of further researches.



## 6. REFERENCES

E.B. Smith, Ph.D., L.H.D., 1938, Egyptian architecture as cultural expression, History of architecture, Princeton University. New York, London.

<https://ia800304.us.archive.org/10/items/egyptiana00smit/egyptiana00smit.pdf>

L. Hatschek, 1900, Patent GB190006455A. The manufacture process of imitation stone plates, slabs or tiles.

<https://worldwide.espacenet.com/patent/search/family/032361881/publication/GB190006455A?q=GB190006455A>

L. Hatschek, 1942, Patent CH234322A. The method of making cellulosic fiber cement products. <https://worldwide.espacenet.com/patent/search/family/005890851/publication/CH234322A?q=CHD234322>

J. Hardie and Coy. Pty. Ltd., 1938, Hardies's Fibrolite building booklet, Queensland. <https://nla.gov.au/nla.obj-296993269/view?sectionId=nla.obj-310593118&partId=nla.obj-297010762#page/n55/mode/1up>

S. Marsden, 1946–1959, The twentieth century heritage survey: post second world war, overview history 2003-4. <https://cdn.environment.sa.gov.au/environment/docs/her-gen-heritagesurvey1-1946-1959.pdf>

The Australian architecture, 1901-51: sources of modernism.

<https://ses.library.usyd.edu.au/bitstream/handle/2123/7701/sup0001.pdf?sequence=1&isAllowed=y>

W. Gropius, 1965, The new architecture and the Bauhaus. [https://monoskop.org/images/b/b7/Gropius\\_Walter\\_The\\_New\\_Architecture\\_and\\_the\\_Bauhaus\\_1965.pdf](https://monoskop.org/images/b/b7/Gropius_Walter_The_New_Architecture_and_the_Bauhaus_1965.pdf)

Arquitectura Viva, Herzog & de Meuron, 1978-2007, <https://www.herzogdemeuron.com/index/search.html>

E.H. Álvaro, 2019, Fiber cement as a material resource for the design of products for collective use, UPV Universitat Politècnica de València.

H.J. Wilke, 1976, New rules issued by the FDA about the use of asbestos containing filter sheets and their consequences in pharmaceutical technology. [https://hero.epa.gov/hero/index.cfm/reference/details/reference\\_id/3660108](https://hero.epa.gov/hero/index.cfm/reference/details/reference_id/3660108)

R.D.T Filho, K. Scrivener, G. L. England, K. Ghavami, 2000, Durability of alkali-sensitive sisal and coconut fibers in cement mortar composites, Cement and Concrete Composites. [https://doi.org/10.1016/S0958-9465\(99\)00039-6](https://doi.org/10.1016/S0958-9465(99)00039-6)

Order of December 7, 2001. The marketing of Asbestos fibers and products containing these fibers intentionally added is prohibited. [https://www.boe.es/eli/es/o/2001/12/07/\(1\)](https://www.boe.es/eli/es/o/2001/12/07/(1))

M. Khorami, E. Ganjian, 2011, Comparing flexural behaviour of fiber–cement composites reinforced bagasse: Wheat and eucalyptus, Construction and Building Materials. <https://doi.org/10.1016/j.conbuildmat.2011.03.052>

H. Savastano, P.G. Warden, R.S.P Coutts, 2003, Mechanically pulped sisal as reinforcement in cementitious matrices, Cement and Concrete Composites. [https://doi.org/10.1016/S0958-9465\(02\)00055-0](https://doi.org/10.1016/S0958-9465(02)00055-0)

R.S.P Coutts, 2005, A review of Australian research into natural fiber cement composites. Cement and Concrete Composites. <https://doi.org/10.1016/j.cemconcomp.2004.09.003>

P. Wambua, J. Ivens, I. Verpoest, 2003, Natural fibers: can they replace glass in fiber reinforced plastics?, Composites Science and Technology. [https://doi.org/10.1016/S0266-3538\(03\)00096-4](https://doi.org/10.1016/S0266-3538(03)00096-4)

E.H. Yang, V.C. Li, 2010, Strain-hardening fiber cement optimization and component tailoring by means of a micromechanical model, Construction and Building Materials. <https://doi.org/10.1016/j.conbuildmat.2007.05.014>

Li. Mi, P.Y. Thomas, V.M. Yoo, C.G. Ozcan, 2020, Recent advancements of vegetable-based natural fiber–reinforced composites and their applications. Composites Part B: Engineering. <https://doi.org/10.1016/j.compositesb.2020.108254>

V. Agopyan, H. Savastano, V.M. John, M.A. Cincotto, 2005, Developments on vegetable fiber–cement based materials in São Paulo, Brazil: An overview, Cement and Concrete Composites. [10.1016/j.cemconcomp.2004.09.004](https://doi.org/10.1016/j.cemconcomp.2004.09.004)

B.J. Mohr, J.J. Biernacki, K.E. Kurtis, 2006, Microstructural and chemical effects of wet/dry cycling on pulp fiber–cement composites, Cement and Concrete Research. <https://doi.org/10.1016/j.cemconres.2006.03.020>

- L.C. Roma, L.S. Martello, H. Savastano, 2008, Evaluation of mechanical, physical and thermal performance of cement-based tiles reinforced with vegetable fibers. *Construction and Building Materials*. <https://doi.org/10.1016/j.conbuildmat.2006.10.001>
- K.G. Satyanarayana, G.G.C. Arizaga, F. Wypych, 2009, Biodegradable composites based on lignocellulosic fibers—An overview, *Progress in Polymer Science*. <https://doi.org/10.1016/j.progpolymsci.2008.12.002>
- J. Claramunt, M. Ardanuy, J.A. García-Hortal, 2010, Effect of drying and rewetting cycles on the structure and physicochemical characteristics of softwood fibers for reinforcement of cementitious composites, *Carbohydrate Polymers*. <https://doi.org/10.1016/j.carbpol.2009.07.057>
- M. Ardanuy, J. Claramunt, R.D. Toledo Filho, 2015, Cellulosic fiber reinforced cement-based composites: A review of recent research. *Construction and Building Materials*. <https://doi.org/10.1016/j.conbuildmat.2015.01.035>
- R.D. Tolêdo Filho, K. Scrivener, G.L. England, K. Ghavami, 2000, Durability of alkali-sensitive sisal and coconut fibers in cement mortar composites. *Cement and Concrete Composites*. [https://doi.org/10.1016/S0958-9465\(99\)00039-6](https://doi.org/10.1016/S0958-9465(99)00039-6)
- R.D. Tolêdo Filho, K. Ghavami, G.L. England, K. Scrivener, 2003, Development of vegetable fiber–mortar composites of improved durability, *Cement and Concrete Composites*. [https://doi.org/10.1016/S0958-9465\(02\)00018-5](https://doi.org/10.1016/S0958-9465(02)00018-5)
- R.D. Tolêdo Filho, 1997, Natural fiber reinforced mortar composites: Experimental characterisation, Rio de Janeiro: DEC/PUC, Ph.D. Thesis.
- Gram HE, 1983, Durability of natural fibers in concrete, Swedish Cement and Concrete Research Institute.
- H. Savastano, V. Agopyan, 1999, Transition zone studies of vegetable fiber-cement paste composites. *Cement and Concrete Composites*. [10.1016/S0958-9465\(98\)00038-9](https://doi.org/10.1016/S0958-9465(98)00038-9)
- H. Savastano, P.G. Warden, R.S.P. Coutts, 2000, Brazilian waste fibers as reinforcement for cement-based composites, *Cement and Concrete Composites*. [https://doi.org/10.1016/S0958-9465\(00\)00034-2](https://doi.org/10.1016/S0958-9465(00)00034-2)
- H. Savastano, P.G. Warden, R.S.P. Coutts, 2005, Microstructure and mechanical properties of waste fiber–cement composites, *Cement and Concrete Composites*. <https://doi.org/10.1016/j.cemconcomp.2004.09.009>
- B.J. Mohr, H. Nanko, K.E. Kurtis, 2005, Durability of kraft pulp fiber–cement composites to wet/dry cycling. *Cement and Concrete Composites*. <https://doi.org/10.1016/j.cemconcomp.2004.07.006>
- P. Soroushian, J. Pil Won, M. Hassan, 2012, Durability characteristics of CO<sub>2</sub>-cured cellulose fiber reinforced cement composites, *Construction and Building Materials*. <https://doi.org/10.1016/j.conbuildmat.2012.02.016>

The #Housing 2030 Report of ONU-Habitat. [https://www.habitatge.barcelona/en/noticia/the-housing-2030-report-of-ONU-habitat-unece-and-housing-europe-acknowledge-barcelona-as-a-pioneering-city-in-housing-policies\\_1109940](https://www.habitatge.barcelona/en/noticia/the-housing-2030-report-of-ONU-habitat-unece-and-housing-europe-acknowledge-barcelona-as-a-pioneering-city-in-housing-policies_1109940)

Economic Commission for Europe 2017, Framework guidelines for energy efficiency standards in buildings.

[https://unece.org/fileadmin/DAM/energy/se/pdfs/geee/geee4\\_Oct2017/ECE\\_ENERGY\\_GE.6\\_2017\\_4\\_EEBuildingGuidelines\\_final.pdf](https://unece.org/fileadmin/DAM/energy/se/pdfs/geee/geee4_Oct2017/ECE_ENERGY_GE.6_2017_4_EEBuildingGuidelines_final.pdf)

S. Moghtadernejad, L.E. Chouinard, M. SaeedMirza, 2020, Design strategies using multi-criteria decision-making tools to enhance the performance of building façades, McGill University, Canada. <https://doi.org/10.1016/j.jobe.2020.101274>

R.S. Teixeira, G.H.D. Tonoli, S.F. Santos, J. Fiorelli, H. Savastano Jr., F.A. Rocco Lahr, 2012, Extruded cement based composites reinforced with sugar cane bagasse fibers. Key Engineering Materials. <https://www.researchgate.net/publication/258227000>

J. Claramunt, L. Fernández, H. Ventura, M. Ardanuy, 2016, Natural fiber nonwoven reinforced cement composites as sustainable materials for building envelopes, Construction and Building Materials. <https://doi.org/10.1016/j.conbuildmat.2016.04.044>

E. García, P. Garcés, S. Chinchón, 2000, General study of alkaline hydrolysis in calcium aluminate cement mortars under a broad range of experimental conditions. Cement and Concrete Research. [https://doi.org/10.1016/S0008-8846\(00\)00396-3](https://doi.org/10.1016/S0008-8846(00)00396-3)

K. Scrivener, J. Newman, B.S. Choo, 2003, Calcium Aluminate Cements. Advanced Concrete Technology. [K.L.+Scrivener,+J.+Newman,+B.S.+Choo,+Calcium+Aluminate+Cements.+Advanced+Concrete+Technology,+Elsevier,+Oxford,+2003.](https://doi.org/10.1016/B978-0-08-045451-1)

K. Scrivener, J.L. Cabiron, R. Letourneux, 1999, High-performance concretes from calcium aluminate cements. Cement and Concrete Research. [https://doi.org/10.1016/S0008-8846\(99\)00103-9](https://doi.org/10.1016/S0008-8846(99)00103-9)

V. Antonovič, J. Keriene, R. Boris, M. Aleknevičius, 2013, The effect of temperature on the formation of the hydrated calcium aluminate cement structure, Procedia Engineering. <https://doi.org/10.1016/j.proeng.2013.04.015>

N.B. Singh, S. Rai, S. Chaturvedi, 2002, Hydration of composite cement, Progress in Crystal Growth and Characterization of Materials. [https://doi.org/10.1016/S0960-8974\(02\)00045-1](https://doi.org/10.1016/S0960-8974(02)00045-1)

S.M. Park, J.G. Jang, H.M. Son, H.K. Lee, 2017, Stable conversion of metastable hydrates in calcium aluminate cement by early carbonation curing. Journal of CO2 Utilization. <https://doi.org/10.1016/j.jcou.2017.07.002>

H.M. Son, S.M. Park, H.Y. Kim, J.H. Seo, H.K. Lee, 2019, Effect of CaSO4 on hydration and phase conversion of calcium aluminate cement. Construction and Building Materials. <https://doi.org/10.1016/j.conbuildmat.2019.07.004>

H.M. Son, S.M. Park, J.G. Jang, H.K. Lee, 2018, Effect of nano-silica on hydration and conversion of calcium aluminate cement. Construction and Building Materials. <https://doi.org/10.1016/j.conbuildmat.2018.03.011>

- A. Bentur, S. Diamond, 1986, Effects of Direct Incorporation of micro silica into GFRC Composites on Retention of Mechanical Properties After Aging, Proceedings—Durability of Glass Fiber Reinforced Concrete Symposium, Prestressed Concrete Institute.
- H. Schreiner, L. Holmen, 2002, The effect of microsilica dispersion in fiber cement mixes. *8th International Inorganic-Bonded Wood and Fiber Composite Materials*. <https://www.researchgate.net/publication/258689432>
- B.J. Mohr, J.J. Biernacki, K.E. Kurtis, 2007, Supplementary cementitious materials for mitigating degradation of kraft pulp fiber-cement composites. *Cement and Concrete Research*. <https://doi.org/10.1016/j.cemconres.2007.08.001>
- D. Jian, Y. Fu, J.J. Beaudoin, 1995, Strätlingite formation in high alumina cement-silica fume systems: significance of sodium ions, *Cement and Concrete Research*. [https://doi.org/10.1016/0008-8846\(95\)00124-U](https://doi.org/10.1016/0008-8846(95)00124-U)
- A. Hidalgo, J.L. García Calvo, M.C. Alonso, L. Fernández, C. Andrade, 2009, Microstructure development in mixes of calcium aluminate cement with silica fume or fly ash. *Journal of Thermal Analysis and Calorimetry*. <https://doi.org/10.1007/s10973-007-8439-3>
- Sakai et al., 2010, Mechanical properties and micro-structures of calcium aluminate based ultra high strength cement. *Cement and Concrete Research*. <https://doi.org/10.1016/j.cemconres.2010.01.001>
- N.K. Lee et al, 2017, Microstructural investigation of calcium aluminate cement-based ultra-high performance concrete (UHPC) exposed to high temperatures, *Cement and Concrete Research*. <https://doi.org/10.1016/j.cemconres.2017.09.004>
- L. Barbara, P. Durdzinski, K.D. Weerd, 2015, Thermogravimetric analysis, A practical guide to microstructural analysis of cementitious materials. <https://doi.org/10.1201/b19074>
- M. Khorami, E. Ganjian, 2013, The effect of limestone powder, silica fume and fiber content on flexural behaviour of cement composite reinforced by waste Kraft pulp, *Construction and Building Materials*. <https://doi.org/10.1016/j.conbuildmat.2013.03.099>
- H. Pöllmann, 2012, Calcium aluminate cements – raw materials, differences, hydration and properties, *Rev. Mineral. Geochem.* <https://doi.org/10.2138/rmg.2012.74.1>
- M.U. Okoronkwo, F.P. Glasser, 2016, Stability of strätlingite in the CASH system. *Materials and Structures/Materiaux et Constructions*. <https://doi.org/10.1617/s11527-015-0789-x>
- A. Hidalgo, J.L. Garcia, O.J. Garcia, S. Petit, C.M. Alos, 2008, Microstructural evolution of calcium aluminate cements hydrations with silica fume and fly ash addition by scanning electron microscopy, and mid and near-infrared spectroscopy. *Journal of the American Ceramic Society*, 91. <https://doi.org/10.1111/j.1551-2916.2008.02283.x>
- A. Hidalgo, S. Petit, J.L. García Calvo, C. Alonso, C. Andrade, 2007, Microstructure of the system calcium aluminate cement-silica fume: application in waste immobilization. *Studies in Surface Science and Catalysis*. [https://doi.org/10.1016/S0167-2991\(07\)81039-1](https://doi.org/10.1016/S0167-2991(07)81039-1)

- H.G. Midgley, 1967, The mineralogy of set high alumina cement. *Trans. Brit. Ceram Soc.* 66, 161-187.
- H.G. Midgley, 1968, The composition and possible structure of the quaternary phase in high alumina cement and its relation to other phases in the system CaO-MgO-Al<sub>2</sub>O<sub>3</sub>. *Trans. Brit. Ceram. Soc.* 71, 55-59.
- S. Bentsen, A. Seltveit, B. Sanderg, 1990, Effect of microsilica on conversion of high alumina cement Calcium aluminate cement. London (UK): Chapman and Hall.
- A.J. Majumdar, B. Singh, 1989, Cement compositions. European patent no. 0/312/323. [https://doi.org/10.1016/0008-8846\(92\)90040-3](https://doi.org/10.1016/0008-8846(92)90040-3)
- A.J. Majumdar, R.N. Edmonds, B. Singh, 1990, Hydration of calcium aluminates in presence of granulated blastfurnace slag. Calcium aluminate cement. In: Chapman and Hall.
- A.J. Majumdar, B. Singh, 1992, Properties of some blended high-alumina cements. *Cement and Concrete Research*. [https://doi.org/10.1016/0008-8846\(92\)90040-3](https://doi.org/10.1016/0008-8846(92)90040-3)
- C. Xiandong, R. J. Kirkpatrick, *Journal of American Ceramic Society*, 76 (1993) 409.M.
- Colleparidi, S. Monosi, P. Piccioli, *Cement and Concrete Research*, 25 (1995) 961.
- J. Bensted, 2002, Calcium Aluminate Cement, Structure and performance of cements, <https://doi.org/10.1201/9781482295016>
- J. Bensted, 1996, The influence of pozzolanic materials on the mechanical stability of aluminous cement, 26(4), 649–650.
- J.M. Rivas Mercury, X. Turrillas, A.H. de Aza, P. Pena, 2006, Calcium aluminates hydration in presence of amorphous SiO<sub>2</sub> at temperatures below 90°C, *Journal of Solid State Chemistry*. <https://doi.org/10.1016/j.jssc.2006.05.017>
- N.Y. Mostafa, Z.I. Zaki, O.H. Abd Elkader, 2012, Chemical activation of calcium aluminate cement composites cured at elevated temperature. *Cement and Concrete Composites*. <https://doi.org/10.1016/j.cemconcomp.2012.08.002>
- H.K.A. El-Hamid, M.M. Radwan, 2019, Influence of nano-silica additions on hydration characteristics and cytotoxicity of calcium aluminate as biomaterial. *Heliyon*, 5(7), e02135. <https://doi.org/10.1016/j.heliyon.2019.e02135>
- M. Ramirez, 2020, Evaluation of the mechanical performance and durability of binary blended CAC-MK/natural fiber composites. *Construction and Building Materials*. <https://doi.org/10.1016/j.conbuildmat.2020.118919>
- M. Idrees, O. Ekinoglu, M. Sarmad, 2021, Hydration behaviour of calcium aluminate cement mortars with mineral admixtures at different curing temperatures. *Construction and Building Materials*. <https://doi.org/10.1016/j.conbuildmat.2021.122839>

- J.F. Zapata, H.A. Colorado, M.A. Gomez, 2020, Effect of high temperature and additions of silica on the microstructure and properties of calcium aluminate cement pastes. *Journal of Sustainable Cement-Based Materials*. <https://doi.org/10.1080/21650373.2020.1737593>
- B.J. Mohr, H. Nanko, K.E. Kurtis, 2005, Durability of kraft pulp fiber–cement composites to wet/dry cycling. *Cement and Concrete Composites*. <https://doi.org/10.1016/j.cemconcomp.2004.07.006>
- P. Soroushian, M. Elzafraney, A. Nossoni, H. Chowdhury, 2006, Evaluation of normal- weight and light-weight fillers in extruded cellulose fiber cement products. *Cement and Concrete Composites*.
- H. Savastano, A. Turner, C. Mercer, W.O. Soboyejo, 2006, Mechanical behavior of cement-based materials reinforced with sisal fibers. *Journal of Materials Science*. <https://doi.org/10.1007/s10853-006-0218-1>
- G.H.D Tonoli, H. Savastano, E. Fuente, C. Negro, A. Blanco, F.A. Rocco Lahr, 2010, Eucalyptus pulp fibers as alternative reinforcement to engineered cement-based composites. *Industrial Crops and Products*. <https://doi.org/10.1016/j.indcrop.2009.10.009>
- G.H.D Tonoli, U.P. Rodrigues Filho, H. Savastano, J. Bras, M.N. Belgacem, F.A. Rocco Lahr, 2009, Cellulose modified fibers in cement based composites. *Composites Part A: Applied Science and Manufacturing*. <https://doi.org/10.1016/j.compositesa.2009.09.016>
- J. Claramunt et al., 2013, Mechanical performance of cement mortar composites reinforced with cellulose fibers.” 9th International conference on Composite Science and Technology. [https://upcommons.upc.edu/bitstream/handle/2117/20588/ICCST-9\\_Sorrento\\_PortadaIndexPonencia.pdf](https://upcommons.upc.edu/bitstream/handle/2117/20588/ICCST-9_Sorrento_PortadaIndexPonencia.pdf)
- J. Claramunt, M. Ardanuy, L. Fernandez, 2015, Wet/dry cycling durability of cement mortar composites reinforced with micro and nanoscale cellulose pulps. *BioResources*. <https://doi.org/10.15376/biores.10.2.3045-3055>
- M. Ardanuy, J. Claramunt, R.D. Toledo Filho, 2015, Cellulosic fiber reinforced cement-based composites: A review of recent research. *Construction and Building Materials*. <https://doi.org/10.1016/j.conbuildmat.2015.01.035>
- H. Ventura, 2017, Development of New Composites Reinforced Lightweight Green Structures of Flax with Nonwoven Fibers, 330. <http://hdl.handle.net/2117/110896>
- N. Balaguru, S.P. Shah, 1992, Fiber-reinforced cement composites. <http://worldcat.org/isbn/0070564000>
- P. Wambua, J. Ivens, I. Verpoest, 2003, Natural fibers: Can they replace glass in fiber reinforced plastics? *Composites Science and Technology*. [https://doi.org/10.1016/S0266-3538\(03\)00096-4](https://doi.org/10.1016/S0266-3538(03)00096-4)
- A. Bentur, S. Mindess, 2006, Fiber Reinforced Cementitious Composites. *Fiber Reinforced Cementitious Composites*. <https://doi.org/10.1201/9781482267747>

- M. Ardanuy, J. Claramunt, R.D. Toledo Filho, 2015, Cellulosic fiber reinforced cement-based composites: A review of recent research. *Construction and Building Materials*. <https://doi.org/10.1016/j.conbuildmat.2015.01.035>
- M. Sriram, K.R.A. Sidhaarth, 2022, Various properties of natural and artificial fibers with cementitious composites in hybrid form – A review, *Materials Today*. <https://doi.org/10.1016/j.matpr.2022.01.266>
- J. Biagiotti, D. Puglia, J.M. Kenny, 2004, A Review on Natural Fiber-Based Composites-Part I. *Journal of Natural Fibers*. [https://doi.org/10.1300/J395v01n02\\_04](https://doi.org/10.1300/J395v01n02_04)
- M. Jawaid, H.P.S. Abdul Khalil, 2011, Cellulosic/synthetic fiber reinforced polymer hybrid composites: A review, *Carbohydrate Polymers*. <https://doi.org/10.1016/j.carbpol.2011.04.043>
- U. Huner, 2015, Effect of Water Absorption on the Mechanical Properties of Flax Fiber Reinforced Epoxy Composites. *Advances in Science and Technology Research Journal* <https://doi.org/10.12913/22998624/2357>
- Z.N. Azwa, B.F. Yousif, A.C. Manalo, W. Karunasena, 2013, A review on the degradability of polymeric composites based on natural fibers. *Materials and Design*. <https://doi.org/10.1016/j.matdes.2012.11.025>
- R.S.P Coutts, 1992, From forest to factory to fabrication, RILEM PROCEEDINGS. CHAPMAN & HALL <https://books.google.es/from forest to factory to fabrication>
- D.B. Dittenber, H.V.S. Gangarao, 2012, Critical review of recent publications on use of natural composites in infrastructure. *Composites Part A: Applied Science and Manufacturing*. <https://doi.org/10.1016/j.compositesa.2011.11.019>
- S. Mathias et al., 2016, Plant Fiber: Molecular Structure and Biomechanical Properties, of a Complex Living Material, Influencing Its Deconstruction towards a Biobased Composite. *Materials* <https://doi.org/10.3390/ma9080618>
- H. Ventura, J. Claramunt, A. Navarro, M.A. Rodriguez-Perez, M. Ardanuy, 2016, Effects of wet/dry-cycling and plasma treatments on the properties of flax nonwovens intended for composite reinforcing. *Materials*. <https://doi.org/10.3390/ma9020093>
- K.L. Pickering, M.G.A. Efendy, T.M. Le, 2016, A review of recent developments in natural fiber composites and their mechanical performance. *Composites Part A: Applied Science and Manufacturing*. <https://doi.org/10.1016/j.compositesa.2015.08.038>
- J.A. García Hortal, 1988, *Constituyentes fibrosos de pastas y papeles*, Edicions UPC, Terrassa (Spain).
- L. Gonzalez-Lopez, J. Claramunt, L. Haurie, H. Ventura, M. Ardanuy, 2021, Study of the fire and thermal behaviour of façade panels made of natural fiber-reinforced cement-based composites, *Construction and Building Materials*. <https://doi.org/10.1016/j.conbuildmat.2021.124195>
- G.W. Beckermann, K.L. Pickering, 2008, Engineering and evaluation of hemp fiber reinforced polypropylene composites: Fiber treatment and matrix modification. *Composites Part A: Applied Science and Manufacturing*. <https://doi.org/10.1016/j.compositesa.2008.03.010>

- L. Yan, N. Chouw, K. Jayaraman, 2014, Flax fiber and its composites - A review. *Composites Part B: Engineering*. <https://doi.org/10.1016/j.compositesb.2013.08.014>
- L.A. Titcombe, 1992, Chemically modified cotton linters: Preparations and papermaking properties, *University of Tasmania*. 51(2), 131–143.
- R. Freytag, J.J. Dinze, 1983, *Fundamentals and Preparation Part A, Handbook of Fiber Science and technology: Vol I, Chemical Processing of Fibers and Fabrics*, edited by Menachem Lewin and Stephan B. Sello, Marcel Dekker, N. 1983;111.
- T.P. Nevell, S.H. Zeronian, 1985, in *Cellulose Chemistry and Its Applications* (Ed.s T.P. Nevell and S.H. Zeronian) Ch. 1, p. 15 (Ellis Horwood: Chichester).
- L. Mi, P.Y. Thomas, V.M. Yoo, C.G. Ozcan, 2020, Recent advancements of vegetable -based natural fiber-reinforced composites and their applications. *Composites Part B: Engineering*, <https://doi.org/10.1016/j.compositesb.2020.108254>
- B. Zawde, 1994, Performance of natural fiber reinforced mortar roofing tiles. *Materials and Structures* 27.6 (1994): 347-352. <https://doi.org/10.1007/BF02473427>
- H. Ventura, M. Ardanuy, X. Capdevila, F. Cano, J.A. Tornero, 2014, The effects of needling parameters on some structural and physico-mechanical properties of needle-punched nonwovens *J. Text. Inst.* <https://doi.org/10.1080/00405000.2013.874628>
- J. Claramunt, L. Fernández, H. Ventura, M. Ardanuy, 2016, Natural fiber nonwoven reinforced cement composites as sustainable materials for building envelopes, *Construction and Building Materials*. <https://doi.org/10.1016/j.conbuildmat.2016.04.044>
- J. Claramunt, M. Ardanuy, 2017, Using vegetable fiber nonwovens cement composites as sustainable materials for applications on ventilated façade systems, *Construction Materials using Inorganic Bonded Fiber Composites*, Woodhead Publishing. <https://doi.org/10.1016/B978-0-08-102001-2.00016-4>
- J. Claramunt, H. Ventura, M. Ardanuy, 2018, The rheology of CAC-based cement pastes and the relationship to penetrability through nonwoven fabric reinforcements. *Cement and Concrete Composites*. <https://doi.org/10.1016/j.cemconcomp.2018.08.014>
- L. Gonzalez-Lopez, J. Claramunt, L. Haurie, H. Ventura, M. Ardanuy, 2021, Study of the fire and thermal behaviour of façade panels made of natural fiber-reinforced cement-based composites, *Construction and Building Materials*. <https://doi.org/10.1016/j.conbuildmat.2021.124195>
- P. Sadrolodabae, J. Claramunt, M. Ardanuy, A.D. la Fuente, 2022, Experimental characterization of comfort performance parameters and multi-criteria sustainability assessment of recycled textile-reinforced cement facade cladding, *Journal of Cleaner Production*. <https://doi.org/10.1016/j.jclepro.2022.131900>
- A. Geremew, P.D. Winne, T.A. Demissie, H.D. Backer, 2021, Treatment of Natural Fiber for Application in Concrete Pavement, *Advances in Civil Engineering*. <https://doi.org/10.1155/2021/6667965>

- F. Medina, N. Barluenga, F. Hernández-Olivares, 2014, Enhancement of durability of concrete composites containing natural pozzolans blended cement through the use of Polypropylene fibers. *Composites Part B: Engineering*. <https://doi.org/10.1016/j.compositesb.2014.01.052>
- R.A.A. Shanks, 2014, Chapter 2-Chemistry and Structure of Cellulosic Fibers as Reinforcements in Natural Fiber Composites, Woodhead Publishing Limited, Sawston, UK.
- Y. Shireesha, G. Nandipati, 2019, State of Art Review on Natural Fibers, *Materials Today*. <https://doi.org/10.1016/j.matpr.2019.06.272>
- J. Claramunt, L. Fernandez, H. Ventura, M. Ardanuy, 2016, Natural fiber nonwoven reinforced cement composites as sustainable materials for building envelopes, *Constr. Build. Mater*. <https://doi.org/10.1016/j.conbuildmat.2016.04.044>.
- M. George, M. Chae, D.C. Bressler, 2016, Composite materials with bast fibers: Structural, technical, and environmental properties. *Progress in Materials Science*. <https://doi.org/10.1016/j.pmatsci.2016.04.002>
- O. Onuaguluchi, N. Banthia, 2016, Vegetable -based natural fiber reinforced cement composites: A review. *Cement and Concrete Composites*. <https://doi.org/10.1016/j.cemconcomp.2016.02.014>
- Gram HE, 1985, Durability of natural fibers in concrete, Swedish, Cement and Concrete Research Institute, Research Fo. 1:83, Stockholm.
- A. Bentur, S.A.S. Akers, 1989, The microstructure and ageing of cellulose fiber reinforced cement composites cured in a normal environment. *International Journal of Cement Composites and Lightweight Concrete*. [https://doi.org/10.1016/0262-5075\(89\)90120-6](https://doi.org/10.1016/0262-5075(89)90120-6)
- H. Savastano, V. Agopyan, 1999, Transition zone studies of vegetable fiber-cement paste composites. *Cement and Concrete Composites*. [https://doi.org/10.1016/S0958-9465\(98\)00038-9](https://doi.org/10.1016/S0958-9465(98)00038-9)
- R.D. Tolêdo Filho, K. Scrivener, G.L. England, K. Ghavami, 2000, Durability of alkalisensitive sisal and coconut fibers in cement mortar composites. *Cement and Concrete Composites*.
- M. Ardanuy, J. Claramunt, J.A. García-Hortal, M. Barra, 2011, Fiber-matrix interactions in cement mortar composites reinforced with cellulosic fibers. *Cellulose*, 18(2), 281–289. <https://doi.org/10.1007/s10570-011-9493-3>
- B.J. Mohr, H. Nanko, K.E. Kurtis, 2005a, Durability of kraft pulp fiber-cement composites to wet/dry cycling. *Cement and Concrete Composites*. <https://doi.org/10.1016/j.cemconcomp.2004.07.006>
- B.J. Mohr, H. Nanko, K.E. Kurtis, 2005b, Durability of thermo-mechanical pulp fiber-cement composites to wet/dry cycling. *Cement and Concrete Composites*.
- V. Agopyan, H. Savastano, V.M. John, M.A. Cincotto, 2005, Developments on vegetable fiber-cement based materials in São Paulo, Brazil: An overview. *Cement and Concrete Composites*. <https://doi.org/10.1016/j.cemconcomp.2004.09.004>

- M. Ramírez, J. Claramunt, H. Ventura, M. Ardanuy, 2020, Evaluation of the mechanical performance and durability of binary blended CAC-MK/natural fiber composites. *Construction and Building Materials*, <https://doi.org/10.1016/j.conbuildmat.2020.118919>
- R.D. Tolêdo Filho, K. Ghavami, G.L. England, K. Scrivener, 2003, Development of vegetable fiber-mortar composites of improved durability. *Cement and Concrete Composites*. [https://doi.org/10.1016/S0958-9465\(02\)00018-5](https://doi.org/10.1016/S0958-9465(02)00018-5)
- V.M. John, M.A. Cincotto, C. Sjöström, V. Agopyan, C.T.A. Oliveira, 2005, Durability of slag mortar reinforced with coconut fiber. *Cement and Concrete Composites*. <https://doi.org/10.1016/j.cemconcomp.2004.09.007>
- B.J. Mohr, J.J. Biernacki, K.E. Kurtis, 2007, Supplementary cementitious materials for mitigating degradation of kraft pulp fiber-cement composites. *Cement and Concrete Research*. <https://doi.org/10.1016/j.cemconres.2007.08.001>
- F.A. Silva, R.D. Tolêdo Filho, J.D.A. Melo Filho, E.D.M. Rego Fairbairn, 2010, Physical and mechanical properties of durable sisal fiber-cement composites, *Construction and Building Materials*. <https://doi.org/10.1016/j.conbuildmat.2009.10.030>
- F.A. Silva, N. Chawla, R.D. Tolêdo Filho, 2010, Mechanical behavior of natural sisal fibers. *Journal of Biobased Materials and Bioenergy*. <https://doi.org/10.1166/jbmb.2010.1074>
- J. Claramunt, M. Ardanuy, J.A. García Hortal, A. Clemente Escuin, 2009, Effect of drying and rewetting cycles of cellulosic fibers on resistance of cementitious composites. <https://upcommons.upc.edu/e-prints/handle/2117/6356>
- J. Claramunt, M. Ardanuy, J.A. García-Hortal, 2010, Effect of drying and rewetting cycles on the structure and physicochemical characteristics of softwood fibers for reinforcement of cementitious composites. *Carbohydrate Polymers*. <https://doi.org/10.1016/j.carbpol.2009.07.057>
- J. Claramunt, M. Ardanuy, J.A. García-Hortal, R.D. Tolêdo Filho, 2011, The hornification of vegetable fibers to improve the durability of cement mortar composites, *Cement and Concrete Composites*. <http://dx.doi.org/10.3989/mc.2015.05514>
- S.F. Santos, G.H.D Tonoli, J.E.B. Mejia, J. Fiorelli, H. Savastano, 2015, Non-conventional cement-based composites reinforced with vegetable fibers: A review of strategies to improve durability. *Materiales de Construcción*. <https://doi.org/10.3989/mc.2015.05514>
- J. Claramunt, M. Ardanuy, L. Fernandez, 2015, Wet/dry cycling durability of cement mortar composites reinforced with micro- and nanoscale cellulose pulps. *BioResources*, <https://doi.org/10.15376/biores.10.2.3045-3055>
- U. Weise, H. Paulapuro, 1999, Effect of drying and rewetting cycles on fiber swelling. *Journal of Pulp and Paper Science*.
- S.R. Ferreira, P.R. Lima, F.A. Silva, R.D. Tolêdo Filho, 2014, Effect of Sisal Fiber Hornification on the fiber-matrix bonding characteristics and bending behavior of cement based composites, *Key Eng. Material*.

- B.J. Mohr, J.J. Biernacki, K.E. Kurtis, 2006, Microstructural and chemical effects of wet/dry cycling on pulp fiber–cement composites, *Cement and Concrete Research*.  
<https://doi.org/10.1016/j.cemconres.2006.03.020>
- G.H.D. Tonoli, M.N. Belgacem, J. Bras, M.A. Pereira-da-Silva, F.A.R. Lahr, H. Savastano, 2012, Impact of bleaching pine fiber on the fiber/cement interface, *J. Mater Sci*.
- R. Ahmad, R. Hamid, S.A. Osman, 2019, Physical and chemical modifications of vegetable fibers for reinforcement in cementitious composites. *Advances in Civil Engineering*.  
<https://doi.org/10.1155/2019/5185806>
- B.J. Mohr, N.H. El-Ashkar, K.E. Kurtis, 2004, Fiber-Cement Composites for Housing Construction: State-of-the-Art Review. Proceedings of the NSF Housing Research Agenda Workshop. <http://www.pathnet.org/si.asp?id=1075>
- R.D. Tolêdo Filho, K. Joseph, K. Ghavami, G.L. England, 1999, The use of sisal fiber as reinforcement in cement based composites. *Revista Brasileira de Engenharia Agrícola e Ambiental*. <https://doi.org/10.1590/1807-1929/agriambi.v3n2p245-256>
- M. Ardanuy, J. Claramunt, F. Pares, E. Aracri, T. Vidal, 2012, Nanofibrillated cellulose as reinforcement for high performance cement mortar composites. ECCM 2012 - Composites at Venice, Proceedings of the 15th European Conference on Composite Materials.
- M.R. Hamidian, P. Shafigh, 2021, Post-peak Behaviour of Composite Column Using a Ductile Lightweight Aggregate Concrete. *International Journal of Concrete Structures and Materials*.  
<https://doi.org/10.1186/s40069-020-00453-6>
- AMERICAN CONCRETE INSTITUTE (ACI), 2009, Aci 544.1R-96: Report on Reinforced Concrete (Reapproved). ACI Committee 544. [http://indiafiber.com/Files/ACI report.pdf](http://indiafiber.com/Files/ACI%20report.pdf)
- TFR1-Test , 1984, The determination of modulus of rupture and limit of proportionality of thin fibre reinforced cement sections. *Material Structure*;17(102).
- TFR4-Test, 1984, The determination of energy absorption in flexure of thin fibre: reinforced cement sections. *Material Structure*;17(102).
- RILEM Recommendations, 1990, 7 Vegetable and their Fibers as Building Materials Salvador, Bahia, Brazil, Edited by H.S. Sobral.
- RILEM International Symposium, 1992, Fiber Reinforced Cement and Concrete Proceedings of the Fourth, edited by R.N. Swamy.
- Swamy RN (ed) (1988) Natural fiber reinforced cement and concrete. Blackie, Glasgow
- H.S.Sobral. (1990). *Vegetable plants and their fibers as building materials*.